TITANS AE

Tradespace Investigation of a Telescope Architecture for Next-generation Space Astronomy and Exploration
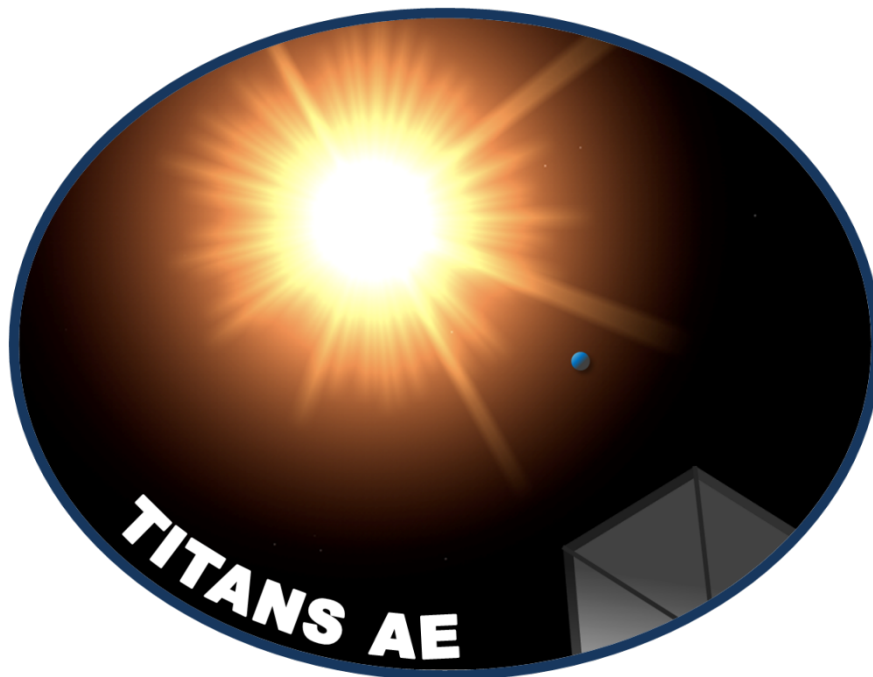
Final Report

May 2013

16.89 Space Systems Engineering

Department of Aeronautics and Astronautics

Massachusetts Institute of Technology

Students: Giuseppe Cataldo, Mark Chodas, Pratik Davé, Atray Dixit, Sherrie Hall, Robert Harris, Dustin Hayhurst, Fernando Hicks, Chris Jewison, Ioana Josan-Drinceanu, Brandon Karlow, Bryan McCarthy, Andrew Owens, Eric Peters, Margaret Shaw, David Sternberg, Kathleen Voelbel, Marcus Wu

Instructors:
Prof. David Miller, Prof. Alessandro Golkar, Prof. Kerri Cahoy, Dr. Rebecca Masterson, Gwendolyn Gettliffe

ACKNOWLEDGEMENTS

TABLE OF CONTENTS

LIST OF FIGURES

LIST OF TABLES

1 EXECUTIVE SUMMARY

NASA has been engaged in a number of space missions aimed to further our understanding of the universe through the development and deployment of space telescopes such as Hubble, Herschel, Spitzer, Chandra, and Kepler, as well as the James Webb Space Telescope (JWST) currently under construction. Such instruments cover a large band of the electromagnetic spectrum, from the X-ray to the infrared, providing valuable information on a number of phenomena of interest to the entire scientific community. The 2010 Decadal Survey for Astronomy and Astrophysics calls for a medium-scale space mission that will hunt exoplanets in a wide field as an attempt to find stellar systems similar to this solar system and Earth-like planets. The Wide-Field InfraRed Survey Telescope (WFIRST) would be the candidate for this type of mission, which would play a preparatory role in the development of a large-scale space-based mission intended to image Earth-like planets in the habitable zones of nearby stars and study their atmospheres. Thus, a telescope for imaging and spectroscopy of exoplanets from the ultra-violet to near infra-red spectra will be one of the top-priority areas in the 2020 decade.

In order to lay the bases for this endeavor, NASA has commissioned the Massachusetts Institute of Technology's Space Systems Laboratory to perform a tradespace exploration analysis for a large, segmented telescope, referred to as a Large Telescope Array (LTA), with the capabilities necessary to achieve the above-mentioned scientific objectives. Specifically, this task involves the identification of a set of architectural decisions, which, once made, define an architecture that can be assessed based upon quantitative metrics (e.g., cost, mass, complexity, risk, performance, serviceability, assemble-ability). By varying the architectural decisions, a family of architectures can be compared, via these metrics, to identify the attributes that are common to the better performing architectures. To accomplish this task, then, the following questions were answered:

1. *Who are the stakeholders and what are their needs and desires?*
   The stakeholders are scientific organizations, high-tech companies, and universities interested in a tradespace study for a next-generation telescope capable of opening new horizons to science and stimulate the development of new technologies.
2. *Based on the results of this stakeholder analysis, are there any assumptions that need to be taken into account and that would limit the scope of such a tradespace analysis?*
   The assumptions were made based on the stakeholder needs and desires, the technical requirements of similar technologies, and the necessity to keep the scope of this project at a level manageable by a one-semester graduate course.
3. *What are the technical requirements to build an LTA?*
   Derived from NASA's Advanced-Technology Large-Aperture Space Telescope (ATLAST) concept, the requirements are: a 16.8-m-diameter primary mirror, operation at Sun-Earth Lagrangian Point 2, on-orbit assembly, launch in 2028, technology readiness level (TRL) 6 by 2020.
4. *What architectural decisions can be made?*
   The following seven were selected: communications architectures, modularity, location of servicing, frequency of servicing, assembly and servicing technique, primary mirror segmentation, and primary mirror segment support method.
5. *What metrics can be employed to evaluate such architectures?*
   The following four metrics were chosen: cost, utility to science, failed downtime, and servicing margin.

6. What are the best-performing architectures resulting from a Pareto-front analysis?
    The Pareto-optimal solutions are represented by those which generate high utility to science at low cost.

The ultimate goal of the project was to develop a model that would take as inputs the assumptions, enumerate the architectural decisions, and develop a tradespace characterized by the selected trade metrics. The model would also determine how requirements affect architectural choices and examine the interactions between the different subsystems of the LTA. The following sections will illustrate the main steps taken during this process, leaving an exhaustive description of all their details to the dedicated sections of the present report.

1.1 Stakeholder Analysis

The following groups have been interested in similar architectural trade studies and were our points of contact throughout the project:

- NASA Goddard Space Flight Center (GSFC)
- NASA Headquarters (HQ)
- The Jet Propulsion Laboratory (JPL)
- The Space Telescope Science Institute (STScI)
- ITT (formerly Kodak)
- MIT
- Skoltech

Such a diverse set of stakeholders provided a broad range of perspectives on the key assumptions and technical requirements needed to define our architectures. They were asked questions related to mission goals, budget and cost models, mirror and detector technologies, data management, launch vehicle options, and inclusion of other potential stakeholders. All this information became the basis for the enumeration and downselection of our architectural decisions.

1.2 Technical Requirements and Assumptions

The technical requirements for our telescope architectures are derived directly from NASA's Advanced-Technology Large-Aperture Space Telescope (ATLAST) concept. The decision to use ATLAST as a starting point was made because it presented several similarities with the case discussed in this report. In particular, ATLAST is a concept for a space-based optical telescope with a 16.8-meter-diameter primary mirror meant to achieve the scientific objectives discussed above. This was a choice of the MIT team, who remains aware that other similar concepts were explored in the past.

Assumptions used in the model were derived from three main areas: the results of the stakeholder analysis, the requirements for ATLAST, and the need to keep the scope of the tradespace analysis limited to what can be achieved within the time frame of a one-semester graduate course. The assumptions provided a clear definition of the scope of the problem, which made the process of enumerating the various architectures more efficient and manageable form a computational perspective. The assumptions are summarized in Table I.

Table I: Assumptions derived from the ATLAST requirements, stakeholder analysis, and model complexity reduction

ATLAST requirements	16.8-m segmented primary mirror
	On-orbit assembly
	Operation at Sun-Earth Lagrangian Point 2
	Launch in 2028
	Technology at TRL 6 by 2020
Stakeholder analysis	40-year lifetime
	Serviceability required
	Implementation of a Federated Satellite System (FSS)
Model complexity reduction	Scheduled servicing
	No mirror replacement
	Included coronagraph

1.3 Architectural Decisions

In order to enumerate all possible architectures, a total of seven architectural decisions were selected. They are described below.

1.3.1 Communications Architecture

Data gathered by the LTA will need to be transferred to Earth for processing and utilization by the scientific community. In addition, specific commands may be have to be sent to the LTA in order for it to accomplish correction maneuvers or accomplish certain tasks. Efficient communications systems are thus essential to mission success and will have to maintain optimal communications quality and high data volume rates within cost constraints. Among several options, the following architectures were selected:

- Direct radio using either the Track and Data Relay Satellite System (TDRSSS) or the Deep Space Network (DSN)
- Laser communications
- Federated Satellite System (FSS) – exploiting the potential of underutilized space commodities by trading and sharing previously inefficiently allocated and unused resource commodities that are available in space assets at any given time

1.3.2 Modularity

It is the level at which components are grouped into physically separate, easily replaced modules with simple interfaces, from level 1 (no modularity) to level 7 (all instruments bus components divided into separate modules). It is important to note that the scientific instruments and engineering components are modularized separately, and therefore the modularity level does not correspond directly to the number of modules. A more complete description of the modularity architectural decision is provided in the body of this report.

1.3.3 Location of Servicing

All servicing is assumed to be robotic and four different locations were identified: Sun-Earth L2 (SE-L2), Earth-Moon L2 (EM-L2), Earth-Moon L1 Orbit Trajectory Used for Servicing

(LOTUS), and Low Earth Orbit (LEO). Each location of servicing has its own challenges affecting ∆V requirements, propellant mass, launch cost, latency of communications, and total downtime for servicing.

1.3.4 Frequency of Servicing

This indicates a scheduled evaluation for replacement or improvement of failed parts or instruments every 3, 5, or 10 years.

1.3.5 Assembly and Servicing Technique

Three methods for assembling and servicing the LTA were identified:

- Self-assembly using self-deployment mechanisms and robotic arms (e.g., JWST)
- Independent tugs or tenders (e.g., DARPA Phoenix Project)
- Formation flying (e.g., SWARM robotics)

1.3.6 Segmentation of Primary Mirror

It represents the characterizing permutations of how the primary mirror could be segmented for launch packing efficiency and ease of on-orbit operations.

1.3.7 Primary Mirror Segment Support Method

The precision of the shape of the primary mirror plays a critical role in obtaining high-resolution images from a space-borne telescope. Given its large diameter, the mirror cannot be thick; therefore, a back-structure made of trusses or ribs needs to be employed to maintain the precise shape of each mirror segment, as well as its positioning with respect to the other surrounding segments. Three methods were chosen to support this function:

- **Surface-normal**: a rigid support of mirror segments using backplane structure
- **Surface-parallel**: relative positioning of mirror segments without backplane structure
- **Hybrid**: a combination of both surface-normal and surface-parallel actuation

1.4 Trade Metrics

The above architectures were evaluated against each other by means of four system-level trade metrics, which allow quantifying the variations in cost, risk, and performance among the different architectures.

1.4.1 Cost

It is the lifecycle cost of the designed telescope. It includes flight system development (based on Stahl 2005 paper, the Unmanned Space vehicle Cost Model 8th edition - USCM8, and NASA Instrument Cost Model - NICM), launch (based on historical and projected launch vehicle costs), assembly, and servicing (Baldesarra 2007).

1.4.2 Utility to Science

Utility to science reflects the lifecycle science output of the telescope. It is defined as the discovery efficiency of each individual instrument integrated over instrument lifetime

(Baldesarra 2007). Instruments are assumed to gain utility with time and the telescope utility to science will increase as more advanced instruments are added.

1.4.3 Failed Downtime

The failed downtime is defined as the time during which no science can be done due to the failure of a component, and thus is a measure of the technical risk involved in the mission. Although downtime will also occur during the Assembly/Transit Phase and Servicing Phase of operations, this downtime is a part of normal telescope operations and thus is not a measure of the risk of a particular architecture.

1.4.4 Servicing Margin

It is a measure of the ease with which the telescope can be serviced. Serviceability is reported as a cost margin (the difference between the lifecycle cost of a repair and a replacement case mission architecture) per kilogram serviced over mission lifetime (Baldesarra 2007). Subsystem-level metrics were also developed to evaluate variations of each of the subsystems the telescope is composed of for all the different architectures. Complexity, mass, power, volume, and lifetime are metrics common to all subsystems; however, metrics specific to each subsystem were also identified and will be discussed more in detail in this report.

1.5 Model Structure and Results

In order to enumerate and characterize telescope architectures within the tradespace, a MATLAB code was developed to take inputs for architectural decisions and parameters based upon assumptions, generate a telescope architecture, simulate that architecture over the entire lifecycle, and characterize the architecture using the trade metrics described above. This code consists of three primary sections: the Architecture Generator, the Lifecycle Simulator, and the Trade Metric Characterizer.

The Architecture Generator consists of nine sub-functions, which map to nine systems within space telescope design (Optics, Communications, ADCS, Avionics, Propulsion, Power, Thermal, Structures, and Systems). The code executes these sub-functions in order, and uses the architectural decisions to generate a telescope architecture consisting of a set of components from a given component database. The architecture indicates which components are used, how many of them are present, and how they are grouped into modules; the component database supplies data such as component mass and Mean Time Between Failures (MTBF).

The Lifecycle Simulator performs a simulation of telescope operations over the assumed lifetime of 40 years, from launch to decommissioning. This simulation models the week-by-week operation of the telescope, including the Assembly, Science Gathering, and Servicing operational phases. During operations, the utility to science of the telescope is calculated for each time step and a random number generator is used along with MTBF data and operational time of telescope components to simulate random failures within the component set. When a time step corresponding to a scheduled servicing mission is reached, servicing is performed. This involves upgrading instruments and replacing modules as needed as well as calculating the serviced mass and servicing downtime. Scientific operations only resume once the servicing downtime is complete; there is no utility to science during servicing. In order to account for the stochastic nature of the random component failures, this simulation is repeated 10 times and the results are

averaged for each architecture. The outputs of the simulation are a time vector of utility to science and the amount of mass serviced during each servicing mission.

Finally, the Trade Metric Characterizer takes the outputs of the Lifecycle Simulator as well as characteristics of the generated architecture and uses them to calculate the four primary trade metrics: Cost, Utility to Science, Serviceability, and Risk. For each architecture, these results (and other metrics of interest) are saved with the architectural vector for later identification. The code is executed for every combination of the architectural decisions in order to enumerate the entire tradespace, and the results are plotted for analysis.

Discussion of Results

Results generated by the model illustrate several dependencies and trends among metrics. It will be seen that utility to science mainly depends on both servicing frequency and servicing location while upgrading the instruments often and minimizing the failed downtime. Cost is instead mostly affected by modularity level and servicing frequency with architectures requiring a large serviced mass being most expensive. Servicing frequency will be shown to have the largest effects on failed downtime since architectures with infrequent servicing are expected to experience more failures, which lead to lengthy downtimes. Finally, serviceability most strongly depends on modularity, servicing frequency, and assembly/servicing technique. Indeed, architectures with strong modularity which are serviced often and with cheap servicing techniques exhibit the lowest cost per unit serviced mass. A sensitivity analysis was also performed in terms of reliability threshold and mean times between failures. Results show that utility to science is the sole trade metric that is significantly affected by changes in such parameters.

The 2-D tradespace representation in Figure I illustrates the interactions between three different trade metrics. Points closest to the utopia point are considered "Pareto Optimal" and are highlighted in red. The utopia point has the lowest cost, highest utility to science, and highest servicing margin. Conversely, the so-called "bad" designs are characterized by high cost, low utility to science, and low servicing margin. In Figure 51I, clusters of architectural point solutions can clearly be seen on the tradespace, with a high concentration of points in the region with low utility to science and increasing cost. Clusters of larger points are seen closer towards the utopia point, reflective of designs with increasingly lower costs, higher utility to science, and higher servicing margin.

An analysis of the points directly reveals that the subset of "Pareto Optimal" solutions is dominated by the "7-1-1" architectural vector elements. "7-1-1" represents the identification numbers of the assigned alternative for the first three architectural decisions in order: the highest modularity level possible of 7, Sun-Earth L2 as the servicing location, and a servicing frequency of 3 years. A modularity level of 7 would constitute the combination of highest instrument modularity and spacecraft bus modularity. A servicing location at SE-L2 will ensure that the space telescope never experiences downtime, thereby providing the highest utility to science. A servicing frequency of 3 years also ensures that onboard instruments and component families remain in pristine operating condition throughout their mission lifecycles. These reasons thus collectively explain why solutions with the "7-1-1" architectural vector would be dominant in the "Pareto Optimal" subset closest to the utopia point.
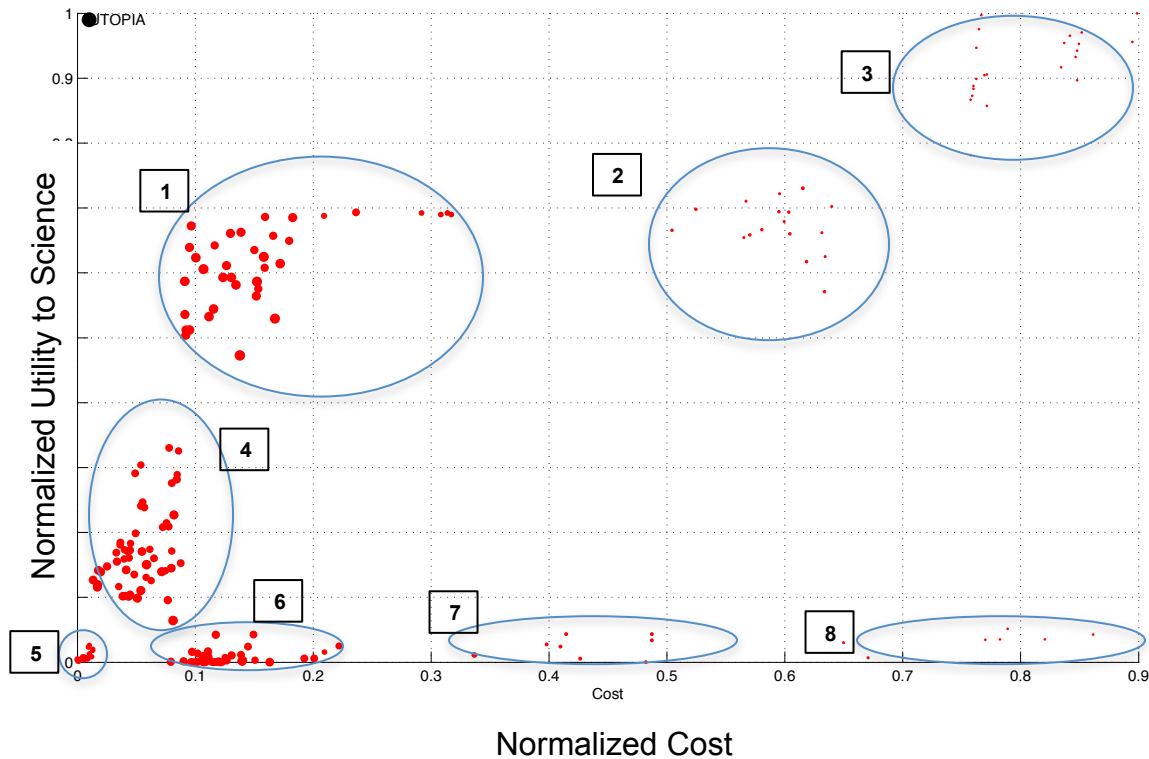
Figure I1: 2-D tradespace of "Pareto Optimal" solutions for the LTA, bounded by normalized utility to science and cost.

In Clusters 2 and 3, the dominant architectural alternatives are still the Sun-Earth L2 servicing location and a servicing frequency of once every 3 years ("X-1-1"). However, modularity is no longer as dominant in this cluster. In fact, lower levels of modularity become more prominent, and this results in increased cost due to higher launch costs required for high launch masses of instrument packages instead of individual components. As such, the solutions of Clusters 2 and 3 are located just to the right of Cluster 1 and in a region with higher normalized cost.

The architectural alternatives of Level 7 modularity, servicing location at LEO, and servicing frequency of one every 10 years dominate the solutions in Cluster 4 ("7-3-3"). Modularity Level 4 is also prominent, thus accounting for the presence of "4-3-3" solutions amongst the majority of "7-3-3" solutions. Cluster 4 is located below and to the left of Cluster 1 because servicing at LEO is a lot cheaper, but it also incurs higher downtime. Also, servicing the telescope once every 10 years means that there is a higher probability that certain instruments or components could fail without being replaced for long periods. This results in a loss of utility to science. Cluster 5 is almost similar to Cluster 4 ("7-3-3"), except that it reveals some alternatives for other architectural decisions have become more prominent. "4-3-3" points are also present in this cluster. These alternatives are laser communications architecture, surface-normal primary mirror actuation, assembly and servicing with tugs and 36 mirror segments. Cluster 6 has modularity level 7, servicing location at LEO, and servicing frequency of once every 3 years as the dominant architectural alternatives ("7-3-1"). While it might be cheaper to service at LEO, a much higher

18

frequency of servicing would result in higher total launch costs for the space telescope across its mission lifecycle. As such, the solutions in this cluster would have a higher normalized cost and they are located to the right of Clusters 4 and 5.

Finally, Clusters 7 and 8 are generally characterized by modularity levels 2 and 3, servicing location at LEO and servicing frequency of once every 3 years as the dominant architectural alternatives ("2/3-3-1"). Lower levels of modularity, near-Earth servicing location and high frequency of servicing collectively imply that large instrument packages or component families are being taken out and replaced frequently during its mission lifecycle. The high frequency of servicing drives the normalized costs up, while servicing a minimally modular spacecraft means that downtime will be a common occurrence, leading to lower utility to science. As such, these solutions are located in the region of increasing costs and low utility to science.

Through analyzing the clusters of solutions in the tradespace of "Pareto Optimal" points, it is evident that the architectural decisions of modularity, servicing location and servicing frequency have huge leverage on the spatial distribution of solutions in the utility-cost space. Higher modularity, servicing at its SE-L2 operating location, and high servicing frequency generally drive solutions towards the utopia point. Low modularity will generally drive solutions towards the high cost end while servicing at LEO or at a lower frequency will drive solutions towards the low-cost/low-utility end.

1.6 Conclusions

The analysis presented in this report will show that servicing frequency, servicing location, and modularity are the most important decisions when architecting a space telescope, while the other four architectural decisions affect the trade metrics in minor ways. In addition, the model developed will serve as a preliminary tool for the stakeholders with which it will be possible to explore the tradespace of large telescope architectures to perform unprecedented science. Several sources of uncertainty remain in the existing model, but the further steps that can be taken to improve its fidelity will be briefly described at the end of this report to allow for follow-on developments.

2 INTRODUCTION

Humanity's endeavor to further its scientific understanding of the celestial heavens has led to the creation and evolution of increasingly powerful and complex space telescopes. Space telescopes provide a view of the solar system, galaxy, and universe unobstructed by Earth's atmosphere and have profoundly changed the way people view space. In an effort to further advance space telescope capability and achieve the accompanying scientific understanding, the Massachusetts Institute of Technology (MIT), specifically, course 16.89 Space Systems Engineering, explored the tradespace of architectural enumerations encompassed within the design of an ultraviolet-optical-infrared (UVOIR) space telescope located at Sun-Earth Lagrangian Point Two (SE-L2). SE-L2 presents several advantages as an operating location for a UVOIR telescope such as a thermally stable environment and an orbit that allows the telescope to maintain a constant orientation with respect to all of the primary sources of heat and light. The main disadvantages associated with SE-L2 are caused by its relatively large distance from Earth, which marginalizes the effectiveness of real-time telerobotics because of latency and increases the cost of communications, launch, and servicing. Course 16.89 believes that, for this UVOIR application, the strengths of this operating location outweigh its weaknesses and therefore decided to explore the family of opportunities associated with SE-L2.

This course used appropriate performance and system metrics to quantify the effectiveness of the aforementioned architectures and create a Pareto front of viable architectures. Evaluating the designs along the Pareto front allowed the course to characterize and group architectures and present these group-types to stakeholders for the selection of an optimal space telescope according to stakeholder requirements and resources. This course also developed sensitivity analysis, which allowed for a greater understanding of how architectural decisions affect the performance of the satellite. Segmentation, modularity, assembly, autonomy, and servicing were key aspects of this multidimensional analysis given the 16.8-meter class size and location of the telescope. Within the respective operating environment and for a spacecraft of similar characteristics, this model will allow stakeholders to predict the long-term operational effectiveness of different space telescope architectures and capture the synergistic effects of combining various architectural decisions into a spacecraft design.

The following sections step through the aforesaid analysis and design efforts conducted in 16.89 beginning with Section III, which explicitly performs the stakeholder analysis and articulates the requirements of the mission. Section IV gives an overview of past designs and expands upon the architecture enumerations pertinent to this project, while Section V presents the methods and metrics by which those architectures will be evaluated and the system metrics which will be balanced and optimized in the creation of this space telescope. Section VI will present the model validation of this project and Section VII will discuss the results and analyses of the project. Finally, Section VIII will explore the future work opportunities of this project, while Section IX will present the conclusions and recommendations drawn from this project.

3   TELESCOPE STAKEHOLDER ANALYSIS

3.1   Stakeholder Analysis

A stakeholder analysis was performed to determine what the specific needs and desires are of relevant stakeholders at this stage of telescope design. This analysis also helped to define areas of interest for the TITANS AE trade study, as well as what applications stakeholders might seek to use this model for in the future. A set of questions on telescope performance, architecture, and cost was sent to various stakeholders around the country. Potential stakeholders with an interest in programs of this kind include:

- NASA Goddard Space Flight Center (GSFC)
- NASA Headquarters (HQ)
- The Jet Propulsion Laboratory (JPL)
- The Space Telescope Science Institute (STScI)
- ITT (formerly Kodak)
- MIT
- Skoltech
- The European Space Agency (ESA)
- Other international universities and space agencies
- The National Reconnaissance Office (NRO)
- Department of Defense (DoD)
- Other governmental organizations

The stakeholder responses were compiled into a set of assumptions and requirements. The list of stakeholders from outside MIT who responded to the questionnaire is shown in Table II. An effort was made to include a diverse set of stakeholders to represent a wide spectrum of views on the goals of our trade study. The stakeholder questions and answers are listed in Appendix B.

Table II: List of surveyed stakeholders

Stakeholder	Organization
Dan Lester	University of Texas
Lee Feinberg	NASA GSFC
Swati Mohan	JPL
Tupper Hyde	NASA HQ

The stakeholder answers to the questionnaire helped scope the model in a number of ways. The responses helped set the scientific goals of the mission, the timeframe of the mission, the size of the primary mirror, and the operating location. These responses also gave an indication of the range of opinions on different facets of our architecture. The stakeholders were adamant that the next-generation large space telescope should be a UVOIR telescope that primarily investigates exoplanets. Additionally, the stakeholders were consistent in their desire for a very serviceable telescope to achieve both a long lifetime and enable instrument replacement. There were some areas in which the stakeholders differed. The recommended primary mirror diameter ranged from 16 m to 30+ m. Also, the stakeholders disagreed on the magnitude of the available budget, ranging from < $5B to $15B. In instances where stakeholders differed, reasonable assumptions

were made that combined the stakeholder input with modeling constraints to arrive at sensible assumptions.
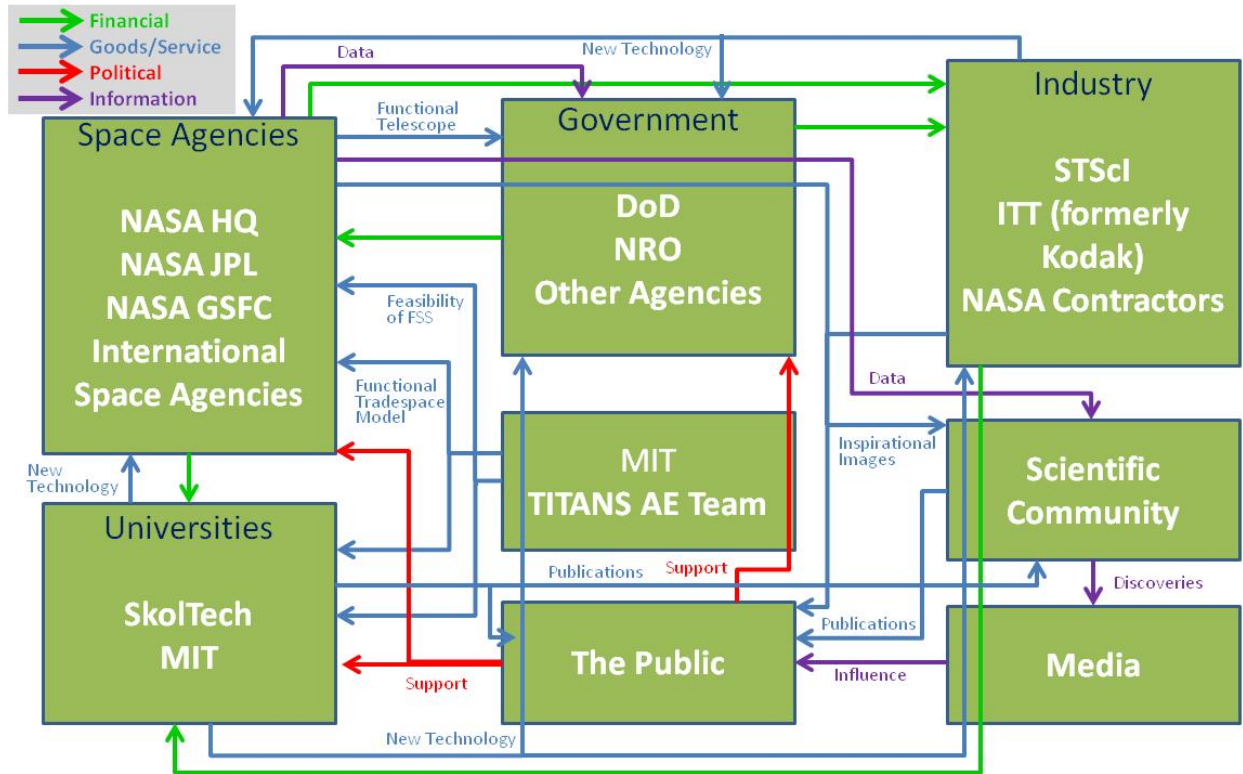
Figure 2: Map of stakeholder needs

```
A defined tradespace for a large
             space telescope        →
                                         ┌─────────────┐        →  A functional telescope
        A functioning model  →           │    NASA     │
                                         │ (HQ, Goddard,│       →  New scientific data
      First-order analysis  →            │    JPL)     │
        of design options                │             │       →  Inspirational images
   Feasibility of LTA as part  →         │             │
     of an FSS structure                 │             │
    New space technologies  →            └─────────────┘


   Feasibility of LTA as part  →         ┌─────────────┐        →  Publications
     of an FSS structure                 │   Skoltech  │        →  Research Programs
        A functioning model  →           └─────────────┘        →  New Technologies


  Images and data of exoplanets  →       ┌─────────────┐        →  Analyses/scientific
                                         │The Scientific│          advancement
                                         │  Community  │        →  Research papers and
  Observations of distant objects  →     └─────────────┘           publications


       Inspirational images  →           ┌─────────────┐        →  Renewed interest in space
                                         │ The Public  │           science and space technology
                                         └─────────────┘


                                         ┌─────────────┐        →  Publications
                                         │             │        →  New technologies
                                         │     MIT     │        →  Research Programs
               Funding  →                │             │        →  A functioning model
                                         │             │           (An adaptable tool, easily
                                         │             │           modified for future use,
                                         │             │           updatable as the project
                                         └─────────────┘           progresses)
```

Figure 3: Needs of major stakeholders, organized as by inputs and outputs

As understanding of individual stakeholder desires came into focus, a list of high-level stakeholder groups was constructed, and the basic needs of those stakeholders identified. The needs and the interactions between all stakeholders are shown in Figure 2. For the high-level groups, these needs are displayed as inputs and outputs for each group in Figure 3. Understanding and organizing these needs enabled identification of what MIT's primary outputs to stakeholders should be (see last block in Figure 3). Specific to the TITANS AE team, this identified the primary output to be a functioning model that may be used throughout future telescope development.

Of particular interest to NASA and Skoltech is including the concept of using Federated Satellite Systems (FSS) in the tradespace as major architectural decision. Using FSS, the final LTA would share processing power and access time with other satellites in its system, creating more efficient allocation of spacecraft resources. FSS use would be a sweeping paradigm shift in spacecraft technology and communications, and thus a key consideration for any new, long-term spacecraft design[1].

3.2 Requirements Definition

In order to identify requirements for the overall telescope design and the tradespace model that apply directly to the scope of this project, two stakeholder needs area were analyzed in detail – goals for data provided to the scientific community and goals for the model itself to make it functional for future use. These areas specifically have been chosen for further analysis because the TITANS AE team is fulfilling the need for a tradespace model, and the mission of the telescope will directly inform the potential telescope architectures explored by the model. Thus, the goals of the model itself and the science goals that affect model design are the needs areas that drive requirements for the TITANS AE project. The model must also incorporate the stakeholder-specified potential for FSS architectures, which will be taken into account directly as an architectural option.

3.2.1 Science Goals

To first understand the potential scientific objectives for a new large-scale space telescope, as well as which objectives are concurrent with needs of NASA and the larger scientific community, a study was conducted through review of the 2010-2020 decadal survey of astronomy and astrophysics[2]. This survey represents a clear summary of the highest priority needs in terms of data for the scientific community and science drivers behind potential NASA missions. The first priority space-based medium-scale mission in the decadal survey is a New Worlds Technology Development Program. That is, laying the groundwork and beginning to explore possible technologies for an exoplanet-imaging telescope whose critical development would take place in the 2020-2030 decade. The main goal for such a telescope mission would be to image Earth-like planets in the habitable zones of nearby stars and provide insight on their atmospheres. It would rely on knowledge obtained from the Kepler and Wide Field InfraRed Survey Telescope (WFIRST) exoplanet finders for observable target selection. Such a mission would require understanding of zodiacal light (light scattered by dust around a star) levels around potential target stars and the ability to distinguish rocky planets through this light.

The first priority large-scale space mission from this decadal survey is the WFIRST telescope, designed to measure a wide field and detect exoplanets using near-infrared detection. WFIRST would determine the range of orbital parameters that permit an Earth-like planet to exist, which will help define the optical requirements necessary to resolve exoplanets. It is now likely that a recently donated National Reconnaissance Office (NRO) telescope will be repurposed to accomplish these goals[3]. The James Webb Space Telescope (JWST), though not ranked in this decadal survey, is recognized as an important mission in the near-infrared spectrum that will investigate the origins of planetary systems and the universe. The science goals of understanding the origins of the universe, galaxies, stars, and planets are still recognized as high-priority in this survey, and will likely still be of interest in the next decade.

From the rankings in this survey, a telescope for imaging and spectroscopy of exoplanets is in line to become the first priority large-scale space mission of the 2020 decade. This would build on the current New Worlds Technology Development Program, and serve as a logical next step following the WFIRST/repurposed telescope mission. Furthermore, the description of the program discussed here fits the timeline of this project, enhancing the impression that exoplanet studies should be one of this mission's primary goals. Such a mission calls for observational capabilities in the visible-to-ultraviolet wavelength regimes. If this project is also to complement the mission of JWST, this new telescope will require the additional ability to make observations in the near-infrared spectrum and observe distant objects such as galaxies in early formation.

Based on review of the decadal survey, the main science objectives for the telescope are defined in Table III. These objectives, defined here as goals, are high-level mission requirements that apply to the final telescope design and correspond with stakeholder needs for science for this project.

Table III: List of mission goals from stakeholder analysis

Goal 1	To observe known Earth-like exoplanets in the habitable zones of their stars at UVOIR wavelengths
Goal 2	To analyze the atmospheres of these exoplanets through spectroscopy and obtain a clearer assessment of their potential to sustain life
Goal 3	To observe distant objects such as forming galaxies and solar systems in order to understand the origins and formation processes of these far-field objects

These science goals are similar to those of the Advanced Technology Large-Aperture Space Telescope (ATLAST). ATLAST was a NASA study performed several years ago that looked at the design of a large, next-generation UVOIR telescope primarily designed to determine if an exoplanet can harbor life[4]. Basing the key performance requirements on those from ATLAST means that the telescope being investigated will achieve the goals stated in Table III. These optical performance attributes are far more stringent than what has previously been achieved on Hubble and JWST. Based on stakeholder recommendations and desires, the technical requirements for the ATLAST optics are used as a baseline for this study. These hardware specific requirements are listed in Table IV.

Table IV: ATLAST key optical performance requirements[5]

Requirement Name	Minimum Requirement	Target Requirement	Science Drivers
Optical Bandwidth	0.2 – 2.5 µm	0.11 – 2.5 µm	Solar system exploration
Aperture Size	16.8 m		
Angular Resolution	6 – 12 mas	3.5 mas	
Field of View	5 arcmin		Extragalactic star formation
Pointing Stability	1 mas		Exoplanet characterization, life detection
Spectroscopic Resolution	300	120000	Extragalactic star formation
Contrast	1e+07	1e+10	Exoplanet characterization, life detection
Inner Working Angle	50 -100 mas	40 -50 mas	Exoplanet characterization, life detection
Wavefront Error	37 nm	0.07 nm	Exoplanet characterization, life detection
Wavefront Stability	10 nm	0.07 nm	Exoplanet characterization, life detection
Uninterrupted Observation Time	2 hours		
Operational Efficiency	90%		

Definitions of these technical requirements and descriptions of how they are considered in the model may be found in Appendix I.

3.2.2 Model Goals

Based on stakeholder needs for the TITANS AE model itself, the main goal of this project is to produce a tool that characterizes the tradespace for a large UVOIR telescope design, and not down-select to any single architecture. This tool must be flexible for future use and robust to major changes in the telescope architectural tradespace. Understanding this, the goals specific to the TITANS AE project are listed in Table V.

Table V: List of goals for TITANS AE model based on stakeholder analysis

Goal 1	To create a robust model that generates a fully enumerated tradespace for a large scale space telescope
Goal 2	The model shall be flexible and modular, such that it may be adapted to the telescope technical requirements desired by the user
Goal 3	The model shall provide data presented in a manner that will assist the user in determining what architecture characteristics are optimal for their needs, without down-selecting or defining an "optimal"
Goal 4	The model code shall be developed such that new trade metrics or variables may be added to suit future user needs without altering the fundamental model structure

3.3 Architectural Assumptions

To simplify the architecture development process, several assumptions have been made:

3.3.1 Operate at Sun-Earth L2

This is the location currently proposed for both JWST[6] and ATLAST[4]. Sun-Earth L2 is a benign environment where the main heat and stray light inputs are always on one side of the telescope, simplifying design. Other operational locations that were considered and could be analyzed in future studies are Low Earth Orbit (LEO), Earth-Moon L2 and Earth-trailing.

3.3.2 16.8-meter-diameter primary mirror

This size is significantly larger than anything previously flown and on par with the largest size considered for the ATLAST design[4]. A 16.8-m mirror provides unprecedented light gathering and resolution capabilities enabling new science. Future studies may look at the science capabilities of even bigger mirrors in the 20–30-m range, comparable with future ground telescope mirror sizes.

3.3.3 On-orbit assembly is necessary

A 16.8-m mirror is significantly larger than any current or planned launch vehicle fairing. Therefore, on-orbit assembly will be required, chiefly for the primary mirror. Novel folding and packing schemes were not looked into.

3.3.4 Segmented primary mirror

The primary mirror must be composed of smaller hexagonal segments, as there is no current infrastructure that would allow the construction of a 16.8-meter monolithic mirror.

3.3.5 Launch in 2028, Phase A in 2020, Technologies be TRL 6 by 2020

These dates represent the next available slot for a large astrophysics mission. JWST will be operational, freeing up funds for the next large telescope.

3.3.6 Lifetime of 40 years

Lifetime is a main driver of lifecycle science value. A 40-year lifetime will allow this telescope's capabilities to be fully utilized before a presumably more capable telescope surpasses it. Lifetime is a significant driver of cost as well. Future studies can look at the effects of varying lifetime.

3.3.7 Autonomous servicing, no human servicing

The lifetime assumption drives the need to service the telescope as no space system has ever lasted 40 years on its own. Servicing also provides an opportunity to upgrade the instrument suite and enable the science output of the telescope to continue to increase over its lifetime. Human servicing capability in 2028 and beyond is highly uncertain and the technology for robotic servicing was assumed to be available and economically advantageous by 2028.

3.3.8 Scheduled servicing

Scheduled servicing, as opposed to on-demand servicing, simplifies the design and costing process since the interval between servicing and the number of servicing missions is known.

Additionally, the long travel times to Sun-Earth L2 mean that on-demand servicing would result in large downtimes.

3.3.9   No servicing of optical surfaces, only instruments and engineering components

Serviceability will be limited to instruments and engineering components as servicing mirrors introduce alignment and contamination concerns that would place strict constraints on the servicer. Additionally, optical services are unlikely to need servicing.

3.3.10   No formation-flying coronagraph

An external, formation-flying coronagraph was proposed for ATLAST[4], but that architecture is neglected as it introduces unnecessary complexity in the form of another spacecraft design.

3.3.11   Federated Satellite System (FSS) considered as a downlink architecture

The FSS downlink architecture introduces multiple satellite-to-satellite links in the downlink chain. This pseudo-constellation allows data to be continuously transmitted from the telescope to the ground without concern for ground station line of sight. This capability potentially can reduce the mass and power of the communications and command and data handling subsystems.
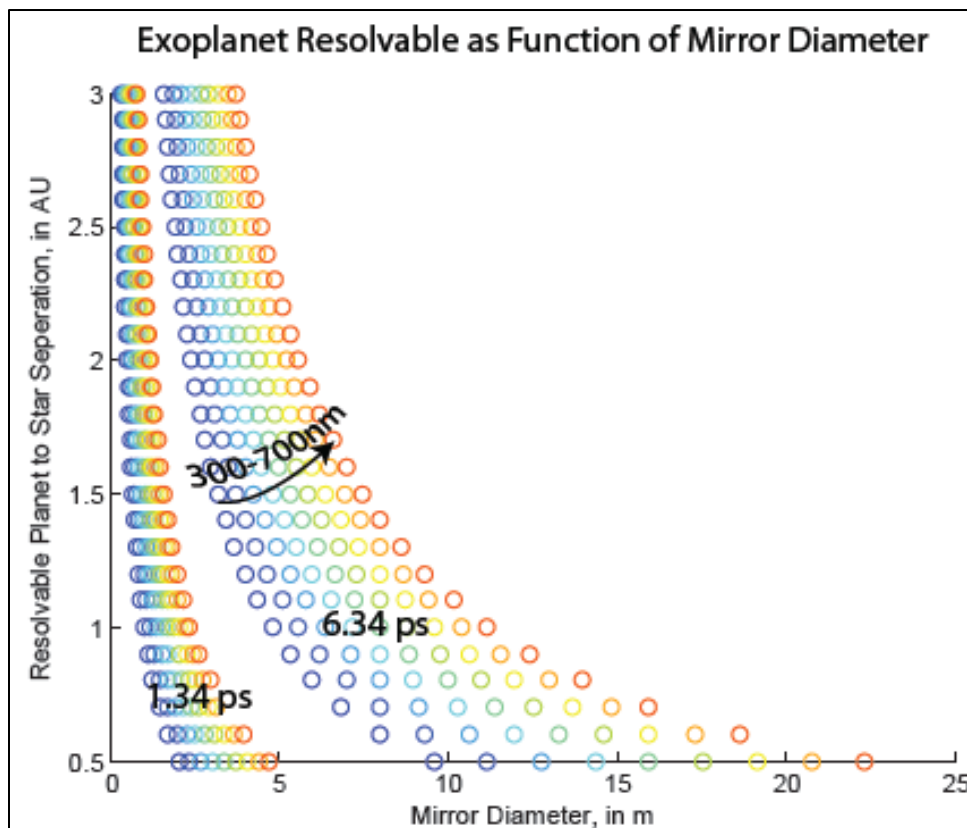
Figure 4: Resolvable exoplanets as a function of mirror diameter

4 ARCHITECTURAL ENUMERATION

4.1 Historical Analysis of Past Missions

Previous architectures can be described as a set of functions and forms developed to address various aspects of established science requirements. Functions are defined as the actions for which each system is created, and forms are the shapes, configurations, arrangements, or layouts that are implemented to achieve the system functions. The study of past forms and functions in previous architectures allowed the team to analyze past telescopes and space systems to gain insights into how different subsystems interact, how the science requirements lead to architectural decisions, and how to determine which architectural decisions were the most important to include in tradespace analysis. Consequently, the analysis of past designs facilitated the determination of a set of functions that each subsystem team needed to address. This analysis also determined sets of forms corresponding to each of these functions for each mission, since the previous missions provided a historical basis for scoping possible forms to study.

The example missions of the Hubble Space Telescope, James Webb Space Telescope, and Kepler Telescope were chosen because they span the tradespace of the current project goals and science requirements. Additionally, the Iridium Constellation was chosen to provide a basis for different communication architectures to analyze the Federated Satellite System concept. Specifically, the past missions permitted the analysis to incorporate several aspects of the different systems including: primary mirrors of various segmentation levels, wavelengths of study, and number of spacecraft in the systems. These telescopes and space systems also spanned a range of launch dates and revealed the progression in scientific and technical capabilities. The aim of the team analysis was the primary subsystem-related functions and forms for these four selected missions.

The result was a mapping of various forms to each analyzed subsystem function, which were then mapped to the architectural decisions. A list of these forms and functions for each of the historical missions can be found in Appendix J. Each subsystem team analyzed all of the historical missions to gather as much information about their respective subsystems and their implementation aboard these spacecraft as possible. In particular, each team focused on determining the methodology by which each historical mission's subsystems were designed and engineered to then determine a suite of forms and functions that historically were deemed the optimal designs and architectures. For example, the Structures and Mechanisms subsystem analyzed all four of the historical missions to determine the functional role of the Structures and Mechanisms subsystem for each mission, as well as how the structure was built for each mission and which mechanisms were selected to enable to spacecraft to perform their respective missions. Subsequently, the Structures and Mechanisms subsystem team was able to determine that the primary Structures and Mechanisms functions for the four analyzed missions were: protecting, supporting, pointing, preventing jitter, deploying, stowing, interfacing, access providing, and on-orbit assembling. These primary functions were then broken down into several additional sub-functions as required to fully define the various spacecraft architectures. The form by which each of the missions provides these functions was then listed on the row corresponding to each function. In this way, similarities between the missions could be determined. The architectural decisions arose from these functions, whereby the forms enabled the telescope to achieve the demands set forth by the architectural decisions.

4.2 Function and Form Mapping

The historical missions have several very similar functions that can be attributed to the missions' overall goal of collecting images of distant objects. With these sets of forms and functions, the teams were able to determine the most applicable functions with sample forms to be applied to the 16.8-m-total-width hexagonal-segment primary mirror telescope of the project. In addition, the forms allowed the teams to begin the determination of metrics to resolve differences between various architectural decisions as they are analyzed by an automated code. These metrics are quantitative in that they are based on relevant calculations. Additionally, the decisions themselves stem from the functions that must be performed by each subsystem, meaning that the architectural decisions made by each subsystem must be able to accomplish all of the respective functions as analyzed in the historical study. Figure 5 shows the top architectural decisions, functions, and forms for each subsystem as determined by observing which forms and functions best describe each subsystem across the different historical missions.

Figure 6 presents architectural decisions with their associated forms across all of the subsystems for the LTA project. The historical missions allowed these seven architectural decisions to be determined as those that provide a basis that spans the possible LTA architectures. These decisions, therefore, represent the most crucial design decisions that most greatly affect the overall design of the telescope. The historical examination was necessary for the LTA analysis team to both narrow the architectural decision list to these seven, as well as to populate the table with the appropriate forms for each decision. By studying the historical missions, the team was able to select forms that are applicable to the LTA while providing a set of forms that fully describe the types of methods for instantiating each of the architectural decisions. Therefore, the historical analysis proved to help scope the LTA project by defining the possible space of forms to be analyzed in the team's code.

ID	Architectural Decisions	Function	Possible Forms				
Systems 1	Location of Servicing	Provide an effectively servicable/upgradable system	Humans/Robots at Earth-Sun L2	Humans/Robots at LEO or MEO			
Systems 5	Science Instrumentation Modularity		Fully Integrated (No Servicing)	Sub-system modularity	Component modularity		
Systems 6	Optical Pathway Modularity		Fully Integrated (No Servicing)	Sub-system modularity	Component modularity		
Systems 7	Engineering Equipment Modularity		Fully Integrated (No Servicing)	Sub-system modularity	Component modularity		
Comm 1	Communications Type	Provide a communciations link with gound	DSN	Laser			
Comm 2	Relay Type		FSS	Direct			
Comm 3	Processing Architecture		Centralized,hierarchic	Centralized,Non-hierarchic	Distributed, hierarchic	Distributed, Non-hierarchic	
Propulsion 1	Propulsion Type	Maintain orbit (station keeping) and move system to new location if needed	Pulsed chemical thrusters	Constant-fire electric thruster	None		
Structures 1	Jitter Prevention Method	Prevent jitter	Electromagnetic	Fluid	Mechanical	None	
Structures 2	Primary Mirror Articulation Method	Provide mirror structural support	Surface parallel	Surface normal	Both		
Structures 3	On-orbit Assembly Technique	Assemble telescope structure	Robotic Arm(s)	Mechanical Tug(s)	Electromagnetic Tug(s)	Swarm Robotics	Deployment (unfolding)
Thermal 1	Insulation from Sun, Earth	Insulate spacecraft form Sun, Earth	No sun-shield	Sun-shield			
Thermal 2	Cooling instrument and/or detectors	Maintain instrument temperature within operational range	Purely passive thermal design	Thermo-electric cooler	Cryocooler	Cryogenic dewar	
Thermal 3	Controlling temperature of optics, bus and other subsystems	Maintain temperature of bus and subsystems within operational range	Purely passive thermal design	Active thermal components			
Science 1	Telescope/Optical Train Architecture	Collect and focus light	Fully Unified Telescope Structure	Fully Distributed Telescope Architecture	Unified Primary, Detached Secondary, Detached Science Instruments	Unified Primary, Detached Secondary, Attached Science Instruments	Hybrid (e.g., Center of Primary Mirror Fixed, Outer Segments free-flying)
Science 2	Instrument/Optical Bench Architecture	Detect light and make observations	Multiple Primary Instruments with or without Secondary Science Payloads	Single Primary Instrument and Secondary Science Payloads			
Science 3	Coronagraph	Observe and characterize Earth-like exoplanets	Occultation disk (separate)	Coronography built into optical train (Lyot-TR6)	Optical vortex coronagraph	No hardware Coronography element	

Figure 5: Reduced architectural decisions and forms for each subsystem

Architectural Decisions	Possible Alternatives						
Servicing Location	Earth-Sun L2	Earth-Moon L2	LEO	LOTUS			
Servicing Frequency	Every 3 years	Every 5 years	Every 10 years				
Modularity Level	Level 1 (no modularity)	Level 2	Level 3	Level 4	Level 5	Level 6	Level 7
Communications Architecture	Direct, DSN	Direct, Laser	TDRS	FSS (LEO)			
Primary Mirror Actuation	Surface Parallel Actuators	Surface Normal Actuators	Both Surface Normal and Parallel Actuators				
Assembly/Servicing Technique	Self-Assembling (Use of Robotic Arms with Unfolding)	Tug	Swarm Robotics/Formation Flying				
Structural segmentation of Primary Mirror	36 Segments, 1 Mirror Each for 36 Structural Segments Total	6 Symmetric Segments (6 Mirrors Each) for 6 Structural Segments Total	1 Center Segment and 6 Symmetric Segments (4 Mirrors Each) for 7 Structural Segments Total	6 Symmetric Inner Segments (3 Mirrors Each) and 6 Symmetric Outer Segments (3 Mirrors Each) for 12 Structural Segments Total	Assymetric (1 Central Segment and 2 Identical "Chord" Segments) for 3 Structural Segments Total		

Figure 6: LTA architectural decisions and forms

4.3 Architectural Decisions

4.3.1 Communications Type

Efficient communications are critical to the successful execution of space missions and architectural frameworks for space exploration. As operating a space telescope at L2 presents unprecedented challenges in maintaining optimal communications quality and high data volume rates within cost constraints, a number of existing and emergent technologies are being considered as prime candidates for the primary communications architecture. Existing technologies considered for architectural enumeration comprise radio-frequency (RF) communication platforms such as the Deep Space Network (DSN), Tracking and Data Relay Satellite System (TDRSS), and Federated Satellite Systems (FSS). An emergent technology is direct FSO (Free-Space Optical) or laser communications, which may eventually evolve to become the dominant option for space communications in future.

Radio-Frequency communications have long been the primary medium for space communications. Commonly used to provide communications support to interplanetary spacecraft missions, the DSN consists of a worldwide network of large antennas and communication facilities located in three locations spaced equally along the Earth's circumference: Goldstone, California; Madrid, Spain; and Canberra, Australia. These facilities contain extensive data processing platforms and several antennas varying from 11 to 70 meters in diameter. A distant spacecraft leveraging the DSN for communications support can thus potentially remain in contact with at least one site. With necessary infrastructure already in place and high reliability in its usage history, the DSN can provide the two-way communications link for guidance, control, telemetry, and scientific data transmission for the space telescope. Furthermore, telecommunications is continuously evolving to meet growing demands in data quality and quantity for commercial, military, and space applications. As such, using the DSN can provide flexibility to the space telescope in adapting to changing mission requirements over the system lifecycle.

Figure 7: Large ground-based antennas of the Deep Space Network[7]

The TDRSS is also a RF communications platform and it is a network of communication satellites and ground stations, where each satellite within the network is defined as a TDRSS. It has provided reliable communications support to existing spacecraft such as the Hubble Space Telescope and International Space Station, and is continuously being expanded with more planned launches of new data and relay satellites to manage increasing data rates and volumes. Also, its usage of the S-, Ku-, and Ka-bands will enable higher bandwidth communications for multi-spectral science instruments and reduce their susceptibilities to radio interference. With existing infrastructure to accommodate multiple users and achieve notable success in many state-

of-the-art applications, the TDRSS also presents an effective and practical communications architecture option for the space telescope. An existing TDRSS is the Iridium satellite constellation, which is a large group of Earth-pointing satellites providing voice and data coverage to satellite phones and other integrated transceivers over the Earth's entire surface.
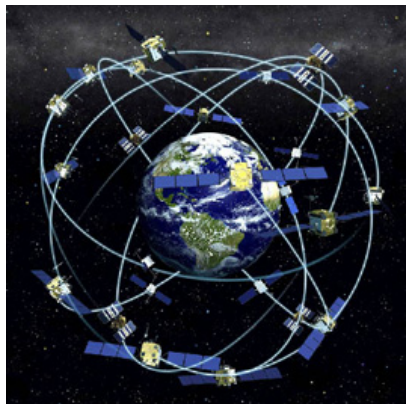
Figure 8: Iridium satellite constellation for global communications[8]

While the DSN and TDRSS offer more direct communication paths between the spacecraft and ground stations, the FSS provides additional routing and relay capabilities for the space telescope. As such, the space telescope can operate as part of an infrastructure of an FSS architectural concept. The FSS is an emergent concept that leverages opportunistic cloud computing and which can potentially "increase the sustainability, cost effectiveness, robustness, and reliability of space-based assets, and hedge demand uncertainty while creating in-orbit markets of space resources."[9] The FSS concept is based on distributed satellite systems, where spacecraft within the federated network share unused space resources such as link capacity, storage capacity and data processing time. With the availability of communications resources already in orbit, designing the space telescope as part of an FSS can significantly reduce infrastructure costs and immediately achieve compliance with existing space communication regulations.

Providing the option for data relay through the FSS can influence further design decisions of the space telescope such as the onboard data storage capacity, antenna power, system reliability and complexity. For storage capacity, direct communications via the DSN or TDRSS will require significant onboard data storage since the communications link window has been stated to be approximately 4 hours per day and it is necessary to preserve all recorded science information throughout its mission lifecycle. Being part of an FSS, however, can allow data recorded outside the link window to be transmitted via cross-links to other federated satellites for storage before rerouting back to Earth, thus reducing the need for large data storage platforms.

With the FSS, antenna power may be reduced since the only transmission destinations are nearby satellites. While compensation for path loss may be required, power overheads for the space telescope can be significantly reduced if there is no need to overcome atmospheric attenuation. Despite its possible benefits, the FSS may also pose problems to system reliability since it is a concept still in its stages of developmental infancy. Without the presence of an existing or robust FSS in operation, there exists technical and bureaucratic obstacles involved in establishing a new

FSS and this incurs significant risk and uncertainty associated with its communications performance.

Complexity of the system is also increased with the FSS since efficient routing protocols and resource scheduling among the space telescope and other satellites will be required. Satellites that are FSS suppliers, i.e., satellites that receive, process, and transmit data from FSS customers will most likely have increased power, mass, and volume requirements. Increased usage may also negatively impact the lifetime of the communications sub-system. Nonetheless, the FSS is a concept that is achievable within current technological means, and designing the space telescope as part of the FSS to leverage on existing communication capabilities is a valuable option that should be seriously considered within the design tradespace.

Figure 9: Visualization of FSS network and an individual satellite Error! Bookmark not defined.

The final option for communications architecture is direct FSO or laser communications. Laser communications recently surfaced as a prospective alternative to RF communications with the successful application of the SILEX (Semiconductor-Laser Inter-satellite Link Experiment) communications payload onboard the Artemis satellite owned by the European Space Agency (ESA).[10] With NASA's recent launch of the Laser Communications Relay Demonstration (LCRD) mission, laser communications offer potential improvements in terms of larger bandwidth, higher data capacity, lower power consumption, more compact equipment, greater security and higher immunity from electronic interference. At equivalent data rates, laser communications may also be implemented with lower mass for greater capability, which will circumvent the requirements for high antenna masses and heavy feed systems archetypal of RF communications. As such, laser communications may be feasible if there is a regular and sufficient period of time during which the space telescope remains within direct line of sight with ground stations.

Figure 10: Satellite-to-ground laser communications[11]

There is also a remote possibility where laser communications can be deployed for inter-satellite data relay similar to FSS operations. Optical communications offer the potential of operating at unprecedentedly high data rates because optical frequencies allow the use of very narrow transmit beams, which can produce high received signal levels with comparatively small antenna packages[12].

However, infrastructures for relay-centric laser communications are currently under-developed. A general concern for laser communications would be its reliability and usage history as compared to RF communications. While laser communications have been validated for terrestrial systems, near-Earth and deep space applications are still in their infancy stages. For relay-centric laser communications to be possible, other laser-based satellites must first be deployed before a laser-based space telescope can begin providing value to stakeholders. As such, it is unlikely that current knowledge and infrastructure available during the early-phase design timeframe of the space telescope will enable relay-centric laser communications to become a worthwhile option. Therefore, only direct and not relay-based laser communications architecture will be considered within the design tradespace.

With differing performance specifications, complexity, implementation costs and scope of application, the selection of DSN, TDRSS, FSS or direct laser as the primary communications system will be an imperative architectural decision in the design of the space telescope. As the cost and complexity of integrating, launching, and deploying a communication system is contingent upon the form and capability, the choice of communication systems will be a key architectural design driver.

4.3.2 Modularity

The modularity of the telescope – defined as the extent to which components are grouped into physically separate, easily replaced modules with simple interfaces – plays a large role in the cost of the telescope. The number of modules impacts the cost of the telescope in two opposing ways. First, a higher number of modules will result in a higher development and launch cost due to an increased engineering effort to define and package modules as well as increased total mass and volume from module encapsulation materials and interface components. Second, a higher number of modules will result in decreased servicing costs; as the number of modules increases, the number of components per module decreases, therefore lowering the number of components that must be replaced to rectify a single component failure. Another way to consider the benefit

of increased modularity would be to think of wasted component time – if a single component within a module fails that component must be replaced, and therefore functional components within that module will also be replaced, even though they have not failed. As the number of components in a module decreases, the amount of useful component time that is lost due to a module replacement after a single component failure also decreases, thus it is more cost-effective for servicing to have more modules. This cost-effectiveness is magnified if modules are created by combining items with similar failure rates and will be discussed later. The combination of these two effects – low development/launch costs and high servicing costs for a small number of modules, high development/launch costs and low servicing costs for a large number of modules – is expected to produce a lifecycle cost curve with high costs at either end of the spectrum and low lifecycle costs at an intermediate number of modules. This trend is depicted notionally in Figure 11. It is important to note that this figure is not based upon any data; it was simply created to illustrate the trends in development/launch, servicing, and lifecycle costs with regard to the number of modules and to enable this discussion of the trade between the number of modules and lifecycle cost.
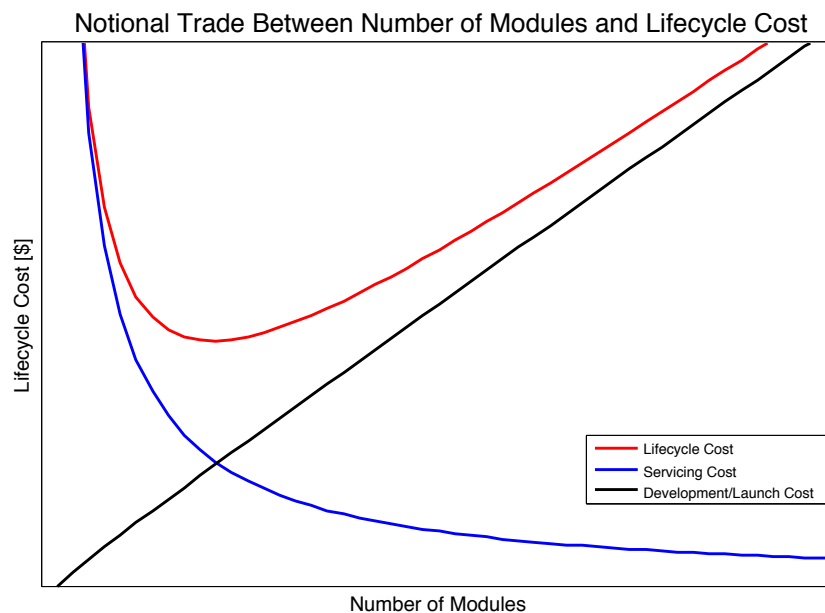
Figure 11: Notional trade between the number of modules in a satellite and the lifecycle cost (red), which is the sum of the costs incurred during the servicing (blue) and the development and launch phases. For the purposes of this analysis, all other factors in cost are assumed to be held constant.

The motivation behind the use of modules in telescope design is to enable servicing, where servicing is defined for our purposes as the action of removing one module and replacing it with another, newer one. Servicing serves two purposes. First, servicing missions can replace failed or unreliable components within the telescope to allow continued operation and extend mission lifetime. This includes the replenishment of consumables such as coolant or fuel. Second, servicing allows for component or instrument upgrades over the mission lifetime. This second purpose is of particular importance to scientific missions, since it allows space telescopes to take advantage of the advancement of instrument technology on Earth[14]. Instrument discovery efficiency increases over time, following a power law described in Baldesarra 2007[13]; servicing

gives space telescopes the capability to replace older instruments with newer ones that have higher discovery efficiencies. In this way, each servicing mission that upgrades an instrument will increase the overall utility to science of the telescope.

In order to capture these two separate purposes of servicing as they affect modularity decisions, the science instruments (the "instrument package") are considered separately from the engineering components (the "spacecraft bus"). This is accomplished by defining a modularity breakdown tree, as shown in Figure 12. In this tree, the overall telescope (top level) is broken down into three branches representing three sections of the telescope: Permanent Infrastructure, which contains telescope components that are not expected to fail within the 40-year lifetime of the telescope, such as the primary mirror and the structural backbone; Instrument package, which contains the scientific instruments; and Spacecraft Bus, which contains the engineering components required to enable the telescope's mission. Gray boxes indicate items that cannot be serviced without replacing the entire telescope.
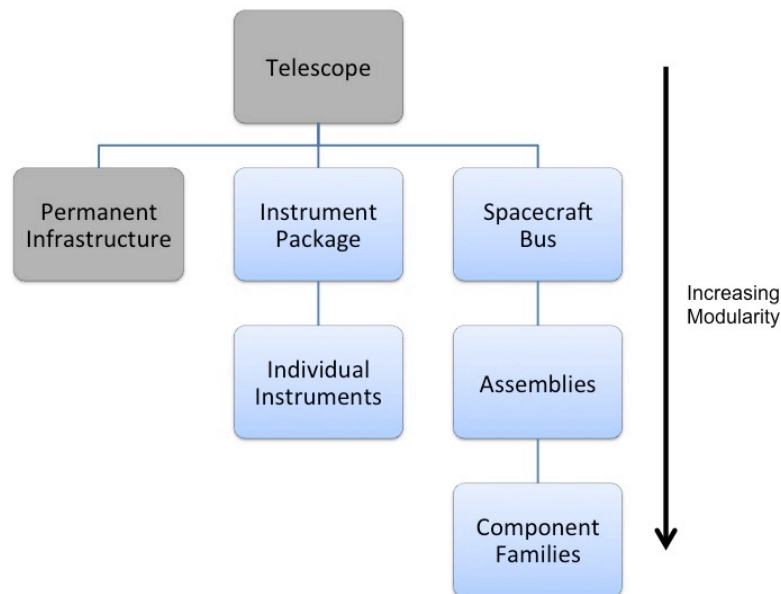
Figure 12: Modularity breakdown tree. This diagram defines the divisions within the telescope that are used to separate components before they are grouped into modules. Each branch of the tree can be modularized at different levels; the number of modules produced increases as one moves further down the branches. Gray boxes indicate permanent infrastructure that cannot be replaced without replacement of the full satellite; this includes components that are expected not to fail, such as the primary mirror and the structural backbone of the telescope.

The Instrument Package and Spacecraft Bus can both independently be broken down further. The second level of Instrument Package modularity involves the separation of individual instruments into their own independent modules. The second level of Spacecraft Bus modularity involves the grouping of components into assemblies for module encapsulation; the third level of Spacecraft Bus modularity involves the grouping of components into component families for encapsulation, meaning that multiple instances of the same component are grouped into the same module. For

the second level of Spacecraft Bus modularity, assemblies (which are encapsulated to create modules) are defined by grouping components within the architecture according to Design Structure Matrix (DSM) connections and Mean Time Between Failures (MTBF) values. In addition, the assembly/servicing technique informs module definitions – a self-assembling architecture adds a robotic arm for every ten modules, and all architectures include Universal Docking Ports (UDPs) in each module except for formation flying architectures, which have electromagnetic (EM) coils (these decisions are described further in the Assembly/Servicing Technique section). Where possible, components with similar MTBF values are grouped in the same module; this is to take advantage of the effect described in the first paragraph of this section. By grouping components with similar MTBF values, the components within a module are projected to fail at approximately the same time. Therefore, when one component fails, it is likely that the other components within that module are near failure and the amount of useful component time lost when a module is replaced is minimized. The full enumeration of all combinations of the levels of each branch of the tree generate 7 discrete modularity levels, described in Table VI. It is important to note that as a result of the separation of the modularity of the instrument package and the modularity of the spacecraft bus, the magnitude of the modularity trade metric does *not* correspond to the number of modules in the telescope. The modularity levels are labeled 1 through 7 simply for identification purposes. The number of modules at a given modularity level may fluctuate depending upon other architectural decisions, but the number of modules in a given architecture are saved for analysis later.

Table VI: Description of the 7 levels of the modularity architectural decision

Modularity Level	Description
1	Full Telescope (No Modularity)
2	Permanent Infrastructure Instrument Package Spacecraft Bus
3	Permanent Infrastructure Instrument Package Spacecraft Bus Assemblies
4	Permanent Infrastructure Instrument Package Spacecraft Bus Component Families
5	Permanent Infrastructure Individual Instruments Spacecraft Bus
6	Permanent Infrastructure Individual Instruments Spacecraft Bus Assemblies
7	Permanent Infrastructure Individual Instruments Spacecraft Bus Component Families

4.3.3 Location of Servicing

The telescope towards which this analysis is directed represents a substantial investment and is expected to provide significant scientific return for a lifetime of approximately 40 years. Since the probability of an event resulting in complete or partial loss of scientific capability increases significantly as time goes on (as illustrated by data from the Hubble Space Telescope, Figure 13) a 40-year lifetime strongly implies the need for servicing in order to repair and replace components[14]. In addition, servicing allows the telescope to maintain scientific relevance by upgrading instruments to take advantage of advancements in instrument technology.
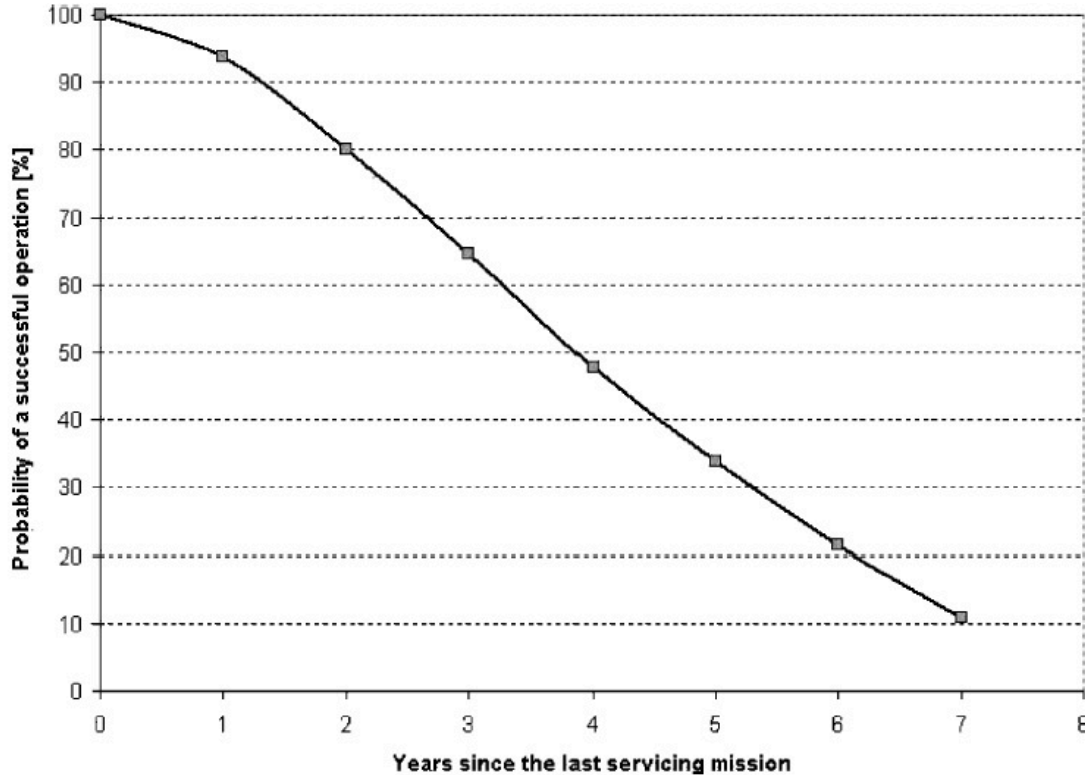
Figure 13: Reliability of the Hubble Space Telescope as a function of time since last servicing mission. Note the significant decline in reliability as time goes on[15].

As mentioned previously, all servicing is assumed to be robotic. Four servicing locations have been identified: Sun-Earth L2 (in-situ servicing), Earth-Moon L2, L1 Orbit Trajectory Used for Servicing (LOTUS – see Figure 14), and Low Earth Orbit. Each servicing location has a different ΔV requirement to move the telescope into place for servicing operations, which incurs a launch cost from propellant mass. This launch cost, associated with the telescope itself, is higher for servicing locations closer to Earth, as the telescope must travel farther on its own. However, the launch cost for servicing (the cost to launch replacement parts) will decrease as the servicing location moves closer to Earth. For this model, the servicers are assumed to launch on a schedule so that they arrive at the servicing location; therefore, the transit time of the telescope must be included in the calculation of total servicing downtime but not the transit time of the servicers. Since transit time is time during which science cannot be done, the telescope architectures with longer transit downtimes due to moving to and from the servicing location are expected to exhibit a lower utility to science. In summary, the location of servicing primarily

affects the cost of the telescope itself via propellant mass, the launch cost of replacement parts during servicing, and the overall downtime and utility to science of the telescope.
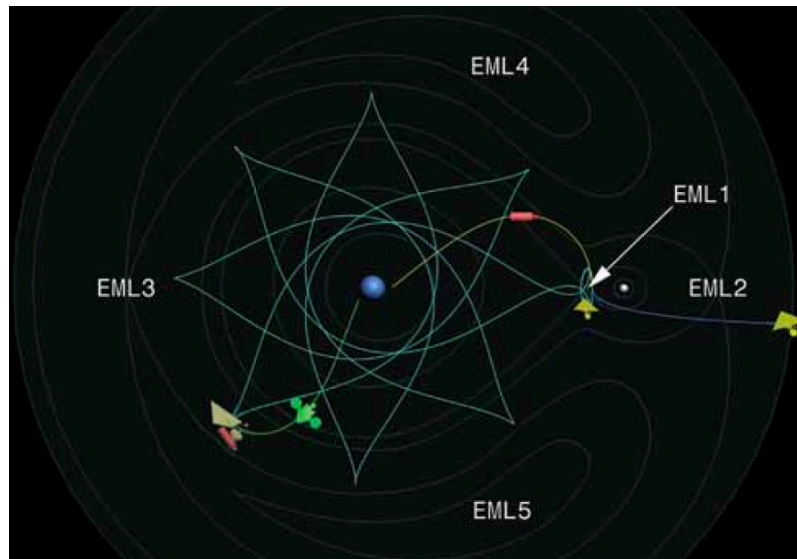
Figure 14: L1 Orbit Trajectory Used for Servicing (LOTUS), one of the orbits under consideration for servicing operations at a greater proximity to Earth. The Earth-Moon system is shown, with green lines indicating the proposed orbital paths of the telescope during servicing operations[15].

4.3.4   Frequency of Servicing

As mentioned before, the servicing of the telescope is assumed to be on a regularly scheduled basis rather than on-demand. The frequency of servicing missions is therefore an architectural decision, and servicing missions may be sent every 3, 5, or 10 years. These values were chosen to represent short, medium, and long inter-servicing periods. 3 years was selected as the minimum because this is estimated to be approximately the time required to prepare and execute a servicing mission; 10 years was selected as the maximum due to the significant increase in instrument technology expected in a 10-year period – estimated to be an approximately 25x increase in discovery efficiency[13] – as well as the increased risk of mission failure as the duration between missions increases (see Figure 13). The servicing schedule determines a minimum threshold for the MTBF of component families on the spacecraft – that is, components must be selected or set up in redundant systems such that they are expected to last at least the time between servicing missions.

The assumption of scheduled servicing as opposed to on-demand servicing was made to reduce model complexity and maintain the scope of this project at a level which could be completed in a one-semester graduate level class. Incorporation of on-demand servicing into the model would have increased model complexity in several ways. First, it would have required the implementation of some form of decision tree or decision rules analysis, which requires the definition of decision threshold values. For example, a parameter would have to be created to indicate what circumstances trigger a servicing mission. In addition, the inclusion of on-demand servicing as an option effectively triples the tradespace by adding the architectural decision of servicing architecture: on-demand, scheduled, or hybrid (on-demand or scheduled, whichever

triggers servicing first); one method to mitigate this would be to simply assume a different servicing architecture, but that would again be an assumption that must be justified. In addition, model parameters would have to be created to describe the duration of servicing mission development, and servicer transit time would need to be incorporated into the model. Currently, since servicing is scheduled, it is assumed that servicers are launched in such a way that they arrive at the servicing location at the start of scheduled servicing. Finally, there is a certain degree of risk associated with programmatic uncertainty – it is more difficult to organize and fund a servicing campaign that is not regularly scheduled – and this uncertainty would need to be factored into the mission risk analysis.

However, the differences between on-demand and scheduled servicing have been investigated for individual architectures by Baldesarra, who investigated the lifecycle effects of servicing on a particular telescope for both on-demand and scheduled servicing cases.[13] His thesis determined that on-demand servicing has the potential to increase the utility to science of a given architecture for roughly the same cost.[13] This makes sense, as on-demand servicing mitigates the problem of long periods of downtime between servicing missions in the event of a component failure. The longest possible downtime is the time it takes to prepare and launch a servicing mission and for that mission to reach the servicing location. Since downtime is time in the telescope's lifetime that has no utility to science, the more downtime a telescope has the lower its utility to science will be. The incorporation of on-demand servicing as an option within the model has the potential to raise the utility to science of certain architectures, or (if servicing architecture were incorporated as an architectural decision) to produce new families of architectures with higher utility to science, but at the cost of a more complex model. This option is further discussed in the future work section.

4.3.5   On-Orbit Assembly/Servicing Technique

Central to this investigation is the evaluation of different methods of on-orbit assembly and servicing of large space structures. At the architectural level, the methods of assembly and servicing are grouped into three families or classes: self-assembly/servicing, tugs, and formation flying. Based on the results of the study, the telescope architectures will be grouped into these classes and compared to predict which of the three techniques performs the best in terms of cost, serviceability, utility to science and risk/schedule as discussed in later sections of the paper.

The self-assembly/servicing method involves only a single spacecraft, encompassing the telescope and supporting systems. The spacecraft is "folded" into one launch vehicle and uses deployment mechanisms to unfold or assemble various appendages once on orbit. This method is therefore very similar to JWST[16] and ATLAST[17], which both rely heavily upon complex deployment schemes. Shown in Figure 15 are the deployment methods for both JWST and ATLAST. If the size of the primary mirror prohibits folding into the selected launch vehicle, this technique requires the use of robotic arms that would access and assemble mirror segments stored in a stack below the spacecraft bus. To facilitate servicing, these robotic arms would also be able to remove and discard failing component modules and install new modules upon the docking of a new cargo shipment.
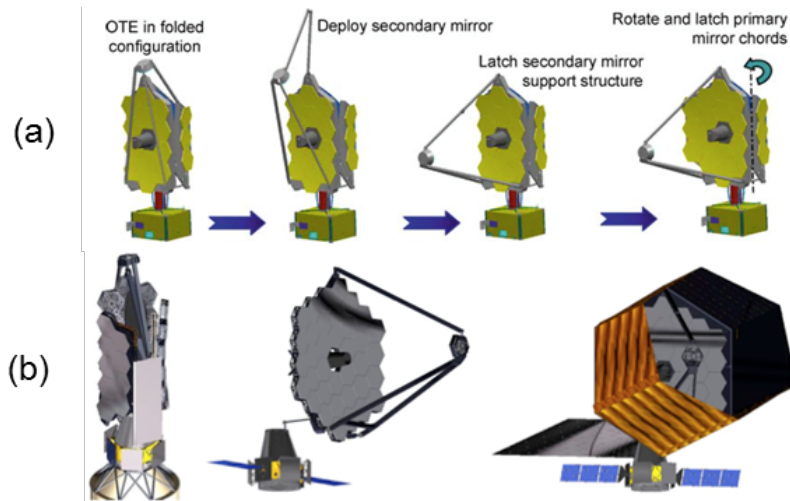
Figure 15: (a) The JWST deployment sequence (mirror only)[16] (b) The ATLAST stowed and deployed configurations[17]

The tug technique[18] involves one or multiple assembler/servicer spacecraft in addition to the main spacecraft containing the telescope and bus. This method allows for the telescope to be launched in several pieces, possibly on several smaller launch vehicles. There can be either one primary tug responsible for assembling the whole system, or several dedicated tugs, each with their own role. The tug(s) would be fully functioning spacecraft with robotic arms or docking ports. Once in orbit, the tug(s) would gather and assemble the mirror segments into the primary mirror, attach the secondary mirror and its support structure, and connect the spacecraft bus appropriately. After assembly, the tug(s) would dock to the main spacecraft and potentially add functionality in actuation and sensing. The tug(s) would also be able to service the telescope by replacing faulty components upon the arrival of new cargo. The tug(s) in this method are akin to the servicer/tender that harvests components from satellites in the geostationary graveyard orbit in DARPA's Phoenix program, shown in Figure 16[19]. Note that the cost or the complexities associated with designing the servicer/tenders is not accounted for in the system cost. This cost is regarded as too difficult to model without a baseline or previous mission to model after and is outside the scope of this model, so this aspect of the technique will not be captured in the architecture enumeration and analysis.
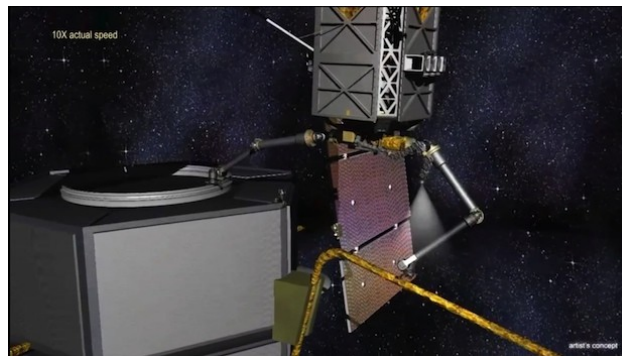
Figure 16: DARPA's Phoenix project. Artist's concept of the servicer/tender (or tug) assembling a space structure[19]

The formation flying technique requires the telescope and bus to be composed of several smaller modules that each has an attitude determination and control subsystem (ADCS). For example, the spacecraft bus, sun shield, primary mirror, secondary mirror, and science instruments would self-assemble by formation flying and then docking to form the completed telescope. This technique will employ electromagnetic formation flying that utilizes superconducting coils on each module to actuate against each other[20]. Having non-contacting servicing and assembly provides added autonomy and flexibility, but will also require stiffer requirements on individual modules. Using the electromagnetic option also removes the need for a propulsion system and fuel in each and every module, as all that is needed is the electromagnetic coils. With this technique, the individual modules would be able to be replaced or serviced individually without impacting the rest of the system. However, if further modularization were required for consumables or short-lifetime components, the spacecraft bus would act as the servicing spacecraft and would require robotic arms. This technique is the riskiest of the options as it involves several stand-alone spacecraft, which increases the probability of a failure that requires servicing, because there are many more subsystems and components. It also uses lower technology readiness level (TRL) components to achieve electromagnetic formation flying, which are inherently riskier.

As one can see from the drastically different architectures described above, the architectural decision of the on-orbit assembly/servicing technique is necessary to include in the investigation. This decision has implications to every subsystem. The structures subsystems vary in each choice from a single, continuous structure to multiple, modular structures. The propulsion and ADCS subsystems play different roles, as do the distribution of communications and avionics. If this architectural decision were not included, the tradespace of the study would be significantly decreased.

4.3.6 Segmentation of Primary Mirror

As previously noted, the immense scale of the observatory envisioned in this study will necessitate some degree of on-orbit assembly and/or deployment to reach an operational configuration. Although the method of assembly, deployment and servicing is treated separately (architecture decision 6), some consideration of the type and configuration of components to be assembled or deployed is merited. Architectures containing a large number of independent components simplify launch considerations such as packing at the cost of increased complexity and risk in on-orbit initialization (and vice versa). Additionally, architectures may consider the degree of symmetry in the selected number of segments. Architectures with a high degree of symmetry will simplify assembly and increase reliability, but may complicate the design and/or manufacturing, particularly if bus or support functions are included within the separate segments (as opposed to located in a single primary bus segment).

The architectural trade described here is mostly clearly observable in the primary mirror element of the observatory. At one extreme, the primary mirror may be launched with the minimum number of structural components, which still permit the assembly to fit in the payload fairing. This option corresponds to a "chord segment" architecture not unlike that in use for JWST (Figure 15)[16]. At the other extreme, the number of structural components is equal to the number

of mirror segments.[*] Such a scenario envisions a higher degree of on-orbit assembly (Figure 17).[21]

(a) Initial Deployment   (b) Docking and Retraction   (c) Insertion into the assembly

(d) Repetition for all modules   (e) Completion of the assembly   (f) Operations
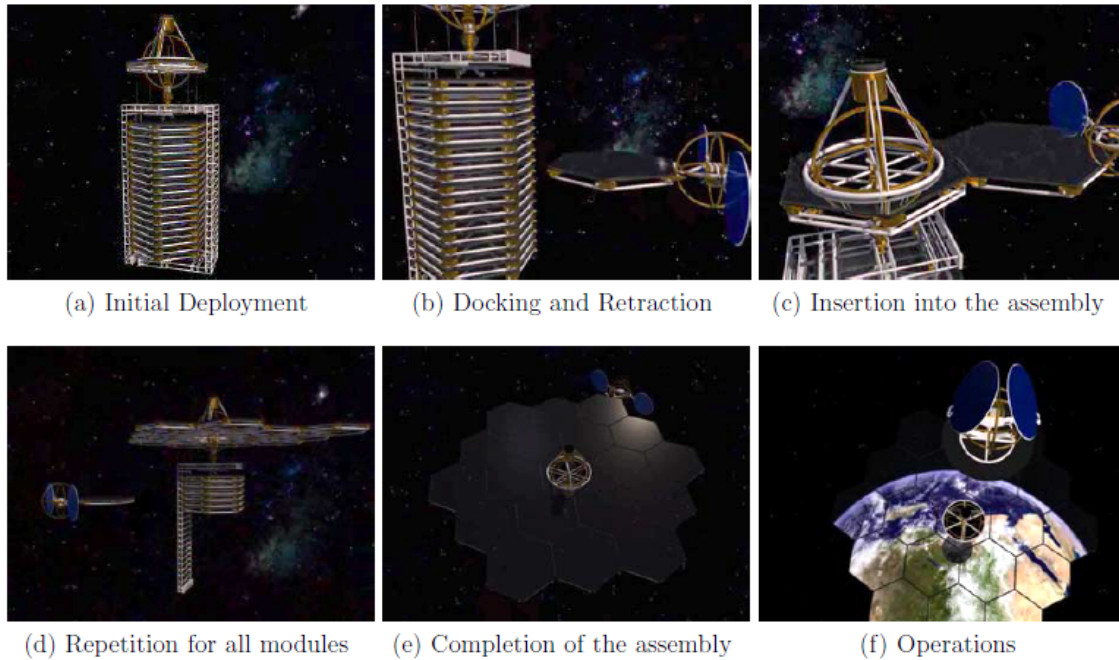
Figure 17: Notional packing and assembly scenario for a highly structurally-segmented primary-mirror architecture.[21]

Between these extremes, a variety of alternative segmentation concepts exist which have not been extensively explored in previous literature. Each offers a compromise between the launch- and packing-optimized high-segmentation approach and the on-orbit assembly- and deployment-optimized "chord segmentation" approach. For the purposes of this investigation, three 6-fold symmetric concepts were selected which provide a range of structural segment counts, dimensions, and volumes (Figure 18).

---

[*] Included in the requirements derived from the ATLAST telescope concept baseline is an assumption that three rings of 2.4 m mirrors will be used in the primary mirror architecture. See Appendix I for a detailed treatment of the ATLAST requirements and their implications. In a more general sense, the size and number of mirror segments is itself an important design consideration, but will not be addressed in the architectural trades treated here.
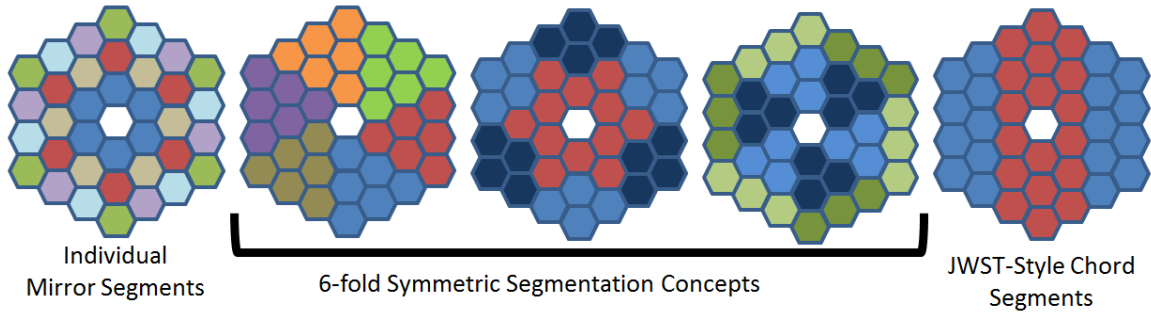
Figure 18: Architectural options selected for exploration in the primary mirror segmentation decision.

From an on-orbit assembly perspective, the complexity of the assembly operation is closely related to the total number of observatory segments to be deployed, the number of operations which must be conducted to deploy them, and the number of unique operations which must be developed to complete the assembly operation. The symmetry of the observatory segments as well as the number of segments thus heavily drive the degree of complexity of the overall assembly operation. By contrast, from a launch payload sizing and packing perspective, the dimensions and volumes of the segments are the most important factors to consider (Figure 19).
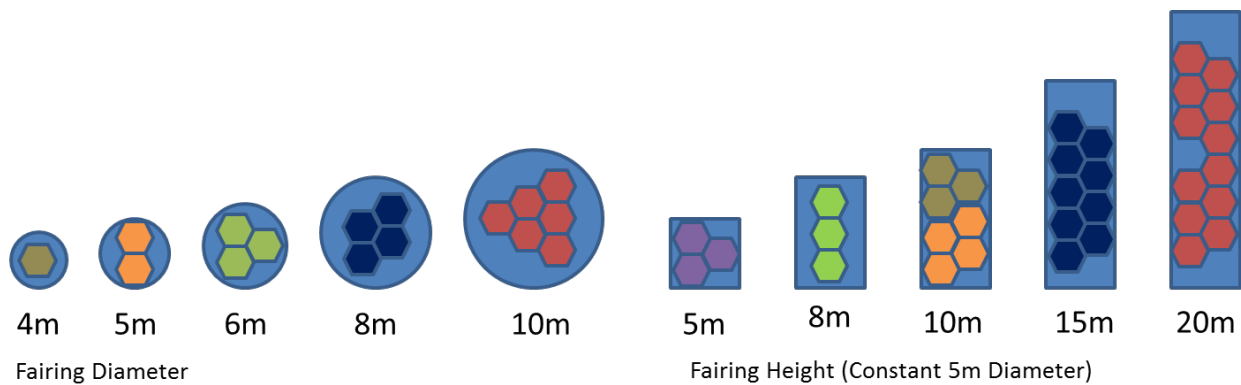
Figure 19: Notional packing of segments into payload fairings of various heights and diameters (sizes are to scale).

More efficient packing of structural segments becomes possible where individual structural segments are allowed to deform to meet the constraints of a given payload fairing. Such an approach would represent a hybrid between the segmentation/assembly and deployment models for telescope construction, where individual segments deploy, and are then assembled into the macro-structure of the observatory. Because these specific variations between segmentation and deployment tread heavily into the design space (as opposed to the architecture space under consideration here), they are not further addressed in this report.

4.3.7 Primary Mirror Segment Support Method

A critical part of obtaining high-resolution images from a space telescope is the precision of the shape of the primary mirror. While a precise shape can be maintained by making the mirror very thick, such a mirror would be too massive to launch, and in the case of a 16.8-meter mirror, too

large for any launch vehicle. Thus, other support methods have been developed. Typically, a large mirror is supported through a backstructure which contacts the back side of the mirror by pins at a discrete number of points. These pins can apply forces to the mirror to accurately articulate its shape. Because these pins are normal to the surface of the mirror, this technique is known as surface-normal actuation. The backstructure is typically made of trusses or ribs[22], as shown in Figure 20.

Figure 20: The Herschel telescope primary mirror with ribbed backstructure[23]

In the case of a segmented primary mirror, not only does each of the segments have to maintain an extremely precise shape, but each segment must also maintain a precise positioning with respect to each of the surrounding segments. Thus, a key architectural decision for the development of the next large space telescope is the primary mirror segment support method. For the purposes of this trade study, the three support methods being investigated are surface-normal, surface-parallel, and a combination of both surface-normal and surface-parallel. Each of these alternatives will be evaluated according to the metrics of utility to science, serviceability, downtime, and cost, which are described in the Trade Metrics Descriptions and Trade Metrics Calculation sections.

In the surface-normal support method, each of the mirror segments is supported directly by a backstructure that links all of the segments. This structure positions the segments relative to each other. In the surface-parallel support method, each of the segments is only relatively positioned. This positioning is done through actuators parallel to the surface of the mirror and between each of the segments. This method removes the need for the backstructure and could simplify assembly and servicing techniques; however, it does increase complexity. The final alternative is a combination of the first two. Figure 21 shows a diagram of surface-normal and surface-parallel techniques for connecting two mirror segments. The entire backstructure is not pictured in the surface-normal diagram.
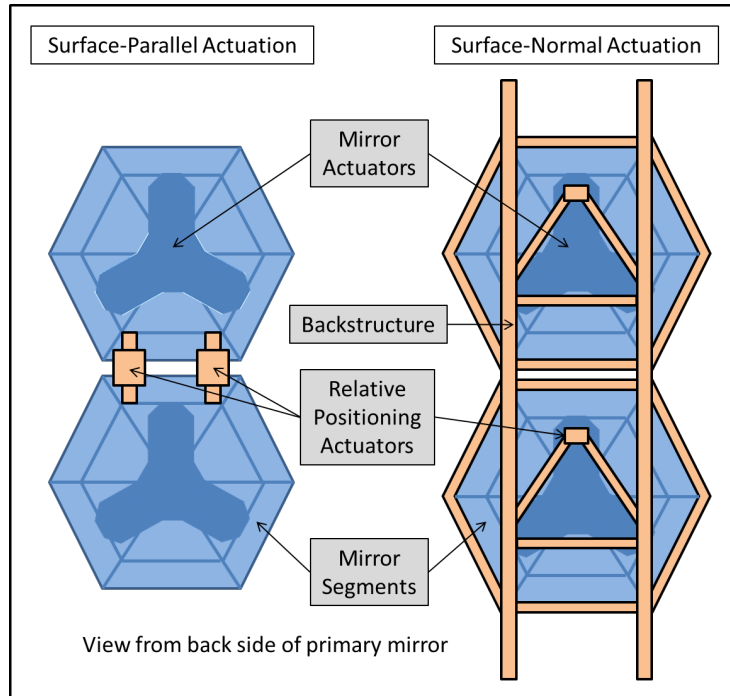
Figure 21: Surface-Parallel vs. Surface-Normal actuation techniques

This architectural decision is important to the investigation for several reasons. Each of the alternatives in this decision is needed to appropriately cover the tradespace. In the past, only surface-normal support techniques have been utilized. However, strictly surface-parallel actuation between segments is an alternative, which could significantly change the structure, assembly technique, and servicing technique of the primary mirror if determined to be more effective with respect to the metrics.

5 METRICS AND MODEL DESCRIPTION

The following sections go into detail regarding the inputs, outputs, and internal processes of the space telescope architecture model developed for this paper. First will be an overview of the layout of the model, followed by detailed descriptions of the trade metrics and the MATLAB code modules that make up the simulation environment.

5.1 Model Overview

The modeling and simulation environment of this project has been implemented in the form of MATLAB code modules that are run in ordered succession by an overarching *Main* wrapper that structures variables, defines constants, provides variable interfaces, and collects results. A detailed list of the code modules and variables tracked throughout the model can be found in Appendix A.

The first set of code modules (*Design Constants*, *Components DB and DSMs*, and *Design Vector*) are all contained within the *Main* wrapper. The *Design Constants* module sets values to important constants that are used throughout the other code modules. The *Components DB and Components DSMs* module captures component family data from Excel workbook files for use within the code. The *Design Vector* module enumerates the full modeling tradespace of architectures by expanding all of the possible combinations of the seven architectural decisions, as found in Section 4.3. Each architecture is captured within a common global variable structure (initialized in the *Main* wrapper as a *struct* data-type) known as an 'LTA' within the code, short for *Large Telescope Architecture*, which is gradually built upon as the design matures through the remaining code modules.

Once the LTAs have been enumerated, the *Main* wrapper iterates through each individual LTA and sends it through the subsystem code modules (in order: *Optics*, *Communications*, *ACS*, *Avionics*, *Propulsion*, *Power*, *Thermal*, and *Structures*), resulting in an architectural design, or a set of selected quantities of component families distributed into defined spacecraft modules. Each architectural design is then sent through the *Systems* code module, which computes the system complexity. Once this is completed, each architectural design is sent through the *Operations* code module, which performs Monte Carlo simulations of the spacecraft's mission. Finally, the *Trade Metrics* code module receives the architectural designs and quantifies desired output metrics for later use in analyzing and evaluating all of the architecture designs against each other. The specific trade metrics (utility to science, serviceability, downtime, and cost) will be discussed further in Section 5.2.

The flow of information and variables between each module can be seen in the N^2 diagram in Figure 22, where the inputs for a given code module can be found in that module's column, and the outputs of that code module can be found in the module's row. Each code module will take the specified inputs and internally use subsystem, operations, and system-level models to compute the subsystem metrics required by other modules. The internal computations of each code module are described in detail in Section 5.3.

	Design Constants	Components DB and DSMs	Design Vector	Optics	Comm	ACS	Avionics	Propulsion	Power	Thermal	Structures	Systems	Operations	Trade Metrics
Design Constants	Design Constants						reliability_req			mirror_diam, mirror_temp_range, R_earth2telescope, reliability_req, shield_efficiency, total_mass_estimate			lifetime_req	lifetime_req, rep_segments, segment_diam, unique_prescr
Components DB and DSMs		Components DB and DSMs		compPowerAvgCol, massCol, volCol	massCol					compPowerAvgCol, massCol, MTBFCol, volCol	compPowerAvgCol, compPowerPeakCol, massCol, MTBFCol, volCol, OverallDSM	DataDSM, OpticalDSM, OverallDSM, PowerDSM, StructuralDSM, ThermalDSM, TRLCol	massCol, MTBFCol	compPowerPeakCol, dimCol, massCol, MTBFCol, volCol
Design Vector			Design Vector		comm_arch		a_s_technique, comm_arch, servicing_freq	servicing_loc, servicing_freq	servicing_freq	servicing_freq	a_s_technique, comm_arch, mirror_segmentation, mirror_support, modularity_level		a_s_technique, modularity_level, servicing_freq	mirror_segmentation, modularity_level, servicing_freq, servicing_loc
Optics				Optics					optics_avg_power_req	optics_power_diss, optics_temp_range, optics_v	optics_components, optics_m, optics_v		discovery_efficiency_inst_a, discovery_efficiency_inst_b, discovery_efficiency_inst_c, discovery_efficiency_inst_d	
Comm					Comm				comm_avg_power_req, comm_peak_frequency, comm_peak_length, comm_peak_power	comm_power_diss, comm_temp_range, comm_v	comm_components, comm_m, comm_v			
ACS						ACS			acs_avg_power_req	acs_temp_range, acs_v	acs_components, acs_m, acs_v			acs_m
Avionics							Avionics		avionics_avg_power_req	avionics_power_diss, avionics_temp_range, avionics_v	avionics_components, avionics_m, avionics_v			
Propulsion								Propulsion	prop_avg_power_req	prop_power_diss, prop_temp_range, prop_v_nd	prop_components, prop_m_nd, prop_v_nd		prop_svc_time	
Power									Power	power_array_area, power_avg_power_diss, power_m, power_m_nd, power_temp_range, power_v, power_v_nd	power_components, power_m_nd, power_v_nd			
Thermal										Thermal	power_m [updated], power_v [updated], thermal_components, thermal_m, thermal_v			thermal_m
Structures											Structures	overall_components	module_definitions, overall_components	comm_m [updated], power_m [updated], overall_components, prop_v, structures_m, sys_mass, sys_vol
Systems												Systems		sys_complexity
Operations													Operations	MC_results.mean_m_serv_vec, p_util_science, time
Trade Metrics														Trade Metrics

Figure 22: N² diagram showing interactions between code modules in the MATLAB model

One very important thing to take away from the N^2 diagram is that the model described in this paper does not have feedback loops, and therefore design decisions cascade through the model without any optimization between subsystems. This is justified in that the model is only meant to perform a first-order architecture evaluation and generate all possible designs, not only those that are optimal. With this in mind, simplifying assumptions regarding computations were made where possible. It is important to note that the order of the subsystem code modules was specifically designed in order to intuitively arrange the necessary inputs and outputs of each subsystem and minimize the number of assumptions to make, thereby simplifying the code and eliminating feedback loops. The code is expandable if feedback loops are desired in the future for more detailed design.

5.2 Trade Metrics Descriptions

5.2.1 Utility to Science

Utility to science reflects the lifecycle science output of the telescope. It quantifies the expected value to the scientific community. There are several methods of quantifying an instrument's utility including productivity rate (the rate that images are taken), number of papers, or discovery efficiency (field of view multiplied by throughput).
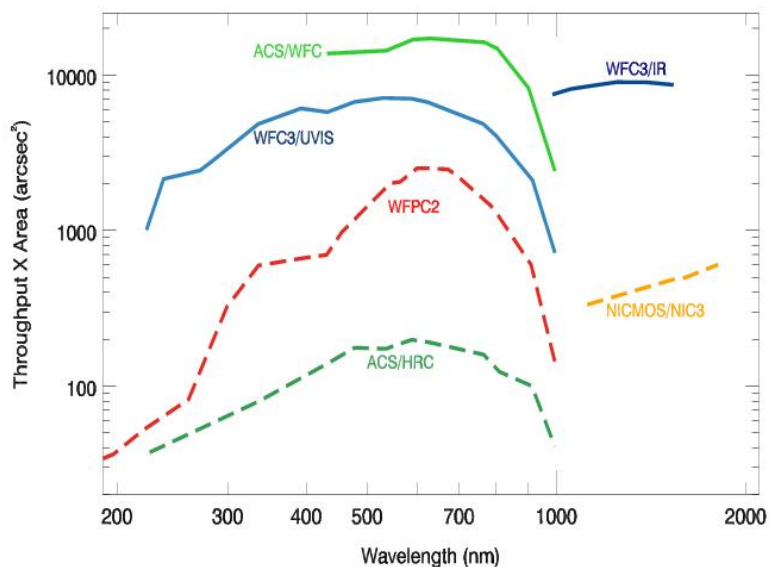
Figure 23: Discovery efficiency for selected Hubble instruments[24]

This model for science utility will use discovery efficiency with an exponential improvement over time, similar to the model in Baldessara.[13] The discovery efficiency for HST instruments is shown in Figure 23.

The two architectural decisions that most directly affect utility to science are servicing location and servicing frequency. Servicing frequency limits the maximum possible rate at which new instruments can be added to the telescope and therefore the maximum rate of increase of utility to science. Additionally, broken components that may have degraded the utility to science can only be fixed during a servicing mission, so more frequent servicing missions help limit the

downtime of the telescope. Servicing location determines the downtime per servicing mission which represents times in which it is impossible to perform science with the telescope.

In this model, utility to science can only be used to compare among telescope architectures. It cannot be used to compare with other telescopes as it has not been calibrated against existing telescopes.

5.2.2 Specific Servicing Margin

The serviceability of a telescope is defined as the ease with which telescope hardware can be changed after the start of the mission, either to replace or repair damaged components or to upgrade telescope systems that have become obsolete. This may be considered as the capability to achieve some benefit at a cost – a more serviceable architecture will have the capability to achieve more repair and upgrade benefits for a lower lifecycle cost. In order to quantify the serviceability of architectures in the tradespace, this report defines the specific servicing margin $\overline{\Delta\$_{serv}}$: the number dollars of budget margin per kilogram of serviced mass for each servicing mission. Effectively, the specific servicing margin is a measure of how much money can be spent per kilogram of replacement parts for a given servicing mission before it becomes more cost-effective to simply replace the entire satellite rather than service it.

Ideally, a model of serviceability would be able to estimate the cost of each servicing mission in order to develop an estimate of the lifecycle cost of servicing for a given architecture. However, space telescope servicing and the technology that supports it are relatively new and are still subject to uncertainty that makes it difficult, if not impossible, to directly model the cost of servicing missions with confidence.[13] Portions of the cost, such as the cost of replacement component development and the launch cost for the mass of replacement components, can be modeled. However, a valid model of the cost of a robotic servicer is beyond the scope of this project due to the wide variety and technological immaturity of robotic servicing architectures. Lacking a valid servicer cost model, any attempt to include the cost of servicers in the lifecycle cost would reduce the validity of the model output. Therefore, a more creative approach must be taken to measure the serviceability of a given architecture. Specifically, a metric must be used which does not require an estimate of the cost of each servicing mission. Hence, the specific servicing margin is defined and is calculated and utilized as described below.

Baldesarra has implemented a method that avoids the estimation of servicer costs.[13] Instead of attempting to estimate the cost of servicing missions directly, the model instead calculates the lifecycle cost of each telescope architecture without including the cost of servicers (both development and launch cost). These lifecycle costs are used to compute the servicing margin, defined as the difference in lifecycle cost between the architecture and a baseline, "non-servicing" case

$$\Delta\$_{serv} = C_b - C$$

Eq. 1

where C_b is the baseline cost for a given architecture, C is a given architecture's lifecycle cost not including servicers, and $\Delta\$_{serv}$ is the servicing margin. All units are in dollars. The baseline cost for each architecture is defined as the lifecycle cost (not including servicers) of the

architecture with modularity level 1 and all other architectural decisions (servicing location, servicing frequency, communications architecture, primary mirror actuation, assembly/servicing technique, and mirror support method) the same. Thus, the only difference between a given architecture and its baseline case is the modularity level. For example, an architecture represented by the architectural vector [4 1 1 1 1 1 1] (where the first element is the modularity level) would use for its servicing margin calculation a baseline architecture with the architectural vector [1 1 1 1 1 1 1]. It is important to note that, while these baseline costs do not include the cost of the servicers – due to the uncertainty in this value described above – they do include the development and launch cost of the replacement parts, as this value can be determined with the same validity as the value of the original cost of the telescope. Thus, costs that can be confidently modeled are included in the lifecycle cost, and costs that cannot (specifically, the cost of servicers) are not.

The baseline architecture is analogous to what Baldesarra called the "replacement case"[13] With modularity level 1, at each servicing mission the only options are to replace the entire telescope or to not take any action. Replacement of the entire telescope is a cost that can be modeled with confidence, as it effectively consists of repeating the development and launch of the telescope. There is no servicer; the new telescope simply replaces the old one. Therefore, the lifecycle cost of a baseline architecture is a value which can be reported with the same degree of confidence as the initial telescope development and launch costs; there are no additional sources of uncertainty. Using this baseline value, the telescopes that are serviceable – that is, architectures with modularity levels 2 through 7 that are capable of replacing a part of the telescope without replacing the whole – can be compared to each other by calculating the servicing margin described above. The servicing margin is a measure of the amount of money that can be spent on servicing over the entire telescope lifetime before it becomes more expensive to service the telescope than to simply replace it.

However, this margin alone does not capture all aspects of servicing. Some telescope architectures may require more servicing than others, either by requiring more replacement parts or more servicing missions. Two metrics are used to capture this aspect: serviced mass and the number of servicing missions. Serviced mass is defined as the mass the modules that are replaced at each servicing mission. It is assumed for the purposes of this model that a module is replaced with another module of identical mass. For each servicing mission in the lifecycle simulation, the mass of each replaced module is known and can be used to calculate the total serviced mass in that mission. The mean of the total serviced mass across all missions is then calculated as a representative value for the amount of mass serviced in a typical mission for the architecture being analyzed. Additionally, during the lifecycle simulation the number of executed servicing missions is counted. It should be noted here that, while the mission lifetime is known and one of the architectural decisions is the frequency of servicing, it is not as accurate to simply pre-calculate the number of servicing missions that occur for a given architecture. Servicing missions only execute in the lifecycle simulation if servicing is required (i.e. if a component has failed or is below the reliability threshold, or if an instrument has become obsolete), so there is potential for one architecture to have fewer servicing missions than another even if they have the same frequency of servicing. Therefore, the number of servicing missions for a given architecture is determined in the lifecycle simulation rather than before it based upon the architectural decisions.

These three metrics – the servicing margin, the mean serviced mass, and the number of servicing missions – are combined to produce the specific servicing margin using the equation

$$\overline{\Delta\$_{serv}} = \frac{\Delta\$_{serv}}{m_{serv} \times n}$$

where $\Delta\$_{serv}$ is the servicing margin in dollars, m_{serv} is the mean serviced mass in kilograms, n is the number of servicing missions, and $\overline{\Delta\$_{serv}}$ is the specific servicing margin in dollars per kilogram per mission. A higher specific servicing margin indicates that more money is available to service for the amount of servicing which occurs; therefore architectures with higher specific servicing margins are considered more serviceable.

As previously stated, the specific servicing margin is a measure of how much money can be spent per kilogram of replacement parts in a given servicing mission before it becomes more cost-effective to replace the telescope than to service it. This can be thought of as analogous to the amount of money that can be spent on servicers, and the metric is reported with the intent of informing stakeholders and mission planners of the budget available to spend on servicing. Specific servicer architectures can be considered independently, and once the cost of a given servicer architecture is estimated the specific servicing margin metric can be used to filter the telescope architecture tradespace to only those architectures for which servicing would be cost-effective. Conversely, the specific servicing margin of a given telescope architecture could be used to set an upper bound on the cost of a servicer, and based on mission-specific data mission planners can use this metric as an aid to decide whether it is feasible to develop a servicer within that budget.

In addition, two interesting artifacts appear in this metric. The first is the fact that, by definition, telescope architectures with modularity level 1 will have a specific servicing margin of 0. This makes sense, as an architecture with modularity level 1 is the non-modular case: it cannot be serviced – it can only be replaced. Therefore, no servicing occurs on these architectures, and the entire budget is spent on non-servicing items. This is the reason that the modularity level 1 family of architectures was chosen as the servicing margin baseline. More interestingly, the definition of this metric provides for the possibility that some architectures may have a negative specific servicing margin. These architectures are those for which it is in fact more expensive to develop and launch the telescope and replacement parts than it is to simply launch a new telescope when components fail, even before servicing costs are factored in. For these architectures, it is always more cost-effective to utilize modularity level 1 and build a non-serviceable telescope which is simply replaced when components fail. In both cases, the specific servicing margin accurately reflects the serviceability of the telescope architecture.

5.2.3 Failed Downtime

The failed downtime is defined as the time during which no science can be done due to the failure of a component. Downtime will also occur during the Assembly/Transit Phase and Servicing Phase of operations, but this downtime is a part of normal telescope operations and thus is not a measure of the risk of a particular architecture. Failure of individual components or subsystems could impact the scientific operations of the telescope, degrading the utility to science of the overall system either partially or completely. Different components will have a

different magnitude of effect; the effect of component failures on utility to science and their representation in this model are described further in the Code Module Description of Operations in the Metrics and Model Description Section. Failed downtime is used as a measure of the risk of a telescope architecture using the assumption that higher risk architectures will experience more failed downtime over the course of a telescope's mission lifetime. Thus, a telescope with more failed downtime is considered a riskier telescope than one with less failed downtime. Failed downtime is reported as a fraction of total mission lifetime.

5.2.4   Cost

The final trade metric is cost. In order to allow a true comparison of the costs associated with each different architecture, the entire lifecycle should be considered. For that reason, cost will be determined in terms of various phases of the space telescope project for each architecture. The phases are flight system development, launch, and on-orbit assembly and servicing. The on-orbit assembly and servicing costs are not estimated. Instead, the costs for a baseline concept in which there is no assembly or servicing are estimated. Then, costs for each mission are estimated without the assembly or servicing costs. The difference between the baseline cost and the cost for each mission is then reported for each decision vector. It is clear that the statistically based models presented here may not provide a highly accurate estimate for the absolute cost of the each design architecture. Rather, the relative costs with respect to the baseline mission cost will be the primary consideration. The goal is to help determine which of the design architectures are more attractive from a cost standpoint rather than to provide a reliable absolute cost estimate.

5.2.4.1   *Flight System Development*

Flight system development is defined here as the design, manufacture, test, and operation of the space telescope system. Several models for flight system development currently exist, and three are being used here. These existing models will be drawn upon in estimating a cost for each architecture. Each of these existing models provides a cost estimate for a portion of the total flight system cost, therefore, the cost estimate output from each will be summed to determine the total flight system cost.

The Stahl Ground-Based Telescope Model is a parametric cost model. It predicts the cost to produce an optical telescope assembly, which consists of the primary mirror, secondary mirror, auxiliary optics, and support structure.[25] The Unmanned Spacecraft Cost Model (USCM8) was developed by Tecolote Research for the US Air Force, Space and Missile Systems Center.[26] The model provides cost-estimating relationships for non-recurring and recurring cost for large spacecraft buses, including the development, ground equipment, launch operations and orbital support, and communications payload. The non-recurring costs included are design and development, manufacturing, and test of one spacecraft, and acquisition of peculiar support equipment.[26] Recurring costs include fabrication, manufacturing, integration, assembly, and test of the spacecraft.[26] The final flight system development model is the NASA Instrument Cost Model (NICM). This model provides cost estimating relationships for several different types of instrumentation.[26]

The three cost models presented for the flight system development each capture a portion of the total cost. These models complement each other and will be summed to provide an estimate for the entire space telescope.

In addition to the architecture decisions captured by the models above, the complexity discussed in the structures subsystem metrics section will have an influence on the cost. To account for this influence, a complexity multiplier is applied to the cost estimate. This multiplier is applied to the non-recurring costs for the space telescope system bus and program overhead. These are the efforts that are directly impacted by the complexity of the design. Complexity is discussed in Section 5.3.3.9.

5.2.4.2   Launch

Launch costs will be estimated using historical launch costs as estimates for future costs from different launch vehicle providers. Launch costs are calculated for both the initial space telescope system launch and the subsequent servicing launches. The initial launch costs are determined based on the mass, volume, and largest dimension of the payload. A particular space telescope assembly must fall within the acceptable ranges for all of these characteristics for a given rocket, otherwise a larger rocket is required. Inflation will also have an effect on the dollars spent for a given launch in the time frame of the proposed space telescope system. The launch cost for the servicing missions, which take place over the 40-year life of the space telescope assembly, are discounted back to the year of launch in 2013 dollars using an assumed annual interest rate of 2.01%. A slight departure for the servicing launch costs involves the volume and largest dimension for each of the servicing payload. These values are not calculated in this model, therefore, only the masses of the service payloads are considered when calculating servicing launch costs. Each design architecture will be associated with a launcher type required as well as the number of launches required based on its mass and volume.

5.2.4.3   Assembly and Servicing

The models for each phase of the space telescope project described above are based on inputs from the subsystem modules. To avoid introducing unnecessary uncertainty into the model, the servicing and on-orbit assembly portions of the mission cost are not estimated. However, as mentioned above, the launch costs for the servicing missions as well as the cost of the replacement components deployed during servicing are being accounted for. These replacement component costs are estimated as a fraction of the original space telescope system cost allocated based on the mass fraction of those components over the mass of the entire system. For example, if 10% of the mass of a given space telescope system is to be replaced, the cost of those components are calculated as 10% of the cost of the original space telescope system.

Based on the inputs from the subsystems, the integrated cost model, composed of each of the individual cost models described above, will provide a lifecycle cost minus the cost of assembly and servicing for each architecture. These assembly and servicing costs are defined as the cost of developing, building, and deploying any object (e.g., tugs, servicer spacecraft) that are not a part of the space telescope system itself. The architectures will be compared based on the funds available for servicing by subtracting the cost of a serviceable telescope from a non-serviceable telescope which requires no assembly. For further details on the Servicing portion of the cost, see the Serviceability discussion below. The cost estimates and the remaining system metrics below can be used to evaluate each of the design architectures.

5.3 Code Module Descriptions

5.3.1 Design Structure Matrix

In order to determine the metrics such as mass, power, and volume for the telescope, two Excel documents were created: a Design Structure Matrix (DSM) and a Components Database (Components DB). These two documents, included as Appendices C through H, are read into MATLAB for the analysis of different architectures in the tradespace. The MATLAB code uses a standardized set of variables, listed in Table VII, across subsystems to capture the various metrics based on the Components DB, thereby allowing ease of use and information transfer.

Table VII: Component Family DB variable names organized by subsystem

	Average Power	Peak Power	Mass	Volume	TRL	Lifetime	Nominal Failure Probability
Structures	struct_avg_pwr	struct_peak_pwr	sruct_mass	sruct_vol	struct_trl	sruct_lifetime	sruct_p_fail
Science/Optics	Science_nominal_power	Science_peak_power	Science_mass	Science_volume	Science_trl	Science_instrument_nominal_lifetime / Science_optical_train_lifetime	Science_p_fail
Communications	comm_avg_pwr	comm_peak_pwr	comm_mass	comm_vol	comm_trl	comm_lifetime	comm_p_fail
Avionics	avionics_avg_pwr	avionics_peak_pwr	avionics_mass	avionics_vol	avionics_trl	avionics_lifetime	avionics_p_fail
Thermal	therm_avg_pwr	therm_peak_pwr	therm_mass	therm_vol	therm_trl	therm_lifetime	therm_p_fail
Propulsion	prop_avg_pwr	prop_peak_pwr	prop_mass	prop_vol	prop_trl	prop_lifetime	prop_p_fail
Power	power_avg_pwr	power_peak_pwr	power_mass	power_vol	power_trl	power_lifetime	power_p_fail

The DSM lists high-level components that will be included in the final telescope. The interfaces between these components include optical, thermal, data, power, and structural, and are enumerated in a format for ease of MATLAB utilization. The DSM is structured so that each of these interface types are listed on individual Excel sheets. The component families are listed across the first row and column to create an N^2 matrix. To accurately sum the interfaces, which are listed as a 1 for an existing interface or a 0 for no interface between two component families at the intersection of a row and column, the resulting matrix is lower triangular. To ensure that the matrix is lower triangular and remove the possibility for human error, the DSM reader MATLAB function forces any upper triangular values to become lower triangular values. The main diagonal is kept as zeros since component families do not interact with themselves, and duplication of interfaces would occur if the matrix were to be fully populated. By keeping the DSM lower triangular, each column can be summed to determine the total interfaces of each component family. Each subsystem adds their component families to the DSM. The MATLAB function sums the DSMs to create an overall interface DSM that defines whether any two components share an interface with any of the five interface types. By grouping component families by subsystem, the interaction between different subsystem component families throughout the telescope can be observed.

5.3.2 Component Family Database

The Component Family DB comprises the complete list of component families for the entire telescope that are included in the DSM. In this manner, each component family is fully described in the Component Family DB so that its interfaces can be recorded in the DSM. Specifically, the database contains for each component a best estimate for its mass, volume, cost, average power required, peak power required, design life, and nominal probability of failure. The Mean Time Between Failures (MTBF) is also computed directly in this spreadsheet based on the design life

and nominal probability of failure, as will be explained in greater detail in Section 5.3.3.8.18. Component families cannot contain specific individual components within each component family. Alternatively, the component family database contains values that are representative of the components within that particular family. In situations where widely varying properties can describe a family, that family can be broken into separate families, of which only one would be used in a particular architecture. Additionally, there are instances where one type of component may be used in widely differing roles, such as a deployment device for a solar panel versus deployment device for an antenna, or where one type of component family is used in very different places within the telescope, such as thermostatic heaters for different components. In these cases, splitting the component families into multiple sub-families allows the code to select the proper number of components for use in different modules of high modularity spacecraft architectures. The added granularity afforded by splitting component families allows for increased accuracy in the model. The DSM also reflects these component family splits, with both families' interfaces listed. Using this component family database, modularity decisions and system mass, volume, and power analyses may be conducted. Just as with the DSM, each subsystem contributes its section to the Components DB, which is kept updated as an Excel spreadsheet that is read into MATLAB each time the main code is run.

In each subsystem code module, the requirements and architectural decision vector dictate which of the component families should be used for a given architecture from the Components DB and incorporated into the architecture for analysis. These component families are recorded by each subsystem in a subsystem specific vector that is passed from module to module. This vector represents integer numbers of each component family that is incorporated into a particular architecture for each particular subsystem. Consequently, this vector is the same length as the number of rows in the Components DB and as the number of rows and columns in the DSM. The vector is used to determine many of the component centric metrics, since the resulting dot product between this component family vector with the DSM is used to determine the complexity of the system, and the dot product between this component family vector with columns in the Components DB is used to determine metrics such as power, volume, and mass. For example, the dot product of the component family vector with the mass column from the Components DB multiplies each component family mass by the number of that particular component family incorporated in the LTA. Summing the resultant provides the mass for that particular subsystem. In this manner, several metrics can be determined, as will be explained in later sections. The Structures and Mechanisms subsystem's code is run as the last subsystem code in order to perform telescope level calculations that require the sum of all components, such as the complete system mass. Consequently, the individual subsystems' values are incorporated into the Structures and Mechanisms code before being sent to the systems level analytics.

In order to determine how varying inputs to the model affects the output trade metrics, a sensitivity analysis was run. Two loops were included in the Main_Servicing.m function for conducting the sensitivity analysis, including a loop for running several cases of a MTBF multiplication factor. The MTBF multiplication factor was run at values of 0.50, 0.85, 0.90, 0.95, and 1.05 to see how varying the mean time between failures for every component family affects the outputs, since the MTBF values greatly affect how servicing missions are performed. All datasets are combined for the sensitivity analysis. The coding structure enables this sensitivity analysis by incorporating this factor in the initialization of the MTBF values, which occurs when

the Components Family DB is read into the LTA MATLAB structure array. A full description of the sensitivity analysis is discussed in Section 7.4.

5.3.3 Subsystem Modules

The code structure uses a series of subsystem modules as initial building blocks that construct the *LTA* structure of variables used to find the Trade Metrics. The following subsystem descriptions include both calculations used in Excel for the Components Data Base and MATLAB code modules. Each of the MATLAB modules is run through the *Main.m* function. Design options derived from the architectural decisions are specified in the *LTA* structure, which is fed into each of the subsystem modules in order. Each module adds to the MATLAB structure, and it is taken in by the next subsystem.

5.3.3.1 Science/Optics Subsystem Module

The Science/Optics subsystem is responsible for calculation of variables pertaining to the optical train and instrument package. The primary outputs from this module are the telescope discovery efficiency, which is found in the MATLAB code module and used for the "Utility to Science" trade metric, as well as the MTBF, power, mass, and volume estimates of the instruments, which appear in the Components Data Base using Excel. Secondary outputs that are required for other subsystem module calculations, such as power dissipation, data rate, and operational temperature range, are also generated in the MATLAB code. The assumptions made to perform the analyses from this module are as follows:

- There will be five instruments total: four optical instruments, plus fine guidance sensors (FGS)
- Mass, Power, Volume, and Temperature range of instruments is based on values for Hubble Space Telescope instruments
- All instruments have equal reliability
- Power dissipation is 20%, the standard used in spacecraft first-order estimations
- Data rate estimates are based on JWST instrument data rate
- Performance analysis used in Baldesarra, 2007[13] can be applied to this system

5.3.3.1.1 Lifetime/MTBF

Instrument lifetime has been determined based on empirical analysis of past space-based telescope instruments and instrument packages. A list was compiled of every space telescope either currently in operation, or whose total operational mission length was ever planned to last longer than ten years. This data set was selected because it encompasses historical failure rates on long-duration telescope missions, as well as data from systems with the most advanced current optical technology. Ten years was chosen as the minimum intended mission length for the data set because it is the maximum time between servicing missions considered for TITANS AE, and thus the minimum time that any given component must last for the telescope to remain in continuous operation with the least amount servicing for potential repairs. Any problem involving direct compromise of instrument function, but not loss of the entire spacecraft, was classified as a failure in this analysis, even if the actual cause was in another subsystem directly related to instrument function (i.e., thermal systems). This extension beyond actual instrument hardware failure allowed all cases of instrument loss to be recorded, and captured the possibility of shorts in instrument-specific electronics in later full-system risk analysis.

For each relevant telescope, the number of instruments and number of instrument failures over the total mission lifetime was recorded. An estimate for the probability that no instrument will have failed by end-of-life on a future long-duration telescope mission was then calculated in two ways. In the first method, an overall probability (total probability of success) was determined by tallying the total number of instrument failures and dividing it by the total number of instruments ever flown on any of the relevant missions. The second method found the average probability of no failure (average probability of success) by dividing the number of failures by the total number of instruments in each instrument package in the data set. A full summary of this process is shown in Table VIII. The more conservative of the two probability values was selected for use in MTBF calculations, as indicated by the highlighted block in the table. This value represents a first-order estimate for the reliability of a space telescope optical instrument at the end of that telescope's anticipated mission duration.

Table VIII: Calculation of probability of no instrument failure

Telescope	Number of Instruments	Number of Failures	Failure Type	Time Before Failure (years)	Mission Length/Time in orbit (years)	Probability of Success
HEAO 3	3	0			11	1
AGILE	3	0			6	1
Fermi	2	0			5	1
Granat	7	0			10	1
INTEGRAL	4	0			10	1
Swift	3	0			8	1
BeppoSAX	11	1			7	0.909091
			MECS power supply	1		
Chandra	4	0			14	1
Rossi	3	0			16	1
Suzaku	4	1			8	0.75
			thermal coolant leaked	0.1		
XMM-Newton	6	0			13	1
COROT	1	0			6	1
Hubble	15	3			23	0.8
			NICMOS thermal failure	8		
			STIS power failure	7		
			ADCS electronics issue	4		
Kepler	1	0			4	1
MOST	1	0			10	1
Herschel	3	0			4	1

Spitzer	3	0			10	1
Odin	2	0			12	1
Plank	2	0			4	1
IBEX	2	0			4.5	1
PAMELA	1	0			7	1
SAMPEX	4	0			12	1
Totals	**85**	**5**	---	---	---	---
Total Probability of Success						**0.941176**
Average Probability of Success						**0.975413**

The reliability estimate was used to determine an expected MTBF (in years) for each instrument by using the equation

$$MTBF = -t/\ln(R)$$

<div align="right">Eq. 3</div>

Where R is the estimated reliability at the end of instrument life and t is the expected lifetime in years. For the purposes of this model, t is set to 40 years. Since at this stage of development no instruments have been selected and detailed instrument characteristics remain rough approximations, each instrument is assumed to have the same reliability. As the project progresses, the trade space for the entire system design narrows, and instrument design is known, the reliability numbers for individual instruments may be changed in the Components Data Base to improve model fidelity.

This calculation was originally coded as a sub-function in the MATLAB code, but was later incorporated into the Components Data Base in Excel, and extended to the MTBF calculations for each subsystem component. Using the Components Data Base method was found to be more efficient for overall code structure and helped shorten total model runtime. If later use of this model involves modifications in which calculation in MATLAB is more efficient, the sub-function may still be found in the Optics/Science module code comments.

5.3.3.1.2 Mass, Power, Volume
Instrument mass, power, and volume were determined based on empirical analysis of past space-based telescope instruments and instrument packages.

<div align="center">

Table IX: Summary of Hubble instrument mass, power, and volume

</div>

Instrument	Type/Function	Mass (kg)	Power (Watts)	Volume (m^3)
High Speed Photometer	Photometer	300	~20	2.00
Goddard High Resolution Spectrograph	Spectrograph	~200	~20	~1.25
WFC3	Wide Field Camera	400	~80	1.78
FGS	Guidance, Astrometry	217	19	1.24
STIS	Spectrograph	374	~80	1.78
COS	Spectrograph	40	62	~1.25

Instrument	Type/Function	Mass (kg)	Power (Watts)	Volume (m³)
NICMOS	NI Camera and Spectrometer	370	~80	1.74
FOS	Camera	329	130	1.78

Based on design requirement, telescope functionality was grouped into four instrument classes. Hubble references were used to assign approximate mass, power, and volume estimates according to instrument type/function. These numbers represent a rough instrument of the instrument payload for the telescope. While the instrument packages can be serviced, none of the architectural decisions explicitly alters specific set of instruments that is selected. Future work can examine the trades involved in how the science requirements translate into a set of science instruments and the associated changes in mass, power, and volume.

Table X: Summary of instrument mass, power, and volume for TITANS AE model

Instrument	Type/Function	Mass (kg)	Power (Watts)	Volume (m³)
Instrument A	Wide Field of View, Low Spectral Resolution, NUV-VIS-VISNIR, Partially coronographic	500	90	1.25
Instrument B	Non-Imaging, Medium/High Spectral Resolution, FUV-NUV-VIS, Non coronographic	500	90	1.78
Fine Guidance Sensors	Orientation navigation	300	45	1.25
Instrument C	Imaging, Low/Medium Spectral Resolution, VISNIR-NIR-ExtNIR, coronographic	500	90	1.25
Totals	Camera	1800	315	5.5

5.3.3.1.3 Optical Performance

Because the current set of architectural decisions and assumptions hold much of the optical train design constant across the tradespace, overall optical performance will not vary substantially across the architectures under analysis. In general, optical performance is closely associated with the total collection area of the observatory primary mirror, the degree of wavefront control and stability, the degree of control over stray light entering the optical pathway and finally, the wavelength range and reflectivity permitted by the mirror coatings. By utilizing the ATLAST design requirements as a baseline, the total collection area, wavefront control parameters, and wavelength ranges were standardized across all architectures. (A detailed treatment of the ATLAST requirements and their implications can be found in Appendix I) Additionally, the selection of a James Webb-style sunshield design (based on engineering considerations) results in a uniform degree of stray light suppression performance across all architectures as well. Jitter and pointing stability do vary to a limited extent with the choice of mirror actuation and primary mirror segmentation. These are specifically addressed separately in the structures code module. As the "optics" module lies upstream from the structures module and feedback loops have been

deliberately suppressed in the code design, any implications derived from the jitter analysis are ultimately addressed in the trade metrics modules at the code terminus. As a result optical performance is initialized here as a constant modifier within the instrument performance module. A more detailed proposal for how optical performance might be addressed in future cases where architectural decisions substantially affect this metric can be found in Appendix K.

5.3.3.1.4 Data Collection/Science/Instrument Performance

Overall science output and performance is heavily dependent on the number and quality of instruments incorporated into the observatory architecture. This proposal uses the ATLAST science instrument set as a baseline for comparison and analysis (Figure 24).

Telescope	TMA Focal Plane Instruments				Cass Focal Plane Instruments		
	Vis/NIR Wide-field Imager	Vis/NIR Multi-Object Spectrograph	Vis/NIR IFU	FGS (FOV per FGS unit)	UV IFU & Spectrograph	Starlight Suppression	Exoplanet Imager & Spectrograph
8-m, 9.2-m	8x8 arcmin	4x4 arcmin	2x2 arcmin	3x3 arcmin	30 arcsec	Internal Coronagraph or Starshade Sensor	~10 arcsec
16.8-m	4x4 arcmin	3x3 arcmin	1x1 arcmin	~1x3 arcmin	15 arcsec		~10 arcsec

Figure 24: Tentative ATLAST science instruments and their FOV[27]

This instrument set was devised by the key stakeholders at NASA, who are also, by virtue of experience and access, best positioned to determine the most useful instruments from a scientific perspective for a given telescope architecture. It is reasonable therefore to assume for our purposes that this selection of instruments represents an optimal balance of resources for each scientific function (otherwise, that instrument would have been given more FOV or more of those instruments would have been added in place of another instrument). As the scope of the architecture tradespace primarily analyzes the engineering and performance – rather than scientific goals – of a 16.8-meter class telescope implementation, this assumption does not substantially alter our analysis, provided the utility is assessed in a relative and normalized fashion.

For the purposes of the TITANS AE architectural model, the functions represented in the ATLAST instrument proposal were packaged into four instrument 'boxes' for the purposes of future assembly, operations and servicing calculations. Each is initialized with a baseline utility value of 10. Accompanying these baseline utilities is an additional value – the utility degradation rate – reflecting the decay in science utility as a result of radiation damage on orbit. Historical values derived from monitoring of Hubble instruments suggest a rate of approximately 1% a year to be in the appropriate range.[28,29] These variables are later employed by the utility-to-science trade metric module to evaluate telescope performance against a variety of architectural decisions.

A more detailed proposal for how instrument performance might be addressed in future cases where architectural decisions substantially affect this metric can be found in Appendix K.

5.3.3.2 Communication Subsystem Module

5.3.3.2.1   Communication Subsystem Metrics

The communications module receives inputs from the design vector and other subsystems, i.e., Optics, and produces outputs for use by subsystems, i.e., Power, Thermal, Structures and Systems.   The majority of the communications module outputs are calculated via the Satellite Communications Design Process (described in the following section).   The communications module outputs required by the Systems module and to calculate the system metrics are calculated separately. The communications module will have the following inputs and outputs, illustrated in Figure 25.
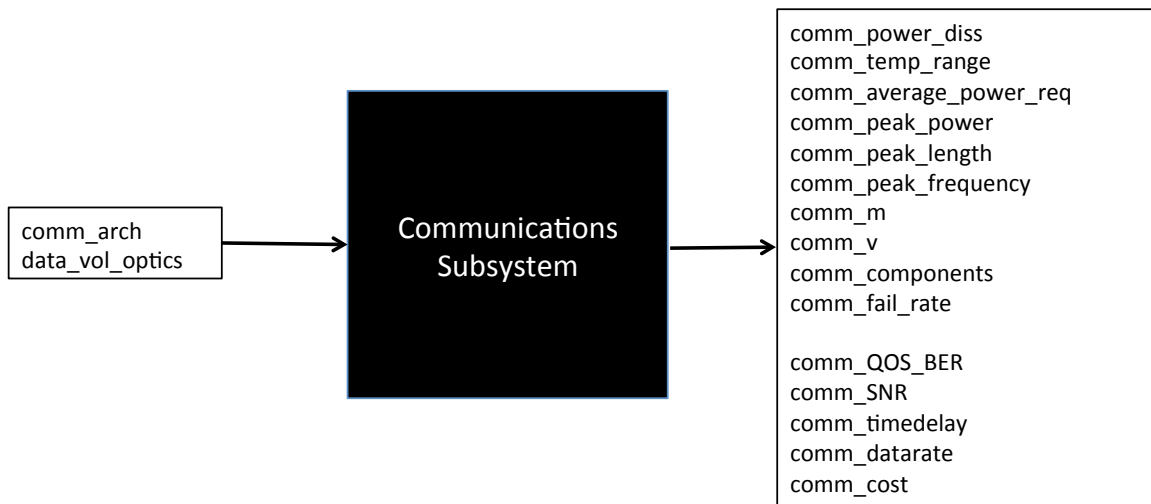
Figure 25: Communication system inputs (left) and outputs (right)

5.3.3.2.1.1 SNR (Signal to Noise Ratio)

The SNR is a basic subsystem metric for assessing communications systems and it is defined as the power ratio of the signal to background noise and it can be calculated at both the transmitting and receiving ends of a communications channel. The signal power will be equivalent to the power of the antennas onboard the space telescope and the relevant values can be tabulated for the high-gain, low-gain, and omni-directional forms after the communications architecture has been finalized. Assumptions will have to be made about the power of cosmic or galactic noise at the telescope's orbit position. High SNRs at both transmitting and receiving ends represent a stable and efficient communications channel, while low SNRs will indicate the need for higher antenna power or more electronic filters.   SNR is constrained to have a minimum performance value in the communications module but the SNR value is also used as an input to systems metrics.

5.3.3.2.1.2 BER (Bit Error Rate)

Like SNR, BER is also a basic subsystem metric for any communications system. Since digital transmission is ubiquitous in satellite communications, the BER will determine the reliability of the communications channel established as it computes the number of bits in error divided by the number of the received bits in a data stream that may be altered due to noise, interference, distortion or bit synchronization errors. This metric can be used to assess the reliability of cross-links between satellites or satellite-Earth channels characteristic of FSS and TDRSS respectively,

or that of laser and RF communications. Choosing the appropriate communications architecture or relay type and making the right design choices by selecting high-power antennas, reliable modulation schemes and error correction codes can minimize BER. Assumptions will have to be made for the parameters required in calculation.

The equation for BER is below:

$$BER \approx \frac{1}{m} erfc \left(\sqrt{\frac{E_b}{N_0}} sin \left(\frac{\pi}{M} \right) \right)$$

Eq. 4

where N_0 is the noise power spectral density, the M-ary PSK modulation scheme encodes m=2^M bits per symbol.

5.3.3.2.1.3 Power Requirements
Power requirements will be used to assess the architectural choices for the communications subsystem as there is always an operational need to regulate power consumption and power budgets may influence the choice of antenna sizes, communications relay and technology. Power will also impact other subsystems as it imposes constraints on the overall power supply and power dissipated by communications infrastructure will contribute significantly to the thermal characteristics of the space telescope. Power can implicitly be calculated through supply voltages and currents from the avionics or via other means such as the link budget equation.

5.3.3.2.1.4 Mass and Volume
Due to the considerable costs of launching a unit weight of load, mass and volume of the communications infrastructure are key considerations for determining the communications type, relay type and final design choices. RF communications require large antennas and heavy feed systems while laser communications may have more compact and lightweight equipment at the same performance level. They can be calculated through dimensions and densities of available communications infrastructure and adjustments may be made to accommodate the space telescope scenario with the appropriate assumptions justified.

5.3.3.2.1.5 Lifetime/MTBF
The predicted lifetime will be a key metric for evaluating the architectural choices, as the large amount of electrical equipment and distribution networks onboard the space telescope have to maintain a high level of reliability through the mission lifecycle. The lifetime of the communications sub-system can be predicted through calculating parameters such as probability of failure and average lifetime for a single or network of components. The communications subsystem is also assumed to be serviceable so that its predicted lifetime metrics do not necessarily have to meet or exceed the in-service lifetime of the entire system. The failure rate of the communications subsystem can thus be calculated via the multiplicative sum of communications components operating in a casual chain, and therefore variable across architectures.

5.3.3.2.1.6 Delay
Calculation of time delays in communications is vital if there are time and cost constraints for direct linkage between a spacecraft and relevant ground control stations. As space

communications entail the exchange of data over vast distances in space, communication channels established between L2 and Earth or other intermediary relay satellites are susceptible to electromagnetic interference and obstruction caused by objects in near-Earth orbits. Both architectural and design choices in communications technology, relay mechanisms and routing protocols have different measures of impact on the time delay experienced during data transmission. Typically, delay should be minimized within the constraints of cost and availability of technology so as to increase overall value and reliability of the communications system in the space telescope.

For example, to perform the delay calculations for the FSS option, the delays in uplink and downlink transmissions in the FSS system (assumed to be RF-based in this study) can be defined as functions of the distance between nodes and the processing time of each node. More specifically, the processing delays can be divided into transmission time, buffering delays, switching delays and data processing time.[30] Likewise, propagation delays can be divided into inter-satellite link delays (in-plane and cross-plane) and uplink/downlink delays with the ground station.

The number of supplier nodes in the FSS network greatly changes the delay; due to orbital alignment, the delay varies with time. For the purposes of this study, a model of the FSS constellation will be developed using documented assumptions (quantity and locations) and will be used as the baseline for communications performance. The model will be developed using Systems Tool Kit (STK).

The processing delays per node will be assumed to be uniform for all FSS suppliers and this delay will be a function of the link access time, data to be transmitted to ground and assumption on the processing speed. The processing speed of each FSS supplier node will be estimated using specification sheets of comparable satellite systems.

$$Propagation\_Delay = \frac{d}{c}$$

<div align="right">Eq. 5</div>

where *d* is distance and *c* is speed of light.

$$Processing\_Delay = \frac{Vol\_data\_ground}{Processing\_speed}$$

<div align="right">Eq. 6</div>

5.3.3.2.2 Communications Design Process

Satellite Communications Design is an iterative process that involves defining the communication mission architecture, specifying the payload architecture, performing the link analysis, designing the payload, estimating impact to key metrics and updating parameters to achieve performance that meets requirements and meets the system level constraints. The design process for the communications module will follow the steps illustrated in Figure 26.
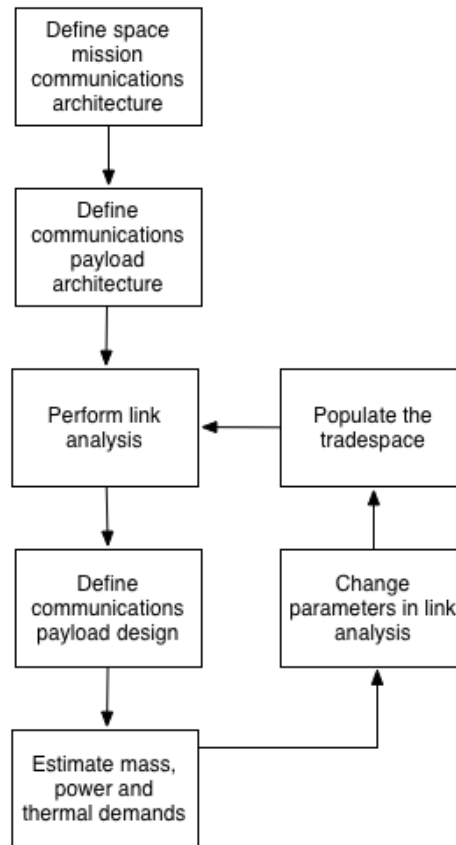
Figure 26: The communication system design and sizing process[30], adapted for the context of this class

The first two steps in the process outlined above involve making architectural decisions. One of the most important decisions for the communications module is fixed for the purposes of this study and that is the orbit and location of the telescope, Sun-Earth L2. It is also pre-determined that the Earth ground stations will be stationary. The ground stations considered are part of the DSN, detailed in the following section.

The first block in Figure 26, define space mission communications architecture, is the step in which the high-level communications architecture is determined. For this study, four options have been considered, which are DSN, TDRSS, FSS and direct laser as dictated by the "Communications Architecture" value in the design vector. The communications module calculations will vary according to the communications architecture.

The "Communications Architecture" impacts the second block in Figure 26, define communications payload architecture. For example, the communications payload for the RF-based communications systems varies greatly from the payload for the direct laser communications system. Furthermore, the payload systems for DSN, TDRSS and FSS have differing processing and transmission requirements, which will be analyzed separately in the following.

The way the communication system design was approached is the illustrated in Table XI.

Table XI: Communication system design process

Step	Step action
1	The system composition was identified – main components (ex. Antennas), other components (filters, amplifiers, modulation units, etc.)
2	STK scenarios were setup. The main goals were to visualize the telescope link to the ground directly, via LEO satellites and GEO satellites and compute the access times
3	Perform link budget calculations for a point design (i.e. having selected an antenna type and dimensions, calculate the maximum allowable downlink data rate for the link to be closed); also determine other relevant parameters for the design (antenna mass, volume, number of antennas, required power etc.)
4	Generalize the results of the link budget analysis – considering a variable antenna size, investigate how the communication subsystem design would scale with this variation
5	Write the MATLAB code for the communication subsystem in the cases analyzed in STK

Step 1 – Identify communication subsystem components
The architecture of the onboard communication system is outlined in Figure 27.
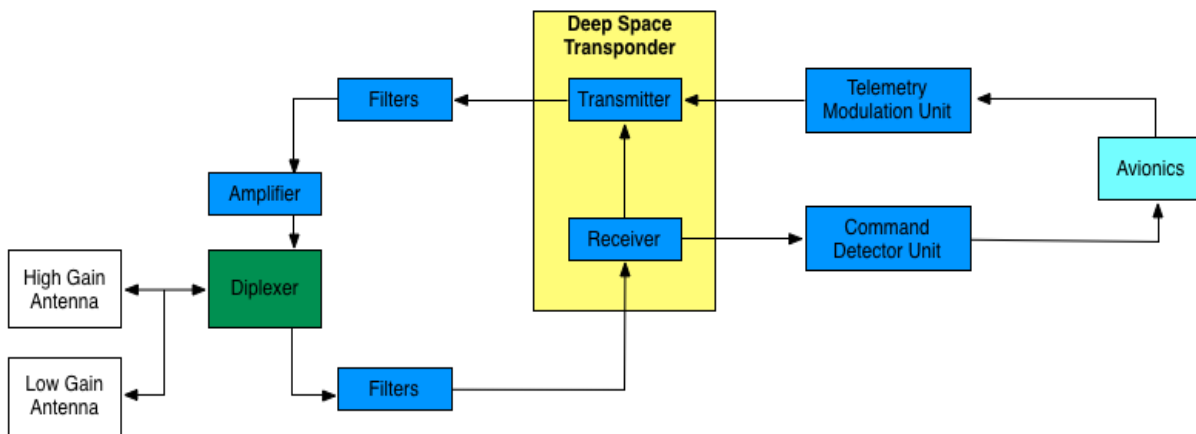
Figure 27: The communication systems architecture considered for the scope of this class[31]

Step 2 – Setup the STK scenario for the mission and calculate access times
Using STK, the orbit for the telescope is illustrated in Figure 28 and Figure 29:
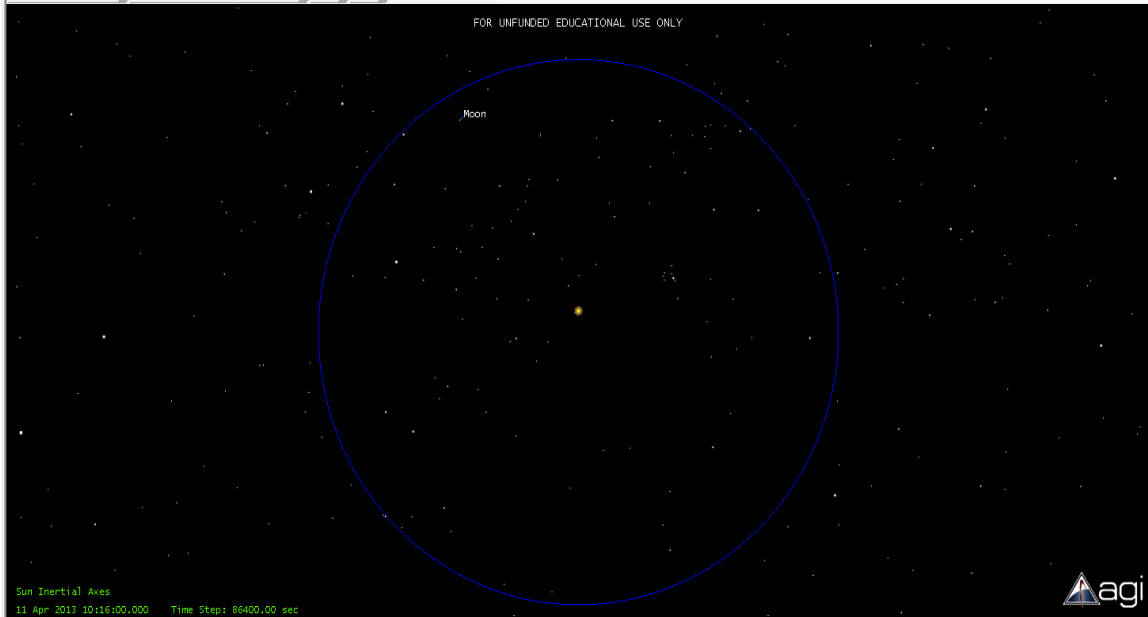
Figure 28: The orbit of TITANS AE in STK – at Sun-Earth L2
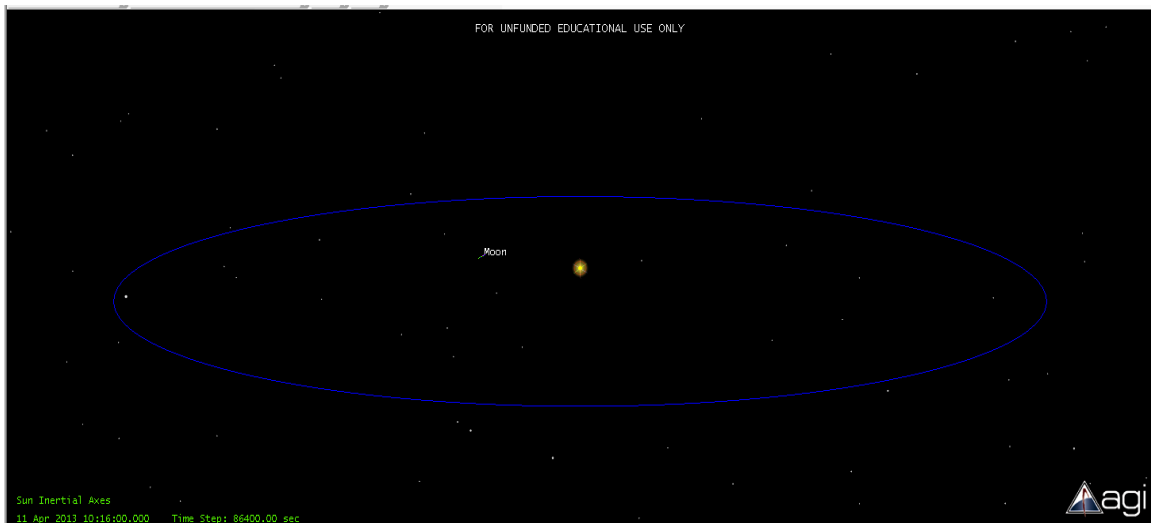
Figure 29: Alternate view of the orbit

The DSN considered is composed out of the following three ground stations:

a) Goldstone Deep Space Network Communication Complex – Barstow, California, USA
b) Robledo de Chavela – Madrid, Spain
c) Tidbinbilla – Australia

The scenarios investigated are:

a) Telescope direct communication with the DSN
b) Telescope communication with the Iridium satellites (LEO) to DSN
c) Telescope communication with the TDRSS satellites (GEO) to DSN
d) Free space optical (FSO) communications (laser).

69

In cases b), c) and d) only the first part of the communication link has been analyzed, since it is the one relevant to the satellite communications architecture sizing.

Direct DSN:
The assumptions made are that the telescope communicates directly with the DSN ground stations. The average access time is 7.4 hours a day, with the three DSN stations. In order to have some margin here, the average access time was considered to be 4 hours a day with the DSN stations, due to additional scheduling factors (ex. Communication with the ISS and other satellites) that may limit the connection time. The STK computed access time was considered to be the best case, and the realistic value of this time will be considered as 4 hours.

LEO:
The satellite constellation considered was Iridium. The problem with this assumption is that the main antennas of Iridium are pointing towards Earth, and in order to establish a high-data rate connection with L2 they would have to point towards L2. However, Iridium also has omnidirectional S-band antennas, which can be used as a contingency scenario, because their gain is low and the supported data rate is also low. The Iridium satellites considered for the link access time calculations are shown in Table XII.

A better assumption would be to consider a LEO satellite network with two antennas: one pointing towards L2 so the telescope can communicate with it, at a high data rate (so a parabolic antenna would be desired), and another antenna pointing towards the Earth, so data collected by the previous antenna can be relayed to the Earth. This would entail a new communication satellite network to be designed, built, and launched for LEO, which translates into an entirely new program, which is considered unfeasible for the scope of this project. Therefore, the LEO case is considered a contingency scenario.

Table XII: Iridium satellites considered for link access calculations

Satellite name	Access time from telescope to satellite
Iridium_13_24840	
Iridium_22_24907	14 access/day, each of 1.1 hours
Iridium_24_25105	

TDRSS:
TITANS AE can see the TDRSS satellites 24 hours a day, so in theory this would be the access time. However, due to the reasons mentioned above, a more realistic value is 4 hours a day. The TDRSS satellites considered for the link access calculations are shown in Table XIII.

Table XIII: TDRSS satellites considered for link access calculations

Satellite name	Access time from telescope to satellite
TDRS3_19548	
TDRS5_21639	24 hour access
TDRS7_23613	

The Iridium and TDRSS constellations are illustrated in Figure 30.
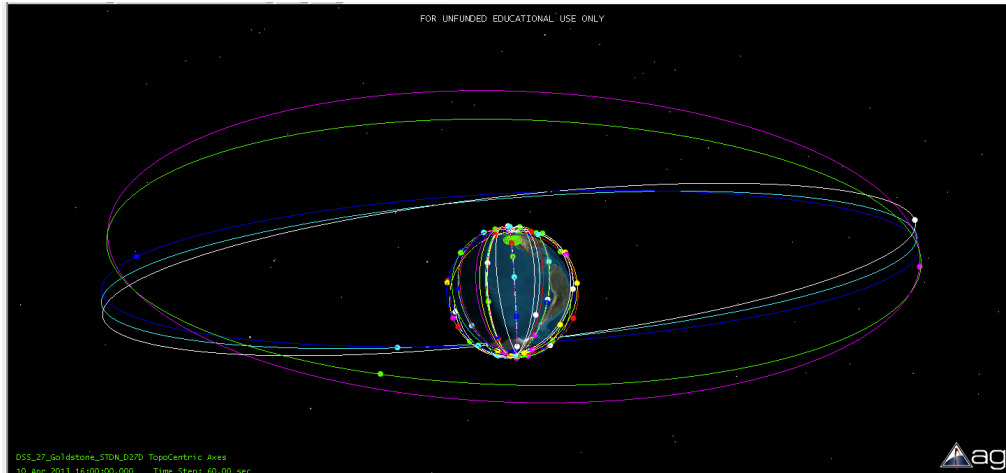
Figure 30: STK scenario with the Goldstone DSN site and the Iridium & TDRSS networks

Step 3 – Link budget calculations

The main process of this step is the link budget design. For this, a few definitions are necessary:

- Satellite Ground Terminal (SGT) – the satellite terminal on the ground, may be large or small, fixed or mobile
- Uplink – the link from the SGT to the satellite
- Downlink – the link from the satellite to the SGT
- Link budget – a quantitative analysis of a communication link, used to assess whether a link is closed (meets requirements) or open (does not meet requirements) and facilitate design.

The main parameters for the link budget are presented in Table XIV.

Table XIV: The main parameters for the link budget[32]

Parameter	Unit	Definition
P_T	dBW	Transmit power
G_T	dBi	Transmit antenna gain relative to isotropic
EIRP	dBW	Effective Isotropic Radiated Power
L_P	dB	Free space loss
L_M	dB	Miscellaneous losses
L_R	dB	Losses due to rain
L_A	dB	Losses due to atmospheric effects
G_R	dBi	Receive antenna gain relative to isotropic
T	dBK	Temperature in degrees Kelvin
G/T	dB/K	Figure of Merit
C	dBW	Receiver carrier power
N	dBW	Noise power
C/N	dB	Carrier-to-noise ratio
B	dBHz	Signal bandwidth
S/N	dB	Signal-to-noise power ratio
R	dBHz	Data rate
k	dbW/K*Hz	Boltzmann's constant
E_b/N_0	dB	Energy per information bit to noise power density ratio

The link budget may be expressed in terms of carrier-to-noise (*C/N*) ratio as:

$$\frac{C}{N} \cong \frac{S}{N} = \frac{E_b}{N_0} = \frac{P_T G_T G_R}{L_A L_R L_M L_P kTB}$$

<div align="right">Eq. 7</div>

It may be decomposed into uplink (UL) and downlink (DL) link budgets.

Since the uplink is mainly used for telecommands, the data rate that has to be supported by this link is small and therefore closing this link will not be as challenging as closing the downlink, in which the science data has to be downloaded and therefore will necessitate a high data rate. Therefore, for the purposes of this analysis, the link budget will focus on the downlink part.

For simplification purposes, the carrier-to-noise ratio was considered to be approximately equal with the signal-to-noise ratio (*S/N*).

The free space loss is given by the following formula

$$L_P = \left(\frac{\lambda}{4 \cdot \pi \cdot \text{range}}\right)^2$$

<div align="right">Eq. 8</div>

where λ is the wavelength (meters) and the range is the path length (meters).

The antenna gain is dependent on the directivity of the beam, for the simplification purposes in this analysis it was assumed (in the first iteration), that the antenna is a parabolic dish, whose gain is given by the following formula

$$G = 10 log \left[\varepsilon \left(\frac{\pi D}{\lambda}\right)^2\right] (dBi)$$

<div align="right">Eq. 9</div>

where ε is the antenna efficiency (usually equal to 0.55), *D* is the diameter of the aperture in meters and λ is the wavelength ($c = f\lambda$).

EIRP is the effective isotropic radiated power of the transmitter

$$10 \log(EIRP) = 10 \log(P_T G_T) = 10 \log(P_T) + 10 \log(G_T) \ (dBW)$$

<div align="right">Eq. 10</div>

The noise power can be expressed as

$$P = \frac{hfB}{e^{\frac{hf}{kT}} - 1}$$

<div align="right">Eq. 11</div>

where $h = 6.62 \cdot 10^{-34} Js$ (Planck's constant), $k = 1.38 \cdot 10^{-23} J/°K$, B is the receiver bandwidth, P is the noise power.

When $hf/kT \ll 1$, the formula above can be simplified and the receiver noise power is

$$P = kTB = N_0B \text{ (W)}$$
$$P_N = GkTB \text{ (W)}$$

<div align="right">Eq. 12</div>

Typical losses that affect the communications link are summarized in Table XV:

<div align="center">

Table XV: Typical communication losses and their values

Loss	Value (dB)
Quantization	0.25
Differential encoding	0.2
Filtering	0.5
Adjacent channel interface	1
Interleaving	1
TOTAL:	**2.95**

</div>

The total value for typical losses is considered to be 3 dB. A margin of another 3 dB was added to give a losses value of 6 dB, which has been considered in the link budget as the miscellaneous losses.

The link analysis or link design for the communications module is performed by a set of interrelated equations used to close the link while maintaining an acceptable level of link performance. The communications module is constrained to have a link margin of greater than or equal to 3 dB and a Signal-to-Noise ratio of 5/10 (-3 dB) or better. These values were selected based on traditional performance standards.[30]

The link analysis takes as one parameter the transmit power required. In combination with the transmit distance (determined by the communications architecture), the antenna type and size can be determined. From there, estimates of mass and volume can be provided for the antenna. Power, mass and volume for the non-antenna communications components will be estimated using specification sheets for comparable systems.

The different antenna types considered are parabolic, horn and array. The helix antenna will not be considered because of its low frequency application spectrum.[30]

The equations for the antennas described above are presented in Table XVITable XVII, and Table XVIII:

Table XVI: Parabolic antenna characteristics[30]
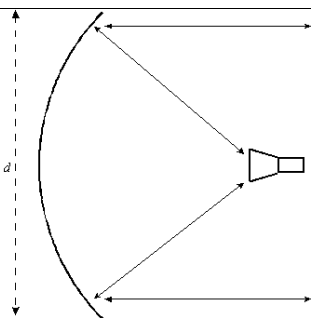
Antenna type	Parabolic reflector
Antenna model	
Beam type	Conical
Typical max gain (dBi)	15-65
Peak gain	$17.8 + 20 \log d + 20 \log f$ ($\varepsilon = 0.55$)
Half-power beamwidth (deg)	21/ (fd)
Size (m)	D
Mass (kg)	10-30

Table XVII: Horn antenna characteristics[30]
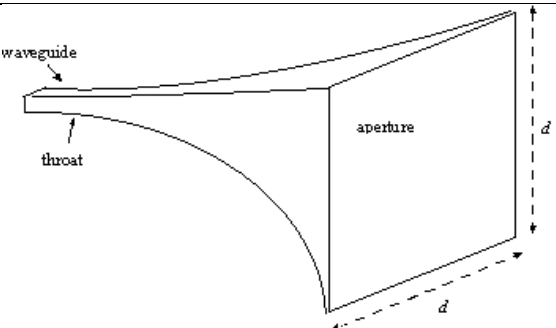
Antenna type	Horn
Antenna model	
Beam type	Conical
Typical max gain (dBi)	5-20
Peak gain	$20 \log (\pi d/\lambda) - 2.8$ ($\varepsilon = 0.52$)
Half-power beamwidth (deg)	$225/(\pi d/\lambda)$
Size (m)	D
Mass (kg)	1-2

Table XVIII: Array antenna characteristics[30]

Antenna type	Array
Antenna model	
Beam type	Conical (scanning)
Typical max gain (dBi)	5-20
Peak gain	$10 \log (A/\lambda^2) + 8$
Half-power beamwidth (deg)	-
Size (m)	A
Mass (kg)	20-40

To simplify the design, two antenna types have been considered:

i)   Parabolic antenna – for the high gain communications. For redundancy purposes, the telescope will have two high-gain antennas, only one of them being powered at a time so that the overall power draw for the communication system will not be impacted by the built-in redundancy in the communication system

ii)   Patch antenna – for low gain communications. There will also be two antennas of this type, with only one of them being powered on at a time.

For the optical communication, TITANS AE will have two telescopes and two corresponding stabilizer units. Each DSN complex consists of at least four deep space stations equipped with ultrasensitive receiving systems and large parabolic dish antennas. There are:

• One 34-meter (111-foot) diameter High Efficiency antenna
• One 34-meter Beam Waveguide antenna (Three at the Goldstone Complex and two in Madrid)
• One 26-meter (85-foot) antenna
• One 70-meter (230-foot) antenna[33]

The best antenna that could be used is the 70-meter antenna, which would give the highest value for the antenna gain. However, in order to ensure a conservative design, it will be assumed that the antenna that is available for communications with TITANS AE is the 34-meter antenna.

The power range for transmission from the DSN antenna is from 16 W to 400 kW. The maximum transmission power is considered to be of 200 kW. The frequencies are separate for Transmit (Earth to Space) and Receive (Space to Earth) and are shown in Table XIX.

Table XIX: DSN transmit and receive frequency range

	Transmit	Receive
S-Band	2110-2120 MHz	2290-2300 MHz
X-Band	7145-7190 MHz	8400-8450 MHz
Ka-Band	34200-34700 MHz	31800-32300 MHz

The transmission frequencies have been chosen to be 34.7 GHz for transmission and 32.3 GHz for reception for the high gain antennas onboard the telescope. For the contingency scenario, the reception frequency is 2.2 GHz (S-band). The link budget was done for the high-gain downlink case and the low-gain downlink case, considered a set antenna size. The link budget main parameters for the high gain case are illustrated in Table XX.

The link budgets for the downlink high and low gain cases are illustrated in the following tables. They represent the core of the communications system design, from which further generalization was done in the following sections.

Table XX: The link budget for the high gain antenna downlink case

Parameter	Unit	Value	Comments
Antenna elevation angle	degrees	30	Assumed high to minimize scattering from buildings or tall mountains
Maximum transmission range	km	1503178.873	L2 distance is 1.5 million km, taking into account the elevation angle this value was calculated
Frequency	GHz	32.3	Chosen from Table XIX
Wavelength	m	0.0093	$\lambda = c/f$
Path loss	dB	-246.2	Eq. 8 $L_P = \left(\frac{\lambda}{4 \cdot \pi \cdot \text{range}}\right)^2$ Eq. 8
Telescope antenna diameter	m	3.5	Chosen as a point design
Gain of the telescope antenna	dBi	58.9	Parabolic antenna
Gain of the ground antenna	dBi	84.9	Assumed 34-m diameter, parabolic
Noise temperature	K	225	Antenna assumed to be shaded from the Sun, to minimize Sun radiation interactions
Telescope antenna radiated power	W	20	Input power to the transmission system is assumed to be 200W, the yield of this is considered 10%
Required E_b/N_0	dB	12	Corresponds to a BER = 10^{-8} (see Figure 31, the coding method selected was QPSK because this is the most commonly used coding technique in satellite communications[34]
Data rate	bps	50M	Arbitrarily chosen
Margin	dB	14.6	Link closed

The link budget main parameters for the low gain case are illustrated in Table XXI.

Table XXI: The link budget for the low gain antenna downlink case

Parameter	Unit	Value	Comments
Antenna elevation angle	degrees	30	Assumed high to minimize scattering from buildings or tall mountains
Maximum transmission range	km	1503178.873	L2 distance is 1.5 million km, taking into account the elevation angle this value was calculated
Frequency	GHz	2.2	Chosen from Table XIX
Wavelength	m	0.136363636	$\lambda = c/f$
Path loss	dB	-222.9	Eq. 8
Telescope antenna diameter	m	1.25	Chosen as a point design, patch antenna
Gain of the telescope antenna	dBi	10	Parabolic antenna
Gain of the ground antenna	dBi	61.55461367	Assumed 34m diameter, parabolic, at the corresponding S-band wavelength
Noise temperature	K	175	Antenna assumed to be shaded from the Sun, to minimize Sun radiation interactions
Telescope antenna radiated power	W	5	Input power to the transmission system is assumed to be 50W, the yield of this is considered 10%
Required E_b/N_0	dB	9.6	Corresponds to a BER = 10^{-8} (see see Figure 31 the coding method selected was QPSK because this is the most commonly used coding technique in satellite communications[34]
Data rate	bps	16k	Arbitrarily chosen
Margin	dB	7.24	Link closed
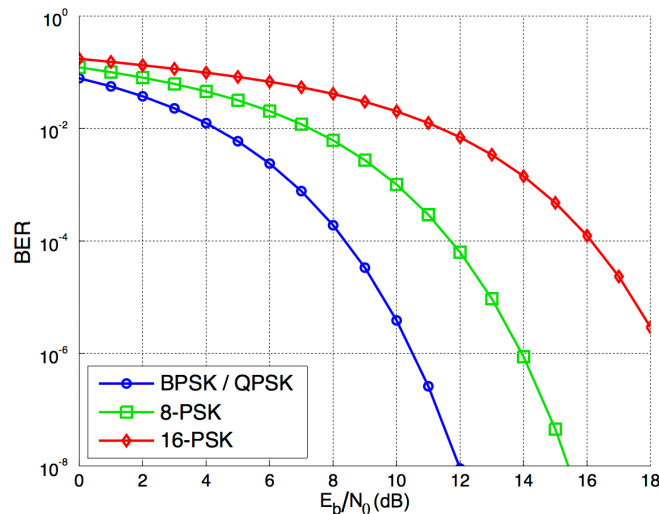
Figure 31: E_b/N_0 values for different coding methods and BER desired values

The laser communication is a novel communication technology, that allows a low satellite transmission power and a low transmit telescope dimensions, in the order of cm. It can also sustain high volumes of data. The problem is that it is cut off by cloudy conditions, therefore, to achieve 99% reliability in the reception link, 9 ground stations are used.[35]

The mass and volume necessary to be accommodated aboard the telescope are about 5 times less than those needed for RF communications[35], but the laser beam has to be very accurately pointed toward the receiving station's direction. In order for this pointing accuracy to not impact the ADCS system, MIT Lincoln Labs have developed an extra stabilizer, which can help improve the telescope's pointing accuracy (The telescope is the optical transmission unit, different from TITANS AE). However, the TRL level for this technology is currently low.

The main mathematical relations describing the laser communications are presented in the following.

$$E_{ph} = \frac{hc}{\lambda}$$

Eq. 13

where E_{ph} is the energy per photon, h is Planck's constant, c is the speed of light and λ is the wavelength. Usually this is 1550 nm.

The energy per pulse can then be written as

$$E_{pulse} = n_s \cdot E_{ph} \cdot q_e$$

Eq. 14

where n_s is the number of photons in a pulse and q_e is the quantum efficiency, equal to 0.8.

The laser communication has M = 16 modulation levels (also called 16-PPM – 16 pulse position modulation).

The received power can be then expressed as

$$P_{received} = E_{pulse} \cdot \frac{R_b}{M}$$

Eq. 15

For the laser communication, the link budget main parameters are illustrated in Table XXII.

Step 4 - Generalize the results of the link budget analysis
MATLAB code was written to investigate how the daily data rate (for 4 hours of contact time) would scale with the TITANS AE antenna size.

The results are illustrated in the following plots.
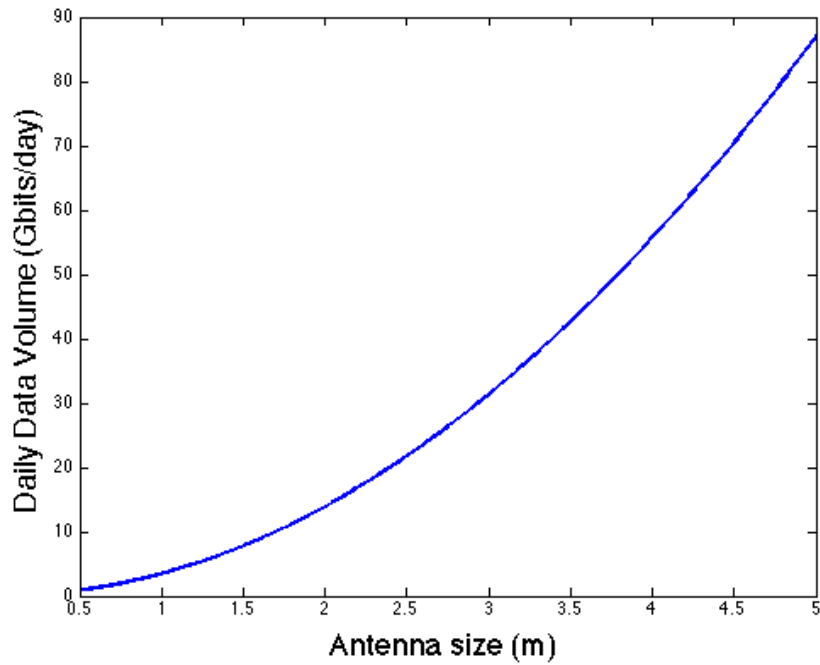
Figure 32: The DSN trade: the increase in daily data volume (Gbits/day) versus the antenna size (meters)

The maximum value of the daily data volume is at 5 m of antenna size, and is of 305 Gbits/day.
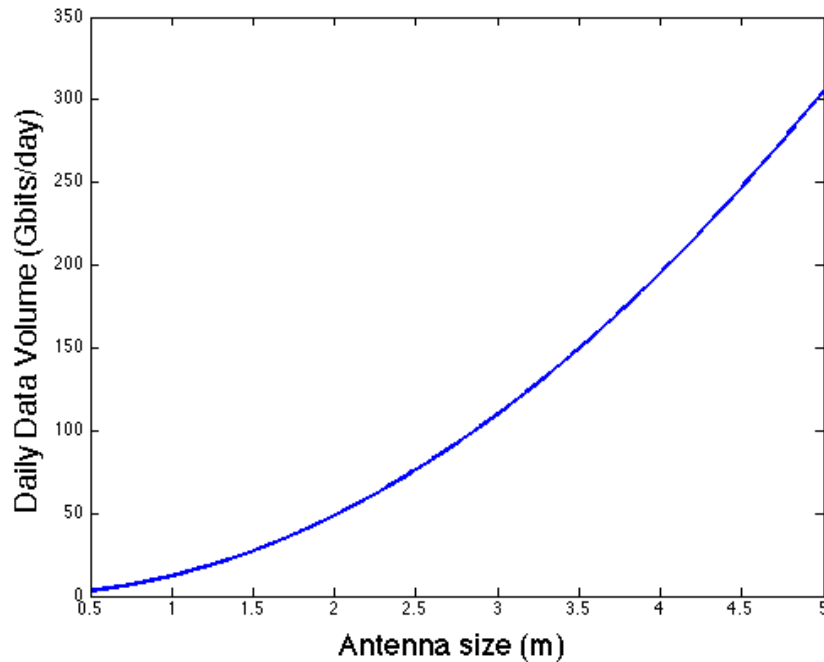
Figure 33: The TDRSS trade: the increase in daily data volume (Gbits/day) versus the antenna size (meters)

The maximum value of the daily data rate is at 5 m of antenna size, and is of 87 Gbits/day.

For both the DSN and TDRSS cases, the antenna size was varied from 0.5 to 5 meters, in increments of 0.01 m. There is an option to have deployable parabolic antennas (Harris) but it this option was not considered for this project.
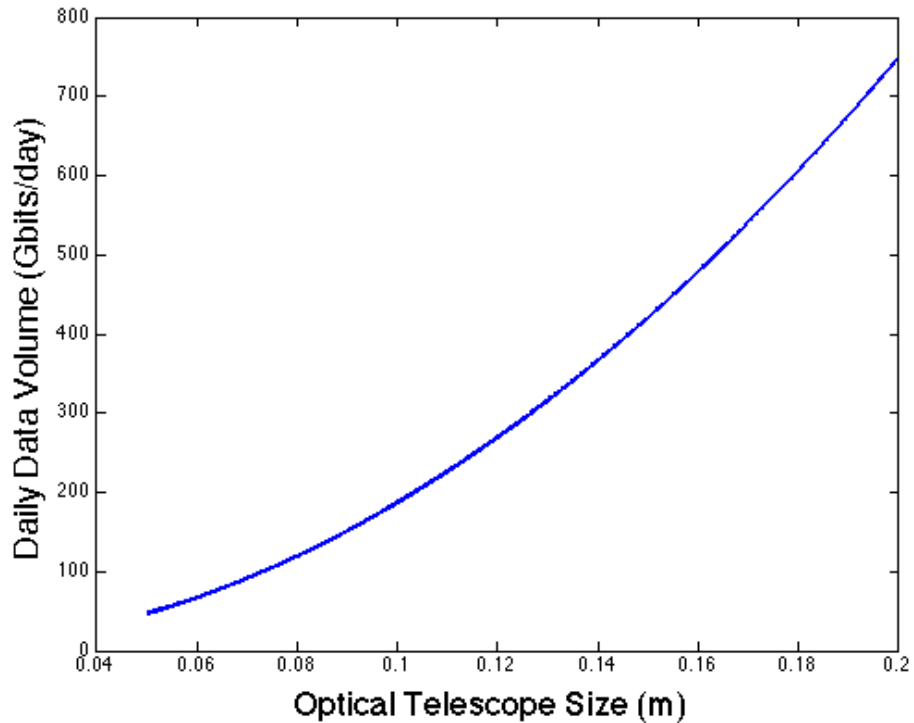
Figure 34: The laser communications trade: the increase in daily data volume (Gbits/day) versus the optical telescope size (m)

The maximum daily data rate is of 748.3 Gbits/day, and it corresponds to an optical telescope size of 0.2 m. The antenna size was varied from 0.04 m to 0.2 m.

Step 5 - Write the MATLAB code for the communication subsystem in the cases analyzed in STK
The MATLAB code for the communications subsystem was hardcoded to include the values determined in the link budgets above for DSN, TDRSS and laser communications.

5.3.3.2.3 Conclusions, recommendations and future work
In conclusion, the options for TITANS AE communications are shown in Table XXII below.

Table XXII: Summary of TITANS AE communication design

Communication type	Gain value	Number of antennas	Band	Communication architecture
Telemetry and telecommand	Low	2	S	LEO (FSS)
Science data	High	2	Ka	TDRSS Laser

In conclusion, based on the results illustrated in Table XXII above, the best options for TITANS AE are as follows:

1. Laser communications – this is the best communication system option because of the advantages it offers: a low weight and power requirement and capability of sending a high data volume. These outweigh the limitations the weather effects may have on this technology
2. Direct DSN – this is the next best communication system option because TITANS AE is located at ESL2 (Sun-Earth Lagrange point 2), the distance from it to the Earth is 1.5 million km. The receiving antenna on the Earth is a DSN 34meter antenna, thus having a big gain and helping close the communication link.
3. TDRSS – this option is following DSN because, although the distance is shorter by 35786 km the receiving antenna aboard the TDRSS satellite is 4.9 meters, so it does not help closing the link as much as the 34 meter antenna on the ground does. So the shorter distance does not compensate the gain lost due to the smaller antenna.
4. LEO (or FSS) – if the FSS is considered to be in LEO (other options are possible too, and should be further explored), the antennas of satellites in LEO usually point towards the Earth and cannot sustain a high data rate communication link to L2. The omnidirectional antennas onboard these satellites would have to be used, which leads to a very small gain and data rate. Due to these considerations, this option is regarded as the contingency case.

As mentioned before, a future work point is to consider other satellite constellations as part of the FSS communication architecture. For example, FSS can include satellites that have highly elliptical orbits so that they can link at their apogees the telescope at L2 and at their perigee other communication satellites in LEO or even a DSN ground station. FSS is considered to be a very promising concept, and all of its aspects should be exploited when analyzing the communication system design in order to come up with novel architectural options.

5.3.3.3 *Attitude Determination and Control System (ADCS) Subsystem Module*

In the context of this project, the primary tasks of the attitude determination and control subsystem (ADCS) are to provide attitude control and stability to the satellite and provide sufficient slew rate and course pointing accuracy to the science instruments on the space telescope. In creating the ADCS model that would accomplish these tasks for this space telescope, much of the work was done without active feedback from other modules given the location of the ADCS module in the N^2 diagram. As a result, some assumptions needed to be made to create an effective ADCS. The primary assumption was that the mass and inertia of this space telescope would be on the same order of magnitude as the mass and inertia of the Advanced Technology Large Aperture Space Telescope (ATLAST) design. Given this assumption, the ADCS was designed such that the torqueing, slew rate, and momentum storage capabilities were on par with the capabilities of the ATLAST design. If this space telescope is created such that it has substantially greater mass or inertia, but that mass or inertia are not an order of magnitude greater than what was assumed, the space telescope will still operate effectively but with a lower slew rate.

While the momentum wheels and star tracker were modeled using established commercial off the shelf parts, the solar sail will be a custom made part. Therefore, in modeling the solar sail in the module code, the volume, mass, and power requirements of the solar sail are estimates, which are based on the design features of other custom-made solar sails. These estimates are adjusted based on the varying sizes and mission requirements of the comparison solar sails.

5.3.3.3.1 Pointing Control and Actuation
The ADCS for this space telescope will use momentum wheels to achieve attitude pointing and stability because of the hardware robustness, flight heritage and proven performance, and the lack of plume impingement associated with this ADCS component. In conjunction with the momentum wheels, this spacecraft will also utilize a solar sail to minimize the distance between the spacecraft center of gravity and the center point of the solar pressure from the sun. Since the only significant external disturbance torque present at SE-L2 is solar pressure, the solar sail will reduce the momentum wheel sizing requirements by an order of magnitude. The relatively small pointing requirement of 1 milliarcsecond (mas) will require the ADCS to have a star tracker and a fine guidance system (FGS) capable of actuating the telescope to that level of accuracy once the momentum wheels have achieved a less accurate pointing accuracy on the order of 0.1 degrees.

While this project explores a family of architectures rather than a single point design, certain components can be used in modeling the characteristics and requirements of a spacecraft. For this space telescope, the Honeywell HR16 Momentum Wheel (100 N-m-s variant) will be useful in modeling the ADCS of the spacecraft. The solar sail will be a customized solution with a two-axis gimbal attached to the boom connecting the spacecraft bus to the solar sail. This two-axis gimbal will allow for solar pressure torque modulation and allow the ADCS to dump the momentum from the momentum wheels without using propellant. The Ball Aerospace CT-633 Stellar Attitude Sensor will be used to model the star tracker on this space telescope.

Using this design architecture, the equations used to determine ADCS module outputs may be developed. These equations with their accompanying explanations are shown below.

The data rate required by the ADCS from Avionics subsystem will not constrain the capability of the Avionics subsystem because the computing requirements of the ADCS will be relatively constant, will not require a significant amount of memory for the inertial measurement unit (IMU) data, and will have allocated software and hardware specifically designed for the ADCS purpose. For the same reason, the data volume required by the ADCS will not be an issue of concern. Furthermore, the data throughput resulting from the images collected by the telescope will be orders of magnitude greater than the data throughput resulting from the ADCS. The required equations are shown below. Examples of support software include Kalman filter, Extended Kalman filter, noise filter, and mixer.

$$D_{Total} = (D_{mw})(N_{mw}) + (D_{ss})(N_{ss}) + (D_{st})(N_{st}) + (ssw)$$

<div align="right">Eq. 16</div>

$$V_D = (D_{Total})(t_d)$$

<div align="right">Eq. 17</div>

D_{Total} represents the total data rate of the ADCS, D_{mw}, D_{ss}, and D_{st} represent the data rate of the momentum wheels, solar sail, and star tracker, respectively. N_{mw}, N_s , and N_{st} represent the number of momentum wheels, solar sails, and star trackers, respectively. ssw represents the support software data rate requirements. V_D represents the total data volume and t_d represents the time over which IMU data is collected.

As stated above, the ADCS will not require any propulsion to be used for momentum dumping. However, if solar pressure modulation will not be allowed or is infeasible, the following equations can be used. Given that nine of the aforesaid momentum wheels would allow the spacecraft to operate for approximately 11 days before reaching momentum saturation and the pointing time requirement for the telescope is only two hours, the frequency of momentum dumps may be arbitrarily selected between 4 to 8 days and still allow a significant margin of error both for pointing time requirements and for momentum wheel saturation. In order to determine the rate at which momentum builds up in the wheels, the following equation may be used.

$$T_{sp} = \left(\frac{F_s}{c}\right) A_s (1 + q) \, cos(i)L$$

<div align="right">Eq. 18</div>

Let T_{sp} represent the solar torque, F_s represent the solar constant, c represent the speed of light, A_s represent the area of the satellite exposed to sunlight, q represent the reflectance factor, i represent the angle of incidence to the Sun, and L represent the distance between the center of gravity of the spacecraft and the center of the solar pressure. It may be assumed that the solar constant at SE-L2 is $1296W/m^2$, the speed of light is 3×10^8 m/s, the surface area is between 1000 and 1500 m^2, the reflectance factor is 0.6, and angle of incidence is 0 degrees, and the distance between the center of gravity of the spacecraft and the center of the solar pressure is less than 0.1 meter. The following equation can be used to determine the amount of momentum build up between momentum dumps.

$$M_T = T_{sp}t_m$$

<div align="right">Eq. 19</div>

Let M_T represent the total momentum and t_m represent the time between momentum dumps.

The operating temperature of the momentum wheels is between -30 and 70 degrees Celsius. The operating temperature of the star tracker(s) is between 0 and 30 degrees Celsius. The operating temperature of the solar sail is between -150 and 110 degrees Celsius.

The power dissipation of the ADCS will be the power required multiplied by some factor of inefficiency as represented in the equation below.

$$P_D = \eta(P_u)$$

Let P_D represent the power dissipation of the ADCS, let η represent the factor of inefficiency of the ADCS, and let P_u represent the power usage of the ADCS. The vast majority of power usage within the ADCS will be used by the momentum wheels. The equations below represent the worst case scenarios for steady state and peak power usage, respectively.

$$P_{uss} = (22 Watts)(N_{mw}) + (25 Watts)(N_{ss}) + (9 Watts)(N_{st})$$

$$P_{up} = (195 Watts)(N_{mw}) + (P_{pss})(N_{ss}) + (P_{pst})(N_{st})$$

Let P_{uss} represent the overall steady state power usage of the ADCS, let P_{up} represent the overall peak power usage of the ADCS, let P_{pss} represent the peak power usage of the solar sail, and let P_{pst} represent the peak power usage of the star tracker.

The momentum wheels are designed to last for over 15 years which is 5 years longer than the servicing option with the lowest frequency. Solar sails can be produced with incredibly low mass and volume, the star tracker(s) are relatively small and light weight, and the FGS will be integrated with the telescope hardware. Therefore, the momentum wheels will dominate the mass a volume requirements of the ADCS. The equations below represent these requirements.

$$M_M = (12 kg)(N_{mw}) + (20 kg)(N_{ss}) + (5.5 kg)(N_{st})$$

$$V_V = \pi \left(\frac{.351}{2}\right)^2 (.178)(N_{mw}) + (.125 m^3)(N_{ss}) + (.002025 m^3)(N_{st})$$

Let M_M represent the total mass of the ADCS and let V_V represent the total volume of the ADCS. Since the telescope architecture tradespace does not encompass an option with multiple non-physically connected segments in operational use and the lifetime of the components far exceeds the longest servicing period, the architectural choices will not have a dynamic impact on the design of the ADCS. As a result, the Pareto front could be characterized largely without the use of the ADCS module. However, the ADCS module does provide comprehensiveness and continuity in the model.

5.3.3.4 Avionics Subsystem Module

The avionics subsystem serves as the backbone for the data interface among all subsystems; it collects, processes, and stores data from the subsystems, schedules tasks, and transmits commands to the subsystems. The avionics subsystem is also responsible for formatting, packing

and unpacking data to/from the ground stations. The largest drivers of the avionics subsystem are the data rate/volume expected from optics, the communications architecture, and the assembly servicing technique. The science data from optics is the largest contributor to the processing and storage demands of the avionics system while in operation. The assembly/servicing technique could have a significant impact on the avionics system during assembly or servicing phases of operation, especially in the case of robotic arms or swarm robotics, which will be intensive from a processing and scheduling standpoint.

comms_arch
assem_service_tech
observatory_struct
data_rate_optics
data_rate_ACS
data_vol_ACS

avionics_m
avionics_power_diss
avionics_v
avionics_data_rate

avionics_temp_range
avionics_power_req
avionics_components
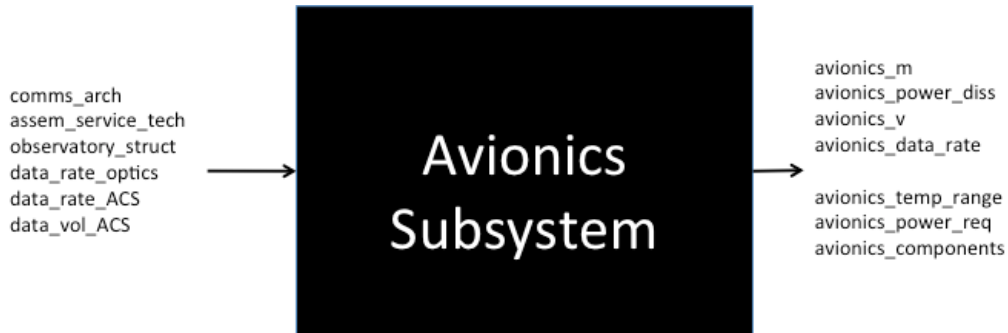
Figure 35: Avionics subsystem inputs (left) and outputs (right)

The majority of the avionics subsystem outputs (see Figure 35) are highly dependent on the selection of technology for each component. Advances in electronics have demonstrated that in less than a decade, data storage capacities, for example, have increased dramatically while form factors have decreased dramatically. As such, the approach for quantifying the avionics outputs will be to leverage the specifications of avionics components used in comparable systems or that have been space qualified by other means.

A typical avionics subsystem is depicted below in Figure 36. Using this diagram and documentation for the Hubble Avionics subsystem, the avionics components in the model are the Central Processing Unit (CPU), Random Access Memory (RAM), Data Management Unit (DMU), Data Interface Unit (DIU) and Power Converter Unit (PCU). The main computer in the model is based off of the specifications for the Hubble Advanced Computer which is 20 times faster, 36% lighter and has 6 times more memory than the DF-224/coprocessor combination that was initially launched with Hubble and developed in the 1970's.[36] Maxwell's Synchronous Dynamic RAM (SDRAM) is used for the volatile memory in the model as it represents one of the latest technologies in its class.[37,38] The DMU and DIU are architecturally the same as Hubble. The DMU controls the central clock, interfaces with the DIUs and the CPU, whereas the DIUs are the data interface with the other subsystems.[39] The PCU essentially consists of a number of DC-DC converters that step down a common voltage supply provided by the solar panels to a series of lower voltage levels suitable for various avionics components as specified by their voltage-current operation requirements. The PCU specifications used in the model are based on the TDK: Lambda PXD Series of radiation-hardened DC-DC converters, which have been chosen as candidate component choices for a number of satellite-based science instruments.[40]
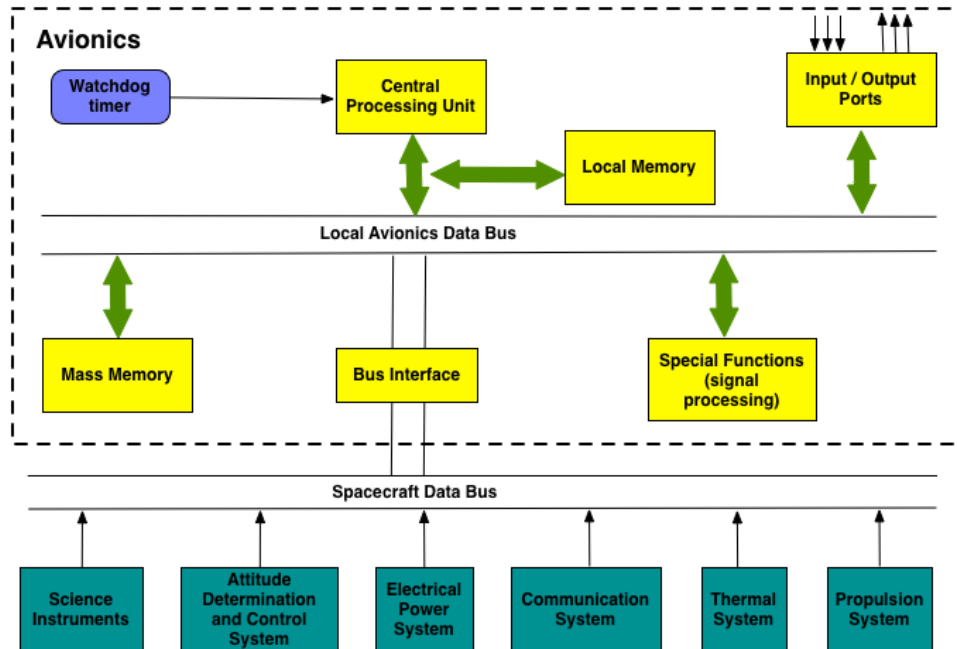
Figure 36: Typical Avionics subsystem for satellite systems[41]

The architecture of the avionics subsystem remains the same throughout all of the architectural decisions, i.e., data and physical connections are constant, but the quantity of each component changes in accordance with processing, memory, and reliability requirements. Redundancy is a common practice with avionics components; for example, the Hubble DIU is composed of two complete units where each unit is capable of performing all of the required functions.

The following sections briefly describe the key outputs of the avionics subsystem to other modules in the model.

5.3.3.4.1 Processing Speed
Processing speed represents the amount of data that a computer system can process in a given amount of time. Processing speed can play an important role in determining the amount of science data that can be collected, how that data is processed, and whether the data is processed on the satellite or on the ground. The amount of processing speed that a computer has impacts its ability to do onboard processing tasks that can improve the effectiveness of the satellite. Specifically, satellites can use onboard processing to overcome rain attenuation, utilize more efficient encoding, modulation, and multiplexing schemes, reduce the bit error rate, accelerate internet related throughput, mitigate problems associated with transmission delay, and allow the use of smaller aperture user antennas.

The communications architecture, on-orbit assembly and servicing technique, and the primary mirror actuation method will all have dynamic impacts on the processing requirements of the satellite. Using a Federated Satellite System, increasing the autonomy of the satellite, and increasing the number and complexity of tasks the satellite is expected to perform are all aspects of the design that will levy greater demands on the processing capability of the onboard computer.

Furthermore, the effective processing speed of a computer is dependent upon several aspects of the onboard computing system including clock speed of the central processing unit, front side bus speed, back side bus speed, the amount of random access memory, the amount of cache memory, how the data protocols are set up, how well the software has been optimized, the temperature of the computer, and what information the computer is expected to process. For this reason, establishing a closed-form solution for the required computing capability will not be feasible. Extensive design analysis, experience, and intuition are all required to determine the processing requirements of a satellite.

5.3.3.4.2 Mass and Volume
Similar to the communications subsystem, mass and volume of all avionics will affect the form and architecture of the space telescope. This should be lightweight and compact without any compromise in its value or performance. They are estimated via dimension ranges of electronics subsystems onboard existing spacecraft.

5.3.3.4.3 Power
Power requirements of satellite avionics components such as microprocessors, memory and other electronic equipment are generally similar to that of Hubble or James Webb space telescopes. An estimation or extrapolation may be derived from them since their overall function and purpose are equivalent. A more accurate method would be to use peak and average voltage and current ratings obtained from component datasheets of potential avionics components. The overall power consumption for the avionics subsystem is simply the sum of the power consumptions of individual components. As every component has its own power efficiency rating, power loss and dissipation is expected. The overall power dissipation for the avionics subsystem is then the sum of the power losses of individual components.

5.3.3.4.4 MTBF
This metric will be similar to that used in the communication subsystem. The lifetime of the avionics subsystem can be predicted through calculating parameters such as probability of failure and average lifetime for a single or network of electronic components. These values may be available in component datasheets of existing avionics systems. The avionics subsystem is also assumed to be serviceable so that its predicted lifetime metrics do not necessarily have to meet or exceed the in-service lifetime of the entire system. The failure rate of the communications subsystem can thus be calculated via the multiplicative sum of communications components operating in a casual chain.

5.3.3.5 Propulsion Subsystem Module

The propulsion system must carry enough fuel to correct for orbital disturbances over the lifetime of the mission (station-keeping) as well as allow for servicing missions to be conducted. From an operational standpoint, there are two servicing decisions being traded: in-situ servicing and servicing at a lower orbit. For the latter case, enough propellant must be carried to allow for round-trip travel from Sun-Earth L2 to the servicing orbit multiplied by the desired number of servicing missions. For the former case, it is useful to calculate the amount of propellant required to transport a robotic servicing probe to Sun-Earth L2 to facilitate a cost comparison between the two servicing options.

5.3.3.5.1 Assumptions

Several assumptions were made in order to minimize the complexity of the propulsion system calculations. For the various servicing locations, transit times were referenced directly from texts. This eliminated the need to calculate transit times from Sun-Earth L2 to the various servicing orbits for each of the propulsion systems under consideration. Furthermore, this also eliminated the need to consider the thrust capabilities of individual models within the engine families under consideration.

5.3.3.5.2 Lifetime

This metric is set by the Operations team. There are three critical inputs: mission duration, which impacts the amount of propellant required for station-keeping maneuvers; servicing location, which determines whether extra propellant will be required for servicing; and servicing frequency, which will determine the amount of propellant required for servicing, given that servicing does not occur in-situ.

5.3.3.5.3 Mass and Volume

The propulsion system mass will be calculated as a fraction of the entire satellite mass, as the fuel required to achieve a specific velocity change (ΔV) increases as the spacecraft mass increases. The required ΔV for the mission is influenced by two factors: station-keeping and servicing. For spacecraft in halo orbits around the Sun-Earth L2 point, it is recommended that a ΔV of 4 m/s per year be allocated for station-keeping[26]. The total ΔV required for station-keeping is then simply 4 (m/s)/year multiplied by the number of years in service.

$$\Delta V_{stationkeeping} = n_{years\ in\ service} \times 4$$

Eq. 25

The ΔV required for servicing missions varies based on the servicing option specified in the design vector. For in-situ servicing, zero additional ΔV capability is required on the spacecraft. However, propellant is still required for the transit of the servicing probe from a parking orbit around Earth to the L2 location. This has been calculated for the transit of the James Webb Space Telescope beginning from a 250 km parking orbit, and will therefore be hard-coded into the module.[42]

$$\Delta V_{probe} = 3.21 \times 10^3$$

Eq. 26

For the case where the telescope is brought closer to Earth for servicing, a separate method for finding the required ΔV must be employed. It has been shown that transfers between a halo orbit around the Sun-Earth L2 point to a halo orbit around the Earth-Moon L2 point can be accomplished with little ΔV – between 0 m/s to 20 m/s, depending on the initial and final orbital radii.[43] Other studies have shown that transfers from Sun-Earth L2 to lunar orbit and to geosynchronous Earth orbits are possible, along with the required ΔV and transit times.[44]

Figure 37 and Table XXIII summarize the ΔV requirements and transit times for several transfer trajectories.

Earth-Moon Az [km]	Sun-Earth Az [km]	ΔV [m/sec]	Earth-Moon Az [km]	Sun-Earth Az [km]	ΔV [m/sec]
16,000	113,000	17.9	16,000	111,000	0
18,000	133,000	10.6	18,000	142,000	0
20,000	161,000	11.0	19,000	140,000	0
22,000	115,000	7.5	22,000	126,000	0
24,000	124,000	4.2	24,000	130,000	0
26,000	129,000	0.9	26,000	131,000	0
28,000	154,000	1.4	28,000	155,000	0
30,000	155,000	2.8	30,000	157,000	0

Figure 37: ΔV requirements for transfers between various SE-L2 and EM-L2 orbits[43]

Table XXIII: ΔV requirements for tarious transfer trajectories

Trajectory	ΔV (m/s)	Transit Time (days)	Reference
LEO to SE-L2	3210	63	Cattrysse
SE-L2 to Lunar Circular	1200	101	Truesdale
SE-L2 to GEO	5000	109	Truesdale

With the ΔVs known, the non-dimensionalized propellant mass (as a fraction of the total spacecraft mass) can be calculated as

$$\frac{m_{\text{propellant}}}{m_{total}} = 1 - e^{-\Delta V/c}$$

Eq. 27

where c is the thruster exhaust velocity. Since the propulsion module is independently trading the performance of chemical and electric propulsion systems, the propellant mass calculation is performed for three characteristic thrusters. For station-keeping and orbital maneuvering, a monopropellant hydrazine thruster is the preferred engine, while arcjets and Hall Effect thrusters are candidate electric propulsion solutions.[45,46]

Table XXIV: Performance characteristics for various thrusters[45,46]

Thruster	Isp (sec)	Propellant	Reference
Monopropellant Hydrazine	230	N_2H_4	Sutton
Arcjet	1000	H_2	Lozano
Hall Effect	1800	Xe	Lozano

The volume of the propulsion system is determined by the propellant mass fraction and propulsion system type. For the chemical propulsion design option, hydrazine is used as the propellant and has a density of 1011 kg/m^3. Additionally, a tank containing a pressurized inert

gas (likely helium) will be needed to provide the desired mass flow rate of hydrazine. The specific volume (per unit spacecraft mass) can then be calculated as:

$$V_{chem} = \frac{m_{prop}}{\rho_{N_2H_4}}$$

$$v_{chem} = V_{chem}/m_{total} = \frac{1}{\rho_{N_2H_4}}\left(\frac{m_{prop}}{m_{total}}\right)$$

<div align="right">Eq. 28</div>

For the pressurization system:

$$\frac{m_{gas}}{m_{total}} = \frac{p_p v_{chem}}{RT_0}\left(\frac{\gamma}{1 - p_g/p_0}\right)$$

<div align="right">Eq. 29</div>

where p_p is the pressure in the propellant tank, v_{chem} is the specific volume of the propellant tank, p_g is the final pressure in the gas tank, and p_0 is the initial pressure in the gas tank. Values for the aforementioned variables were collected from Tables 6-3 of Sutton[45], and are summarized below in Table XXV.

Table XXV: Values for pressurization system variables

Variable	Value
P_p	1 atm (101 kPa)
P_g	1 atm (101 kPa)
P_0	3600 psi (2.5 MPa)

The total mass fraction for the chemical propulsion system is therefore the sum of the propellant specific mass and the pressurization system specific mass.

$$\frac{m_{chem}}{m_{tot}} = \frac{m_{propellant}}{m_{total}} + \frac{m_{gas}}{m_{total}}$$

<div align="right">Eq. 30</div>

For the electric propulsion design case, if one assumes a particular exhaust gas, with a molar mass of M_{gas} and a tank pressure of P, then the specific volume (per unit spacecraft mass) can be calculated from the ideal gas law as:

$$PV = m \left(\frac{\mathcal{R}}{M_{gas}} \right) T$$

$$v_{elec} = \left(\frac{m_{prop} R_{spec} T}{P} \right) \Big/ m_{total} = \left(\frac{m_{prop}}{m_{total}} \right) \left(\frac{\mathcal{R}T}{M_{gas}P} \right)$$

<div align="right">Eq. 31</div>

5.3.3.5.4 <u>Power and Thermal</u>

Values for average power consumption and efficiency for each thruster were taken from Table 19-7 of Wertz[30], and are replicated in Table XXVI below. No power data was found for the monopropellant hydrazine thruster. It was assumed that since the propellant is gas-pressurized and undergoes catalytic decomposition, power would only be needed to actuate the flow valves, which is negligible compared to the power required by electric propulsion systems.

Table XXVI: Power consumption and efficiencies for selected thrusters

Thruster Architecture	Power Required (W)	Efficiency
Monopropellant Hydrazine	0	0.9
Arcjet	1000	0.4
Hall	1000	0.5

Average power dissipated was calculated based on the thruster efficiency and the input power, per the equation below

$$P_{dissipated} = (1 - \eta) \times P_{input}$$

<div align="right">Eq. 32</div>

5.3.3.6 *Power Subsystem Module*

The electrical power system generates, stores, regulates, and distributes electrical power to instruments and other subsystems. Electrical power is vital for the operation of the whole spacecraft. If there is a fault in the power system, all the other systems are lost including the mission. Challenges for the power system include maximizing efficiency, safety, reliability, and radiation tolerance. Providing a solution with minimal mass, volume, thermal characteristics, and costs is of extreme importance. The power subsystem analysis relies on several important informed assumptions. These suppositions build upon several operational aspects of the telescope. For future explorations and research these assumptions will have to be revised to make sure the model is still accurate. A list of the assumptions made for the power system is presented:

- The telescope will operate in a halo orbit around Sun-Earth L2, the spacecraft will orbit around this point at a radius much bigger than the Earth. This position is very benign for the power system since it guarantees a constant solar flux with no eclipses, the large radius of the orbit also ensures the antumbra of the Earth does not obstruct solar flux reaching the solar panels. This advantage simplifies the solar array design along with the power storage unit (batteries).

- One of the architectural decisions is modularity. It was decided to model the power system as one module always. Its importance and size govern this decision. It is illogical to replace each individual solar cell when all of them will have the same level of degradation; same logic applies to the batteries. Power distribution systems will reside in each spacecraft module; this will allow servicing them in each segment, where they will be grouped with components that have similar failure rates. The power distribution scheme will be similar to a decentralized power architecture.

- For this study all the spacecraft subsystems will be considered as a constant power demand system except for communications. Uploading and downloading data to the telescope will have a very profound effect on the peak power demands and therefore on the battery capacity. This implies that the communications system is the only one that has an effect on the battery sizing. To be more accurate, a small fraction (10%) of the total power demanded by the subsystems is stored on the batteries as a safety measure. Parameters of the communications system that affect the battery design are peak power demand, frequency of download, and download time. State of the art lithium-ion batteries will be evaluated for this study.

- Solar arrays analysis is simplified due to the advantageous orbit of the spacecraft. The sun always points in the same direction during operation and there are no eclipses. Following these characteristics the solar panels are fixed within the spacecraft and do not rotate or track the sun. Educated predictions on the performance of triple junction GaAs solar cells for 2020 are used on the model.

- Besides power generation and storage, electricity has to flow to every subsystem that needs it. Distribution takes an important role on the whole system design. Since the specific electrical requirements of each subsystem are not known, the model relies on a general factor based on the total power generated. The factor is derived from averaging previous space missions, specifically the distribution mass per watt. This factor is the one with the most uncertainty on the power model. Further work and research can be done to model the distribution system with better accuracy.

Due to our trade study architecture with no feedback loops, the power system is responsible for generating an estimate of the mass and volume for the spacecraft taking into account each system electrical requirements. The structures and thermal subsystems (located lower on the N^2 diagram than power) will require a way to calculate the mass and volume needed for the power system once the electrical power equations have been solved. The best approach is to use a non-dimensionalized volume and mass factor with units of kg/watts and m^3/watts respectively. The solution will provide the most accurate results based on the total power requirements of the spacecraft.

The following metrics will evaluate the performance of the electrical power system.

5.3.3.6.1 Power and Power generation
Generating enough power for all the subsystems is a vital element in the design. Power scheduling is also included in this metric (only communications subsystem is taken into account for power budget). To calculate the total power, all the power requirements of the subsystems are added together plus the power required to charge the batteries.

$$TotalPower = (Power_{Subsystems} + Battery_{ChargingPower})$$

<div align="right">Eq. 33</div>

The power allocated to the batteries is based on the assumption that communications will happen few times a day, and not on a regular schedule. Therefore it is assumed that the battery has to be charged each day, giving 24 hours of allowable charging time. The battery power required is listed in Eq. 36, and it is derived from the communications peak power demand requirements. The next step is to calculate the array's specific power. This is a factor that takes into account the amount of solar flux available at the operation point, the efficiency of the solar cells used and the degradation by radiation at the end of life,[47]

$$ArraySpecificPower = SolarFluxL2 * ArrayEffieciency(1 - Degradation)^{ServicingPeriod}$$

<div align="right">Eq. 34</div>

Using this factor the total solar array area needed is calculated as follows:

$$Area_{Array} = \frac{TotalPower}{ArraySpecificPower}$$

<div align="right">Eq. 35</div>

As mentioned previously solar flux will be constant, batteries are only needed for peak power demands. The only system that has considerable peak power demands is the communication subsystem. A safety margin will be added to the battery capacity in order to accommodate unplanned peak demands. The servicing frequency drives the Depth of Discharge (DOD) for the energy storage system. A relationship of DOD and number of cycles is calculated from SMAD.[47] Using this relationship, an allowable DOD is calculated from number of cycles required:

$$BatteryCapacity = (1 + (1 - DOD))(PeakPower * PeakPowerTime * PeakPowerFrequency)$$

<div align="right">Eq. 36</div>

5.3.3.6.2 Lifetime/MTBF
Few systems really dictate the lifetime of the mission, power is the most obvious one. Being able to generate the necessary power for the required time generates constraints in the power generation scheme and size. This metric will measure the power generating performance of the system at the beginning and end of life. The system will be designed to be replaced with a predetermined servicing frequency. Servicing frequency will act as the lifetime of the whole system due to inherent degradation.

5.3.3.6.3 Mass
The mass of the power system will be dependent on the amount of power needed. The solar array plus all the necessary power switches, distribution systems, batteries, harness overhead, and different voltage buses will account for the total mass of the system. The total mass is calculated by adding the solar array mass, the energy storage unit mass, and the overhead mass. These are the main divisions of the power system.

$$TotalMass = ArrayMass + BatteryMass + OverheadMass$$

<div align="right">Eq. 37</div>

Array mass is calculated using a specific mass factor extracted from SMAD[47] also taking into account the inherent degradation and the lifetime of the system. State-of-the-art triple-junction Gallium-Indium cells will be considered for this study.

$$ArrayMass = \frac{SpecificMass*PowerRequired}{(1-Degradation)^{Servicing\ Period}}$$

<div align="right">Eq. 38</div>

A similar approach is used to calculate the battery mass, using Lithium-Ion cells.

$$BatteryMass = \frac{Capacity}{SpecificEnergy}$$

<div align="right">Eq. 39</div>

The mass of power switches, distribution systems, and harness overhead are difficult to calculate without going into a detailed component design, which is out of scope of this study. A standard factor will be used taking into account the solar array mass. Previous space missions have provided information that suggests that the overhead mass is proportional to the power required by the spacecraft and therefore the solar array mass. The overhead mass factor is extrapolated from SMAD data.

$$OverheadMass = ArrayMass * OverheadMassFactor$$

<div align="right">Eq. 40</div>

5.3.3.6.4 Volume
The volume of the power system will be dependent on the amount of power needed. The solar array plus all the necessary power switches, distribution systems, modularity overhead and different voltage buses will account for the total volume of the system. The available volume is calculated in the same fashion as the mass metric.

The total volume of the system is divided by the array, batteries, and overhead parts.

$$TotalVolume = ArrayVolume + BatteryVolume + OverheadVolume$$

<div align="right">Eq. 41</div>

The array volume is calculated by multiplying the array area by the array thickness. Thickness is derived from SMAD information.

$$ArrayVolume = ArrayArea * ArrayThickness$$

<div align="right">Eq. 42</div>

Similar to the mass metric, the volume of the energy storage system is calculated using a power density factor taken from SMAD.

$$BatteryVolume = Capacity * PowerDensity$$

<div align="right">Eq. 43</div>

Following the mass metric, the overhead volume is derived using an overhead volume factor, extrapolated from previous space missions.[47]

$$OverheadVolume = TotalPower * OverheadVolumeFactor$$

<div align="right">Eq. 44</div>

5.3.3.7 Thermal Subsystem Module

In order to control the temperatures of the many critical subsystems on the spacecraft, paths for heat transfer will need to be designed in or around the assemblies throughout the space telescope. Different thermal control concepts will provide varying degrees of thermal balance, where thermal control mechanisms must be selected to maintain a component within its operating temperature range. Thermal balance is dictated by the following equation:

$$Q_{abs} + Q_{diss} + Q_{design} = A_r \varepsilon \sigma T^4 = Q_{emit}$$

<div align="right">Eq. 45</div>

where Q_{abs} is the heat energy absorbed from the environment, Q_{diss} is the internal heat energy from dissipated power loads, Q_{design} is the heat energy that is put in or taken out of the system by design (by a thermal control mechanism), A_r is the radiative surface area, ε is the emissivity, σ is the Stefan-Boltzmann constant, and T is the desired operating temperature. Typically, this equation is used to compute a temperature for a given thermal design; this model does the opposite by computing how much energy must be applied or removed in order given a desired operating temperature. Also, thermal modeling typically performs this calculation over a range of environmental absorption and internal power load conditions; however, this model assumes these conditions to be constant.

For this paper, the spacecraft's thermal control was designed separately for three thermal-evaluation blocks: (1) the Optics block, which is chiefly focused on controlling the temperature of the primary mirror; (2) the Instruments block, which contains three instruments to be kept at room temperature and one IR instrument to be kept near 60 K; and (3) the Bus block, which focuses on the electronics associated with the ADCS, avionics, communications, power, and propulsion subsystems. The differences in how each thermal-evaluation block is handled within the thermal subsystem module code are shown in **Table XXVII**.

The heat energy absorbed by each thermal block is dictated by the following equation:

$$Q_{abs} = SA_p\alpha$$

<div align="right">Eq. 46</div>

where S is the absorbed flux from the environment (assumed in this case to only be from the sun), A_p is the external surface area projected towards the flux source, and α is the absorptivity. The Optics block and the Instruments block area assumed to be behind a thermal shield, blocking the absorbed flux from the sun at a designed efficiency. For this project, this shield efficiency

was assumed to be 80%. For several reasons (primarily thermal isolation), the Bus block is not assumed to be behind the thermal shield. However, the Bus block is assumed to be marginally shielded by the solar-cell arrays. Thus, a shielding efficiency of 50% is assumed for reduction of solar flux on the Bus block.

The internal heat energy from dissipated power loads for each thermal block is computed by the following equation:

$$Q_{int} = \sum \left[(1 - eff)P\right]_{subsys}$$

Eq. 47

where *eff* is the energy conversion efficiency of a given subsystem, and *P* is the average power draw of that subsystem. These values are summed up for each subsystem present per block. The Optics block is assumed to have zero power draw, the Instruments block adds up the power draw of each instrument, and the Bus block adds up the power draw from the ADCS, avionics, communications, power, and propulsion subsystems.

The desired operating temperature of a given thermal block is selected by first determining the restrictive operating temperature range for a given thermal block. This is done by selecting the highest minimum threshold from all of the subsystems within the block as the minimum restrictive operating temperature, and the lowest maximum threshold as the maximum restrictive operating temperature. For the Optics block, the mirrors are assumed to be operated near room temperature (between 22 and 24 degrees Celsius), just as Hubble's mirrors are. The Instruments block only considers the single cryogenic instrument's temperature range, assuming that the other instruments thermal control will be eclipsed by the cryocooling for the IR instrument. The Bus block considers the operating temperature ranges from the ADCS, avionics, communications, power, and propulsion subsystems. Now, an all-encompassing operating temperature range has been established for all of the components/subsystems within the thermal block. The desired operating temperature is simply the average value of this restrictive range. An additional estimation is made for the radiative surface area, A_r, and the surface area projected towards solar flux, A_p, of each thermal block. These surface areas are estimated using the volume of each subsystem, where each subsystem is modeled as a cube. In the case of the Bus block, the propulsion subsystem (dominated by the propellant tanks) is not considered in the area calculations.

Each thermal block contains one heating mechanism, one cooling mechanism, and a package of thermal sensors. **Table XXVII** displays the heating and cooling mechanisms per thermal block. Because this thermal model does not evaluate performance over a range of variable conditions, either a heating mechanism is selected for thermal balance, or a cooling mechanism. In other words, the model does not account for a thermal block requiring both heating and cooling needs. The quantity of a heating or cooling mechanism is determined to satisfy the requirement set by solving for Q_{design} in Eq. 45.

The Instruments and Bus blocks are modeled to have a variable quantity of thermal blankets for insulation and shielding. Thermal blankets are employed on the entire surface area of the Instruments block, and any surface area of the Bus block not used for an external radiator. In total, there are 11 thermal component families that can be selected for a given spacecraft architecture design: 3 heating mechanisms, 3 cooling mechanisms, 3 suites of thermal sensors,

and 2 thermal blankets. See the Components Database in Appendix C to see individual properties of each thermal component family.

Table XXVII: Summary of Thermal-evaluation Blocks and Assumptions

	Optics Block	Instruments Block	Bus Block
Contents	Primary mirror and optical train to instruments	3 Instruments at Room Temperature, 1 Instrument at 60 K	Electronics from ACS, Comm, Avionics, Power, and Propulsion
Heating Mechanism	Thermostatic Heater(s)	Thermostatic Heater(s)	Thermostatic Heater(s)
Cooling Mechanism	Thermoelectric Cooler(s)	Cryocooler(s)	Heatpipes + Radiator
# of Thermal Sensors	150	50	75
Thermal Blankets	--	Yes	Yes
Absorptivity	0.06 (gold coating)	0.05 (thermal blanket)	0.05 (thermal blanket)
Emissivity	0.02 (gold coating)	0.02 (thermal blanket)	0.02 (thermal blanket)
Solar Shielding	80% shielded by thermal shield	80% shielded by thermal shield	50% absorbed by solar-cell arrays

The mass, power, volume, and lifetime performance metrics have been selected as most relevant to the thermal considerations of a next-generation space telescope design. Each metric will dictate the cost and certain design and development choices for the overall spacecraft, and will thus be used to determine and compare the values of varying architectures within the tradespace. The main resources for estimating the values of these metrics and other properties of the thermal control mechanisms (e.g., emissivity and absorptivity of the thermal blankets) are the *Spacecraft Thermal Control Handbook* by Gilmore[48] and Donabedian[49], along with parameterization from previous space telescope designs[50,51] and currently available technologies[52]. Validation of the thermal subsystem code module was performed by comparing mass and power output metrics to true values for the Hubble Space Telescope and the James Webb Space Telescope.

5.3.3.7.1 <u>Mass</u>

Different thermal control concepts will contribute varying ranges of mass to the overall spacecraft, though it is not as simple as claiming passive components to be less massive than active components. For instance, a network of heat pipes leading to external radiators (passive) could be more or less massive than a thermal fluid loop (active) depending on the size, quantity, and degree to which components need cooling. However, because this model has been simplified to only consider a single heating mechanism or cooling mechanism in order to satisfy the thermal balance, mass is not traded over various thermal design concepts. Instead, it is simply summed up over the selected number of components, by the following equation:

$$mass_{total} = \sum_{i=1}^{n_{components}}(mass_i)$$

<div align="right">Eq. 48</div>

The mass of individual thermal component families is catalogued in the Components Database, which can be seen in Appendix C.

5.3.3.7.2 Volume

Similar to mass, different thermal control concepts will demand varying ranges of volume from the overall spacecraft. The total volume of the thermal subsystem is computed by adding up the selected number of components, by the following equation:

$$volume_{total} = \sum_{i=1}^{n_{components}}(volume_i)$$

<div align="right">Eq. 49</div>

The stowed volume of individual thermal component families is catalogued in the Components Database, which can be seen in Appendix C.

5.3.3.7.3 Power

Power is another performance metric that is dependent on the types of thermal control components that will be used to maintain thermal stability for all components. Most active thermal control components, such as thermo-electric coolers, pumped fluid loops, and heaters, require power to operate, while passive thermal control components do not. The total average power draw of the thermal subsystem is computed by adding up the selected number of components, by the following equation:

$$power_{total} = \sum_{i=1}^{n_{components}}(power_i)$$

<div align="right">Eq. 50</div>

The average power draw of individual thermal component families is catalogued in the Components Database, which can be seen in Appendix C.

5.3.3.7.4 Lifetime/MTBF

The lifetime metric is of particular interest to the overall mission of the space telescope, as the lifetime of thermal components will directly affect the lifetime of the on-board instruments. The mass, volume, and power metrics are directly affected by the reliability requirement (design constant) of the spacecraft architecture, where redundant units of a component family are designed into the spacecraft in order to satisfy the minimum reliability threshold, increasing the total mass, volume, and power of the thermal subsystem. The lifetimes of individual thermal component families is catalogued in the Components Database, which can be seen in Appendix C. The Mean Times Between Failures (MTBF) of individual thermal component families is derived using the following equation:

$$MTBF = \frac{-lifetime}{\ln{(reliability)}}$$

<div align="right">Eq. 51</div>

The reliability of individual thermal component families is also catalogued in the Components Database.

5.3.3.8 *Structures and Mechanisms Subsystem Module*

The Structures and Mechanisms team is responsible for analyzing the structural components of the telescope and the mechanisms that actively modify the shape or performance of the structural elements. Consequently, the team is generally responsible for giving the telescope its overall shape and support, from integration into the launch vehicle through launch and transit to its operating orbit, to its assembly, operation, and periodic servicing.

For the telescope on which the MIT team is conducting a tradespace analysis, the Structures and Mechanisms team has developed a suite of MATLAB functions that analyzes the metrics of: the level of jitter of the primary mirror; the mass, volume, and power of all structures and mechanisms; and the precision of assembly in assembling the structure for operation. Additionally, the telescope is divided into modules according to the aforementioned modularity metric. These metric functions are subsequently incorporated into the system level analysis MATLAB scripts in order to automate the analysis of the full tradespace for the telescope. This tradespace is fed a series of trades from each subsystem, and the Structures and Mechanisms team has generated a collection of trades that are analyzed by the Structures and Mechanisms metrics in the full code. Therefore, with these metrics, architectural decisions can be evaluated in a Pareto front analysis at the full system level.

5.3.3.8.1 <u>Structures and Mechanisms Code Description through Assumption and Component Selection</u>

The Structures and Mechanisms subsystem has a wide array of possible components from which to incorporate into the overall components vector for the telescope. The architectural decisions guide the determination of the structural components and the mechanisms required to operate the telescope. The Components Family DB contains the full properties of each of these components and the values assigned for each parameter. Though hardcoded in the database, they can easily be changed from their values, which have been determined through analysis of historical components and structures, if more accurate data are provided in the tradespace study.

5.3.3.8.2 <u>Mirror Actuation</u>

The mirror support decision constitutes one of the driving architectural decisions for the Structures and Mechanisms subsystem because of the number of components that are added to fully actuate the mirror. The mirror can be actuated with surface-normal actuators, surface-parallel actuators, or a combination thereof, with surface-parallel actuators having a TRL value of 5 (as opposed to flight-proven TRL 9 surface-normal actuators) because they have not yet flown on large space missions. Table XXVIII shows the number of these actuators that are employed to shape the primary mirror based on the mirror support architectural decision chosen for a particular iteration.

Table XXVIII: Number of primary-mirror actuators for mirror support architectural decision

	Surface-Normal Decision	Surface-Parallel Decision	Combination Decision
Surface-Normal Actuators	252	0	144
Surface-Parallel Actuators	0	306	168
Total	252	306	312

As can be seen in this figure, the total number of actuators is least for the surface-normal decision, but highest for the decision to incorporate both surface-normal and surface-parallel. Importantly, a backstructure element is added for each mirror segment in both the surface-normal and combination architectural decision cases in order to provide a structure against which the surface-normal components could actuate. In the surface-normal case, seven degrees of freedom are achieved per mirror segment with the total number of actuators representing seven surface-normal actuators for each of 36 mirror segments. In the surface-parallel case, three actuators are used at each of 84 mirror segment boundaries, one actuator is used on the back of each mirror segment for segment curvature, and an additional actuator is given to the 18 segments on the outer ring because of the decreased number of segment neighbors. In the combination case, four surface-normal actuators are placed at each mirror segment, and two surface-parallel actuators are placed at each of the 84 mirror segment boundaries. In this manner, it is believed that full 7-degree-of-freedom motion can be attained by any mirror segment. These placements can easily be modified to incorporate better placement data to improve the model.

5.3.3.8.3 Secondary Mirror

Secondary mirror components are added to complete the optical train. A single mirror segment with a back frame element is used to represent the secondary mirror, and three bus structure elements are added in order to represent the booms that hold the secondary mirror in place. The mirror segmentation architectural decision also affects the support of the secondary mirror, so additional surface-normal and surface-parallel actuators are added to provide action to the secondary. It is believed that full seven degree-of-freedom is achieved using the coded numbers of each: seven surface-normal, 18 surface-parallel, and a combination of six surface-normal and six surface-parallel actuators for the three mirror support decisions, respectively. Again, it is trivial to modify these values as additional information regarding mirror support with surface-parallel actuators is included in the model analysis.

5.3.3.8.4 Communications Structure and Mechanisms

The communication architecture decision affects the number of gimbals, antenna deployment devices, and added bus structure mass in the Structures and Mechanisms code. The number of gimbals is incremented by two in each decision to account for the requirement that each antenna will need to be pointed in different directions than the optical direction of the telescope to allow for communications to occur. Additionally, the number of antenna deployment devices is incremented by two in order to deploy the antennas when the telescope is operational. To account for the increased structural support for the larger antennas required for all

communication types relative to laser communications, an added bus structure element is added to represent the added mass of this structural support.

5.3.3.8.5 Solar Array Gimbals

Gimbals are added not only for the antennas required for communications, but also for the solar panels. It is assumed that one gimbal is required for every kilowatt of generation power. These gimbals are added to allow the solar panels to track the sun for optimum power generation capability while the telescope is pointed in a different direction. Additionally, these added gimbals increase the jitter during operation, so a damper is added to the telescope architecture for each.

5.3.3.8.6 Jitter Control Devices

Determining the type of jitter control device to employ is based on the level of jitter as output from the separate jitter calculation code. A telescope was analyzed to determine the fundamental frequencies of the mirror and the wavefront error that is expected. Using these values, the jitter function generates a value for jitter to be used in the Structures and Mechanisms code. This value then determines the type of damper to be used, either magnetic isolation devices for jitter values less than 0.5, active dampers for jitter values above 1.5, or viscoelastic devices for all other jitter values. These three types of dampers are used because they represent three of the most common types of dampers used on spacecraft; their effective jitter ranges can be easily adjusted in the code in order to specify certain types or part numbers of each. Since the jitter is caused primarily by reaction wheels and gimbals, one damper of the jitter-level-determined type is added for each reaction wheel and gimbal included in the telescope.

5.3.3.8.7 Modularity Level Overhead Mass

The modularity decision is crucial in determining the overhead mass required for increasing the number of modules into which the telescope is divided. To obtain the mass overhead itself, the number of additional mass units, each 100 kg, was to be determined. By analyzing the increasing surface area cubes within an initially cubic structure, following the pattern of $8^{number\ of\ cubings}$ (1, 8, 64, etc.), with the *number of cubings* representing the number of times each cube was divided into eight cubes of identical volume, it was determined that the increase in surface area follows the following equation:

$$Mass_{added} = 6x^{1/3}$$

<div align="right">Eq. 52</div>

In this equation, *Mass_{added}* represents the added number of mass elements added for the *x* number of modules. By determining the mass overhead after the modularity creation script is run, it is possible to adjust the mass overhead to each particular architecture. Eq. 52 was derived from comparing the ratio of surface area to volume, which means that it represents a square/cubed law. Therefore, the added mass is hardcoded into the code for each modularity level, though it is possible to add a more continuous and module size dependent model in the future.

5.3.3.8.8 Assembly and Servicing Components

The assembly/servicing technique architectural decision causes a large variability in the number of components due to the method selected for aggregating the modules together. In order to assemble the telescope with the first technique, the use of telescope robotic arms, it is assumed

that 1 arm is able to maneuver 10 modules, and each module includes 2 docking ports. Therefore, the number of arms is 1/10 the number of modules that are created in the module creation function. Additionally, it is assumed that all docking ports are of the same size and load-bearing capacity. With these assumptions, the number of docking ports is twice the number of modules. In the second technique, the use of a separate servicer tug, arms also are used on the telescope to assist, and each module requires 2 docking ports. However, it is assumed that there is 1 arm per 20 modules because of the added capabilities of the tug itself. In the third technique, the use of self-assembling modules which maneuver with electromagnetic coils, it is required that each module be able to maneuver in all 6 degrees of freedom. Therefore, each module is equipped with 3 electromagnetic coils, which when assembled would be mounted orthogonal to one another. Additionally, it is again assumed that each module is equipped with 2 docking ports. Regardless of the number of docking ports, the numbers of power and communication interfaces are equal to the number of docking ports, since each docking port must be associated with both communications and data transfer capabilities. The code is able to add additional granularity, should it be required, because the modularity level can affect these current multiplication factors in determining the number of components per module. To cope with future changes, this section is already coded in a way that will allow separate component selection laws to be implemented for the seven different modularity levels.

5.3.3.8.9 Light Protection
A light shield is included to provide light protection for the optical train and instruments. The ATLAST light shield offers a baseline for the properties of the light shield.[53] The other method of light protection, a tubular baffle, is encoded in the Structures and Mechanisms code, though it is not incorporated into this model. The design parameters for the baffle are obtained by scaling the Hubble Space Telescope's baffle by the increased radius of the LTA design.[54] The specific mass, volume, and other properties are listed in the Components Family DB. Therefore, the analysis code is able to adjust as needed to an additional architectural design choice in future iterations of the code. The analysis team has made the assumption for the current analysis that only the light shield will be incorporated.

5.3.3.8.10 Structures and Mechanisms Subsystem Metrics
The Structures and Mechanisms subsystem metrics are determined once all of the structural components have been selected. Using the Components Family DB, it is possible to determine the mass and volume of the subsystem directly by summing the dot product of the structures components vector with the respective column from the database. The average and peak power of the Structures and Mechanisms subsystem, however, adds the power required to operate the Communication subsystem's antenna gimbals to the structures specific component power requirements because of the validation method chosen: since the Hubble Space Telescope included the mass of the gimbals in the Communication subsystem, the mass is treated as a Communications property, but the power is treated as a Structures and Mechanisms property because it is from a Structures and Mechanisms component family.[54]

5.3.3.8.11 Finalizing Module Definitions
The last operation conducted by the Structures and Mechanisms subsystem is to call the module creation function. Though called once before to determine the number of modules in the subsystem code, it must be called again to place the components added to the telescope after the initial call into module. These added components include the bus structure overhead based on

modularity level, robotic arms, docking ports, electromagnetic coils for assembly and servicing, and docking port data and power transfer units. Once these components are placed into their proper modules according to modularity level, this information is passed to the Systems function.

5.3.3.8.12 Finite Element Model

Accurate imaging through a space-based telescope requires very accurate pointing of the optical telescope assembly. Any oscillations in the primary mirror will cause wavefront error and therefore limit the science output. Thus, the amount of jitter that the mirror experiences due to reaction wheels, thrusters, or other active components on the spacecraft bus is important to quantify. In order to quantify this behavior, a finite element model (FEM) of the system must be created to analyze how vibrations in one area of the spacecraft affect motion in another area through a normal modes analysis.

5.3.3.8.12.1 Creating the Model of the Telescope

In this modeling scenario, it is important to simplify the model to a level of abstraction that will be relatively constant between the different architectures, but be able to differentiate between all combinations of the segmentation of the primary mirror and primary mirror actuation method architectural decisions. At this stage in the trade study, the structural design of the telescope bus has not been developed, so the 36-segment, 16.8-m mirror must remain the primary focus of the model. The bus is modeled as a concentrated point mass representing the sum of subsystem masses. The effective response of the reaction wheel set accounting for damping comes out of this bus node. This is the disturbance input to the jitter analysis. The model also takes the primary mirror actuation method and the segmentation of the primary mirror as inputs. In general, these inputs affect the FEM according to the diagram in Figure 38.
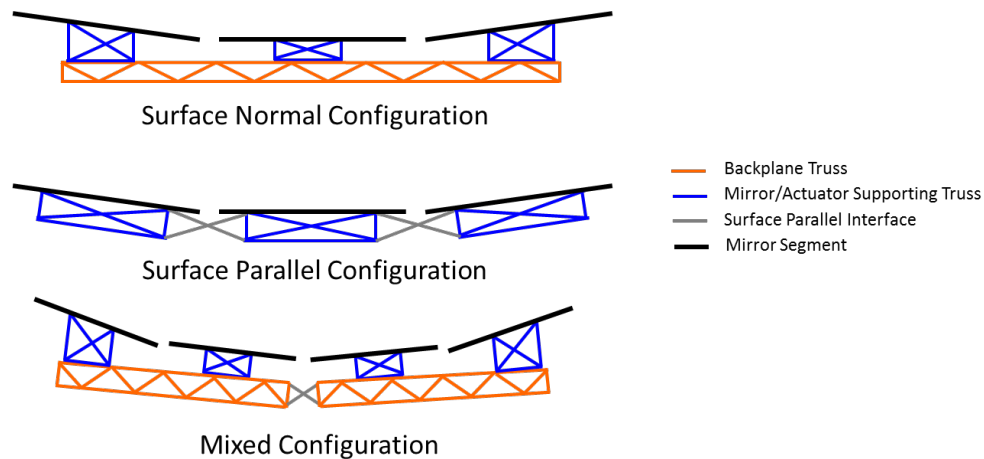
Figure 38: Simplified visualization of surface-parallel vs. surface-normal configurations in the FEM

The mixed configuration assumes that each major segment, or raft, from the segmentation of the primary mirror architectural decision will use surface-normal actuation internally, but surface-parallel actuation is used between rafts. The trusses in Figure 38 show a visualization of the layout of connections only, and do not reflect actual truss structural members. Not all segments or mirrors are pictured in these diagrams for simplicity. To simplify the model, each segment of the mirror is considered to include and represent the mass and stiffness of a primary mirror

segment, its actuators and its individual backstructure. The connections between segments represent the overall backstructure stiffness and vary based on the architecture decision to be more or less stiff.
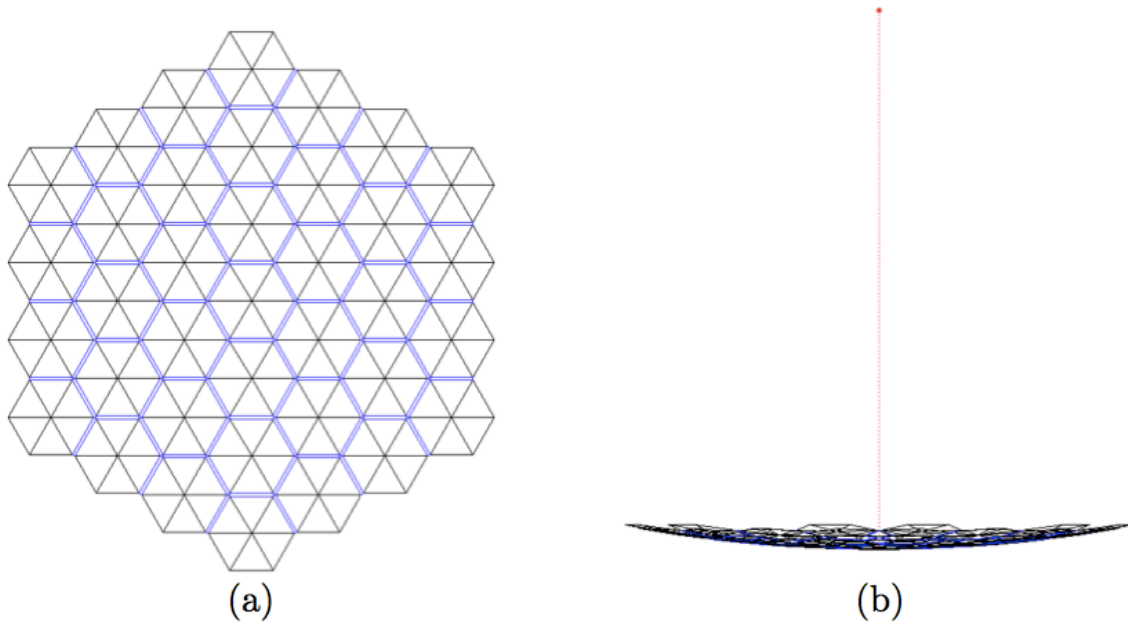
Figure 39: Primary mirror mesh for the FEM of the 16.8-m, 36-segment, *f*/1.5 telescope, where (a) is a top-down view and (b) is a side view with the focal point

The primary mirror is divided into 259 nodes or grid points in the mesh. One node is placed at the center of the segment and one node at each corner. These nodes are connected in a series of triangle and quadrilateral mesh elements with corners at the grid points. The final mesh of the mirror is shown in Figure 39, where the black lines show edges of triangle elements and the blue lines show edges of quadrilateral elements. The connection to the bus node is not shown, although the bus is connected with rigid bars to the edges of the first ring in the shown mesh. Shown in Figure 39, each grid point is also displaced vertically corresponding to the telescope's *f*# of 1.5. The quadrilateral elements represent the connection between segments and their properties change depending on the architectural decisions. For example, a surface-normal configuration would have a uniform higher stiffness for all of these quadrilateral elements, while a surface-parallel configuration would have a uniform lower stiffness for all of these elements. In the mixed case, the edges between rafts are considered lower stiffness while internal connections within a raft are considered higher stiffness. See Figure 40, for a depiction of these mixed cases, where red represents the surface-parallel, lower-stiffness interface and the blue represents the backstructure, higher-stiffness interface.
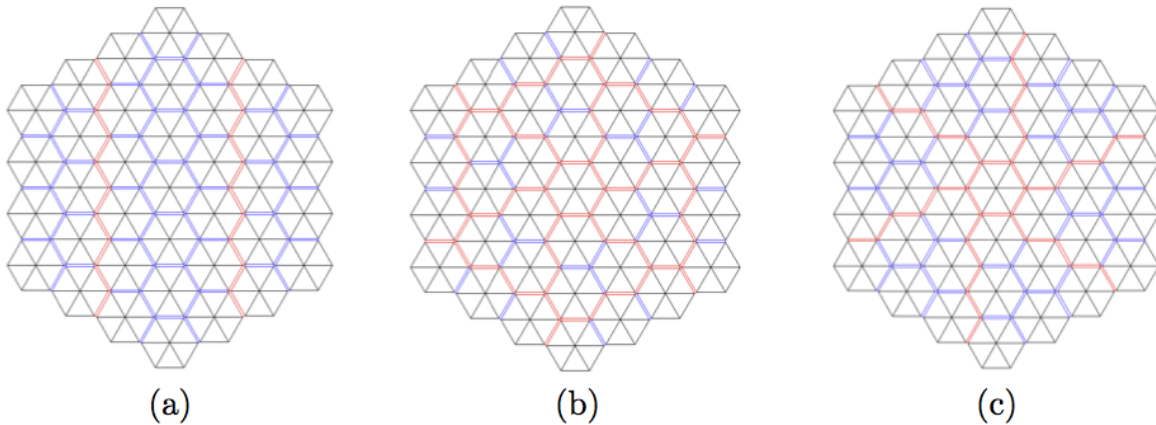
Figure 40: Raft segmentation in the FEM where red shows surface-parallel connection between rafts and blue shows backstructure connection within rafts. Shown for three segmentations where (a) is the JWST-style fold, (b) the 12-segment, and (c) the 6-segment.

5.3.3.8.12.2   Implementation and Output of the Model

The development and coding of this model, mesh and normal modes analysis uses a combination of MATLAB functions and NASTRAN finite element analysis software. The MATLAB functions are used to generate the grid points, elements and material properties for a particular architecture. NASTRAN requires this information to be input in different "cards," along with information on what type of analysis to perform. These cards each need to be written to a data text file before sending to NASTRAN. NASTRAN is executed from the MATLAB function and runs the normal modes analysis on the inputted cards. NASTRAN returns a large text file of output that includes mass properties, normal mode frequencies, and mode shapes for all six degrees of freedom at each node in the model. This text file is subsequently parsed to return a diagonal matrix of natural frequencies and a dense matrix of mode shapes. These matrices are computed for each of the architectural decision options: surface-normal, surface-parallel, and five mixed cases corresponding to the segmentation of the primary mirror options. These seven matrices are output to the jitter calculation code discussed in the next section.

5.3.3.8.12.3   Validation of Results

An important aspect of running this analysis is the verification that the outputted results accurately predict the natural frequencies and mode shapes of the particular architecture. To discuss this, comparisons between previous FEM model outputs and mode shapes must be shown to reasonably match. Scott Uebelhart[55] analyzed a similar space telescope with hexagonal segments in his PhD thesis and saw a first mode of the primary mirror behave as a saddle bending mode at 6.15 Hz. Shown in Figure 41, the model used in the analysis outputs the first saddle bending mode at 6.09 Hz. Also, Rebecca Masterson, in an analysis of an interferometer, reports first bending modes of the mirrors to occur at 5.99 Hz.[56] The remaining modes in the model behave similar to increasing order Zernike polynomials as expected. While this only validates the surface-normal case, due to the lack of information one must assume that the other architecture choices will be correct modifications of this validated model. As expected, architectures with more surface-parallel interfaces tend to react to lower frequency responses. In addition it is important that the model represents an appropriate mass when compared with the telescopes in the architecture enumeration. The average total system mass across all of the

architectures in a full enumeration is 13,982 kg compared to the FEM model average output of 14,379 kg. With a difference of less than 3% from the computed average, it can be said that the model accurately represents the average architecture mass.
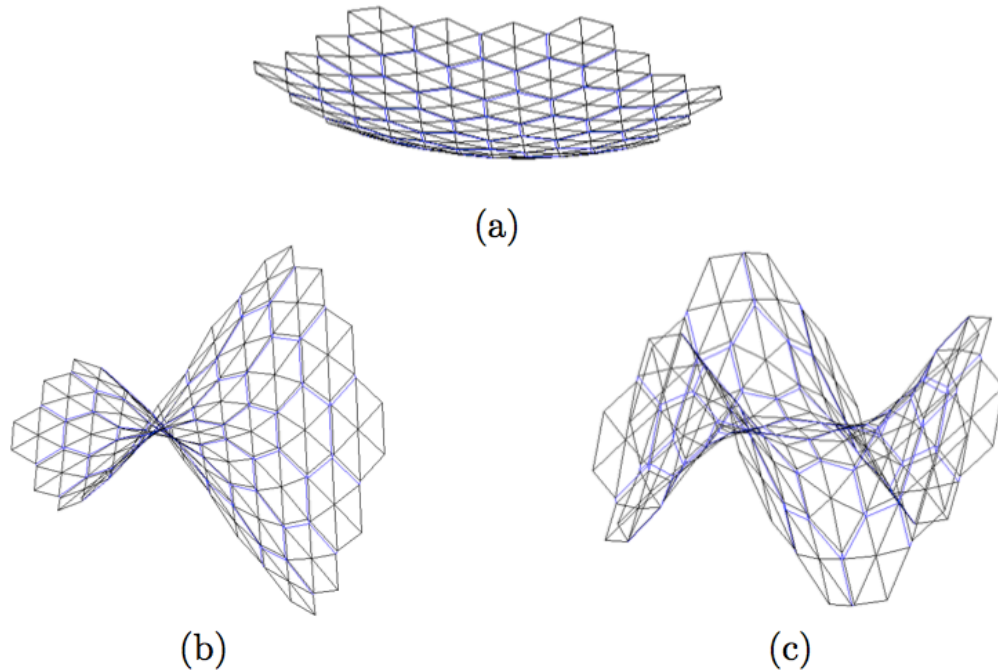
Figure 41: Normal modes for the primary mirror where (a) is the undeflected mirror, (b) is the 6.09 Hz, 1ˢᵗ, saddle bending mode and (c) is the 13.06 Hz, 7ᵗʰ bending mode

5.3.3.8.13 Jitter

The jitter analysis was done in a similar manner as that of Rebecca Masterson**Error! Bookmark not defined.**. The first step in the jitter analysis was to create a Finite Element Model (FEM) to represent the telescope, described in the previous section. Once this FEM was created, there were three important steps to complete the analysis: creation of a transfer function for the system from the disturbance input to the performance outputs, modeling of the disturbance input, and propagation of the disturbance input through the transfer function to calculate the performance outputs.

5.3.3.8.13.1 Creation of the Transfer Function
The normal modes analysis described in the previous section determined the modal frequencies and shapes of the FEM. NASTRAN outputted Ω, a diagonal matrix of natural frequencies, and Φ, which is a matrix containing the mode shapes, for each mirror support and mirror segmentation method, according to the various architectural decisions. These matrices were used to create a state-space model in MATLAB according to Eq. 53 and Eq. 54:

$$\begin{Bmatrix} \dot{q} \\ \ddot{q} \end{Bmatrix} = \begin{bmatrix} 0 & I \\ -\Omega^2 & -2Z\Omega \end{bmatrix} \begin{Bmatrix} q \\ \dot{q} \end{Bmatrix} + \begin{bmatrix} 0 \\ \Phi^T B_{\hat{x}\omega} \end{bmatrix} \omega = A \begin{Bmatrix} q \\ \dot{q} \end{Bmatrix} + B\omega$$

Eq. 53

$$z = \begin{bmatrix} C_{z\hat{x}}\Phi & 0 \end{bmatrix} \begin{Bmatrix} q \\ \dot{q} \end{Bmatrix} = C \begin{Bmatrix} q \\ \dot{q} \end{Bmatrix}$$

Eq. 54

where q are modal coordinates, Z is a diagonal matrix of damping ratios, $B_{\hat{x}\omega}$ is a mapping matrix between the disturbance forces and the physical degrees of freedom, ω is the disturbance input, z is the performance output, and $C_{z\hat{x}}$ is a mapping matrix from physical states to the output.

The matrix Z was set to 0.001 along the diagonal, according to Masterson's thesis**Error! Bookmark not defined.**. The matrix $B_{\hat{x}\omega}$ was set to all zeros with ones along the diagonal of the final six rows, meaning that the six degrees of freedom of the disturbance input map to the six degrees of freedom on the single bus node. Finally, the matrix $C_{z\hat{x}}$ was calculated using the function *zernikes2_hex.m*, taken from code used in an analysis done for the Modular Optical Space Telescope (MOST), which was an MIT Space Systems Laboratory project to develop a parameterized model for large space telescopes.[56] The function *zernikes2_hex.m* takes in each of the grid points used in the FEM, along with the diameter of the mirror, and, using Zernike polynomials 3-48, composes the matrix $C_{z\hat{x}}$. Several of these Zernike polynomials are pictured in Figure 42.
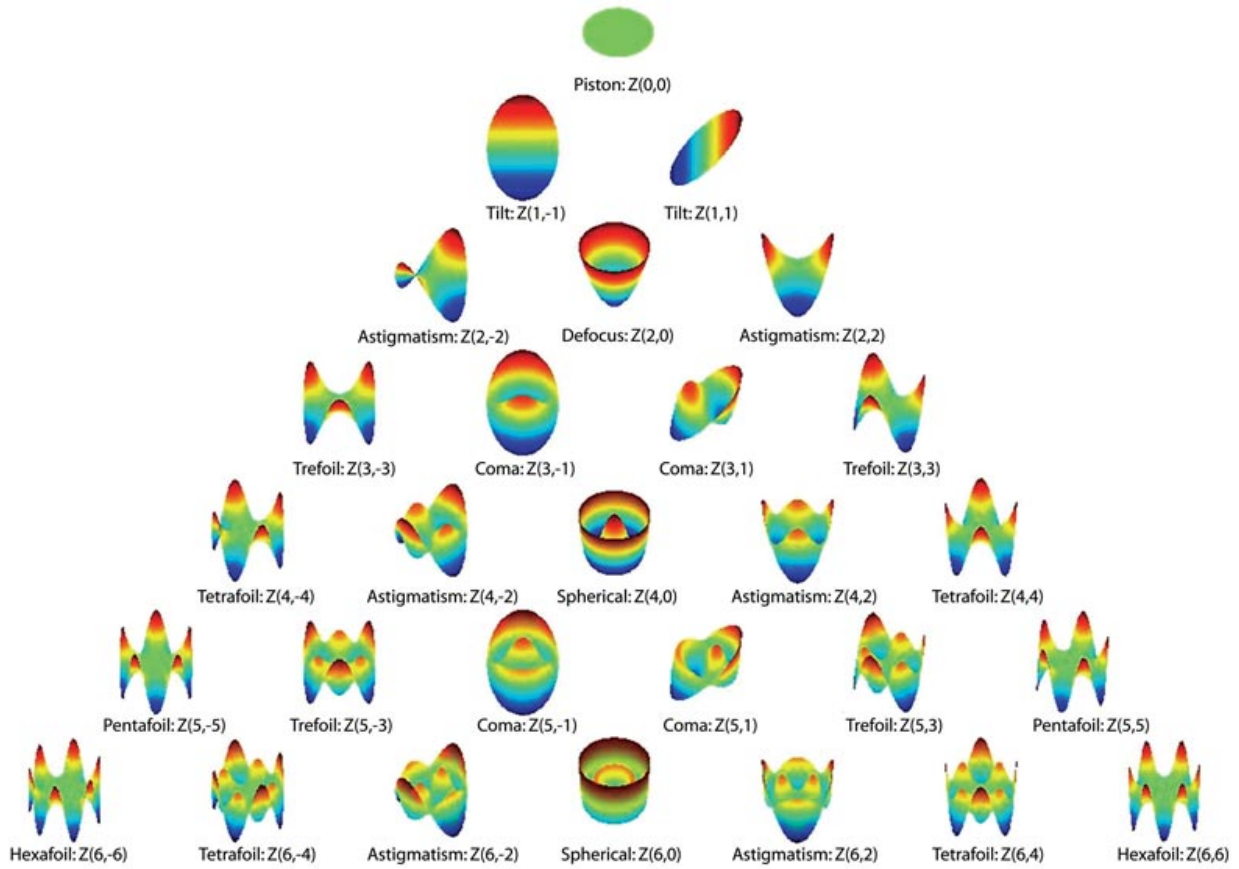
Figure 42: Zernike modes, which describe how a wavefront is distorted by a specific aberration[57]

Matrices *A*, *B*, and *C*, given in Eq. 53 and Eq. 54, are typically combined according to Eq. 55 to generate a transfer function, $G_{z\omega}$.

$$G_{z\omega}(s) = C(sI - A)^{-1}B$$

Eq. 55

For the purposes of this analysis, transfer functions were calculated using a function called *qbode.m*, which was written by Etienne Balmes in 1992. The function calculates the transfer function of the system from each input to each output at each frequency in a frequency vector. This frequency vector was generated using the function *freq_gen.m*, written by Homero Gutierrez.

5.3.3.8.13.2   Modeling of the Disturbance Input

The model was subjected to a single source of vibration for the analysis—a set of reaction wheels located at the single bus node. The reaction wheel assembly is typically considered the dominant disturbance source, which, for the purposes of this study, was modeled according to parameters taken from Ithaco E Reaction Wheel data in Masterson's Master's Thesis.[58] The reaction wheel disturbance Power Spectral Density (PSD) was calculated using the function

psd_rwa_dist.m, written by Gutierrez and modified by Olivier de Weck in 1998. Inputs to the function include parameters taken from Gutierrez's PhD Thesis[59]: nominal reaction wheel speed of 1500 RPM, variation in reaction wheel speed of 1500 RPM, uniform wheel speed distribution, Euler angles from the spacecraft axes to wheel axes, and the type of reaction wheel model. This function output the PSD shown in Figure 43.
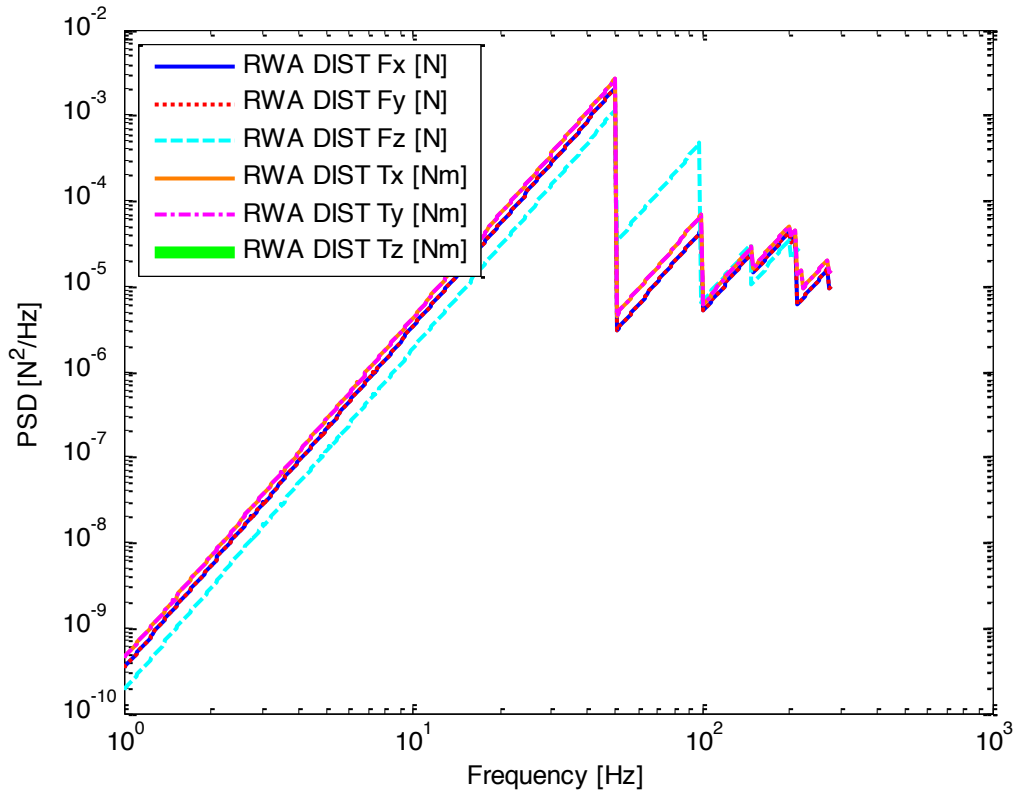
Figure 43: Ithaco E reaction wheel PSD

This figure shows the expected "sawtooth" pattern as seen in Gutierrez[59].

5.3.3.8.13.3 Calculating the Performance Output

With the transfer functions at each frequency and the reaction wheel PSD, $S_{\omega\omega}$, the PSD of the output signal is calculated according to Eq. 56

.

$$S_{zz} = G_{z\omega}S_{\omega\omega}G_{z\omega}{}^{H}$$

Eq. 56

where ( )^{H} is the matrix Hermitian. The output signal PSD, S_{zz}, is then integrated over all frequencies to get the output covariance matrix, Σ_z, as shown in Eq. 57.

.

$$\Sigma_z = \int_{-\infty}^{\infty} S_{zz}(\omega)d\omega$$

Eq. 57

where the diagonal elements of the covariance matrix are the performance variances. This process was taken from Masterson's thesis**Error! Bookmark not defined.**. Finally, the root-sum-square of the performance variances gives wavefront error, in meters.

5.3.3.8.13.4   Results

The requirement on wavefront error, taken from the ATLAST optical performance requirements given in Section 3.2, is 37 nm, with a goal of 0.07 nm. Thus, the output is expected to be near that range. The results for each case are shown in Table XXIX.

Table XXIX: Jitter analysis results*

Primary Mirror Segment Support Method	Structural Segmentation of the Primary Mirror	Wavefront Error [nm]
Surface-normal	36 individual segments	2.12
Surface-parallel	36 individual segments	0.39
Mixed	3 "ring" segments	0.60
Mixed	6 symmetric segments	0.51
Mixed	7 segments (1 large, 6 small)	1.99
Mixed	12 segments	0.45
Mixed	3 JWST-style segments	1.89

*These results are subject to an unknown scaling error suspected to be due to unit mismatch which could not be resolved before the writing of this report. However, comparisons between results are still valid.

These results make sense when compared against each other. The surface-normal segment support method, with its more rigid backplane, translates the jitter though the structure more than the flexible surface-parallel support method, which performs the best. Likewise, the cases in which the primary mirror is divided into many smaller segments perform more similar to the surface-parallel support method than do the cases with only a few segments, such as the JWST-style segments.

According to these results, wavefront error is approximately proportional to the stiffness of the structure. This may be due to the fact that most of the energy from the reaction wheel

disturbances is concentrated at high frequencies, and most of the structural modes with high energy are at lower frequencies. With less stiffness, these structural modes drop in frequency, so the wavefront error scales appropriately.

The calculations were done offline and these results are implemented in the model using a simple switch-case architecture based on the primary mirror segment support method and the structural segmentation of the primary mirror.

5.3.3.8.14 Module Creation Code

As described in Section 4.3.2, the architectural decision about modularity presents seven options: modularity levels 1-7. This section describes how these seven levels were implemented in the code.

The module creation code takes in the overall components and MTBF columns of the component database, the DSM, and the architectural decisions of modularity level and assembly/servicing technique. The output is an m x n matrix containing the module definitions, where m is the number of modules and n is the number of component families in the component database. Therefore, each column represents a module. A sample module definitions matrix is shown in Figure 44.

$$
n = 4 \left\{ \overbrace{\begin{bmatrix} 5 & 0 & 0 \\ 0 & 3 & 1 \\ 0 & 4 & 0 \\ 3 & 1 & 0 \end{bmatrix}}^{m = 3} \right.
$$

Figure 44: Sample module definitions matrix with three modules

In this example, module one contains five instances of component one, zero instances of component two, zero instances of component three, and three instances of component four. Similarly, module three only contains one instance of component two. The module creation code utilizes a switch-case architecture to create the appropriate module definitions matrix depending on the modularity level.

Modularity level 1 is the full telescope (no modularity). Thus, the module definitions matrix for level 1 only has a single column, and that column is simply equal to the overall components column in the component database.

Modularity level 2 is the permanent infrastructure, the instrument package, and the spacecraft bus. Permanent infrastructure components include the bus structure and any instances of the light shield, primary mirror baffle, and secondary mirror segments, which are all placed into module one. All of the instruments are placed into module two, and every component that has not already been dealt with is placed into module three.

Modularity level 3 is the permanent infrastructure, the instrument package, and spacecraft bus assemblies. The permanent infrastructure and instrument package modules are dealt with the same as in modularity level 2. The bus assemblies are broken out according to the following rule: components with connections in the DSM and similar MTBFs are put in the same module (with the exceptions of propulsion components, thermal bus components, thermal optical components, and thermal instrument components, which are placed in their own modules). The code begins by working across each row of the DSM, placing connected components into the same module and components with similar MTBFs in the same module, and placing components into a new module when they have no connections or similar MTBFs as any component already placed in another module. Currently, the code checks to see if the difference in MTBFs between any two components is less than one, effectively checking if they are equal. In the future, this should be modified to be a more meaningful number.

Modularity level 4 is the permanent infrastructure, the instrument package, and spacecraft bus component families. The permanent infrastructure and instrument package modules are dealt with the same as in modularity level 2. Then for each component family not already dealt with, a new module is created.

Modularity levels 5, 6, and 7 are divided the exact same way as modularity levels 2, 3, and 4, respectively, with the only difference being that the four instruments broken out into their own modules for levels 5, 6, and 7.

The final step for each modularity level is to add the appropriate number of assembly/servicing components to each module. Two UDPs are added to each module in every case. One robotic arm is added for every ten modules for each case besides formation flying; in that case, three electromagnetic coils are added to each module.

5.3.3.8.15   Mass

The mass of the structure and mechanisms within the telescope acts as one of the most tractable metrics, since the mass of the system must be kept low for cost, number of required launches, ground operations, and many other areas of the telescope's lifespan.[18,58] The mass is also crucial to determine the inertia of the assembled telescope, which subsequently drives the attitude determination and control design for the spacecraft. Consequently, the mass of the system must be analyzed as one of the key values to be determined by the Structures and Mechanisms team.

To determine the mass of a particular architecture of both the Structures and Mechanisms subsystem mass and the entire telescope mass, two areas of the telescope must be massed and summed: the bus and connecting or supporting structures, as well as the mechanisms aboard the telescope themselves.

The mass of the Structures and Mechanisms subsystem is determined based on the number of components that are selected from the Components Family DB. Given the number of each component as listed in the structures component vector, a dot product with the mass column from the Components Family DB provides the total subsystem mass. This subsystem mass is then added with the masses of the other subsystems to determine the overall telescope's mass, as described in Eq. 58:

$$LTA.sys\_mass = \begin{pmatrix} LTA.optics\_m + LTA.comm\_m + LTA.acs\_m + LTA.avioncs\_m + LTA.thermal\_m \\ + LTA.structures\_m + LTA.power\_m + (LTA.structures\_pow\_avg \times LTA.power\_m\_nd) \end{pmatrix}$$
$$+ (1 + LTA.prop\_m\_nd)$$

<div align="right">Eq. 58</div>

In this equation, *LTA.sys_mass* is the total system volume in cubic meters, *LTA.optics_m* is the total Optics subsystem mass, *LTA.acs_m* is the total ADCS subsystem mass, *LTA.avionics_m* is the total Avionics subsystem mass, *LTA.thermal_m* is the total Thermal subsystem mass, *LTA.structures_m* is the total Structures and Mechanisms subsystem mass, *LTA.power_m* is the total Power subsystem mass, *LTA.structures_pow_avg* is the average power used by the Structures and Mechanisms subsystem in Watts, *LTA.power_m_nd* is the Power subsystem's nondimensional value in kilograms per Watt, and *LTA.prop_m_nd* is the Propulsion subsystem nondimensional parameter for propellant mass fraction per unit system mass.

Because the Structures and Mechanisms coding module is the last subsystem module to be run and there are no feedback loops, non-dimensional values for both Power and Propulsion are used to determine the overall mass of the telescope. As can be seen in the above equation, the masses for all subsystems are added, though there are two non-standard mass terms. The Power and Propulsion subsystems have provided to the Structures and Mechanisms subsystem non-dimensional values to be used in determining mass. The power-based non-dimensional value is used to determine the added mass of power management and distribution electronics and wiring harnesses required to power the various mechanisms that are used by the Structures and Mechanisms subsystem. The propulsion-based non-dimensional value, however, is used in determining the required propellant mass; as the propulsion system is required to move the telescope in its entirety, the total propellant mass cannot be determined until all other components have been determined. Therefore, the mass of required propellant is added to the system mass with the use of a non-dimensional value as calculated by the Propulsion subsystem. To account for these mass effects in both the Power and Propulsion subsystems, their respective values are updated immediately following this system mass calculation. Additionally, the Components Family DB is updated to reflect the mass of the propellant that is used in each iteration for use in other sections of the code.

Additionally, the validation process led to a change in the way that antenna gimbals are treated in the code. The mass of the gimbals required to operate the communication antennas have been incorporated not to the Structures and Mechanisms subsystem mass, but to that of the Communications subsystem. Though these components are added to the Structures and Mechanisms component vector, their mass properties are added to the Communication subsystem to aid in the validation process, since Hubble Space Telescope values combined gimbal and telescope mass together within the Communications subsystem.[54]

5.3.3.8.16 Volume
Due to the constraint of the limit on launch volume imposed by the launch vehicles' fairings, only architectures that can be packed into launchable units may be deemed feasible architectures. Naturally, the fewer launches required, the less cost in launching the telescope's components. Therefore, the volume of each architecture must be determined in order to ensure that each architecture can meet this launch constraint. This volume metric, however, is opposed by the

complexity metric. For example, although the packed volume of one architecture may be less than another, the complexity of the resulting on-orbit assembly may render the less voluminous architecture less desirable overall.

To determine the volume of a particular architecture for both the Structures and Mechanisms subsystem and the entire telescope, the volume of the stowed configuration must be analyzed. This stowed configuration is determined in the Structures and Mechanisms coding module in a manner much like the calculation of system mass. To determine the total volume, the following simplified equation is executed:

$$
\begin{aligned}
LTA.sys\_vol = & \left(\begin{aligned} & LTA.optics\_v + LTA.comm\_v + LTA.acs\_v + LTA.avionics\_v + LTA.thermal\_v \\ & + LTA.structures\_v + LTA.power\_v + \left(LTA.structures\_pow\_avg \times LTA.power\_v\_nd \right) \end{aligned} \right) \\
& + \left(LTA.sys\_mass \times LTA.prop\_v\_nd \right)
\end{aligned}
$$

<div align="right">Eq. 59</div>

In this equation, *LTA.sys_vol* is the total system volume in cubic meters, *LTA.optics_v* is the total Optics subsystem volume, *LTA.acs_v* is the total ADCS subsystem volume, *LTA.avionics_v* is the total Avionics subsystem volume, *LTA.thermal_v* is the total Thermal subsystem volume, *LTA.structures_v* is the total Structures and Mechanisms subsystem volume, *LTA.power_v* is the total Power subsystem volume, *LTA.structures_pow_avg* is the average power used by the Structures and Mechanisms subsystem in Watts, *LTA.power_v_nd* is the Power subsystem's non-dimensional value in cubic meters per Watt, *LTA.sys_mass* is the total system mass, and *LTA.prop_v_nd* is the Propulsion subsystem non-dimensional parameter in cubic meters per kilogram. Just as in the system mass calculation, non-dimensional parameters are used by both the Power and Propulsion subsystems in determining the total volume of the telescope. Like the mass-based non-dimensional values, these values are necessary because the Structures and Mechanisms subsystem determines its components after the Power and Propulsion subsystems. They allow the system volume to be determined, and both the Power and Propulsion subsystem volumes are then immediately updated following this equation.

Additionally, just as with the determination of the system mass, the volume of the gimbals required to operate the communication antennas have been incorporated not to the Structures and Mechanisms subsystem volume, but to that of the Communications subsystem. Though these components are included in the Structures and Mechanisms component vector, their volume properties are added to the Communication subsystem to aid in the validation process, since Hubble Space Telescope values combined gimbal and telescope volume together as part of the Communications subsystem.[54]

5.3.3.8.17 Power
The power of the Structures and Mechanisms subsystem is closely coupled with the Power subsystem, since the Power subsystem is responsible for generating, regulating, and distributing electricity throughout the telescope. In order to reduce the size and mass of solar panels, the power demands of all mechanisms must be kept low; the power metric allows the team to compare different architectures based on the power required to operate all components at both average and peak levels.

While the structure of the telescope itself does not have any power demands, there are mechanisms of the Structures and Mechanisms subsystem that levy power demands on the power management and distribution system. The trade decisions made at high systems levels, such as the modularity of the system, has a substantial effect on the total mechanism-required power of the telescope. Deployment mechanisms, such as high temperature superconductors, frangibolts, or burn wires significantly affect the peak power, but not the average power, because these large powered mechanisms are operated for only a few, short duration periods during the telescope's operational phases. The average power, however, is dominated by the mirror segment actuators during image collection. The following equations are used in determining the power required of the power generation system:

$$LTA.sys\_pow\_avg = \sum_{i=1}^{N} LTA.overall\_components(i) \times LTA.compPowerAvgCol(i)$$

<div align="right">Eq. 60</div>

$$LTA.sys\_pow\_peak = \left(\frac{LTA.sys\_mass}{LTA.power\_m\_nd} \right) + LTA.structures\_pow\_peak$$

<div align="right">Eq. 61</div>

In these equations, *LTA.sys_pow_avg* is the total average system power in Watts, *LTA.overall_components* is the vector of all telescope components, *LTA.compPowerAvgCol* is the vector of the average required power in Watts for each component family as listed in the Components Family DB, *LTA.sys_pow_peak* is the total peak power for the system in Watts, *LTA.sys_mass* is the total system mass in kilograms, *LTA.power_m_nd* is the Power subsystem non-dimensional parameter in kilograms per Watt, and *LTA.structures_pow_peak* is the peak power required by the Structures and Mechanisms subsystem in Watts. The bounds for the summand range from the first to the Nth component.

As can be seen, the Components Family DB is used in determining the average power for the telescope, and the non-dimensional parameter from the Power subsystem is used in determining the peak power of the telescope, since this non-dimensional parameter takes into account the duty cycling of upstream components. With these values of peak and average power, it is possible to determine the mass of the associated solar arrays and the power management and distribution system required to supply sufficient power. This mass calculation is conducted as part of the system mass calculation.

5.3.3.8.18 Lifetime/MTBF
Because the mechanisms of the Structures and Mechanisms subsystem have much shorter MTBFs than the spacecraft structure itself, the focus of the lifetime/MTBF analysis for this subsystem will be on the mechanisms rather than the structure itself. The permanent infrastructure – mostly structural components such as the mirror backframe, bus structure, secondary boom, and light shield – will not be able to fail in the analysis as their lifetimes are orders of magnitudes higher than the other components. Depending on the architecture selected, the MTBF of the appropriate components will be retrieved from the Components DB shown in Appendix C. After parsing the data from the database, the MTBF will be output in a predefined data structure to the operations module. The MTBF that are stored in the database are estimated

based on typical component family MTBFs and do not represent precise numbers, only estimates. In the operations module, these MTBFs are used to compute component reliabilities in the Monte Carlo simulation to determine if a component fails during operation. The fault tree diagram shown in Figure 45 shows which component failures lead to system failure. When any of these conditions are met, the telescope will fail and the utility to science will drop to zero until the next servicing mission.
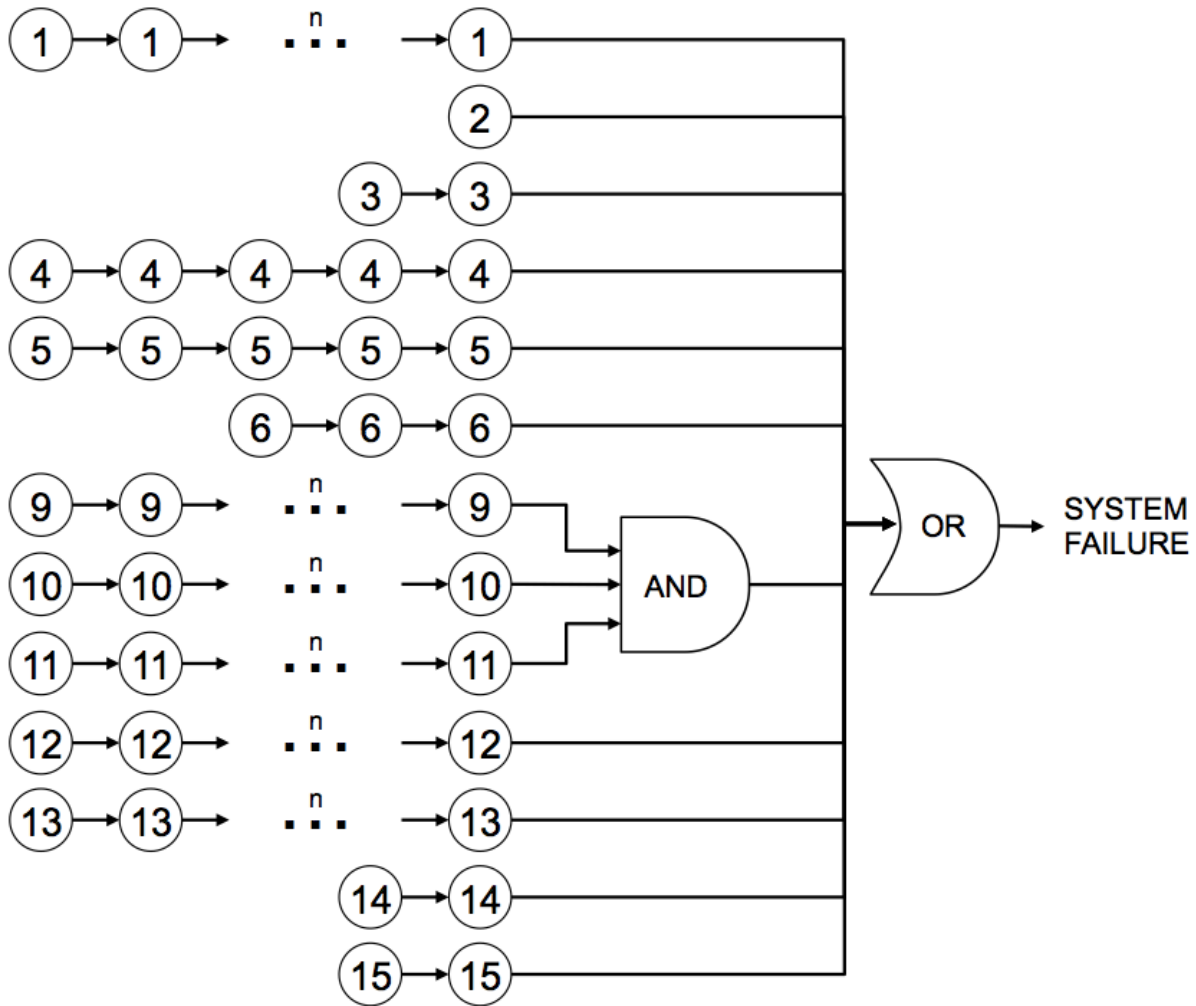
Figure 45: Fault tree diagram for the Structures and Mechanisms component failures that lead to system failure, where the numbers represent the corresponding row/component number in the Component DB shown in Appendix C.

As shown in the fault tree diagram in Figure 45, different components lead to system failure in various ways. Some components can only cause system failure if all of them fail. These are depicted with an ellipsis (e.g., components 1, 9, 10, 11, 12, and 13). Others can cause system failure if a specific number of them fail. For example, components 2, 3 and 4 require 1, 2 and 5 failures respectively. Components that only cause system failure when other components have also failed are grouped with an AND gate (e.g., components 9, 10, and 11). Components that will

cause system failure by themselves are linked together with an OR gate leading to system failure as are most in the fault tree.

The numbers in the fault tree diagram represent the components from the Component DB located in Appendix C. For example, robotic arms are component 1, electromagnetic coils are component 2, and docking ports are component 3. All robotic arms (component 1) need to fail before mission failure, as the design assumption is that all assembly/servicing maneuvers are able to be carried out by a single arm and others are included in the design for redundancy and ease of operation. One electromagnetic coil failure will cause that particular module to be unserviceable, since there are no robotic arms in those architectures in which electromagnetic coils are employed. Two docking port failures as well as the corresponding data and power interface failures (components 3, 14, and 15) are required to fail because all modules have two docking ports, so data and power could theoretically be routed to the module in two ways. Five failures of primary mirrors and surface-normal actuators (components 4 and 5) are assumed to degrade science utility to a level corresponding to mission failure. Alongside this five-mirror failure requirement, three surface-parallel actuators (component 6) would affect six mirror segments and thus drop the science utility below the threshold again. All vibrational dampers (components 9, 10, and 11) are required to fail before system failure. Nonetheless, in the Monte Carlo simulation, the utility to science parameter is scaled down for each failure of a component affecting science utility (e.g. mirrors, actuators, and dampers). Components in the primary infrastructure of the telescope are not included in the fault tree and are assumed to function for the full 40-year lifetime of the satellite.

5.3.3.9 Systems Module

5.3.3.9.1 Complexity
The computation of a structural complexity metric for the telescope architecture has been developed by Sinha and the MIT Phoenix Team.[60,61] The architectural study employs a simplified structural complexity metric because it has been shown to be a predictor of development cost across several types of complex systems.[60] This complexity metric was chosen because of its ability to be applied to a wide array of systems covering a broad spectrum of both complexity and function. Specifically, its use in determining the complexity of a highly fractionated architecture for the DARPA Phoenix Project was a key benchmark, since the LTA will be comprised most likely of several modules, not dissimilar from Phoenix satlets. The structural complexity metric used in the cost analysis contains three complexity factors:

$$C = C_1 + C_2 C_3 = \left(\sum_{i=1}^{n} \propto_i \right) + \left(\sum_{i=1}^{n} \sum_{j=1}^{n} \beta_{ij} A_{ij} \right) \left(\gamma E(A) \right)$$

Eq. 62

In this equation, C_1 represents the complexity due to the number and flight readiness of the components, C_2 represents the complexity due to pair-wise component interactions, and C_3 represents the complexity due to the topology of the system architecture and the associated complexity of system integration.[60] These three complexity terms are determined with the following equation with variable values from the DSM and the Components DB:

$$C(n, m, A) = \left(\sum_{i=1}^{n} \alpha_i\right) + \left[\sum_{i=1}^{n} \sum_{j=1}^{n} \beta_{ij} A_{ij}\right]\left(\gamma E(A)\right)$$

<div align="right">Eq. 63</div>

In Eq. 62, n is the number of components, m is the number of interfaces, A is the Design Structural Matrix (DSM), α is a function of Technology Readiness Level (TRL) as described by Eq. 63, β is the complexity of each connection between pairs of components, γ is $1/n$, and $E(A)$ is the graph energy of the DSM, which is the sum of the singular values of the DSM as determined using the "svd" command in MATLAB.[60] In the complexity analysis, higher values of β were given to components that have greater software and integration effort required when they are present in the system. The values of the β terms are currently based upon those from the DARPA Phoenix Project[61], though in the future, further iteration should occur to determine the proper values. The addition of an optical-type interface is necessary for the telescope architecture, whereas in Phoenix no such interfaces existed.

$$\alpha = 9\left(\frac{TRL_{max} - TRL}{TRL_{max} - TRL_{min}}\right)$$

<div align="right">Eq. 64</div>

The structural complexity metric for each subsystem is included in the cost metric, since it is an input to the development cost. Sinha has shown that a power law relationship exists between complexity (*X*) and development cost (*Y*), as denoted in Eq. 65. Sinha demonstrated the wide applicability of this approach for both terrestrial and space applications, including those in development stages.[60]

$$Y = aX^b.$$

<div align="right">Eq. 65</div>

Because the team is architecting, not designing, systems that fulfill the given high-level requirements, component families are included in the DSM and Components DB instead of specific components. There is no resultant specific design, but rather an estimate of the performance of the telescope system based on representative components for each component family. For this reason, the DSM and Components DB are constructed at a higher level with rather generalized representations of each subsystem that go into enough design detail necessary to distinguish between different architectures. Consequently, the application of these complexity relationships is novel and unique to this project. The values of β have been adjusted to reflect the complexity of integrating different groups of subsystem components.

5.3.3.9.2 Risk Analysis
The complexity of the mission discussed in this report in terms of mission objectives, design and manufacturing, test and verification, operations and maintenance requires a risk analysis in order to study the impact of failures on mission capability, as well as understand how to best use the available resources to maximize mission success. If something does not work as planned or a failure occurs, the entire mission could be lost along with large amounts of money, time, and effort. It becomes thus imperative to invest in such resources to protect against anomalies very early in the design process. By so doing, a risk analysis becomes an integral component throughout this process and will guide the designer in his choices and decisions.

In order to quantify the concept of risk, risk is defined as the product of the probability of a negative event occurring and its impact.[47] A risk analysis, therefore, encompasses a measure of the impact of the negative event, which can span from reduced performance to total mission failure. Two types of risk exist in practice: mission risk and programmatic risk. The former, also known as technical failure risk, has an impact on the total return from the mission and can be thought of as the amount of mission objectives that would be lost if the negative event occurred. In the case discussed here, the utility to science would be negatively affected by a mission failure as no data could be collected and no discoveries would be made. The latter type of risk, also known as implementation risk or management failure risk, affects budgets and reserves of several resources; its impact is translated into the amount of margin used to recover from the negative event. Programmatic risk plays an important role before operations begin, that is during the design and development stages of the mission when schedules slippages are likely, budget variations might occur because of political or leadership changes, engineering resources may not be adequate, etc. Both types of risk have been addressed in this study and will be presented in detail in this section.

5.3.3.9.2.1 Mission Risk

Whenever the overall return of the mission under consideration is affected by the timing of when a failure occurs, an Expected Productivity Analysis (EPA) is deemed appropriate to study technical failure risks.[62] This applies to all missions returning data of some sort throughout time and for which the more data the more successful the mission. This is certainly the case of space telescopes but also robotic missions returning scientific data. As opposed to this, if the most important requirement for mission success is that the end goal be met, then the timing of when a failure occurs does not matter. Such is the case of sample return missions, human spaceflight missions, or commercial satellites needing to operate for a certain number of years to fulfill contract requirements. Under these circumstances, a Probabilistic Risk Assessment (PRA) would be used, because the probability of meeting that specific end goal is what ought to be optimized.[47] Given the context of the mission described in this report, i.e., a large telescope array collecting and returning data to Earth, an extensive discussion of EPA will be carried out and numerical results will be presented.

By definition, the expected productivity of a system is the product of the probability of being in each functional state and the productivity in that state, summed over all states and all time. Here, this is to be considered as the expected value of the utility-to-science function over the entire mission lifetime. The expected productivity is calculated by following three steps:

1. Estimation of the probability of being in each state at each time
2. Estimation of the productivity in each state
3. Combination of the two previous steps to obtain the expected value of the total productivity by the end of mission life

The first step is based on a Markov model applied to each subsystem under the hypothesis that the future states of the subsystems depend only on the current state and not on any previous state. To clarify this assumption, which does apply to the case discussed in this report, if the subsystem under consideration fails if at least 2 actuators fail, it is irrelevant whether the subsystem started with 6 actuators and 4 have already failed, or if the subsystem started with only 2. The conclusion remains the same, that is, from now on the subsystem has remained with only 2 actuators and either one can fail at a given rate. In order to determine the probability of being in

any state at any time, one needs to define the possible states in which a subsystem can be and how it would transition from one state to the next. This can be accomplished by generating a state diagram, where each state is represented by a node and the transitions by the different interconnections among nodes. Transitions occur because components fail; therefore, each transition is associated with the failure rate of the component causing the system to vary its state. As an example, Figure 46 illustrates the state diagram of the Attitude and Determination Control subsystem (ADCS), here modeled with 9 momentum wheels (mw), 1 star tracker (st), and 1 solar sail (ss).
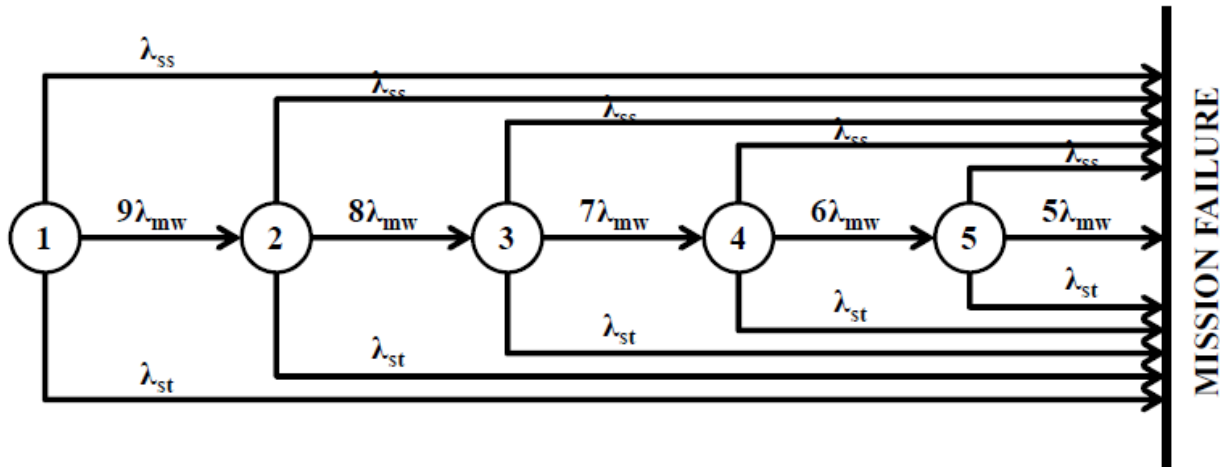
Figure 46: State diagram for the Attitude and Determination Control subsystem. Five different states were identified which lead to mission failure

In order to determine the failure rates (or alternatively, the Mean Time Between Failures – MTBF – defined as the inverse of the failure rates) needed to perform the analysis mentioned above, the following approach was adopted. Reliability values were estimated for all components based either on data available in the literature[47] or assumptions made to extrapolate the values of technology readiness levels (TRL) in the next decade for all components requiring substantial technology development. The following equation was used:

$$\lambda = \frac{1}{MTBF} = \frac{-\ln R}{\Delta t}$$

Eq. 66

where R is the reliability estimated at time Δt. The time span is equal to 40 years if the component being considered is assumed to never fail over the mission lifetime, otherwise it is set to values corresponding to the duration of operations before servicing, that is, 3, 5, or 10 years. The transitions are represented through the transition matrix, $[A]$, which is needed to solve the following system of first-order linear differential equations:

$$\dot{P}(t) = [A] \cdot P(t)$$

Eq. 67

where $\dot{P}(t)$ is the time rate of change of the state probability vector, $P(t)$. The elements of the transition matrix correspond to a different state and are determined by looking at what enters and

exits each node. As an example, for the case shown in Figure 46, the transition matrix would be as follows:

$$\begin{bmatrix} -(9\lambda_{mw} + \lambda_{ss} + \lambda_{st}) & 0 & 0 & 0 & 0 \\ 9\lambda_{mw} & -(7\lambda_{mw} + \lambda_{ss} + \lambda_{st}) & 0 & 0 & 0 \\ 0 & 8\lambda_{mw} & -(7\lambda_{mw} + \lambda_{ss} + \lambda_{st}) & 0 & 0 \\ 0 & 0 & 7\lambda_{mw} & -(6\lambda_{mw} + \lambda_{ss} + \lambda_{st}) & 0 \\ 0 & 0 & 0 & 6\lambda_{mw} & -(9\lambda_{mw} + \lambda_{ss} + \lambda_{st}) \end{bmatrix}$$

Similar matrices were calculated for the following subsystems: Structures, Power, and Thermal. These matrices were then assembled into the final matrix as independent blocks. This rests on the simplifying hypothesis that no failures occur due to subsystems interaction. Although this is in partial agreement with the higher-level assumption that no loops were accounted for in the N^2 diagram (which would show how the different subsystems interact with one another), the subsystems teams reported no failure modes due to possible interactions among subsystems at this level of the architectural study. It is recommended that when more details become available, a more in-depth failure mode analysis be carried out and the transition matrix be updated accordingly to account for such interactions. Moreover, the Communications, Avionics, and Propulsion subsystems teams made the assumption that their subsystems never fail within the maximum time between servicing missions, 10 years, which is the worst-case scenario. Therefore, they are not part of the analysis being discussed in this section. These hypotheses rest on two factors: 1) the subsystems' component families were selected so as to meet the requirement of being functional for at least 10 years, 2) the decision was made to take specific mitigating actions which would assure such a lifetime for these subsystems. For example, extreme temperature and radiation environments in deep space require that measures be taken to avoid environment-related avionics failures. Shielding, redundancy, design/processing methods are often employed in order to protect avionics equipment.[63] Types of radiation effects include total ionizing dose, displacement damage dose, single event effects (SEE), and charging/electrostatic discharged caused by electron deposits.[64] Shielding physically mitigates radon effects on avionics through the use of materials surrounding the electronics. Redundancy involves increasing the number of components, subsystems or internal component parts. Design techniques at the component level include dopant walls, isolation trenches, and chip layout, whereas design techniques at higher levels include decoupling, spacing, and circuit corrections[63]. Processing and manufacturing methods include the use of specific materials and processing techniques[63]. The avionics subsystem has selected all radiation-hardened components and many space-qualified components in order to reduce avionics failures due to environmental factors. Furthermore, the avionics subsystem will also employ redundancy at the component level to mitigate the impact of avionics failures, environmental or otherwise, on the system.

The solution to the system of differential equations[62] provides the probability of the system being in any given state at any given time. Initial conditions are needed to solve these equations. From a purely technical perspective, there is a 100% probability to be in state 1, which is when all subsystems are functioning, and 0% probability to be in all successive states. Indeed, right before launch, everything is expected to be working properly, whereas afterwards components and

subsystems start having higher probabilities of failure due to launch vibrations, environmental factors, degradation, and so on.

In the second step, the productivity, $C(t)$, in any given state is defined as the fractions of elements that can be completed per unit time, where an element is a single unit of the subsystem metric for the given mission. Examples of elements that could be selected in this context are an image, a gigabyte of data, a measurement, etc. In the case presented here, the productivity is the utility-to-science function defined in the Trade Metrics Calculation section.

Finally, in the last step, the expected productivity, $E[Prod]$, can then be computed by the following equation:

$$E[Prod] = \int_0^{lifetime} \sum_{i=0}^{n} C_i(t)P_i(t)\, dt$$

Eq. 68

This methodology was systematically applied at the subsystem level. Namely, failure states in each subsystem were identified at the level of detail allowed by this tradespace study. While some subsystems could be characterized by component failure modes, others did not have this type of information and remained at a more general level (the subsystem level). Indeed, it is beyond the scope of this work to perform a detailed design of the telescope and all its subsystems.

Figure 47 shows the state probabilities as computed by the Markov model. In black are the states corresponding to "all instruments working" for each subsystem (the "1" nodes of the state diagrams), whose probability decreases with time, whereas in different colors all other intermediate states whose probability is 0 at the beginning of mission but increases with time.
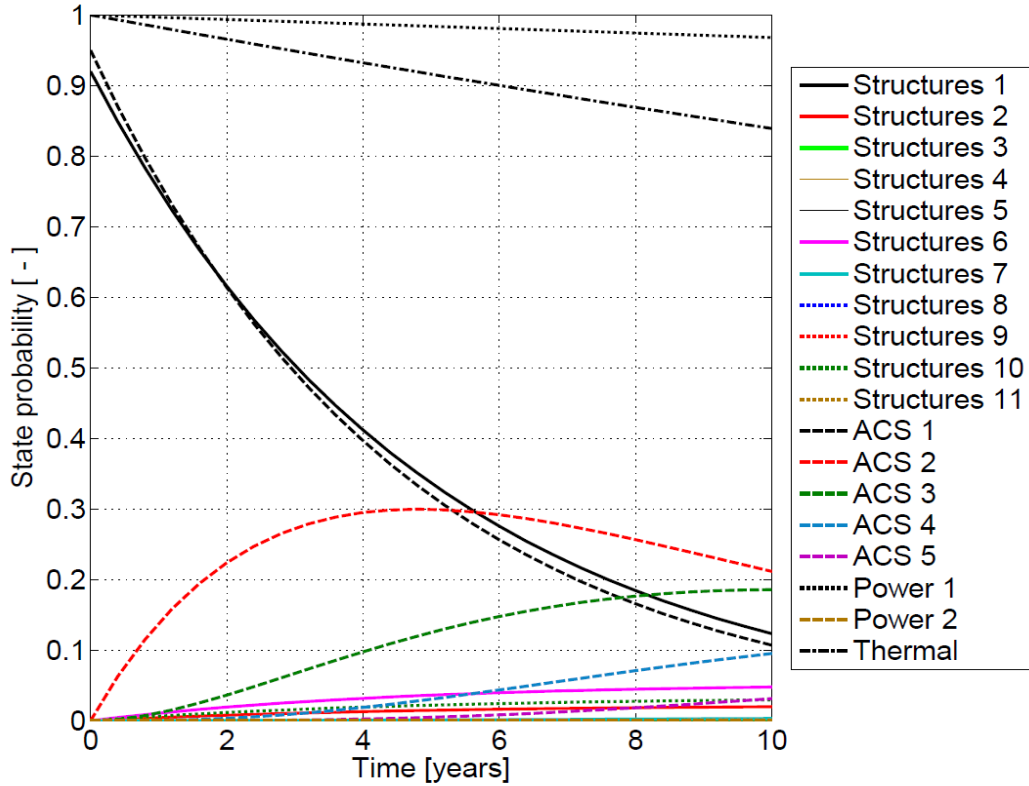
Figure 47: State probabilities as a function of time. The timespan was fixed to 10 years, as this could be the longest time interval without servicing. Since significant technology advancements may occur in such a long period of time, this type of analysis can be rerun for the remaining 30 years of the telescope's lifetime by ensuring the failure rate values are updated.

Figure 48 illustrates the probabilities of failure of each of the subsystems previously analyzed as well as of the telescope. Such probabilities were calculated by estimating the probability that each subsystem will fail entirely due to its not being in one of the states shown in Figure 47. The same applies to the whole telescope. The equation used is the following:

$$P_{f\_sub} = \prod_{i=1}^{n}[1 - P_i(t)]$$

<div align="right">Eq. 69</div>

where P_{f_sub} represents the probability for each of the entire subsystems to be in a non-functioning state, and *i* varies from 1 to the total number of functioning states. By assuming that the telescope will fail if at least one of the abovementioned subsystems fails, the same equation Eq. 69 can be applied, where now $P_i(t)$ is replaced by each P_{f_sub} to yield the probability for the entire telescope to be in a non-functioning state.
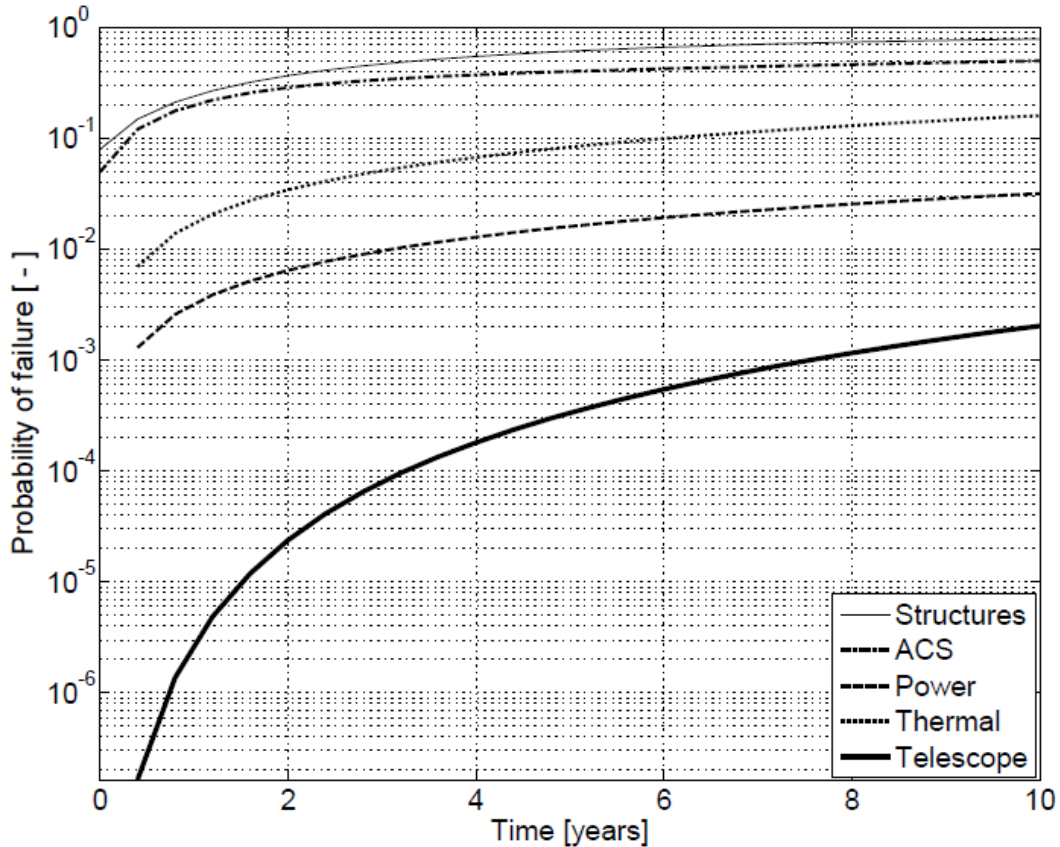
Figure 48: Probability of failure for the subsystems affected by mission risk over a time span of 10 years, which is the longest time interval that could exist between servicing missions

It can be seen the structural system is the one with higher risk, given the large number of mechanisms used. According to this model, the entire telescope could fail with a probability about 0.2% after 10 years of operations.

5.3.3.9.2.2 Implementation Risk and Schedule
As far as management failure risk is concerned, attention was paid to three factors: technology infusion, manufacturing processes, and test and verification. These are risk elements, which either decrease the probability of beginning operations in the nominal state or increase the probability that a particular subsystem will begin operations with degraded performance. These risk elements have a negative impact before launch, and thus before any utility to science is returned. In this sense, they affect the probability that a particular subsystem may be in a perfectly functioning state at $t = 0$. Such risk components result in an immediate change to the initial conditions used to find the probability of being in each state (Eq. 69). This approach enables to quantify potential schedule slippages that might occur due to the three aforementioned risk elements. However, one should remain cautious that this type of risk analysis rests on a number of assumptions made by each subsystem, which affect to some extent the uncertainty of the results discussed previously. These will be discussed separately for the subsystems involved in the remainder of this section. It will be illustrated what the technological challenges to develop

such a new large telescope array are and what their implications are on both programmatic risk and schedule.

5.3.3.9.2.2.1 *Attitude and Determination Control Subsystem*

In ADCS, the solar sail will require further advancements in technology and more testing before it can be qualified for flight with a TRL of 9. It is assumed today that solar sails have achieved a TRL equal to 7. It was thought to be highly likely that they will reach level 9 by 2020, but uncertainties remain which were estimated around 5%. The initial condition was therefore lowered from 1 to 0.95.

5.3.3.9.2.2.2 *Communications*

Free-Space Optical (FSO) solutions have been validated as viable radio-frequency (RF) communications substitutes in terrestrial systems to date. Larger bandwidth and higher data capacity capabilities for FSO, such as those needed for the communications subsystem of telescope system of study, were demonstrated in a recent NASA launch of Laser Communications Relay Demonstration (LCRD). FSO technologies for deep-space communications is a current area of development as evidenced by the NASA LCRD and other funded research activities.[65] As a consequence, FSO readiness by 2020 poses both technical and schedule risk to the telescope for FSO options.

The concept of Federated Satellite Systems (FSS) is a paradigmatic shift in how satellites share resources, e.g., processing capabilities and access time, thus impacting future satellite designs. Resource allocation is dynamic, based on the need, availability, and line of sight of participating suppliers and customers in FSS. These exchanges can be arranged by monetary or reciprocal resource sharing agreements as FSS transforms satellite resources to marketable commodities. Distributed Satellite Systems (DSS), where groups of satellites collectively perform a mission, have been demonstrated by NASA's A-Train and the Iridium satellite constellation. However, a market-based resource-allocation approach for FSS has not yet been implemented, nor has a deep-space multi-system intersatellite link (ISL) network been demonstrated. FSS is still in the conceptual phase and requires significant development of the protocols, algorithms, and technologies that would enable dynamic, secure, timely, and quality transaction. In addition, because FSS is a new paradigm for space operations based on a space market economy, there are also challenges to developing the economic, business, policy, and regulatory infrastructure necessary for FSS.

5.3.4   Operations Module

The Operations code module is a simulation of the telescope architecture's 40-year lifetime from launch to decommissioning. The simulation takes as an input a telescope architecture (defined by a component set generated by the subsystem code modules), as well as mission parameters and the architectural decision vector, and follows the process outlined in Figure 49 to produce data that are analyzed by the trade metric characterization code. Stochastic component failures are included in the simulation in order to model their impact on telescope operations and servicing; in order to account for behavior from probabilistic events, a 10-iteration Monte Carlo simulation loop was utilized for each architecture. The results of each iteration are averaged to produce the final outputs for a given architecture.
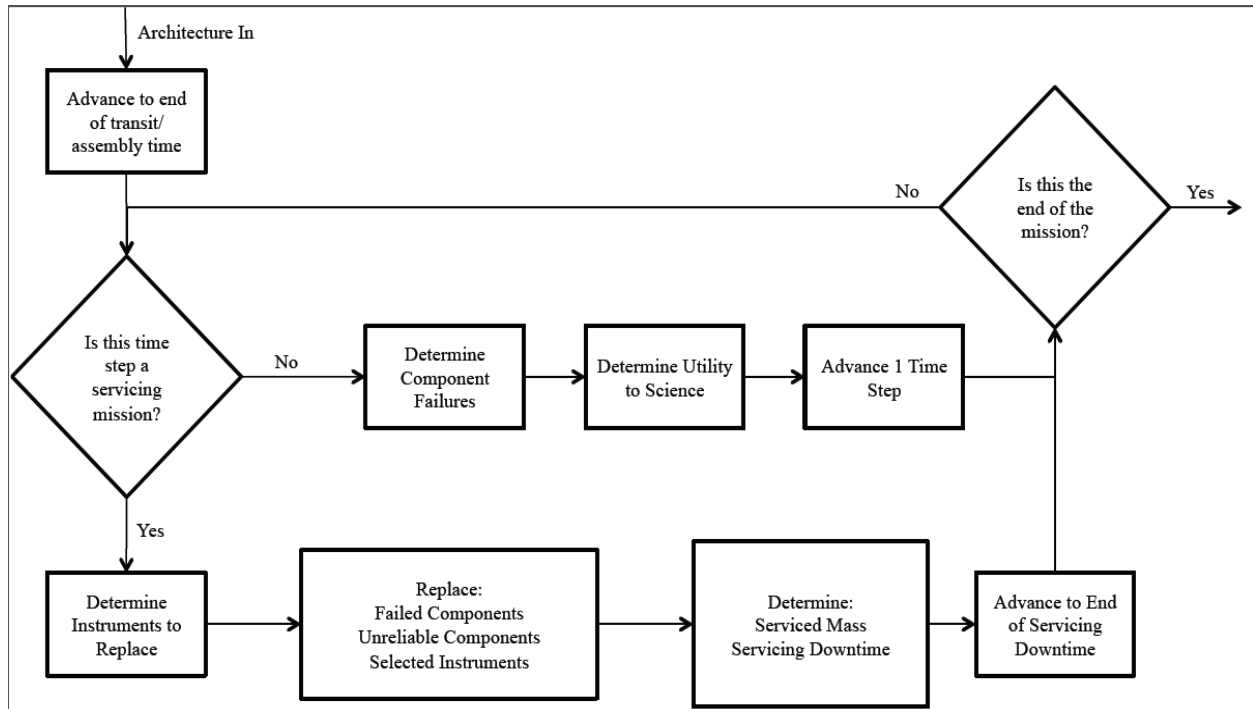
Figure 49: Code structure diagram for the operations module.

When an architecture (in the form of a MATLAB struct) is input into the Operations code module, it is translated into an architecture matrix that encodes the relevant values of the architecture into an easily accessible format. The architecture matrix is an $n \times 7$ matrix, where n is the total number of components within the architecture. Each row of the architecture matrix corresponds to a particular component, and the columns encode the relevant data for that component. In order from left to right, the columns represent:

- Components Database Row Number
- Mass (in kg)
- MTBF (in weeks)
- Module Number
- Clock
- State

The component clock is an entry that documents how long that particular component has been in operation; this entry is updated at each timestep and is reset when a component is serviced. The component state is an indication of whether the component is failed or operational at a given timestep, with 1 indicating an operational component and 0 indicating a failed component. The simulation incorporates a stochastic element that fails components based upon their reliability values to simulate component failure in the real-world telescope. When a component fails, the state flag is set to 0; when the component is serviced, the state flag is reset to 1.

This simulation uses one week as a timestep, and incorporates the three mission phases of the telescope: Assembly/Transit, Science, and Servicing. In order to minimize computational time, the timesteps can advance in jumps over sections of time that have no significant change –

126

specifically, the Assembly/Transit and Servicing Phases – while advancing step-by-step during science operations. The simulation begins at launch and enters the Assembly/Transit Phase. Once the Assembly/Transit Phase is complete, the telescope enters nominal operations, starting with Science. When a timestep corresponding to a servicing mission is reached (as defined by the servicing frequency architectural decision), the simulation enters the Servicing Phase. The timestep then advances to the end of the Servicing Phase and reenters the Science Phase, and the process repeats until the end of mission lifetime. Each mission phase is discussed in more detail in the following sections. The outputs of the simulation are:

- **Utility to Science Vector:** a vector indicating the utility to science of the telescope at each timestep
- **Failed Downtime Fraction:** the fraction of the mission lifetime that the telescope was not producing science because of a component failure
- **Servicing Downtime Fraction:** the fraction of the mission lifetime that the telescope was not producing science because of servicing operations
- **Serviced Mass Vector:** the vector of length n, where n is the number of servicing missions, encoding the amount of mass that was serviced during each servicing mission
- **Mean Serviced Mass:** the mean of the serviced mass vector, indicating the average mass serviced for a given servicing mission
- **Number of Servicing Missions:** the number of times that the telescope was serviced
- **Failure Matrix:** an $n \times m$ matrix, where n is the number of component families in the components database and m is the number of timesteps in the simulation, encoding the number of components of that family (row index) that are in a failed state in that timestep (column index)
- **Module Replacements Matrix:** an $n \times m$ matrix, where n is the number of modules in the telescope and m is the maximum possible number of servicing missions, encoding which module (row index) was replaced during each servicing mission (column index)

Assembly/Transit Phase

The Assembly/Transit phase begins at launch and ends when the telescope is fully assembled and is in place at SE-L2. It is assumed that assembly of the telescope takes place during transit. The transit time from LEO to SE-L2 is 63 days (or 9 weeks) and it is assumed that the telescope is fully assembled by the time it reaches SE-L2.[66] The Operations code module simulates this phase by advancing the timestep to step 9, the week where the telescope arrives at SE-L2 and begins the Science phase.

Science Phase

The Science Phase mode calculates the instantaneous utility to science of the telescope by multiplying the sum of the utilities of the four instruments on-board the telescope by the instantaneous observational efficiency. In addition, timesteps in the science phase "roll the dice" to determine which components fail, using a random number generator and the reliability of each component at that timestep; the instantaneous observational efficiency changes according to which components are failed. The utility is calculated for each week of the 40-year lifetime. The telescope enters Science Phase on all timesteps except for the beginning of the mission when it enters the Assembly/Transit Phase and at the servicing frequency when it enters the Servicing Phase.

Mirroring Baldesarra, the initial discovery efficiency of a given instrument type starts at an arbitrary value and increases in time due to technological advances that enable additional throughput or increased field of view for the same cost, mass, power, etc.[13] Once an instrument is installed on the telescope, its discovery efficiency is assumed to slightly degrade with time due to radiation damage or similar effects. The formula for instrument utility is:

$$u_i(t) = Ae^{b(T-2028-L)} \cdot r^{t-T}$$

Eq. 70

where $u_i(t)$ is the utility of each instrument, A is a constant that specifies discovery efficiency at the beginning of the mission in $arcmin^2*photons/second$, T is the year the instrument was installed on the telescope, L is the latency from ground development and flight implementation of an instrument design in years, b is a constant that specifies the improvement rate of discovery efficiency over time, r is the decay factor, and t is the year of operation. Both r and b were taken from Baldessarra and are 0.99 and 0.3218 respectively.[13] b was then adjusted off its baseline value to examine the sensitivity of utility to science to the assumed growth rate as described in Section 7.4.1.3. A was initialized to 10 for all instruments and L was assumed to be 3 years.

In order to simulate component failures, the reliability of each component at each timestep is calculated and compared to a random number in order to determine via a "dice roll" whether or not a given component fails in the given timestep. The expression used to evaluate whether or not a component has failed is

$$e^{-\frac{t_i}{MTBF_i}} \leq r$$

Eq. 71

where t_i the time in weeks that component i has been in operation (from the component clock entry in the architecture matrix), $MTBF_i$ is the MTBF value in weeks for component i, and r is a random number between 0 and 1. The left side of this expression represents the reliability (between 0 and 1) of component i at a given timestep; this expression evaluates as true if the reliability of component i is less than the random number. If the expression evaluates as true, the component is considered to be failed, and the state flag for the component in the architecture matrix is changed to 0. Thus, a component with a reliability of 0.8 in a given timestep has a 20% chance of failing in that timestep. Once failed, a component remains in a failed state until the next Servicing Phase occurs.

The utilities of all four instruments are then summed and multiplied by the observational efficiency. The observational efficiency will change with time as the telescope changes modes and as components on board fail. In science mode, the observational efficiency will be 90% per the requirement in Table IV. During the initial transit to the operational location and during servicing or transit to or from the servicing location, the observational efficiency will drop to 0% as the telescope is assumed to be incapable of doing science. The observational efficiency will also drop below 100% and possibly to 0% when failures aboard the telescope degrade its ability to conduct science operations. Some component failures result in degradation of the overall scientific output of the telescope (either as a geometric series or proportional to the ratio of failed to operational components for a given component family), while others result in complete loss of scientific output. The instantaneous utility to science equation therefore is:

$$US(t) = O(t) * [u_A(t) + u_B(t) + u_C(t) + u_D(t)]$$

where *US(t)* is the instantaneous utility to science of the telescope, *O(t)* is the observational efficiency, and *$u_i(t)$* is the utility of each instrument. The different Monte Carlo runs in Operations will capture different sets of failures that will yield slightly different instantaneous utilities to science as the set of instruments and the observational efficiency will be slightly different in each case.

Servicing Phase

The Servicing Phase begins when the timestep of the simulation coincides with a servicing mission, at which point the servicing mission counter is increased by 1. First, the model determines which instruments to replace and marks them for replacement. Instrument replacement during servicing missions is the primary means of increasing the utility to science of a given telescope architecture. As the discovery efficiency of instruments improves, the existing instruments on the telescope are replaced with newer, more capable instruments. To model real-world decision-making, instruments were marked for replacement if the discovery efficiency of the new instrument was five times greater than the discovery efficiency of the current instrument. The threshold value of five times the current discovery efficiency was chosen so that every instrument is not replaced on every timestep (as they would be if the rule were to replace any instrument that had seen a rise in discovery efficiency). The threshold creates a balance between the need to upgrade the instrument, the need to allow instruments to operate for a sufficient lifetime to generate enough utility to science to merit their cost, and the need to prevent serviced instrument mass from being the maximum value at every servicing mission.

Next, the components that are in a failed state or below a reliability threshold are marked for replacement. The rows in the architecture with a state flag of 0 indicate that that component is in a failed state, and those indices are marked for replacement. The reliability threshold is a way to enable preemptive replacement – that is, the replacement of a component that has not yet failed. If a component is still operational, but its reliability has fallen below a threshold value, then the probability of that component failing before the next servicing mission is higher than the probability for components that do not have reliabilities below the threshold value. Thus, that component is considered "unreliable" and is marked for replacement. The expression used to determine whether or not a component is below the reliability threshold is

$$e^{-\frac{t_c}{MTBF}} \leq R_{thresh}$$

where t_c is the component time in weeks, $MTBF$ is the component Mean Time Between Failure in weeks, and R_{thresh} is the reliability threshold (unitless). For this simulation, the reliability threshold was taken to be 0.7, meaning that components with a greater than 30% probability of failure are replaced. This threshold value is an operational decision related to how far mission controllers are willing to allow components to degrade before replacing them. As such, the reliability threshold is the subject of a sensitivity analysis to a change in ± 0.05 (i.e., changing the threshold value to 0.65 or 0.75), which is described in Section 7.4 Sensitivity Analysis.

Once all components and instruments needing replacement are marked as such, the modularization of the telescope is taken into account by translating the component and instrument replacement marks into module replacement marks. If any element within a module is marked for replacement, the whole module is marked for replacement. This is due to the fact that for this model "servicing" is defined as the act of removing a module and replacing it with an identical (but potentially upgraded, if the module includes an instrument) module; the smallest unit of the telescope that can be serviced is a module. Thus, when an element is replaced all other elements in its module must be replaced as well.

Finally, all modules that are marked for replacement are replaced, meaning that all elements in that module are replaced. When a component or instrument is replaced, the component clock is reset to 0, which resets the reliability of the component to 1; in this way, the simulation represents the component as being new. In addition, the state flag is set to 1 to indicate that the replaced component is now operational. Once these replacements are complete, the mass of all modules that were replaced is summed to give the serviced mass for this servicing mission, and the value is stored in the serviced mass vector. Next, the servicing downtime is calculated.

The servicing downtime is informed by the assembly/servicing technique and the number of modules replaced. The self-assembly case is assumed to require 2 hours per module, the case using tugs is assumed to require 6 hours per module, and the case using formation flying is assumed to require 4 hours per module. These values were chosen to reflect the relationships between these three techniques. First, in the self-assembling case, the robotic arms which are incorporated directly into the telescope design have a clear and unchanging relationship between end effector location and orientation and the telescope itself; therefore, the arms may perform more complex and rapid preprogrammed motions to remove and insert modules. For this reason, self-assembly is assumed to be the fastest method. The use of a tug for servicing requires that the tug dock with the telescope, implying that there will be more uncertainty in the relative location and orientation of end effectors and telescope modules; therefore arm motions will have to be more carefully and slowly executed. For this reason the servicing by tug is the slowest technique. Finally, formation flying involves more complex movement of modules using electromagnetic (EM) coils. Since all elements are floating in free space and all forces are internal resulting from interactions between EM coils, the center of mass of the system must remain unchanged; therefore the movement of any one component will cause movement in the others. However, complex preprogrammed motion is still available for servicing operations, though it will be more complex than the simple use of robotic arms. For this reason, the formation flying assembly/servicing technique is assumed to be at a medium value, between self-assembly and tugs.

Once the time for actual servicing operations is calculated, the transit time for movement of the telescope from SE-L2 to the servicing location and back is added in to determine the total amount of time that the telescope was offline due to servicing:

$$t_d = t_{serv} + t_{transit}$$

Eq. 74

where t_{serv} is the servicing time, $t_{transit}$ is the transit time to and from the servicing location, and t_d is the total downtime due to servicing. In the servicing code, all of these time values were documented as days; once the value is computed, the total downtime in days is divided by seven

to convert to weeks to match the timestep length. At this point servicing is complete, the timestep is advanced to the end of servicing, and the telescope enters the Science Phase.

5.3.5   Trade Metrics Calculation

5.3.5.1   *Utility to Science*

The Trade Metrics module receives the instantaneous utility to science of the telescope for each week of the forty-year lifetime from the Operations module. Trade Metrics integrates this input against time to find the total utility to science for each Monte Carlo run and then averages across the Monte Carlo runs. The equation for total telescope utility to science is:

$$U = \frac{1}{N} \sum_{i=1}^{N} \int_{0}^{2080} US_i(t)dt$$

<div align="right">Eq. 75</div>

where U is the total utility to science of the telescope, N is the number of Monte Carlo runs, i is a particular Monte Carlo run, $US_i(t)$ is the instantaneous utility to science from the Operations module, and t is the number of weeks the telescope has been operating.

5.3.5.2   *Serviceability*

The Servicing Phase begins when the timestep of the simulation coincides with a servicing mission, at which point the servicing mission counter is increased by 1. First, the model determines which instruments to replace and marks them for replacement. Instrument replacement during servicing missions is the primary means of increasing the utility to science of a given telescope architecture. As the discovery efficiency of instruments improves, the existing instruments on the telescope are replaced with newer, more capable instruments. To model real-world decision-making, instruments were marked for replacement if the discovery efficiency of the new instrument was five times greater than the discovery efficiency of the current instrument. The threshold value of five times the current discovery efficiency was chosen so that every instrument is not replaced on every timestep (as they would be if the rule were to replace any instrument that had seen a rise in discovery efficiency). The threshold creates a balance between the need to upgrade the instrument, the need to allow instruments to operate for a sufficient lifetime to generate enough utility to science to merit their cost, and the need to prevent serviced instrument mass from being the maximum value at every servicing mission.

Next, the components that are in a failed state or below a reliability threshold are marked for replacement. The rows in the architecture with a state flag of 0 indicate that that component is in a failed state, and those indices are marked for replacement. The reliability threshold is a way to enable preemptive replacement – that is, the replacement of a component that has not yet failed. If a component is still operational, but its reliability has fallen below a threshold value, then the probability of that component failing before the next servicing mission is higher than the probability for components that do not have reliabilities below the threshold value. Thus, that component is considered "unreliable" and is marked for replacement. The expression used to determine whether or not a component is below the reliability threshold is

$$e^{-\frac{t_c}{MTBF}} \leq R_{thresh}$$

<div align="right">Eq. 76</div>

where t_c is the component time in weeks, $MTBF$ is the component Mean Time Between Failure in weeks, and R_{thresh} is the reliability threshold (unitless). For this simulation, the reliability threshold was taken to be 0.7, meaning that components with a greater than 30% probability of failure are replaced. This threshold value is an operational decision related to how far mission controllers are willing to allow components to degrade before replacing them. As such, the reliability threshold is the subject of a sensitivity analysis to a change in +/- 0.05 (i.e. changing the threshold value to 0.65 or 0.75), which is described in the Sensitivity Analysis section of this report.

Once all components and instruments needing replacement are marked as such, the modularization of the telescope is taken into account by translating the component and instrument replacement marks into module replacement marks. If any element within a module is marked for replacement, the whole module is marked for replacement. This is due to the fact that for this model "servicing" is defined as the act of removing a module and replacing it with an identical (but potentially upgraded, if the module includes an instrument) module; the smallest unit of the telescope that can be serviced is a module. Thus, when an element is replaced all other elements in its module must be replaced as well.

Finally, all modules that are marked for replacement are replaced, meaning that all elements in that module are replaced. When a component or instrument is replaced, the component clock is reset to 0, which resets the reliability of the component to 1 – in this way, the simulation represents the component as being new. In addition, the state flag is set to 1 to indicate that the replaced component is now operational. Once these replacements are complete, the mass of all modules that were replaced is summed to give the serviced mass for this servicing mission, and the value is stored in the serviced mass vector. Next, the servicing downtime is calculated. This value is informed by the assembly/servicing technique and the number of modules replaced. The self-assembly case is assumed to require 2 hours per module, the case using tugs is assumed to require 6 hours per module, and the case using formation flying is assumed to require 4 hours per module. These values were chosen to reflect the relationships between these three techniques. First, in the self-assembling case, the robotic arms, which are incorporated directly into the telescope design have a clear and unchanging relationship between end effector location and orientation and the telescope itself; therefore, the arms may perform more complex and rapid preprogrammed motions to remove and insert modules. For this reason self-assembly is assumed to be the fastest method. The use of a tug for servicing requires that the tug dock with the telescope, implying that there will be more uncertainty in the relative location and orientation of end effectors and telescope modules; therefore arm motions will have to be more carefully and slowly executed. For this reason the servicing by tug is the slowest technique. Finally, formation flying involves more complex movement of modules using electromagnetic (EM) coils. Since all elements are floating in free space and all forces are internal resulting from interactions between EM coils, the center of mass of the system must remain unchanged; therefore the movement of any one component will cause movement in the others. However, complex preprogrammed motion is still available for servicing operations, though it will be more complex than the simple

use of robotic arms. For this reason, the formation flying assembly/servicing technique is assumed to be at a medium value, between self-assembly and tugs.

Once the time for actual servicing operations is calculated, the transit time for movement of the telescope from SE-L2 to the servicing location and back is added in to determine the total amount of time that the telescope was offline due to servicing:

$$t_d = t_{serv} + t_{transit}$$

<div align="right">Eq. 77</div>

where t_{serv} is the servicing time, $t_{transit}$ is the transit time to and from the servicing location, and t_d is the total downtime due to servicing. In the servicing code, all of these time values were documented as days; once the value is computed, the total downtime in days is divided by seven to convert to weeks to match the timestep length. At this point servicing is complete, the timestep is advanced to the end of servicing, and the telescope enters the Science Phase.

5.3.5.3 Failed Downtime

The Failed Downtime is calculated using the results of the simulation from the Operations Module. The time vector of Utility to Science, which encodes the Utility to Science of the telescope during each week of the telescope's lifetime, is analyzed to determine how many weeks show a Utility to Science of 0. This is accomplished by evaluation of the equation

$$DT_{total} = \sum(US == 0)$$

<div align="right">Eq. 78</div>

where US is the vector of Utility to Science values for each timestep in the simulation and DT_{total} is the total downtime in weeks. By taking the sum of the number of elements in US for which the expression $US == 0$ evaluates to true (and returns a 1), the total number of timesteps for which the Utility to Science was 0 can be calculated. A Utility to Science of 0 indicates that, during that timestep, the telescope was not operational either due to component failures or servicing operations. In order to isolate the number of weeks that the telescope was down specifically for component failures, the number of weeks of downtime due to servicing is calculated by summing the servicing downtime for each servicing mission; this value is subtracted from the total downtime in order to yield the downtime due to failures:

$$DT_{fail} = DT_{total} - \sum DT_{serv}$$

<div align="right">Eq. 79</div>

where DT_{serv} is the vector of servicing down times for each servicing mission in weeks, DT_{total} is the total downtime in weeks (from Eq. 78), and DT_{fail} is the total amount of downtime due to component failures in weeks. The Failed Downtime for each architecture is reported as a fraction of the total mission lifetime spent in a non-operational state due to component failure, therefore the output from Eq. 79 is normalized by the total mission lifetime:

$$FD = \frac{DT_{fail}}{L*52}$$

<div align="right">Eq. 80</div>

where DT_{fail} is the number of weeks of downtime due to a component failure, L is the mission lifetime in years, and FD is the failed downtime metric, the fraction of mission lifetime spent down due to a component failure.

5.3.5.4 Cost

5.3.5.4.1 Flight System Development

As described in the Trade Metrics Descriptions section, the cost of the flight system development, which includes the design, manufacture, and testing for the entire space telescope assembly, is estimated using three models. The function that performed this calculation is called Cost_Flight System. This function simply summed the individual cost of each phase of the mission for each design architecture. The assumptions and characteristics of those models are presented here.

5.3.5.4.1.1 Stahl Ground-Based Telescope Cost Model

The use of the Stahl Ground-Based Telescope model implies the assumption that the costs forecasted by this model is indicative of similar space-based telescopes. The model takes into account the unique prescription segments, the number of repeated segments, the segment diameter, wavelength performance, and the overall diameter of the telescope. Notably, the model takes into account manufacturing learning curve considerations based on the number of repeated segments fabricated. This portion of the code simply outputs a cost for the optical train

of the telescope. The original model estimated this cost in year 2000 dollars, therefore an annual discount rate of 2.01% was assumed to convert these into year 2013 dollars.

The Stahl Ground-Based Telescope Model is a parametric cost model, shown as Eq. 81. It predicts the cost to produce an optical telescope assembly, which consists of the primary mirror, secondary mirror, auxiliary optics, and support structure.[25]

$$C_{OTA} = (0.68)(SF)\, D^{1.8} \lambda^{-0.5} e^{0.04(Y)}$$

Eq. 81

where C_{OTA} is the cost of the optical telescope assembly, SF is a segmentation factor, D is the aperture diameter, λ is wavelength diffraction limited performance, and Y is the difference between the year of development and the year 2000. For segmented mirrors, SF is defined in Eq. 82 as:

$$SF = P_n R_n^{0.7} (D_s/D)^{1.8}$$

Eq. 82

where P_n is the number of unique prescriptions, R_n is the number of repeated segments, D_s is the diameter of the repeated segments, and D is the diameter of the primary mirror. For monolithic mirrors, the SF value is 1. The bounds implied by the data set upon which this model is based include a maximum mirror diameter of 14.142 meter and a segment diameter of 1.0-8.41 meter. The 16.8-meter assumption for the aperture violates this boundary condition. However, as discussed, the absolute cost estimate reliability is less important for this trade than the relative costs, therefore any loss in accuracy resulting from using this model is viewed as acceptable. Moreover, this model is intended for ground-based telescopes. The effects captured in this model, specifically changing cost with segmentation, learning curve considerations, and economies of scale are all expected to provide similar relative results on the optical train of a space telescope. These benefits were deemed to outweigh the loss of absolute accuracy associated with using a ground-based model for a space-based application.

5.3.5.4.1.2 NASA Instrument Cost Model (NICM)

The NASA Instrument Cost Model (NICM)[25] estimates the cost of instrumentation aboard a spacecraft. The specific version of the model used here is intended for interplanetary spacecraft. This was considered the most appropriate model for the mission being considered for this project. The ATLAST requirement of four science instruments was assumed to be the case for this mission, as well. The NICM outputs costs in year 2010 dollars. An annual discount rate of 2.01% was used, and the NICM outputs restated in year 2013 dollars. The model itself takes in peak power, instrument weight, and replacement frequency to determine a lifecycle cost for each of the science instruments aboard individually.

This model provides cost estimating relationships for several different types of instrumentation. The NICM predicts the development and single-unit fabrication costs without management and systems engineering "wrap" factors.[26]

The model is defined in Eq. 83 as

$$C_{NICM} = 328 * M^{0.426} P^{0.414} DL^{0.375}$$

<div align="right">Eq. 83</div>

where C_{NICM} is the cost of instruments, M is total instrument mass in kilograms, P is maximum instrument power in watts, and DL is design life in months.[26] The NICM was produced from 159 instrument cost sets and has some bounds associated with that data set to ensure reliable estimates. The bounds for the mass input are 1-75 kg. The bounds for the instrument power are 1-75 W. The bounds for total design life are 10-150 months. As with the USCM8, the NICM will allow for differentiation of the design architectures based on cost.

5.3.5.4.1.3 USCM8 Cost Model

The Unmanned Spacecraft Cost Model (USCM8) was developed by Tecolote Research for the US Air Force, Space and Missile Systems Center.[26] The model provides cost estimating relationships for non-recurring and recurring cost for large spacecraft buses, including the development, ground equipment, launch operations and orbital support, and communications payload. The non-recurring costs included are design and development, manufacturing, and test of one spacecraft, and acquisition of peculiar support equipment.[26] Recurring costs include fabrication, manufacturing, integration, assembly, and test of the spacecraft.[26] The full model is not presented in this document, however the inputs to the USCM8 are the weights of the various subsystems, the volume of the reaction control system (RCS) tanks, the number of communication channels, burn time to get to the final location, orbit location, and mission of the spacecraft (communications or non-communications). The USCM8 model is a set of cost estimating relationships derived from 44 satellites. Based on the data set provided by these 44 satellites, the USCM8 model has a recommended range for each input. For the entire spacecraft bus, the input range is 114–5,127 kg. Should the architectures fall outside of this or any of other input ranges, as is quite possible, the USCM8 model will be less reliable than intended. However, the relative differences in cost between architectures should still provide useful, discriminating information as discussed earlier.

5.3.5.4.1.4 Complexity

A value for structural complexity is determined in the Systems code module and is incorporated into a "complexity factor" that is used as a multiplier onto the programmatic and spacecraft bus design costs. This is intended to reflect the increased project management and systems engineering workload associated with the design of a more structurally complex system.[60] The calculation of complexity is discussed in Section 5.3.3.9.1. The complexity factor (CF) is of the form

$$CF = \frac{Adjusted\ Development\ Cost}{Unadjusted\ Development\ Cost} = A \times C^{1.2}$$

<div align="right">Eq. 84</div>

where C represents the architecture's structural complexity and A is determined using HST as a validation point, solving the following relation:

$$\frac{Hubble\ Actual\ Development\ Cost}{Hubble\ Unadjusted\ Development\ Cost} = A \times C_H{}^{1.2}$$

<div align="right">Eq. 85</div>

The complexity factor defined above was used to adjust the development cost predicted for HST by our model to HST's actual development cost.[67] This relationship between development cost and complexity has been adjusted from its original implementation.[60,61] This is because only one validation point for complexity (HST) is available, and to get accurate values of β one would need several validation points. Additionally, the value of the exponent here is assumed to be 1.2 based on past space systems[60,61], but ideally that would also be solved for using several validation points. In light of this, complexity is only used as an adjustment onto the predicted development cost of an architecture in the model presented in this report.

5.3.5.4.2 Launch

To find the launch cost for a given telescope architecture, data was collected on various launch vehicles, either currently operational or in development, that may be potentially used for this program (Table XXX). This provided important information such as the mass that each vehicle can send to the desired Geo-Transfer Orbit (GTO), the cost charged per launch, and allowable payload volume.

Table XXX: Launch vehicle properties and cost estimates

| Launch Vehicle | Cost Per Launch (FY2013 Dollars) | Payload Mass (kg) to Specified Orbit | | | Diameter (m) | Height (m) |
		GTO	LEO	LOTUS and EM-L2		
Space Launch System[68]	500000000	23000	70000	35814.6	8.384	17
Falcon 9[69]	56000000	5760	10454	7112.8	4.6	11.4
Falcon Heavy[69]	128000000	12000	53000	20836.2	4.6	11.4
Atlas V[70]	130000000	13605	29400	17967	5	26.5
Delta IV Heavy[71,72]	300000000	12980	22950	15870	5	19.81

To find the total cost required for launch, the number of launches that will be necessary is also required. Determining the number of launches required for a telescope architecture involves, in some manner, packing the telescope into the launch vehicle(s) in order to ensure that the launch system can support the program. The first step in the packing process is to analyze three things: component dimensions, system mass, and system volume. The launch cost MATLAB code checks the maximum dimensions of components included in a given architecture. If the largest component dimension exceeds the payload height offered by a particular launch vehicle, that launch vehicle is immediately removed from the analysis. If the maximum component dimension does fall within the height offered by the payload fairing of the vehicle, the code checks the other dimensions to determine if the component fits within the fairing diameter, possibly in a rotated manner. In the case that it fits with rotation, or in the more common case that all dimensions fall within the payload fairing height and diameter, the vehicle remains a viable option. During this process, the code determines which launch vehicles are able to fit the particular folding/segmentation method of the primary mirror, by far the largest component in the system.

For example, based on the dimensions given in Table XXX, only the Space Launch System (SLS) is capable of fitting Segmentation of the Primary Mirror option #5, the JWST folding style mirror. However, all launch vehicles are capable of launching Segmentation option #1, the case that uses individual uncombined segments. The next step is to determine the maximum number of launches required based on mass and on volume. Total system mass is directly divided by the launch vehicles' capabilities so that there exists a step function of number of launches required for mass. The total system volume is scaled by a conservative packing efficiency of 70%[73] and divided again by the launch vehicles' capabilities. The results of the mass-based and volume-based "number of launches" calculations are compared, and the total number of launches required for a particular vehicle is taken as the larger of the two. Once the total number of required launches is known for each viable launch vehicle, these values are multiplied by the corresponding vehicle's cost per launch (Table XXX) to determine the total launch cost.

A similar approach is used to determine cost of launches for servicing missions. In the servicing case, however, the mass capabilities of each launch vehicle vary depending on the desired servicing location. Also, because the telescope is already in orbit, and the module or component sizes for servicing are known to fit in the various payload fairings, only the mass capabilities of the launch vehicles are considered. By removing unnecessary consideration of volume or dimensional constraints, the code becomes more efficient within the servicing code module.

5.3.5.4.3 Servicing Cost

As described in the Serviceability section, this model does not estimate the cost of a servicer due to the lack of a valid servicer cost model. However, servicing operations still contribute to the overall cost of the mission in two ways. First, the cost of the development of replacement components is considered; second, the cost to launch those components to the servicing location is considered. These two cost elements sum to make up the cost to produce and launch replacement parts over the telescope lifecycle; once again, it is important to note that this cost does not include the cost of a servicer – this only includes the elements of servicing cost which can be estimated with confidence.

In order to calculate the development cost of the replacement components that were produced and used during servicing, it is assumed that the development cost per kilogram of new modules is approximately the same as the development cost per kilogram of the initial telescope. Thus, the total flight system development cost from the first build is multiplied by the ratio of total serviced mass to the system mass:

$$C_{serv}^{D} = C_{FS} \times \left(\frac{\sum m_{serv}}{m_{sys}} \right)$$

<div align="right">Eq. 86</div>

where C_{FS} is the flight system development cost in dollars as described in the Flight System Development Cost section, $\sum m_{serv}$ is the total serviced mass in kg, m_{sys} is the mass of the telescope system in kg, and C_{serv}^{D} is the cost to develop replacement parts in dollars.

In order to calculate the launch cost of replacement parts, the location of servicing, the mean serviced mass per servicing mission, and the number of servicing missions are taken into account along with data for the mass-to-orbit capability as well as the launch cost of various launch

systems to various orbits, displayed in Table XXX. The servicing launch cost is determined for each servicing mission using the same algorithm as the initial launch cost, except that the lift capability of the vehicles is changed to the appropriate values for the servicing location (i.e. if the current architecture utilizes LEO as the servicing location then the launch vehicle's mass-to-LEO capability is utilized instead of its mass-to-SE-L2 capability) and the launch mass is the serviced mass for that particular mission. The sum of the launch cost for each individual mission is the overall servicing launch cost, C_{serv}^{L}.

Once the development and launch costs for servicing have been calculated, the overall servicing cost is calculated by adding them together:

$$C_{serv} = C_{serv}^{D} + C_{serv}^{L}$$

<div align="right">Eq. 87</div>

where C_{serv}^{D} is the cost to develop replacement parts in dollars, C_{serv}^{L} is the cost to launch the replacement parts in dollars, and C_{serv} is the overall servicing cost (not including the cost of servicers).

5.3.5.4.4 Cost Output

As a way of interpreting the outputs of the cost model, historical missions are compared to the outputs of the model. The at-launch cost of the Hubble Space Telescope was $1.5 billion in 1990 US dollars.[74] The five servicing missions of the Hubble Space Telescope had a cost of $9.6 billion in 2009 US dollars.[75] The James Webb Space Telescope (JWST) is estimated to cost at least $8 billion over its lifespan. Figure 50 shows a comparison of those historical costs with the TITANS AE model cost output for both modular (Modularity Level 2-7 and non-modular (Modularity Level 1) architectures averaged over the lifetime of each mission. A breakdown of the sources of these costs is also presented. A "Hybrid Hubble" space telescope architecture was evaluated using the TITANS AE model. This architecture was intended to resemble the Hubble Space Telescope; however, due to assumptions made in the model, this Hybrid Hubble architecture is very different from the actual Hubble mission architecture (e.g., it would be stationed at SE-L2, have a 16.8-m segmented mirror, and have a lifespan of 40 years). Because of these differences, the cost of the Hybrid Hubble is not a highly accurate reflection of the actual Hubble costs. However, it is a useful comparison to make for the purposes of evaluating the output of the model. As can be seen in Figure 50, the Hubble Actual and Hybrid Hubble lifecycle costs are similar. Notably, Average of TITANS AE is slightly more expensive than Hybrid Hubble. This comparison does not reflect the other measures of performance or utility for these architectures, such as utility to science. The Hubble Actual, Hybrid Hubble, and Modular TITANS AE Architectures have lower lifecycle costs than the JWST, though the overall cost estimate of the JWST is smaller than that of the average modular TITANS AE space telescope. This is due to the much shorter lifespan of the JWST, 5 years, relative to the lifespan of the TITANS AE mission, 40 years. It can also be seen, as expected, that modular TITANS AE architectures have lower lifecycle costs (not including most servicing costs) than non-modular TITANS AE architectures. This comparison supports the notion that the cost model is giving reasonable estimates for the lifecycle costs of architectures being evaluated.

<div align="right">139</div>
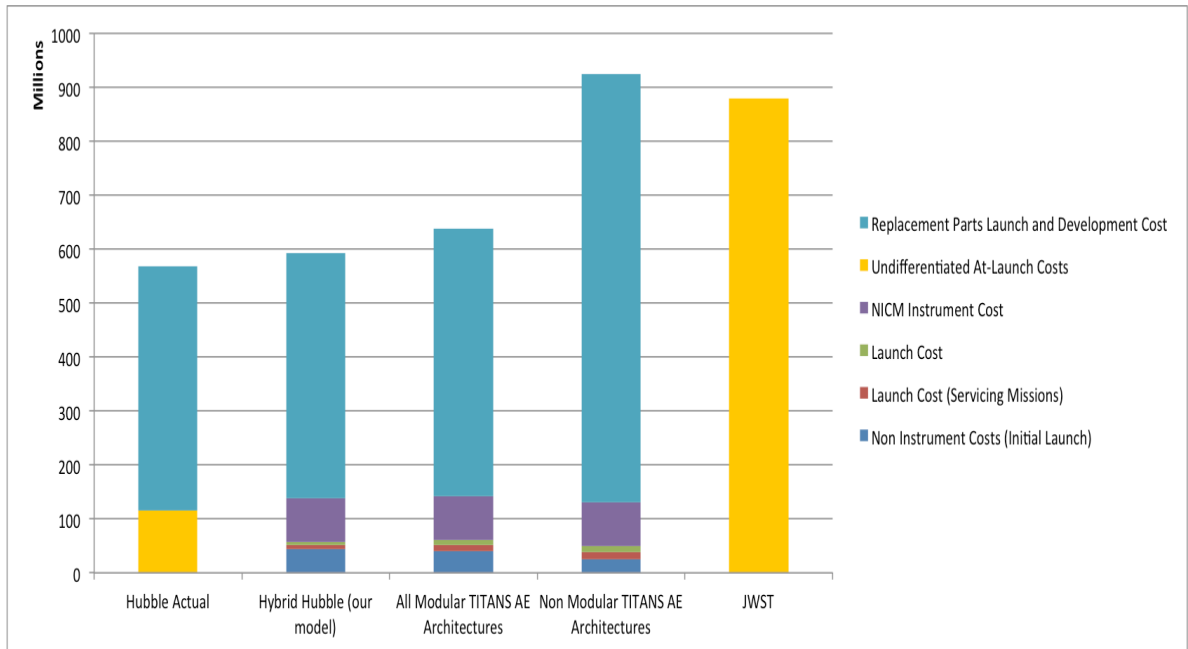
Figure 50: Comparison of cost model output to actual space telescope programs, normalized by total years of operation

6 MODEL VALIDATION

One dimension of validating the accuracy and comprehensiveness of the TITANS AE model encompasses the comparison of the actual Hubble Space Telescope (HST) and James Webb Space Telescope (JWST) mass and power values with the mass and power values of HST and JWST as predicted by the TITANS AE model given architecture decision vectors similar to the actual spacecraft. Ideally, the model predictions would be within ± 30% of the actual HST and JWST values. Given that some of the characteristics of HST and JWST are not captured by the decision vector and the limited scope of the model, this validation was completed with as few code modifications as possible.

The following characteristics of HST and JWST were not captured in the architecture decision vector and were not accounted for in the code modifications: HST uses a monolithic mirror whereas the TITANS AE model uses only segmented mirrors, and JWST has no servicing implemented whereas the TITANS AE model does. Additionally, the model was run with a 40-year lifetime, compared to 23-and-counting for Hubble and a goal of 10 for JWST.

TITANS AE model also exhibits different modularity options; therefore, the code has been run with modularity level 6 for HST, which corresponds to the instruments being in individual modules, and the spacecraft bus is in assemblies. For JWST, the modularity level is assumed 1 (spacecraft level of modularity).

For the communication architecture: Hubble uses TDRSS, so the code has been run with the TDRSS option and JWST uses the DSN, so the JWST validation was run with the DSN option.

Another difference between the design presented here and HST is that HST is in LEO and experiences eclipses. Appropriate modifications in the code were implemented to reflect this: the power subsystem incorporated higher capacity batteries to be able to sustain the telescope consumption during eclipses and the ADCS system incorporated magnetorquers (an added mass of 180 kg). Due to technological advances, the fine guidance sensors are lighter and the batteries in the model are lighter as well.

The results of the validation are illustrated in Table XXVI.

Table XXXI: TITANS AE model validation against HST and JWST

Variable name	Model value	HST value	JWST value	Explanations
Power mass	504 kg	757.1kg[77]	-	The TITANS AE model incorporates lighter batteries (lithium) than HST (nickel metal)
Propulsion mass	0	0[76]	-	HST does not have a propulsion system
Avionics mass	532 kg	600 kg[77]	-	12% difference, attributed to technological advances
ADCS mass	133.5 kg	1074 kg[77]	-	For HST, each fine guidance sensor weighs 220 kg and there are three of them on the HST. The HST also has 4 reactions wheels at 45 kg a piece and 4 magnetorquers at 45 kg apiece. It has an emergency system of computers and IMUs for safe mode which weighs 39 kg. It may be

				assumed that the IMUs weigh something on the order of 15 kg total. If all of these components are added up, it may be determined that the mass of HST ADCS is actually 1074 kg which leaves quite a discrepancy between the HST and the 133.5 kg shown for the TITANS AE model. However, fine guidance system mass in TITANS AE is counted under the science subsystem. Also, TITANS AE does not use any magnetorquers because it is not in LEO. The reaction wheels have less mass on TITANS AE which may cause a slower slew rate. However, this slew rate is on the right order of magnitude and is acceptable within the operational time frame of the mission. Part of the emergency system would fall under the avionics subsystem and IMUs were not accounted for in the code because TITANS AE will probably be able to have IMUs of negligibly small mass, volume, power etc. when TITANS AE is built.
Comms mass	46.79 kg	47.71kg[77]	-	1.9% difference
Optics mass	2300 kg	3860 kg[77]	-	Difference attributed to the different instruments installed on TITANS AE and HST
System mass	11473 kg	11110 kg[77]		3.2% difference, coming mainly from the optics mass difference and the ADCS subsystem
Comm average power	200 W	-	211 W[78]	5.5% difference
ADCS average power	232 W		147 W[78]	The average power is higher due to the fact that the TITANS AE model's ADCS components consume more power than the ones on JWST, thus leading to the 57.8% difference (the reaction wheels take 22W at steady-state, and there are 9 in the design)
Avionics power	200 W		187 W[78]	6.9% difference
Thermal power	207.75 W	-	250 W[79]	The difference comes from the fact that the temperature of JWST's instruments is supposed to be kept at 7K. In the code, the value is 60K, hardcoded in the optics module and was not changed for the purpose of this validation. 20% difference

Some values for JWST or HST were difficult to find on the Internet or in the available references, so the comparison could only be performed on a subset of the model outputs.

7 RESULTS AND ANALYSIS

7.1 Tradespace Exploration and Analysis

Tradespace exploration was applied to the study of the next-generation space telescope design and it facilitated the structured consideration of a large number of design alternatives for the space telescope in terms of desired trade metrics, while avoiding the premature focusing on point solutions. Instead of simply identifying "optimum" or "best" design solutions, this approach uses both graphical and quantitative means to evaluate the architectural decisions that drive the spatial distribution and orientation of all possible alternatives within the considered system design space. "Non-optimal" or "bad" designs will also be evaluated to reveal the multi-dimensional tradeoffs inherent in a complex design problem presented by the space telescope. Ultimately, tradespaces allow the comparison of point designs or sets of point designs to alternatives and accelerate the identification of both physical and preference constraints on feasible solutions.

The tradespace of the space telescope was generated by the complete enumeration of all design variables, which yielded a total of 15,120 design points. The metrics of utility to science, cost, servicing margin, and total failed downtime were previously conceptualized to help identify "good" designs. As these metrics have different units of measurement, they were normalized to facilitate effective and convenient comparison of architectural solution points on a common, quantitative basis. Hence, a solution with a normalized cost near 0 implies that it is relatively cheaper as compared to other solutions in the tradespace, and does not imply that the lifecycle cost is low in terms of absolute monetary value.

2-D and 3-D visualizations of the tradespace bounded by different combinations of metrics were then generated to analyze the interactions, tradeoffs and sensitivities of all design points. In-depth evaluation was then performed on the 2-D tradespaces bounded by cost and utility to science, where sets of design points were evaluated to determine the single or combined architectural decision that would allow one set to dominate another in the tradespace. Complete evaluation also enabled the identification of the Pareto fronts on 2-D and 3-D tradespaces, on which the Pareto Front subset solutions that offer the best tradeoffs between the metrics of interest can finally be identified and analyzed.

7.1.1 2-D visualization of tradespace: normalized Utility to Science vs. normalized Lifecycle Costs
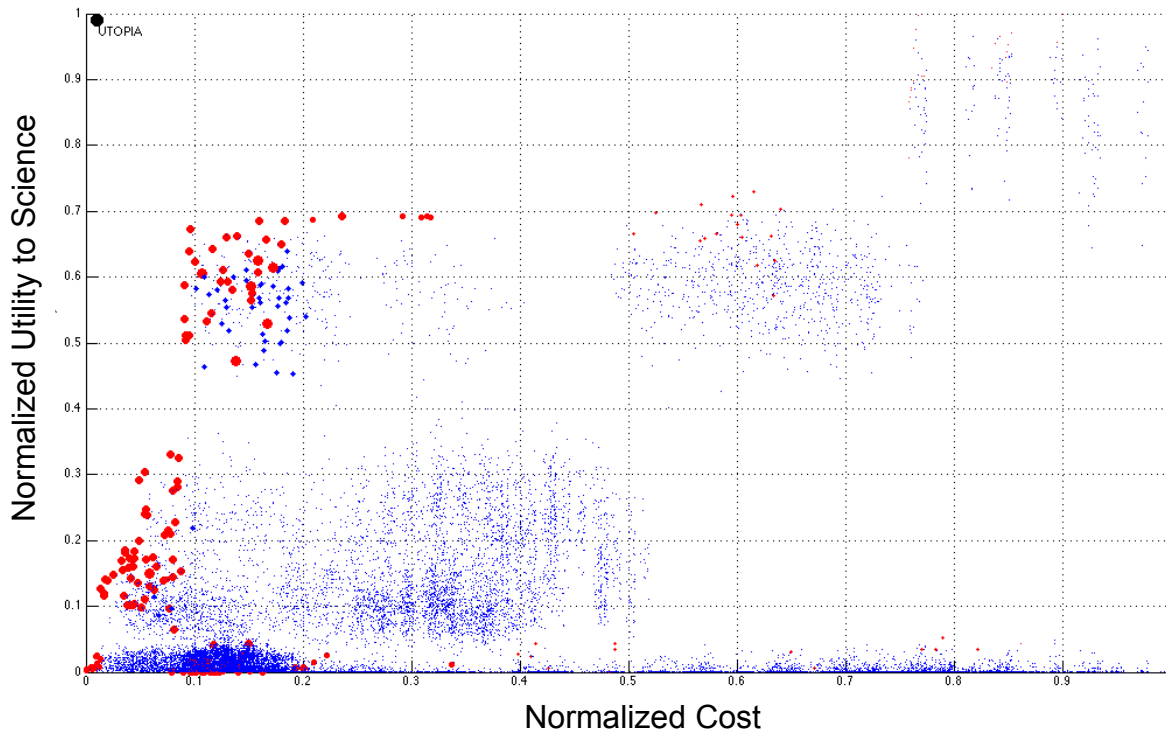
Figure 51: Pareto front solutions (in red) for tradespace bounded by cost and utility to science.

2-D visualizations of system tradespaces were first generated, and a tradespace bounded by cost and utility to science was analyzed and shown in Figure 51. An additional dimension was also reflected in the tradespace to include servicing margin as the third metric, where its value is directly proportional to the size of the point. Therefore, the 2-D tradespace representation can illustrate the interactions between three different trade metrics. The "Pareto Optimal" points were highlighted in red. They were identified using multi-objective optimization and non-dominated sorting, which were algorithms commonly used to establish the Pareto front on a set of points. Points closest to the utopia point would be considered "Pareto Optimal" and the utopia point has the lowest cost, highest utility to science, and highest servicing margin. Conversely, the so-called "bad" designs are characterized by high cost, low utility to science, and low servicing margin.

In Figure 51, clusters of architectural point solutions can clearly be seen on the tradespace, with a high concentration of points in the region with low utility to science and increasing cost. Clusters of larger points are seen closer towards the utopia point, reflective of designs with increasingly lower costs, higher utility to science, and higher servicing margin. Points on the right-hand side are generally smaller, reflecting lower servicing margin. The dominated solutions (in blue) were then removed, leaving a filtered tradespace containing only the "Pareto Optimal" solutions. This is shown in Figure 52 and a total of 8 clusters were visually and cognitively identified in the filtered tradespace for further analysis.

144

Figure 52: 2-D view of filtered 3-D tradespace of "Pareto Optimal" solutions for the space telescope bounded by utility to science and cost.

Cluster 1, which is the identified subset of "Pareto Optimal" solutions closest to the utopia point was further evaluated and each constituent design point was then labeled with its unique architectural vector to determine any commonalities that may be characteristic of the overall subset. This is shown in Figure 53 below. A brief analysis of the points directly reveals that the subset of "Pareto Optimal" solutions is dominated by the "7-1-1" architectural vector elements. "7-1-1" represents the identification numbers of the assigned alternative for the first three architectural decisions in order: the highest modularity level possible of 7, Sun-Earth L2 as the servicing location, and a servicing frequency of 3 years. The same evaluation may also be performed for the other subsets. However, the "7-1-1" subset of architectural solutions will be the focus of evaluation in this report.

Figure 53: "Pareto Optimal" subset solutions closest to the utopia point (Cluster 1) on the filtered tradespace bounded by utility to science and cost, dominated by solutions with "7-1-1" architectural vectors.

A modularity level of 7 would constitute the combination of highest instrument modularity and spacecraft bus modularity. As explained previously, the MTBF of an assembly is equivalent to the lowest MTBF of the components within it and this drives the grouping of component families. As such, the highest level of modularity with each component family as an individual module will yield the most physically robust system with the highest MTBF values for component families and subsequently the entire system. A servicing location at SE-L2 will ensure that the space telescope never experiences downtime, thereby providing the highest utility to science. A servicing frequency of 3 years also ensures that onboard instruments and component families remain in pristine operating condition throughout their mission lifecycles. These reasons thus collectively explain why solutions with the "7-1-1" architectural vector would be dominant in the "Pareto Optimal" subset closest to the utopia point. A small number of solutions identified by the "4-1-1" architectural vector were also observed in the subset, where

'4' represents Modularity Level 4 and the space telescope architecture is defined by instrument packages and spacecraft bus component assemblies.

The "7-1-1" architectural vector for the visually identified "Pareto Optimal" subset of solutions closest to utopia point was reaffirmed using the Polar plot shown in Figure 54 below. The Polar plot illustrates the frequency of occurrence within the filtered Pareto set of solutions for every possible alternative in each architectural decision on a circular plane based on random sampling. Sampling from a smaller set of solution points can help identify architectural alternatives that dominate the same set. With increasing number of samples, the frequencies of occurrence for all architectural alternatives will become equal as a direct result of sampling across a large distribution. Each arrow on the circle corresponds to each alternative, and it is matched in accordance to the legend shown on the left in an anti-clockwise order. Color families distinguish the 7 key architectural decisions. The frequency of occurrence has also been normalized and it is directly proportional to the length of the arrow representing its corresponding architectural alternative. The opaque circle in the center of the plot has a radius of 1 and arrows protruding out of this circle can be easily identified as prominent architectural alternatives.
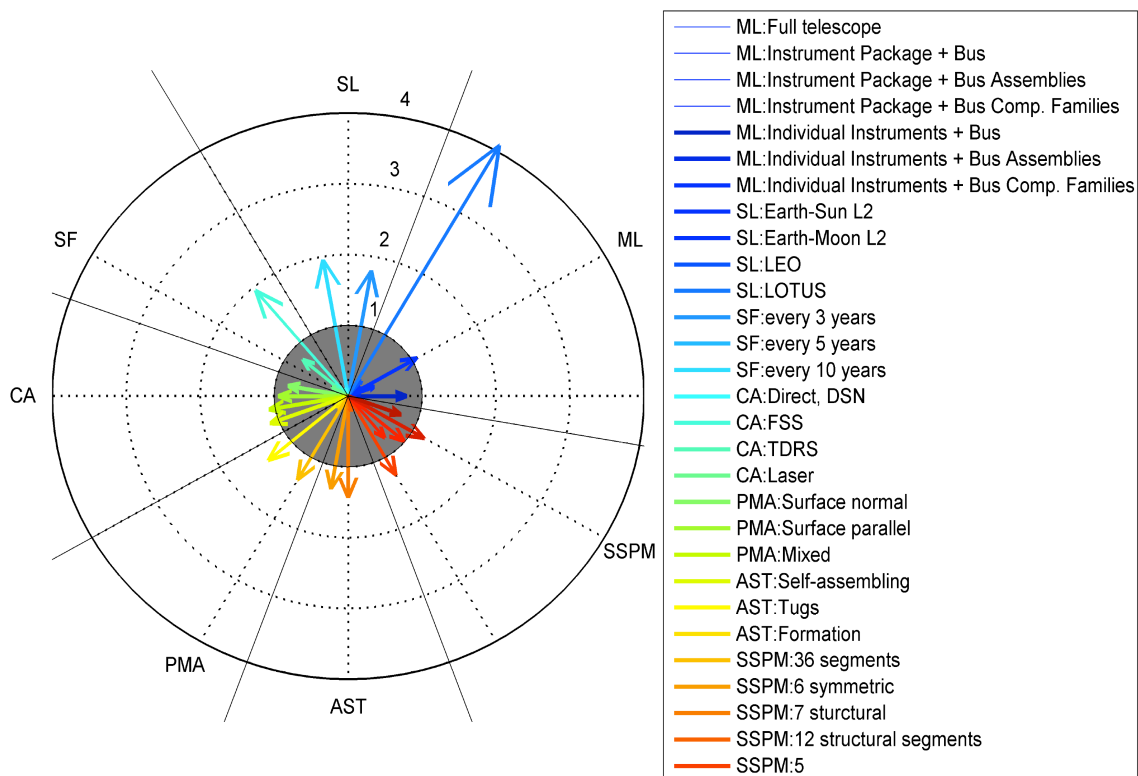
Figure 54: Polar plot indicating frequency of occurrence for every alternative in each architectural decision for Pareto Optimal solutions. ML: Modularity, SL: Servicing Location, SF: Servicing Frequency, CA: Communications Architecture, PMA: Primary Mirror Actuation, AST: Assembly/Servicing Technique, SSPM: Structural Segmentation Primary Mirror Gray circle of radius 1 represents expected radius of any architecture decision if it is not associated with Pareto solutions.

Figure 54 clearly shows that Level 7 (Individual Instruments and Bus Component families) dominates the modularity architectural decision. Both SE-L2 and LEO dominate other solutions

for the Servicing Location decision while a 3-year frequency dominates the Servicing Frequency decision. As such, the "7-1-1" subset of "Pareto Optimal" solutions comprise the dominant alternatives shown in the Polar plot, thereby verifying its close proximity to the utopia point. In other architectural decisions, laser communications is slightly dominant for communications architecture, surface-normal and hybrid assemblies are equally dominant for primary mirror actuation architectures, and space tugs and robotic self-assemblies are also distinctly dominant for assembly and servicing techniques. 36 segments and 12 structural segments are slightly dominant for the decision on mirror segmentation. The large variation in the other 4 architectural decisions thus account for the distribution of architectural solutions in the identified "Pareto Optimal" subset of solutions closest to utopia point.
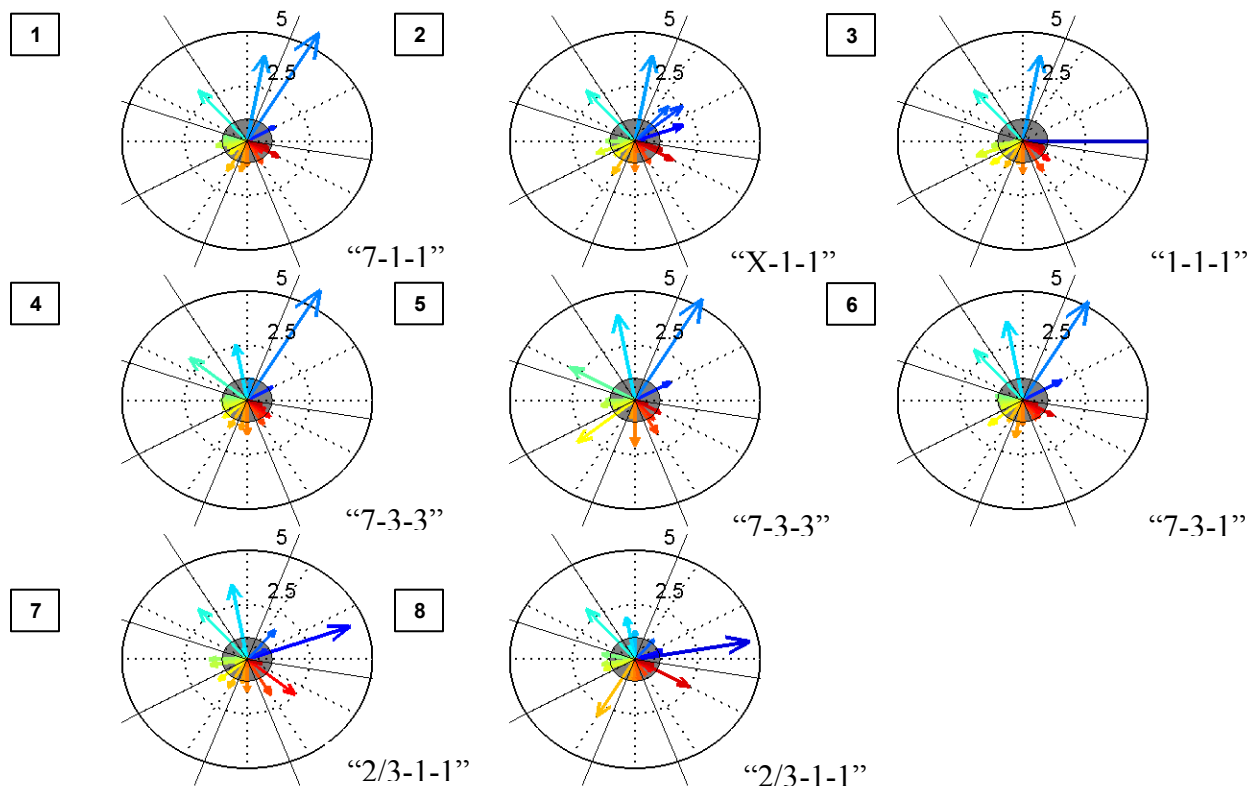
Figure 55: Polar plot array illustrating dominant architectural alternatives in every identified cluster.

The same procedure is then repeated to evaluate the dominant architectural elements in every cluster. An array of Polar plots is shown in Figure 53, where each numbered Polar plot is representative of its corresponding cluster on Figure 52. In Cluster 2, the dominant architectural alternatives are still the Sun-Earth L2 servicing location and a servicing frequency of once every 3 years ("X-1-1"). However, modularity is no longer as dominant in this cluster. In fact, lower levels of modularity become more prominent, and this results in increased cost due to higher launch costs required for high launch masses of instrument packages instead of individual components. As such, the solutions of Cluster 2 are located just to the right of Cluster 1 and in a region with higher normalized cost.

The dominant architectural alternatives in Cluster 3 are Level 1 modularity, SE-L2 servicing location and a servicing frequency of once every 3 years ("1-1-1"). This cluster is located in the top-right region of the tradespace and comprises solutions with generally high cost and high utility to science. Costs are exceptionally high for these solutions, as the lowest level of modularity and the highest frequency of servicing meant replacing the entire telescope once every 3 years. Utility to science is also highest due to regular servicing and replacement of every instrument and component onboard the spacecraft without any downtime.

The architectural alternatives of Level 7 modularity, servicing location at LEO and servicing frequency of one every 10 years dominate the solutions in Cluster 4 ("7-3-3"). Modularity Level 4 is also prominent, thus accounting for the presence of "4-3-3" solutions amongst the majority of "7-3-3" solutions. Cluster 4 is located below and to the left of Cluster 1 because servicing at LEO is a lot cheaper, but it also incurs higher downtime. Also, servicing the telescope once every 10 years means that there is a higher probability that certain instruments or components could fail without being replaced for long periods. This results in a loss of utility to science.

The Polar plot of Cluster 5 is almost similar to Cluster 4 ("7-3-3"), except that it reveals some alternatives for other architectural decisions have become more prominent. "4-3-3" points are also present in this cluster. These alternatives are laser communications architecture, surface-normal primary mirror actuation, assembly and servicing with tugs and 36 mirror segments. Normalized costs of solutions in Cluster 5 are lower than that of Cluster 4 because laser communications and the use of tugs, which are external to the space telescope system, entail lower launch mass. As such, Cluster 5 is located to the left of Cluster 4.

Cluster 6 has modularity level 7, servicing location at LEO and servicing frequency of once every 3 years as the dominant architectural alternatives ("7-3-1"). While it might be cheaper to service at LEO, a much higher frequency of servicing would result in higher total launch costs for the space telescope across its mission lifecycle. As such, the solutions in this cluster would have a higher normalized cost and they are located to the right of Clusters 4 and 5.

Finally, Clusters 7 and 8 are generally characterized by modularity levels 2 and 3, servicing location at LEO and servicing frequency of once every 3 years as the dominant architectural alternatives ("2/3-3-1"). Lower levels of modularity, near-Earth servicing location and high frequency of servicing collectively imply that large instrument packages or component families are being taken out and replaced frequently during its mission lifecycle. The high frequency of servicing drives the normalized costs up, while servicing a minimally modular spacecraft means that downtime will be a common occurrence, leading to lower utility to science. As such, these solutions are located in the region of increasing costs and low utility to science.

Through analyzing the clusters of solutions in the tradespace of "Pareto Optimal" points, it is evident that the architectural decisions of modularity, servicing location and servicing frequency have huge leverage on the spatial distribution of solutions in the utility-cost space. Higher modularity, servicing at its SE-L2 operating location, and high servicing frequency generally drive solutions towards the utopia point. Low modularity will generally drive solutions towards the high cost end while servicing at LEO or at a lower frequency will drive solutions towards the low-cost/low-utility end.

5 architectural solutions were then chosen at random from the "Pareto Optimal" subset ("7-1-1") and plotted on a Pareto Trace plot shown in Figure 56 to demonstrate that they are always on or close to the Pareto front for all the trade metrics of interest. These points may eventually be recommended architectural solutions, but they have chosen simply for illustrative purposes. The Pareto Trace plot is a collective 3-D representation of tradespaces bounded by the fixed axis of cost and each of the remaining trade metrics to illustrate how a single architectural solution point transits across different tradespaces defined by different metrics. The x-axis defines the number of tradespaces, each defined with different metrics, to be plotted for Pareto tracing. Each tradespace in this plot can have different utopia points.

A "Pareto Optimal" point will thus move along the Pareto front for each tradespace shown in this representation. The 5 chosen points were then traced across the three different tradespaces and the traces demonstrate that these points are always on or close to the "Pareto Optimal" region in each tradespace. Therefore, these "Pareto Optimal points can be shown to have the best tradeoffs for utility to science, downtime and service margin against costs. As such, the Pareto trace plot can facilitate the illustration of the position of an architectural solution relative to other points across multiple tradespaces.
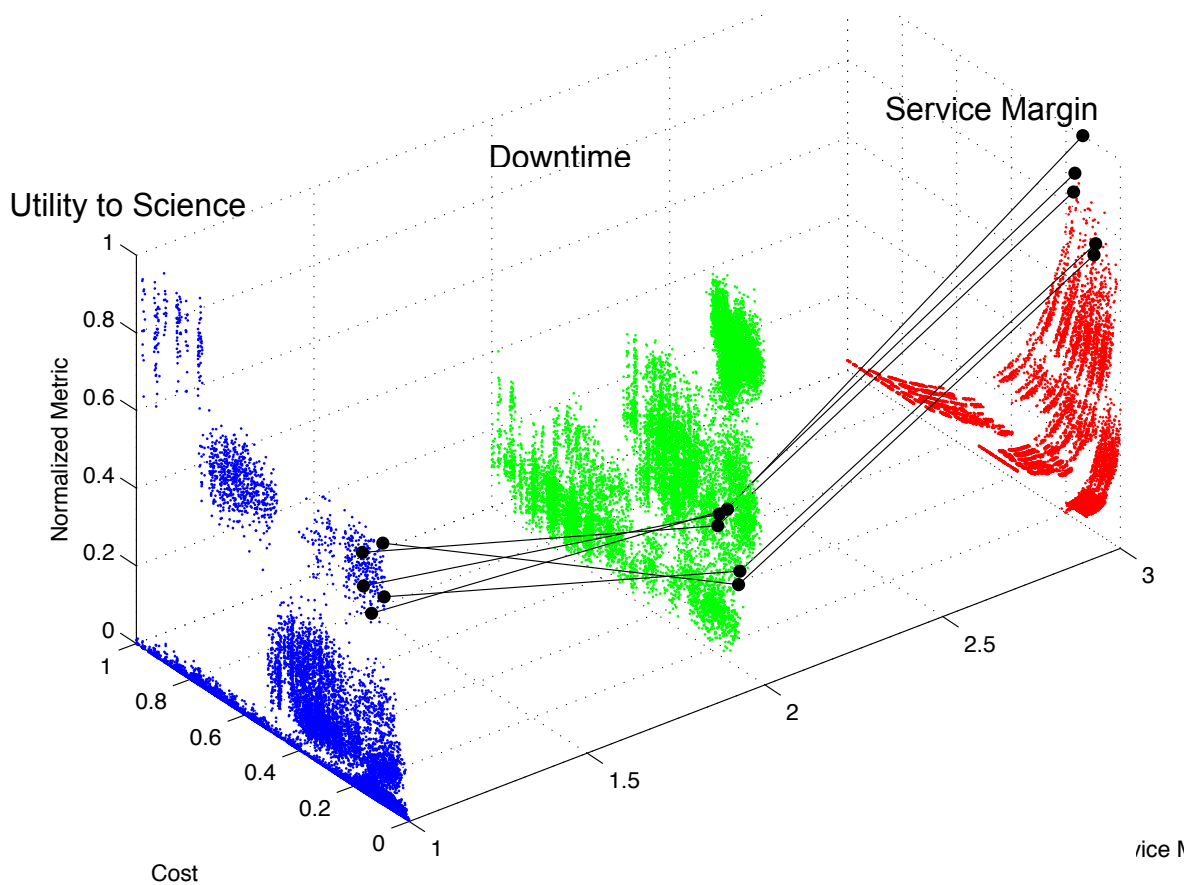
Figure 57: Pareto trace of solutions across different tradespaces defined by combinations of various trade metrics with a fixed bound of cost.

150

This procedure for tradespace exploration and analysis can be conducted for the other trade metrics like downtime or service margin so that further evaluations can reveal the tradeoffs that are driving the distribution and location of other architectural solutions. However, utility to science versus cost will be the focus of analysis and evaluation at this stage.

7.1.2   3-D Visualization of Tradespaces

3-D visualizations of tradespaces can also be plotted for encompassing illustrative purposes. While 3-D tradespaces are much more difficult to interpret, they are reflective of the inherent tradeoffs between the four metrics of interests. The spatial distribution of solutions within a 3-D space can thus provide new and useful insights into performing evaluation and analysis.

Two 3-D tradespace plots were generated for this illustrative, with the X-Y plane established by the dominant metrics of total lifecycle cost and utility to science. The vertical Z-axis was varied in these two plots, with Failed Downtime and Service Margin as the third metric shown in Figure 58 and Figure 59 respectively. The three metrics in each case have been normalized to compare their interactions on a common quantitative basis. A restructuring of the system design tradespace was also clearly evident with the change in third metric.
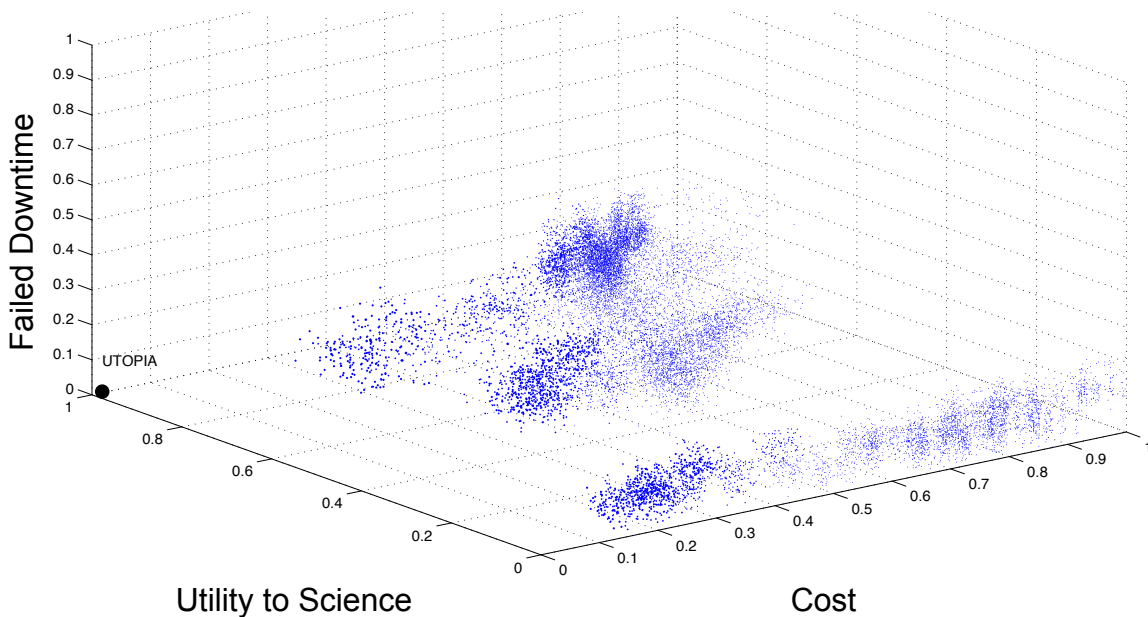
Figure 58: 3-D tradespace of the space telescope bounded by cost, utility to science and failed downtime
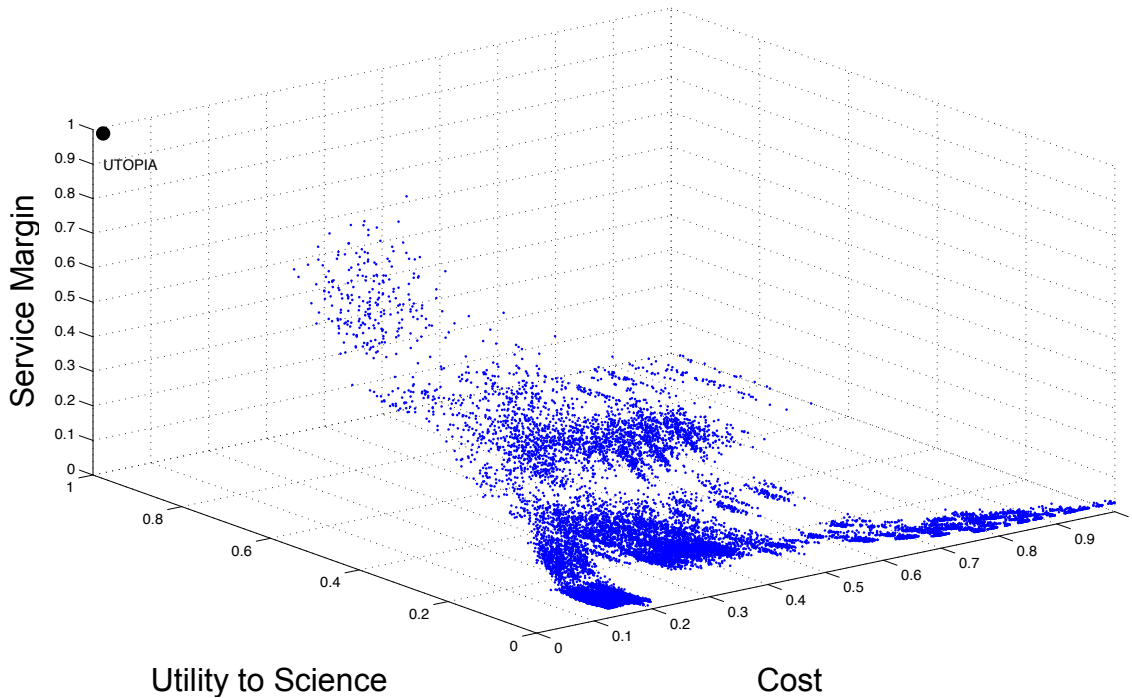
Figure 59: 3-D tradespace of the space telescope bounded by cost, utility to science, and service margin

Figure 59 shows the distribution of the same set of design points restructured by a change in the third metric from downtime to service margin. An elevated slope of design points is observed, with most points concentrated at regions with low utility to science and increasingly spare sets of points tapering towards the utopian point with low cost, high utility to science and high service margin. This distribution can be explained with the underlying scientific principles and assumptions used to develop the trade metrics of interest in this case. The service margin is a monetary metric, quantified by the baseline cost less the development cost, launch cost and servicing cost. Clearly, the lower the costs of launching a particular service mass, the higher the service margin.

New relationships between the metrics have also been observed from these two plots. The servicing location of the space telescope has a direct impact on its downtime, where Sun-Earth L2 is the best location since there is no change in operating location and subsequently no downtime. This is followed by the Earth-Moon L2 location, the Lotus orbit, and finally LEO as determined by proximity from the designated operating location. Utility to science is generally inversely proportional to downtime. However, the cost to launch servicing mass demonstrates an inverse trend, as it entails the lowest cost for LEO owing to close proximity from Earth and the highest cost for Sun-Earth L2. Therefore, the service margin would be inversely proportional to downtime. Combining these two relationships would then imply that the service margin is directly proportional to utility to science. This implied relationship is thus evident in the upward slope observed in the tradespace of Figure 59 as "Pareto Optimal" design solutions move and taper towards the utopia point.

152

Instead of a Pareto front, a Pareto surface can be identified in 3D space and the "Pareto Optimal" points are highlighted in red as shown in Figure 62 below. A total of 202 solutions was found in this Pareto set. Dominated solutions can then be removed to yield the filtered tradespace shown in Figure 63. The procedures used to analyze and evaluate tradespaces in 2D can then be applied in the same manner with the added dimensionality.
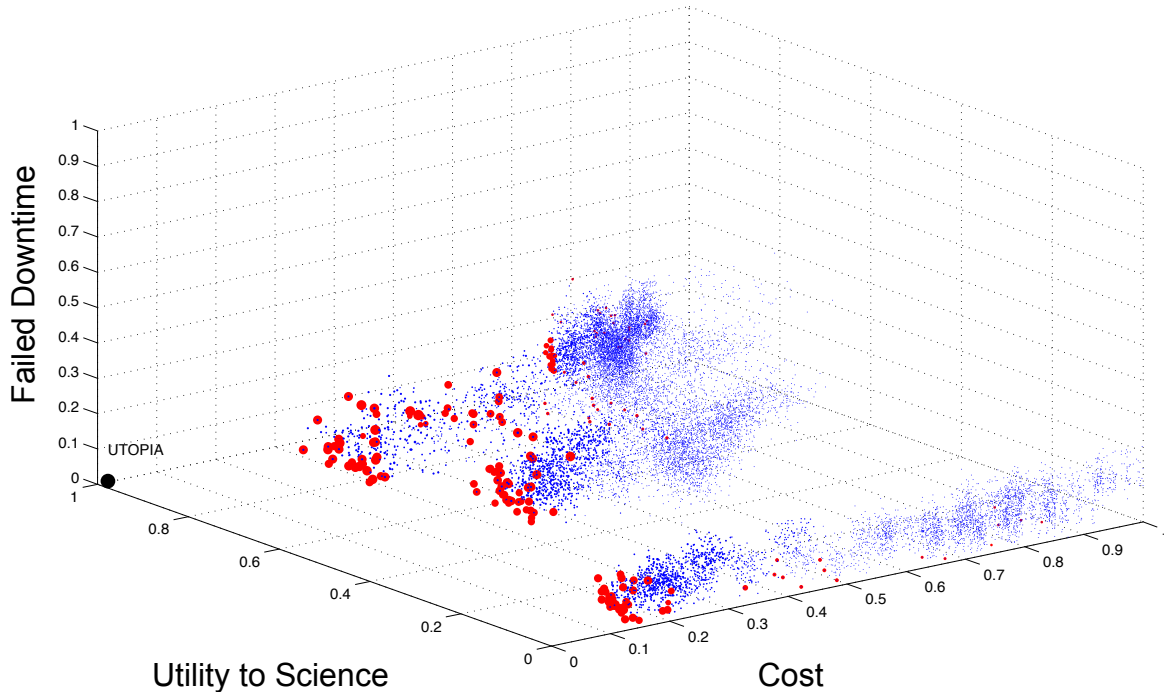
Figure 60: 3-D tradespace of the space telescope bounded by cost, utility to science and failed downtime, with "Pareto Optimal" solutions highlighted in red
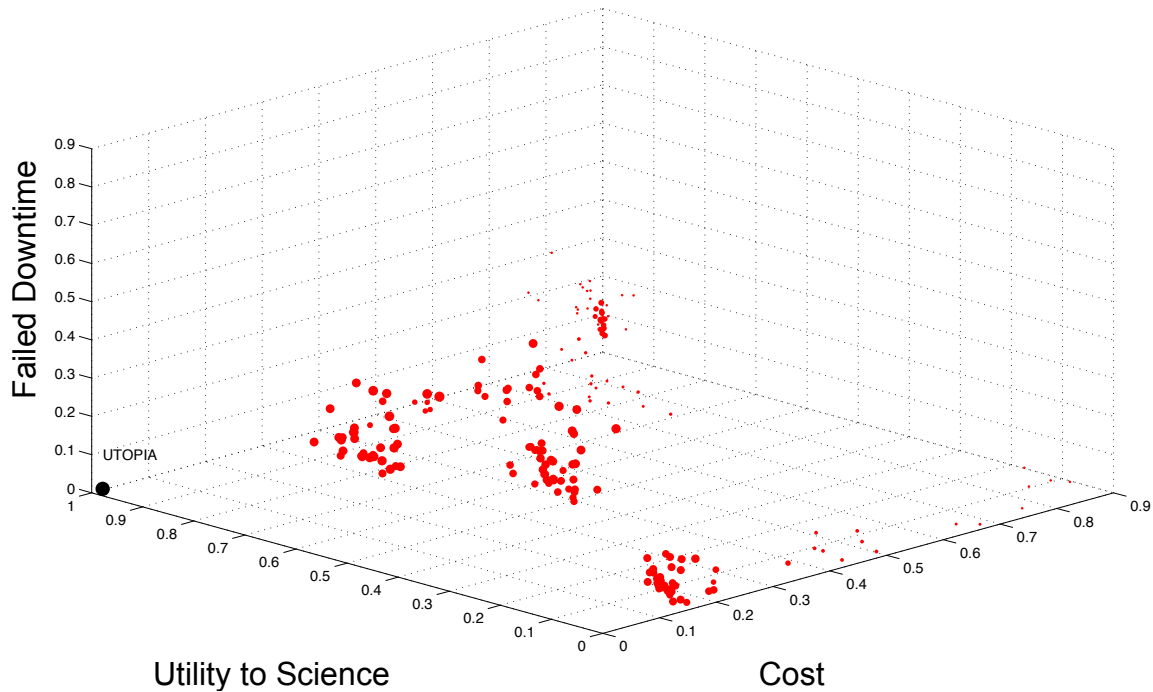
Figure 61: Filtered 3-D tradespace of "Pareto Optimal" solutions for the space telescope bounded by cost, utility to science and failed downtime

Continued exploration and analysis of tradespaces can reveal further complex interactions among trade metrics and architectural decisions. In the evaluation and analysis thus far, architectural solutions with the "7-1-1" configuration of full modularity, SE-L2 servicing location and a servicing frequency of once every 3 years, have been found to constitute the "Pareto Optimal" subset of solutions closest to utopia point. Decreasing modularity generally increases cost due to higher masses of instrument packages required to be launched during every servicing trip. Hence, solutions with lower modularity levels tend to fall on the high-cost/high-utility region of the tradespace.

Servicing locations closer to Earth generally lead to decreased utility to science, as the movement from its original operating location at SE-L2 coupled with high servicing frequency results in increased downtime. As such, solutions with servicing locations at LEO and other alternatives are found in the low-cost/low-utility region of the tradespace. The servicing frequency has a strong proportional impact on cost, but an inversely proportional effect on utility to science. Its variation thus leads to a wide distribution of solutions.

From the analysis of clusters, Polar plots and Pareto trace plots, the effects of different architectural combinations are clearly reflective in the tradespaces. Therefore, tradespace exploration motivates the process of making a priori design or architectural selections that are "Pareto Optimal" through rigorous analysis and consideration of other options.

7.2 Interactions and Main Effects

7.2.1 Science Utility

The main effects plot shows the impact that a single architectural decision has on a particular trade metric. In this case, the trade metric is science utility. Science utility is defined as the contribution of the spacecraft to the scientific community and is calculated by taking the integral of the sum of the field of view multiplied by the throughput of all the science instruments on the spacecraft.
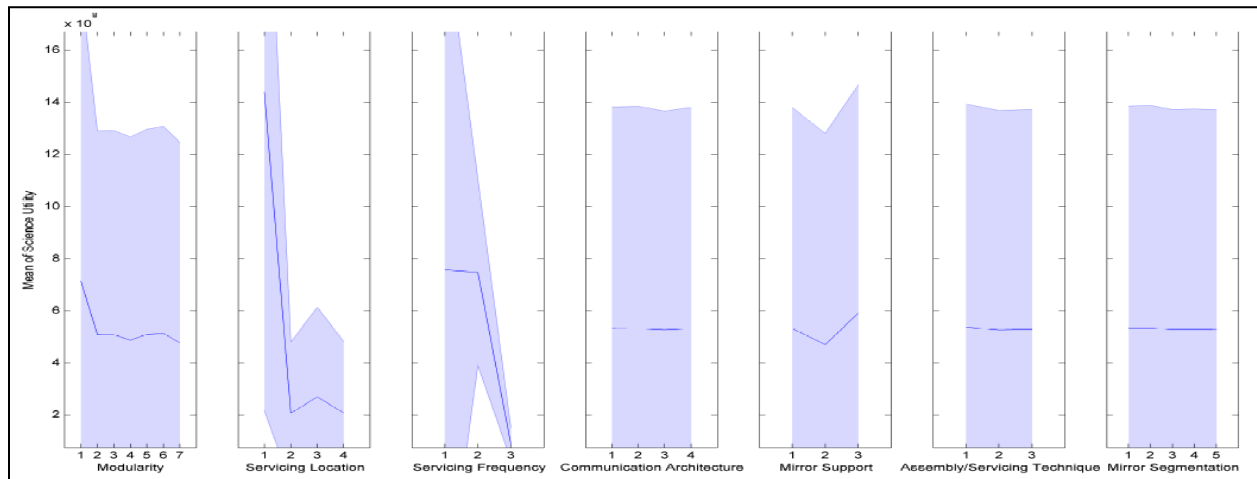
Figure 62: Main effects plot for Science Utility

With respect to modularity level, modularity level 1 is the most useful for science utility while the rest of the modularity levels exhibit approximately the same level of science utility. This occurs because modularity level 1 requires the entire satellite to be replaced, which will rapidly upgrade the science capability: 3-D tradespace of the space telescope. With respect to servicing location, SE-L2 is by far the most useful to science. This is attributed to the fact that the telescope does not have to relocate to be serviced, thus the bounded by cost, utility to science, and failed downtime value is minimized. With respect to the servicing frequency, servicing every three years provides the greatest science utility while servicing every ten years provides a drastically lower science utility. This occurs because shorter frequencies allow for the satellite to be repaired and upgraded more frequently. With respect to communication architecture, no major effects were observed. With respect to mirror support method, mixed surface-normal and parallel actuators provide the most utility to science because they allow for a more effective actuation capability. The surface-parallel option provides the lowest science utility because of the low MTBF values associated with this system. For the servicing and assembly technique, as well as the segmentation method, no major effects were observed.

An interaction plot was generated to show the effect that each architectural decision, in combination with every other architectural decision, had on the total science utility. Because there are seven architectural trades being conducted, the resulting plot was a 7-by-7 grid of graphs, with each sub-plot showing the impact that a given combination of two architectural trades have on science utility. Each row of the plot grid represents one set of architectural trades as data sets, with the number of distinct lines equal to the number of different architectures

within that tradespace. Each column of the plot grid represents the architectural decisions within that particular tradespace as distinct points along the independent axis. For all plots, science utility is represented on the dependent axis.
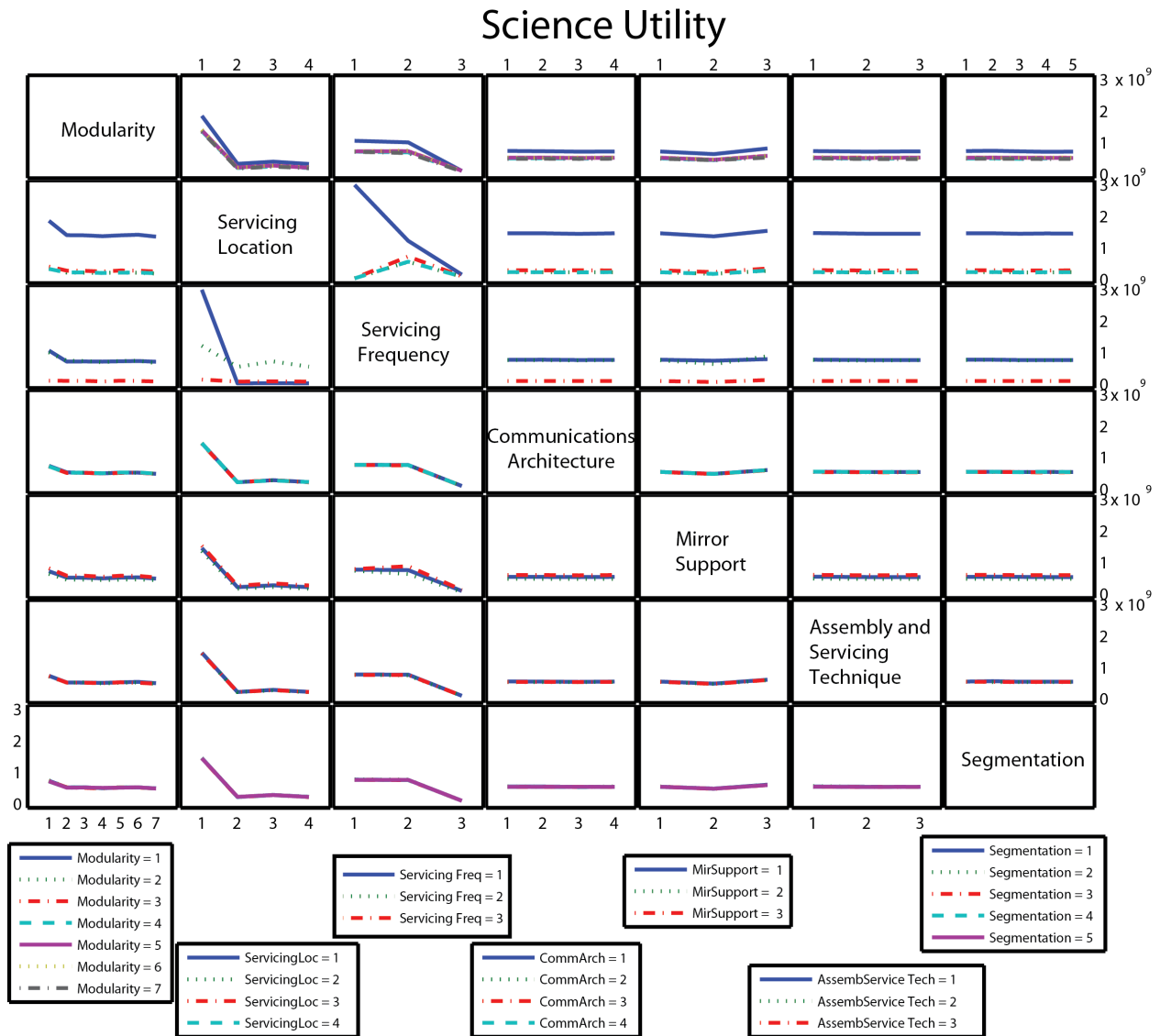
Figure 63: Interaction plot for Science Utility

The most interesting plot encompassed within the graph above shows the interaction between the servicing location and the servicing frequency. The servicing location of SE-L2 provides the greatest science utility when a servicing frequency of three years is used because SE-L2 requires no down time for transit to the servicing location. The science utility falls as the servicing frequency is decreased causing more parts of the space telescope to fail. For all of the other servicing locations, the servicing frequency of three years provides a low science utility because of the tremendous amount of time spent in transit. In these cases, the ten year servicing frequency also causes a low science utility because of the bounded by cost, utility to science, and

156

failed parts. The 5-year servicing time strikes an optimal balance for architectures serviced somewhere other than SE-L2.

7.2.2 Cost

The main effects plot shows the impact that a single architectural decision has on a particular trade metric. In this case, the trade metric is cost.
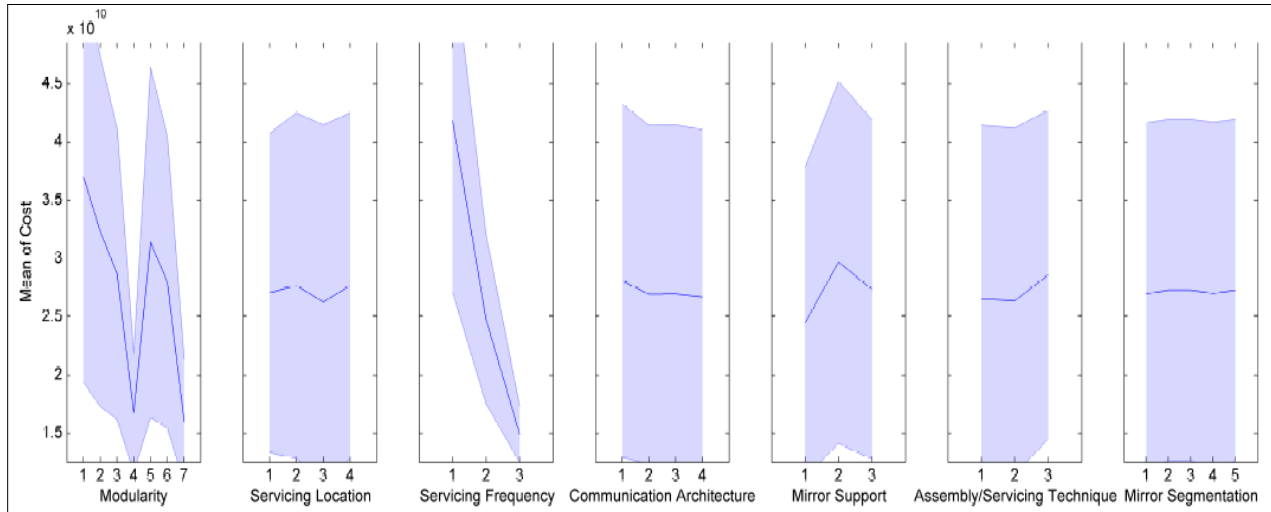
Figure 64: Main effects plot for Cost

Cost most strongly depends on servicing frequency and modularity. Servicing frequency directly affects the number of servicing missions. With each additional servicing mission, the cost will increase due to an additional launch and additional mass being added to the telescope to replace broken or unreliable components. Modularity affects the mass that is replaced in each servicing mission. When many components are grouped together in one module, the entire module must be replaced when any component in the module fails or becomes unreliable. Therefore, as modularity increases, less and less mass is replaced over the lifetime of the telescope. With less mass being replaced, fewer additional components need to be developed and lower cost launch vehicles can be used for each servicing mission. Of the remaining architectural decisions, the biggest dependency is on mirror support method and this dependency is entirely caused by the varying number of actuators involved in the mirror actuation techniques. The remaining architectural decisions (servicing location, communications architecture, Assembly/Servicing Technique, and Mirror Segmentation) have little direct effect on cost.

These interaction plots show the same information as the interaction plots above except for the trade metric of cost.
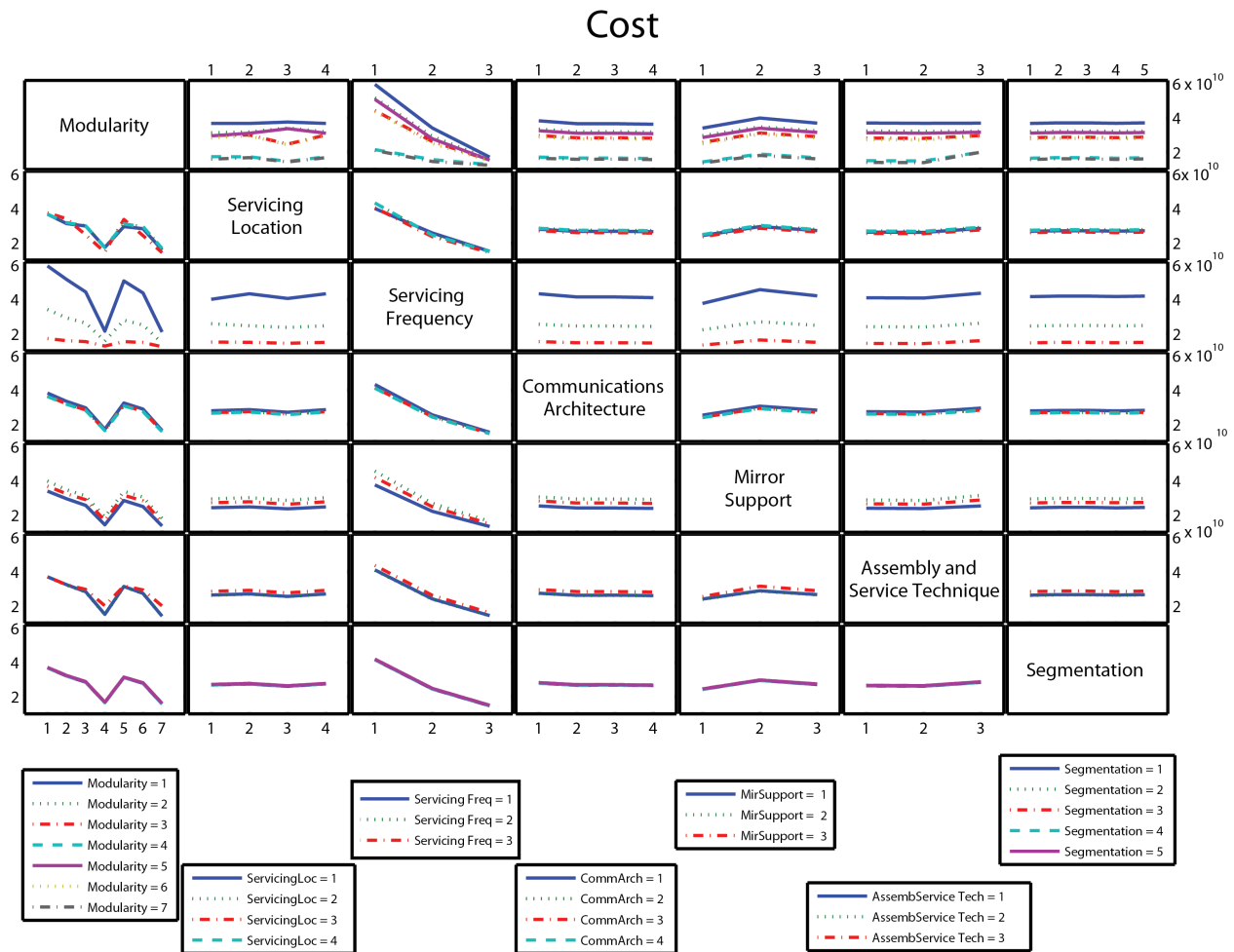
Cost

Figure 65: Interaction plot for Cost

With respect to the interaction between servicing frequency and modularity level, the higher the modularity level of the spacecraft, the less expensive that it will be. However, the cost gap between levels of modularity is greater for more frequent servicing than for less frequent servicing. This dependency on servicing frequency exists because the proportional cost of replacing large modules when only a few components within have failed is decreased with less frequent servicing because modules will tend to have more components that need servicing. Another interesting dependency is the divergence between modularity levels 3/6 and 2/5 for servicing at LEO. This divergence occurs because servicing missions using higher modularity levels and servicing at LEO are able to use smaller rockets whereas servicing missions associated with lower modularity still need to use larger more expensive rockets to move large amounts of mass into LEO and have the added cost of moving the space telescope over large distances. Lastly, there is a small dependence of cost for high modularity levels on assembly/servicing technique. The swarm assembly/servicing technique adds additional equipment necessary for assembly to each module, increasing the mass and cost.

7.2.3   Servicing Margin

The main effects plot in Figure 66 shows the impact that each architectural trade had on down time. Servicing margin was defined as cost difference between the "baseline" design for a given

set of architectural decisions – that is, the design with a monolithic bus (modularity level 1) – and an identical design with a higher level of modularity, normalized by the total mass that can be launched across all of the servicing missions.
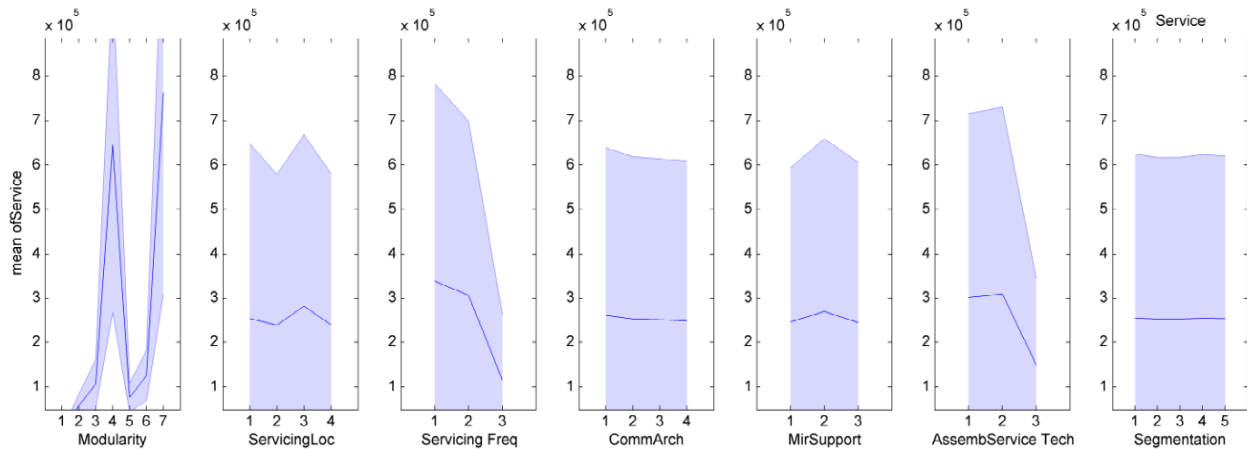
Figure 66: Main effects plot for Servicing Margin

As can be seen from the main effects plot, not all architectural trades had a significant impact on the total mission down time. In particular, Communications Architecture and Mirror Segmentation Method showed nearly flat trends across the different design decisions within those trades. Meanwhile, Modularity Level, Servicing Frequency, and Assembly/Servicing Technique showed noticeable trends across the different design decisions within those trades.

An interaction plot was generated to show the effect that each architectural decision had on the total servicing margin. Because there are seven architectural trades being conducted, the resulting plot was a 7-by-7 grid of graphs, with each sub-plot showing the impact that a given combination of two architectural trades had on serviceability. Each row of the plot grid represented one set of architectural trades as data sets, with the number of distinct lines equal to the number of different architectures within that trade-space. Each column of the plot grid represented the architectural decisions within that particular trade-space as distinct points along the independent axis. For all plots, servicing margin was represented on the dependent axis.

7.2.3.1 Modularity
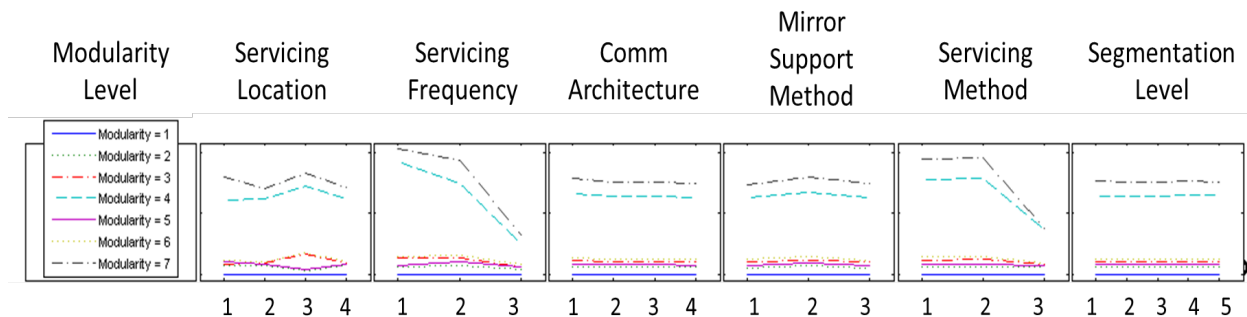
Figure 67: Service margin trends for different modularity levels

It was observed across all of the interaction plots that modularity levels 4 and 7 had the highest servicing margins. This corresponds to the two most modular design options: modularity level 4

159

represents a single instrument package with separate structures for each component family; modularity level 7 represents individual instruments packages with separate structures for each component family. Modularity level 7 was the most serviceable across all other design trades, since individual instruments are less costly to service/replace than a single, integrated instrument package.

7.2.3.2 Servicing Location
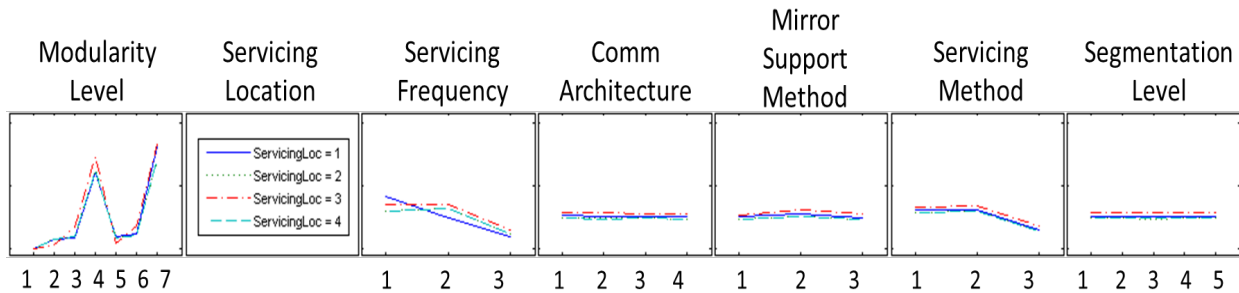
Figure 68: Service margin trends for different servicing locations

Results showed that of the four servicing locations, LEO (servicing location 3) generally provided the most servicing margin. However, interesting trends were detected when looking at both servicing location and servicing frequency. For a servicing frequency of 3 years, servicing at Sun-Earth L2 (servicing location 1) provides the most servicing margin. For servicing frequencies of 5 and 10 years, servicing in LEO provides the most servicing margin. This is thought to happen because the serviced mass at LEO is lower than the serviced mass at other locations as the telescope will use electric propulsion to get to/from LEO. That is, for a fixed payload mass launched to orbit, the mass of propellant required to refuel the telescope for its return journey to L2 is lower than the mass of chemical propellant that would be required to propel the servicing probe to any location outside of LEO. This leads to the launch cost/kg is lowest at LEO.

7.2.3.3 Servicing Frequency
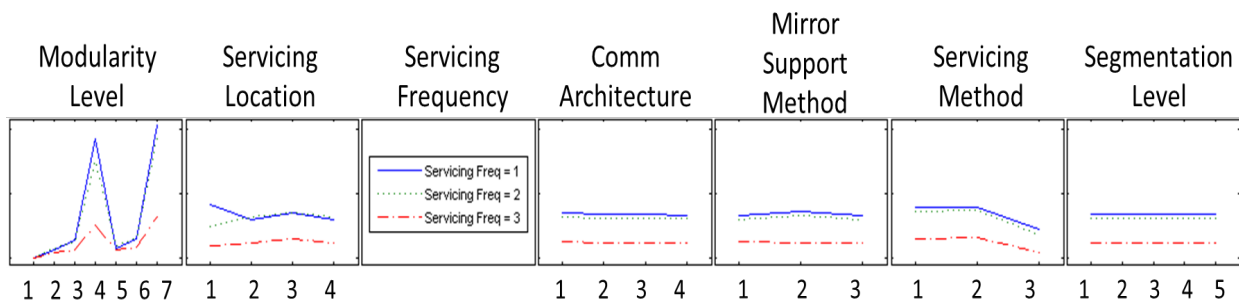
Figure 69: Service margin trends for different servicing frequencies

As can be seen in the above figure, shorter servicing frequencies lead to more servicing margin. The shortest servicing frequency – three years between servicing missions – consistently has the highest servicing margin for all architecture combinations. Likewise, the longest servicing frequency – 10 years between servicing missions – has the lowest servicing margin for all architecture combinations. This is thought to happen because having frequent servicing missions

leads to fewer components being replaced per mission, which cheaper rocket with lower payload capacities can be used. Infrequent servicing missions would be replacing more components per mission, requiring launch vehicles with larger payload capacities.

7.2.3.4 Communications Architecture
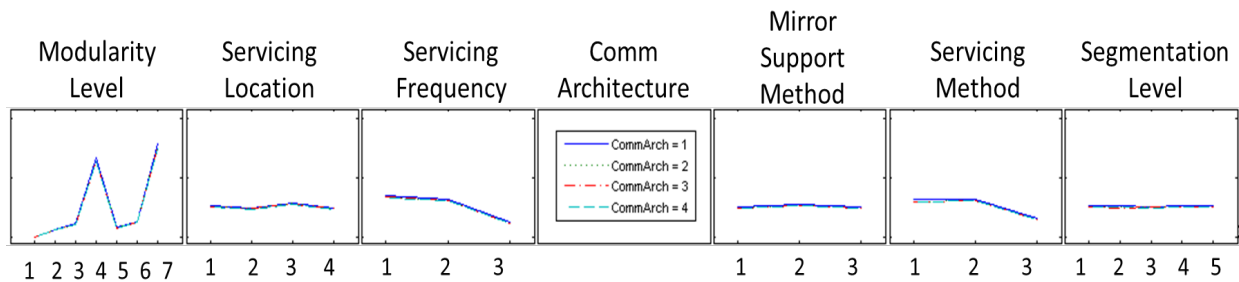
Figure 70: Service margin trends for different communications architectures

Communications architecture has little impact on servicing margin across all other design trades. Communications architecture 1 (DSN) is marginally better than the other three options, which is interesting because it the most massive and most expensive out of the four possible architectures, and therefore should have the lowest servicing margin.

7.2.3.5 Mirror Support Method
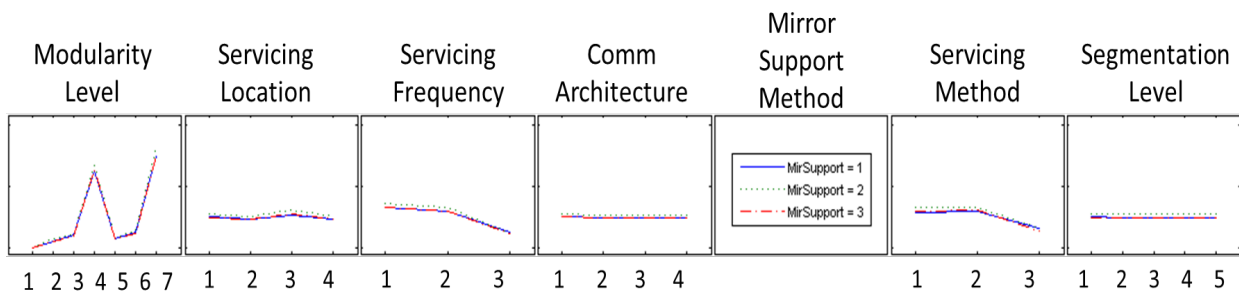
Figure 71: Service margin trends for different mirror support methods

The Mirror Support Method trade also showed little variation across the three possible architectures. Results showed that support method 2 (surface parallel) was provided a marginally higher servicing margin than the other two support methods. This is because the surface parallel support method lacks a back-structure, and therefore has the lowest mass of the three options.

7.2.3.6 Assembly/Servicing Technique
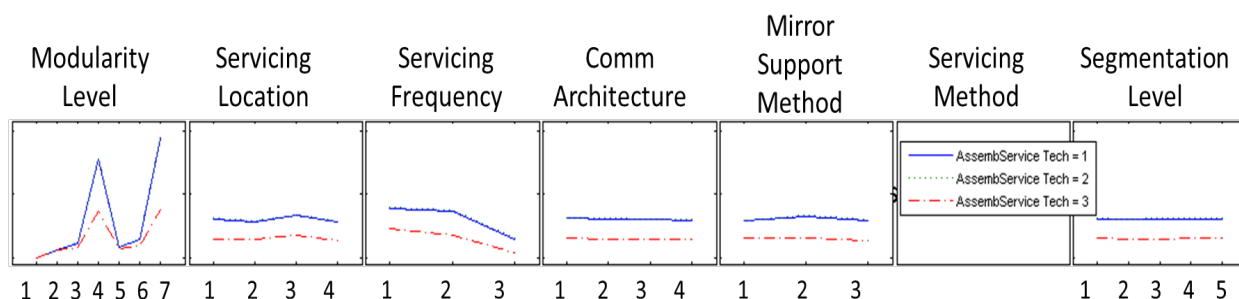
Figure 72: Service margin trends for different assembly/servicing techniques

Assembly/Servicing Technique had a noticeable impact on servicing margin. Techniques 1 and 2 (self-assembly and tugs, respectively) had the highest servicing margins and were nearly identical. Servicing technique 3 (formation flying individual components) had drastically lower servicing margins across all other design trades. Of the three options, servicing technique 2 had the highest servicing margin. It is believed that this is because tugs have the lowest cost.

7.2.3.7 Mirror Segmentation
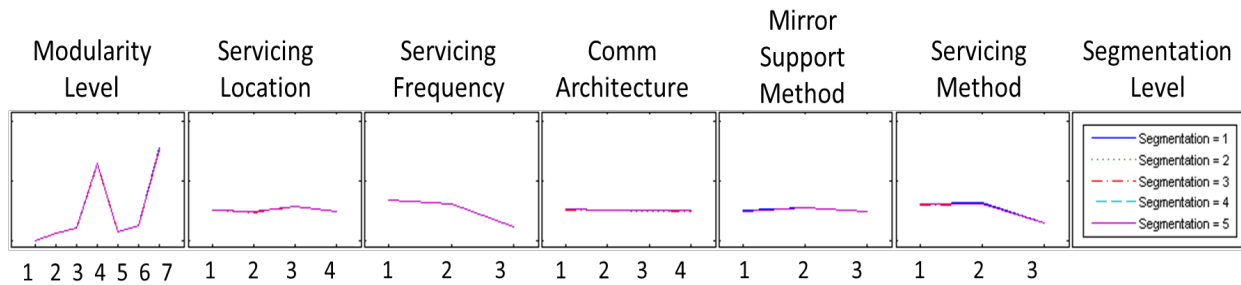
Figure 73: Service margin trends for different mirror segmentation methods

Mirror segmentation has no noticeable effect on servicing margin, as can be seen by the fact that the lines for all five segmentation types overlay each other.

7.2.4   Downtime
The main effects plot shown in Figure 74 shows the impact that each architectural trade had on downtime. Failed downtime is a combination of the time during which no science can be done due to the failure of a component and the time it takes to complete a servicing mission.
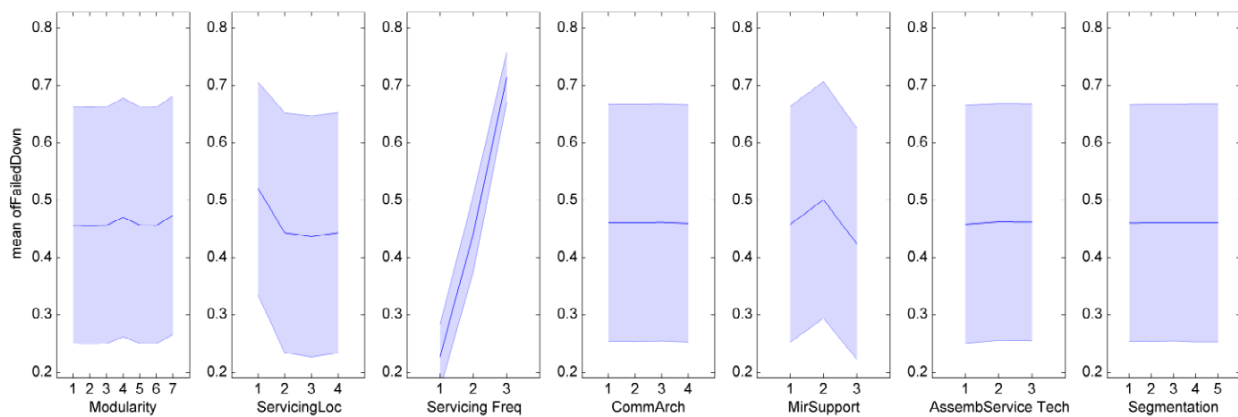
Figure 74: Main effects plot for Downtime

As can be seen from the main effects plot, not all architectural trades had a significant impact on the total mission down time. In particular, Communications Architecture, Assembly/Servicing Technique, and Mirror Segmentation Method showed nearly flat trends across the different design decisions within those trades. Meanwhile, options within the Servicing Frequency trade showed a significant variation between each other, with the most frequent servicing option (3 years between missions) having the least amount of failed down time, and the least frequent servicing options (10 years between missions) having the highest amount of failed downtime.

7.2.4.1 Modularity
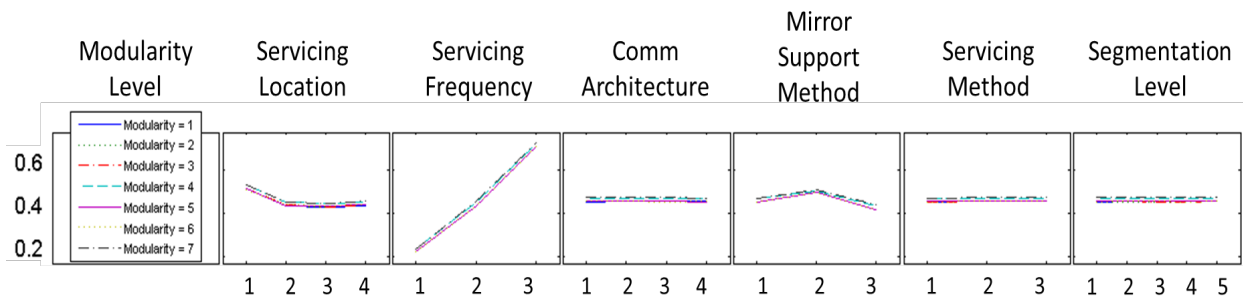
Figure 75: Downtime trends for different modularity levels

The above graphs show that there is little difference in down time between the different modularity levels. Modularity levels 4 and 7, the two most modular levels, have marginally higher down times than the other options. This is due to the fact that more modules require longer time to service.

7.2.4.2 Servicing Location
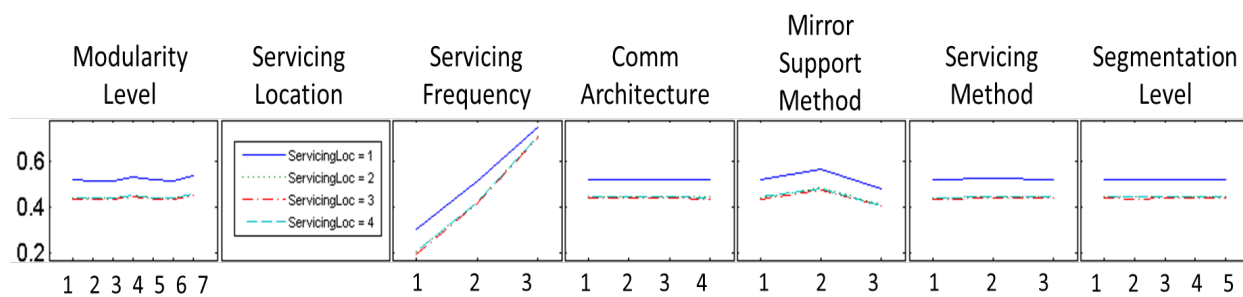
Figure 76: Downtime trends for different servicing locations

Servicing location 1 (in-situ servicing at Sun-Earth L2) has the highest amount of down time out of the four locations. This trend is interesting, considering the travel time from Earth orbit to SE-L2 is shorter than the transit time from ES-L2 back to Lunar or Earth orbit, by about 40 days. LEO, lunar, and LOTUS servicing locations all have similar down times. This makes sense, because the transit times from Earth-Sun L2 to these three locations are similar to within a few days.

7.2.4.3 Servicing Frequency
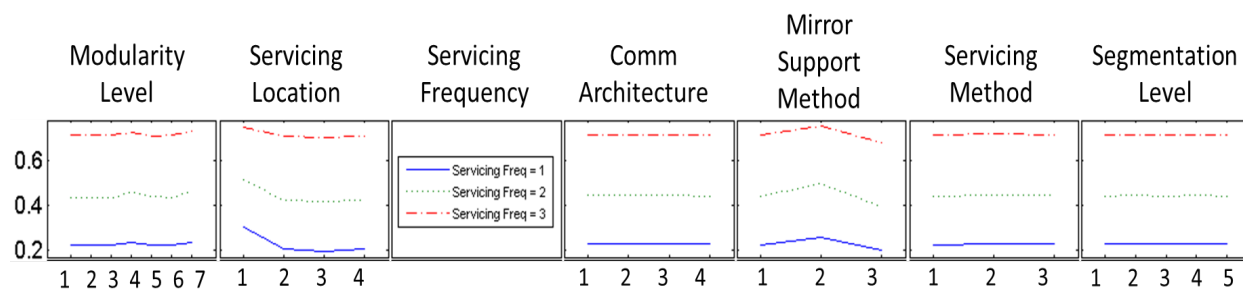
Figure 77: Downtime trends for different servicing frequencies

163

As mentioned in the discussion of the Main Effects plot, the total percentage of failed downtime increased with time between servicing missions. The lowest servicing frequency, 3 years between missions, has the lowest amount of failed down time. The highest servicing frequency, 10 years between servicing missions, has the highest amount of failed down time. If more time is allowed between servicing missions, more components are going to fail, leading to reduced science capacity.

7.2.4.4 Communications Architecture
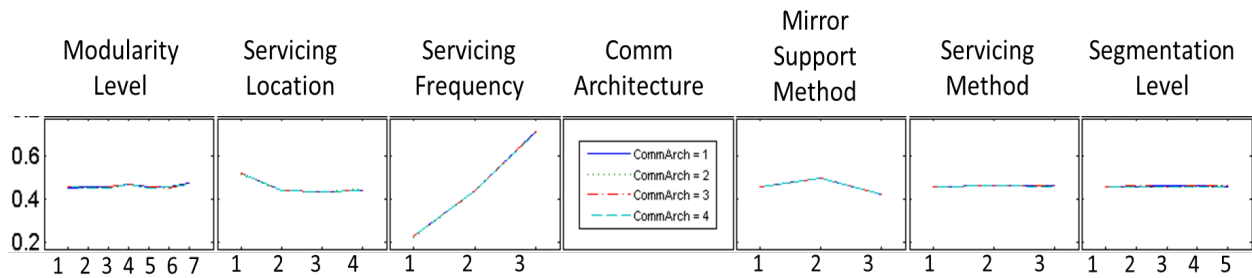
Figure 78: Downtime trends for different communications architectures

There were no noticeable differences between the downtime that resulted from different communications architectures.

7.2.4.5 Mirror Support Method
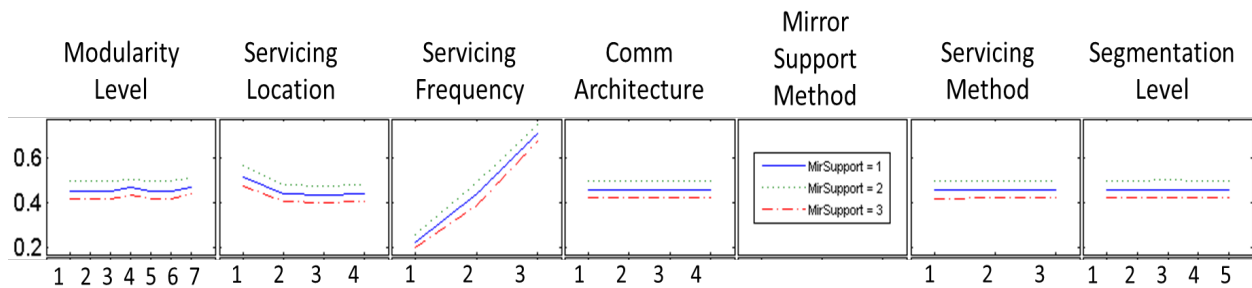
Figure 79: Downtime trends for different mirror support methods

Mirror support method 2 – surface parallel actuators – had the highest downtime out of the three options. Support method 3 – mixed surface normal and surface parallel actuators – had the lowest amount of down time.

7.2.4.6 Assembly/Servicing Technique
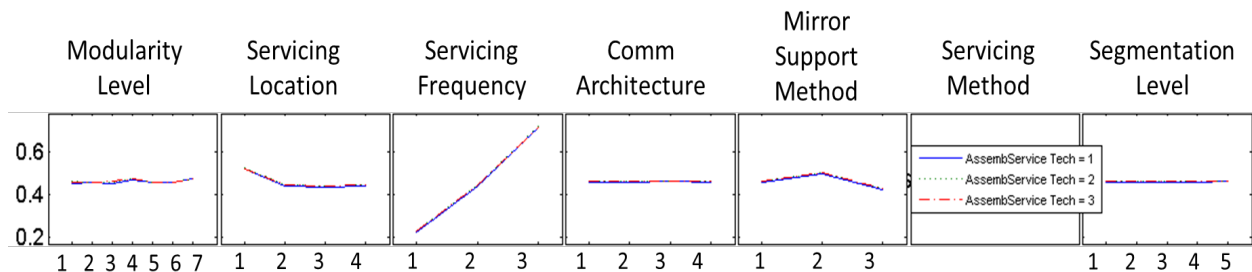
Figure 80: Downtime trends for different assembly/servicing techniques

164

There were no noticeable differences between the downtime that resulted from different assembly/servicing techniques.

7.2.4.7 Mirror Segmentation
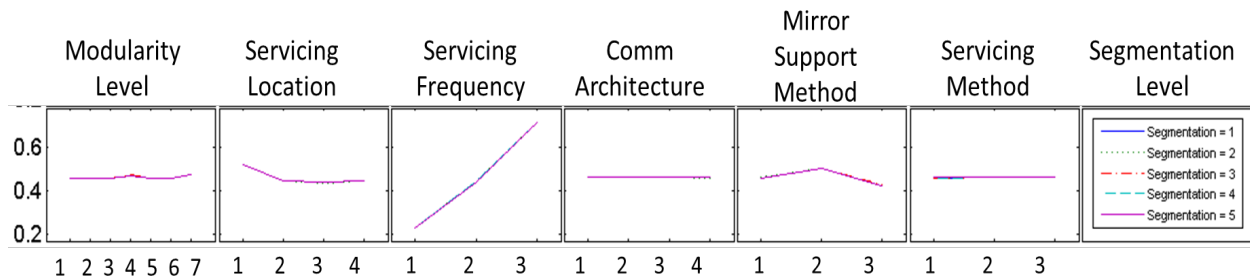
Figure 81: Downtime trends for different mirror segmentation levels

There were no noticeable differences between the downtime that resulted from different mirror segmentation levels.

7.3 Tradespace Characterization

7.3.1 Principle Component Analysis (PCA)

A principle component analysis was performed in order to determine the trade metrics that contributed the most to the overall variation. Principle component analysis decomposes a vector space into orthogonal components, the first of which maximally explains the variation in the data. Successive components explain the maximal amount of remaining variation under the constraint that they must be orthogonal to all previous components. Singular value decomposition (SVD) was used to deconstruct the trade space into principle orthogonal components and associated eigenvalues. The magnitude of the eigenvalue corresponds to the amount of variation explained by that component.
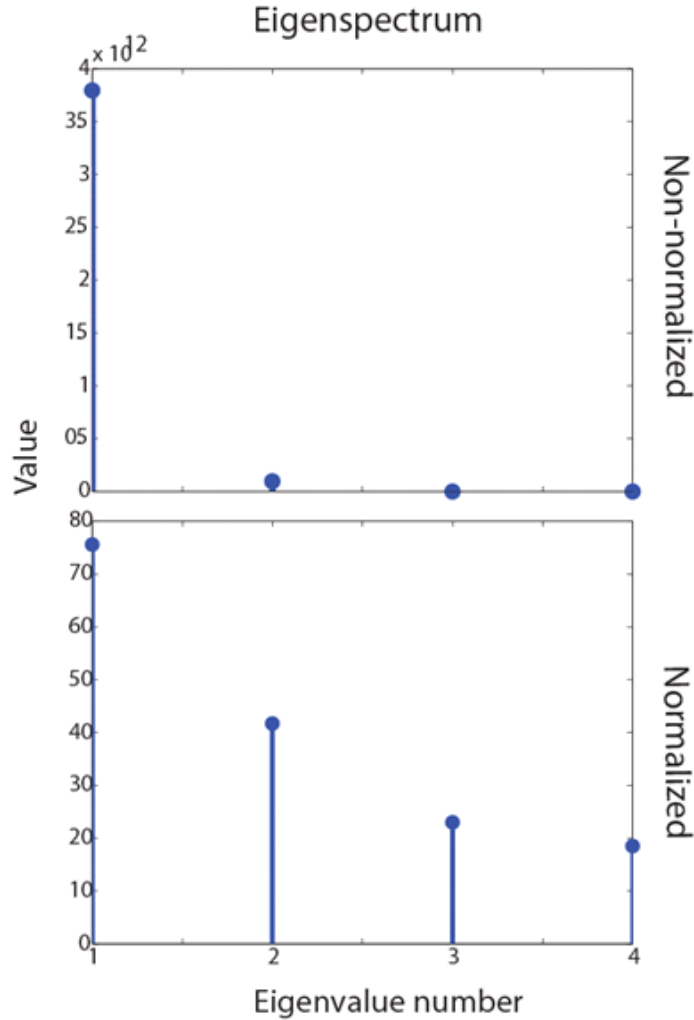
Figure 82: Eigenspectrum of non-normalized (top) and normalized trade metrics after performing PCA.

The eigenvalues corresponding to the first four principle components are shown in Figure 81. The principle component analysis was performed on the raw output trade metrics from our model. We found that the variation in certain trade metrics (particularly cost) was so large that they dominated the eigenspectrum. In order to address this large variation we performed a normalization of the trade metrics as seen in Eq. 88.

$$N_n = \frac{N_o - min(N_o)}{\max(N_o - min(N_o))}$$

Eq. 88

In order to assess which trade metrics contributed the most to the trade space variation, the sum over all eigenvalues for each eigenvalue multiplied by the eigenvector component corresponding to each trade metric was determined per the equation below as seen in Table XXXII.

$$\sum_{i=1}^{i=n} \lambda_i v$$

<div align="right">Eq. 89</div>

Trade space analysis should be performed on trade metrics that are independent, and this analysis allows proper testing of this assumption. It is apparent that cost and failed downtime are primary drivers of tradespace variation. Complexity also appears to an important factor in tradespace variation (Table XXXIII), but since it makes a small contribution to cost. As such it was not considered as an independent trade metric.

<div align="center">

Table XXXII: Contributions of Each Trade Metric to Overall Variation

Trade Metric	Relative Contribution
Cost	47.4
Science Utility	23.6
Service Margin	23.5
Failed Downtime	66.8

</div>

<div align="center">

Table XXXIII: Contributions of Trade Metrics to Overall Variation including Complexity

Trade Metric	Relative Contribution
Cost	45.3
Science Utility	23.6
Complexity	53.4
Failed Downtime	62.8

</div>

7.3.2   Hierarchical Clustering

As a next step in determining the overall structure of the tradespace, hierarchical clustering was performed on the entire tradespace as well as on the Pareto efficient architectures (Figure 82).

This hierarchical clustering was performed on the normalized trade metrics (between 0 and 1). We see two important features, clustering corresponding to similarities in trade metrics (top dendrogram) and similarities corresponding to architectural decisions (left dendrogram). It is apparent from both principal component analysis and hierarchical clustering that our four trade metrics can be reduced to two independent metrics.
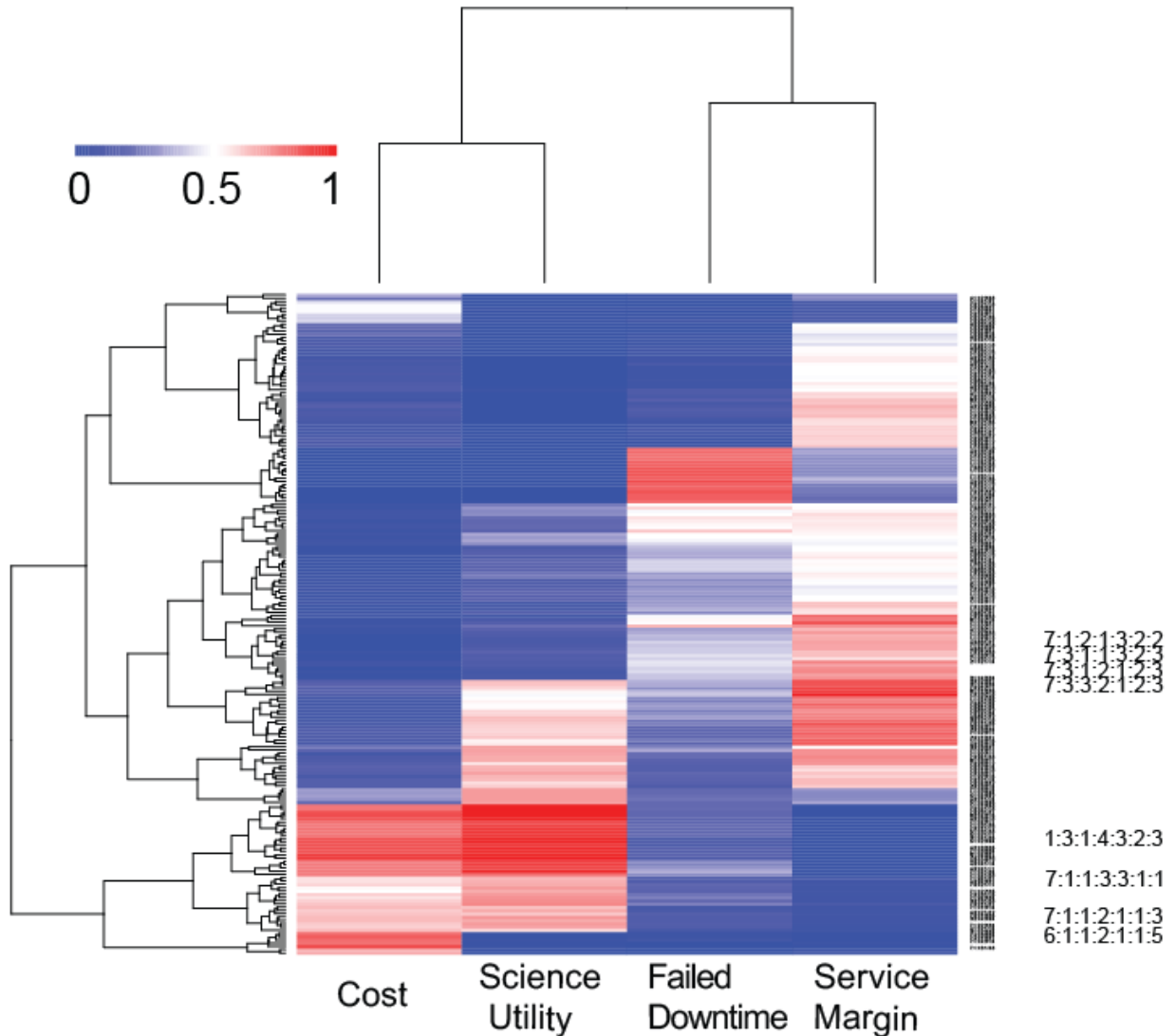
Figure 83: Hierarchical biclustering of Pareto Architectures. There are two main clusters for our trade metrics (1) cost and utility to science (2) failed downtime and service margin. There are also emergent clusters for different Pareto architectures (hierarchical branches on the left) In particular we identify the 7-1-1 set of architectures that was determined to have a high amount of science utility at relatively low cost.

Looking more globally at an assortment of trade metrics and performance metrics collected, it is apparent that there are three primary clusters of trade metrics (Figure 83). Weighting trade metrics according to their relatedness, as quantified in the dendrogram, achieves a similar function to using PCA to deconstruct maximally independent metrics. This approach has the benefit of not being constrained by an orthogonality requirement, and offers a novel means of rationally weighting the contributions of each trade metric or identifying maximally independent trade metrics from a set of performance metrics.
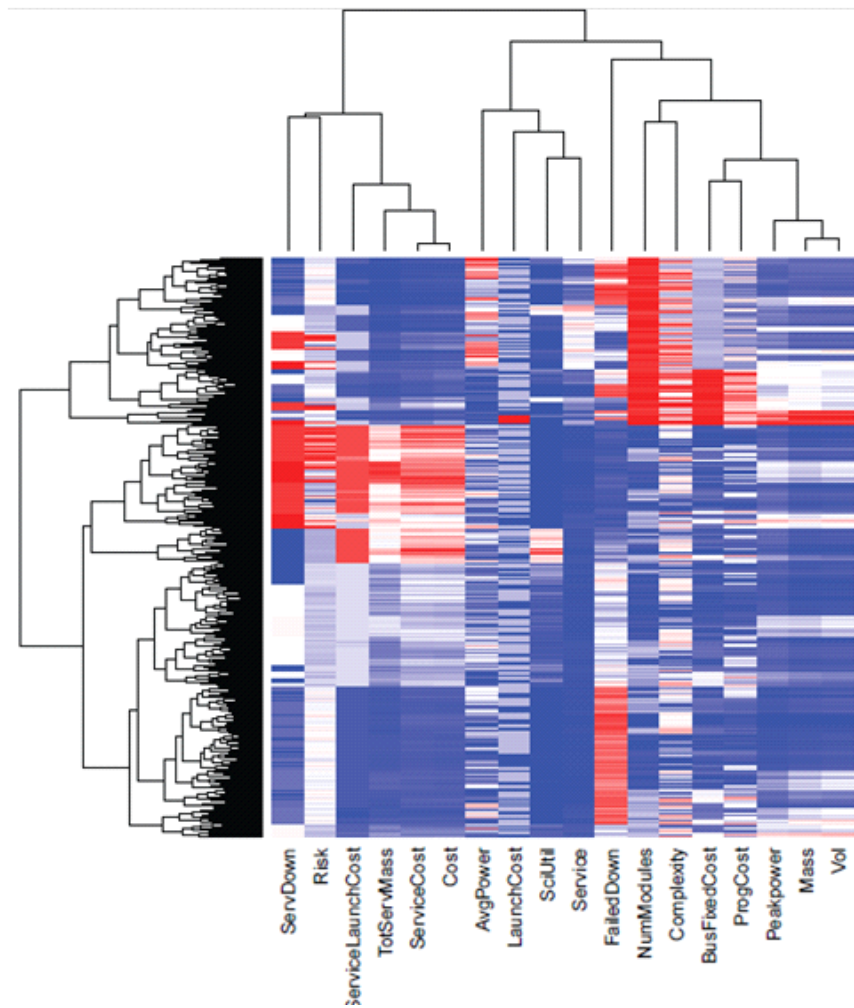
Figure 84: Hierarchical biclustering of all architectures and performance metrics. There are three main clusters for our trade metrics (1) cost and risk dominated (2) science utility and servicing dominated. (3) mass, volume, and complexity dominated. There are also emergent clusters for different architectures (hierarchical branches on the left).

7.4 Sensitivity Analysis

An analysis was conducted in order to understand the model's sensitivities to a selected number of assumptions/design parameters. Sensitivity analysis was performed on assumptions that effected many code modules that were hypothesized to directly impact trade metrics and/or were implemented in the model in such a way it was efficient to vary design parameters and run multiple iterations. These assumptions included the mean time between failure (MTBF) of all components and the Reliability Threshold at which servicing of a component will occur.

7.4.1 Assumptions

This section describes the design parameters or assumptions that were varied in order to conduct the sensitivity analysis.

7.4.1.1 Component MTBF

Component MTBF levels are provided for each component in the model, and are located in the Component Family DB; these values are based on years of lifetime and reliability values from data sheets, or estimates where data sheets are not available or where components leverage to-be developed technologies without existing MTBF analyses. Component MTBF values are used in the calculations of initial system cost and the failure rates. For the sensitivity analysis, the MTBF value for each component was increased or decreased by a certain percentage (this change is constant for all components within a single run). In order to implement this analysis, an MTBF multiplier was added into the code for each sensitivity run to increase or decrease the MTBF values of all of the components by the specified amount. The MTBF multiplier was run at values of [0.50, 0.85, 0.90, 0.95, 1.00, 1.05] to investigate a range of component MTBF values and understand how those values impact the model output.

7.4.1.2 Reliability Threshold

The Reliability Threshold is the threshold at which a decision is made to perform servicing on a non-failed component. During each servicing mission, if a component's reliability has dropped below the reliability threshold, it is replaced. This value is a representation of a program management decision of how far mission managers are willing to allow a component to degrade in reliability before replacement. This design parameter impacts serviced mass and failed downtime. For the sensitivity analysis, the Reliability Threshold was varied over the range of [0, 0.50, 0.60, 0.65, 0.70, 0.75, 0.80, 0.90, 1] in order to investigate a broad range of possible values for the Reliability Threshold. The two extreme values (0 and 1) were selected in order to examine the effect on telescope performance of the two extremes of the programmatic decision of when to service components. A reliability threshold of 0 indicates that components are never serviced due to low reliability; they are only serviced when they fail. A reliability threshold of 1, on the other hand, indicates that every component will be serviced during every mission, since any period of operational time will decrease a component's reliability below 1. The intermediate values were chosen to examine the range of reliability threshold values surrounding the nominal model value of 0.7, using two steps of 0.05 followed by a step of 0.1 in both directions.

7.4.1.3 Instrument Growth Rate Sensitivity

To examine the effect of varying rates of growth of discovery efficiency, each of the four instruments was assigned a different discovery efficiency growth rate by altering the baseline value of 0.3218 from Baldesarra[13]. Instrument A was assigned (4/3)*0.3218 or 0.4291. Instrument B was assigned the baseline value of 0.3218. Instrument C was assigned (2/3)*0.3218 or 0.2145. Instrument D was assigned (1/3)*0.3218 or 0.1073. By looking at the relative contributions of the different instruments to the overall utility to science, the dependence on instrument growth rate can be determined.

Figure 85 shows the utility to science of each instrument for a typical architecture. The x-axis shows time in weeks and the y-axis shows the utility to science on a logarithmic scale. The instruments are clearly sorted according to their assigned discovery efficiency growth. But most importantly, the utility of the fast-developing instruments vastly outpaces that of the slow-developing instruments. The contribution of Instruments C and D to the telescope utility to science is almost negligible. Therefore, the calculation utility to science is highly sensitive to the assumed discovery efficiency growth rate. For use in this model, this sensitivity is acceptable as utility to science is a relative metric for differentiating among architectures. But this sensitivity also illuminates the importance of investing in instrument development. Such investment has a direct payoff in terms of scientific output and a small difference in technology growth rate can greatly affect the scientific utility of a telescope.
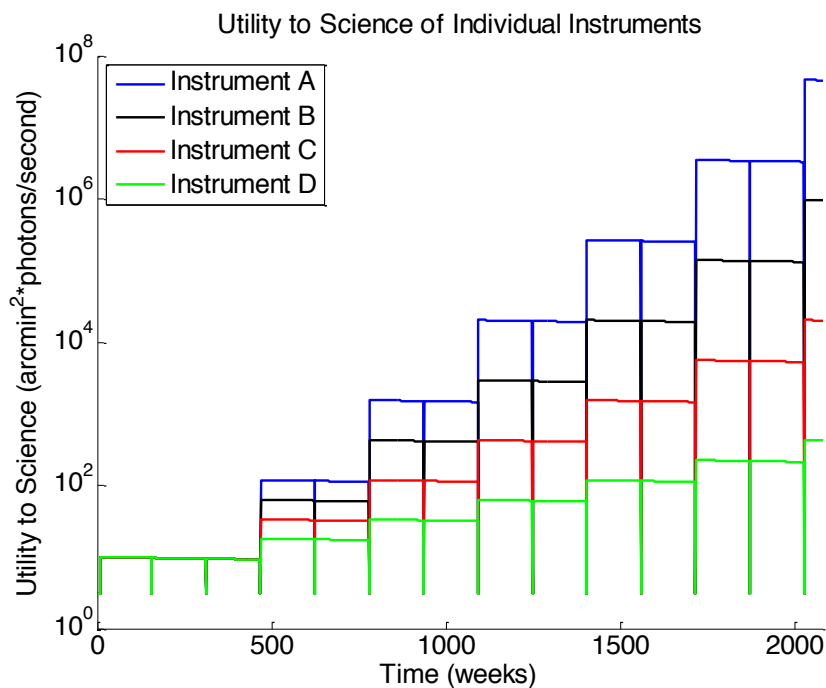
Figure 85: The utility to science of each instrument for a typical architecture. The x-axis shows time in weeks and the y-axis shows the utility to science on a logarithmic scale. The instruments are clearly sorted according to their assigned discovery efficiency growth rate.

7.4.2 Sensitivity of Trade Metrics to Assumptions

7.4.2.1 *Interquartile Range of Percent Change in Trade Metrics*

These charts demonstrate the spread of the differences of trade metric values between each baseline architecture (enumerated with the baseline case for the assumption) and the same architecture enumerated with a variance the assumption of interest. This method enables an examination of the effect of this parameter on an architecture-by-architecture basis, thus illuminating which metric is most affected by the parameter for a given architecture. The following plots show the effect of changing the Component MTBF and Reliability Threshold values across a certain range for all architectures. Each row of the tornado plot corresponds to a trade metric, and shows the 25th and 75th percentile values for the data set of delta values for that metric, defined as

$$T(i) = \frac{m_s(i) - m_0(i)}{m_0(i)} \times 100$$

Eq. 90

where i is the index for a particular architecture, m is the metric under investigation (with m_s indicating the value with the changed parameter and m_0 indicating the value for the baseline case), and T is the trade metric delta value, defined as the percent change in the metric. Figure 86 represents this data for Component MTBF values changed by ±10%. Figure 87 represents this data for Reliability Threshold changed by ±0.05.
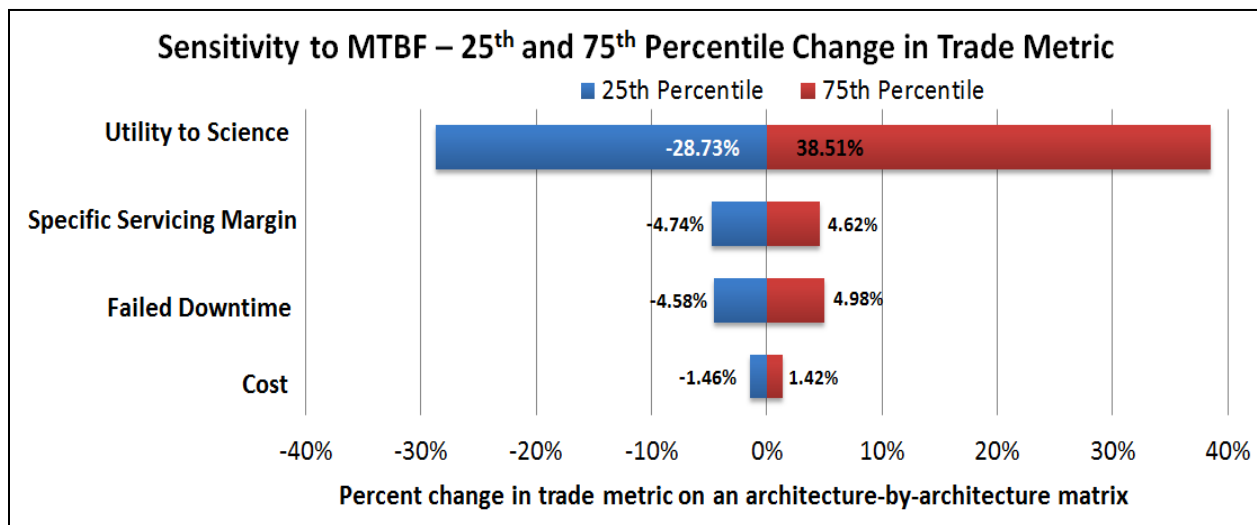
Figure 86: Tornado chart of component MTBF delta values

172
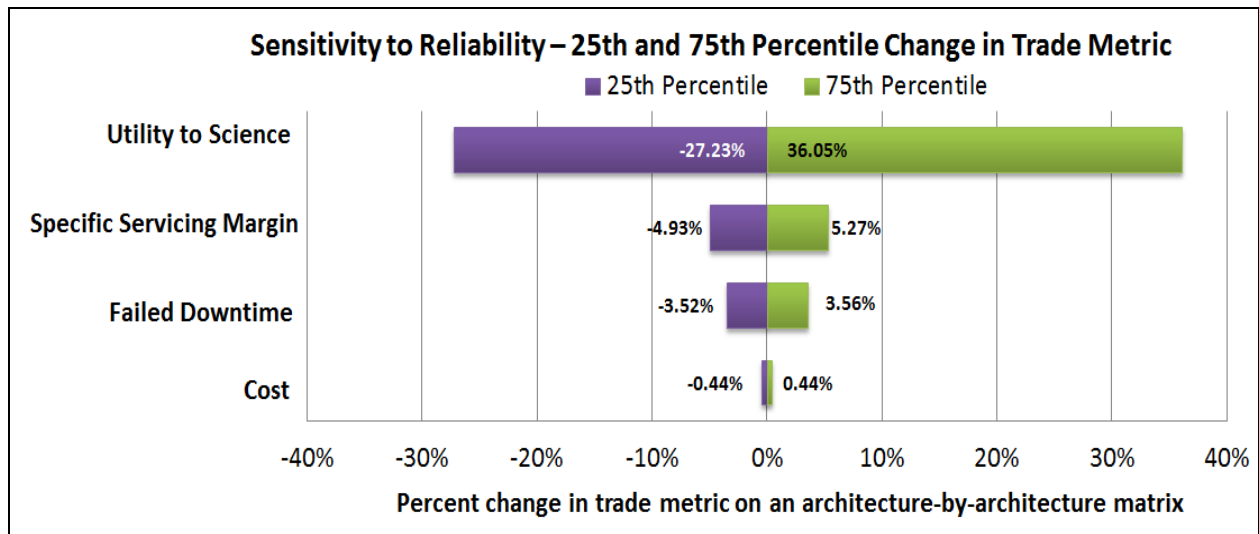
Figure 87: Tornado chart of reliability delta values

As can be seen in both sensitivity analyses, Utility to Science has the largest spread in the interquartile delta values, varying more than 30% in the positive direction, $UtS_s(x_i) > UtS_0(x_i)$, and more than 25% in the negative direction, $UtS_s(x_i) < UtS_0(x_i)$, where x_i is the ith architecture, UtS_0 is Utility of Science for the baseline case and UtS_s is the Utility of Science where a design parameter was altered for the sensitivity analysis. This analysis indicates that over half of the architectures have over 25 percent change in the Utility to Science metric in the independent cases where Component MTBF is varied ±10% (Figure 86) and Reliability Threshold is varied ±0.05 (Figure 87) in comparing architecture to architecture. Therefore, there are many architectures whose Utility to Science Metric is sensitive to both Component MTBF and Reliability Threshold. A closer inspection of the data shows that the Utility to Science produces high variance in values for the extremes in high and low values, making Utility to Science very sensitive to perturbations according to the percent change metric used in Figure 86 and Figure 87. The source of this variance requires further investigation.

Similarly, component family MTBF also produces delta change percentages in the ±5% range for Downtime and Servicing Margin and ±1% for Cost. Most architectures are not as sensitive in the Downtime, Servicing Margin, and Cost metrics as they are for Utility to Science when Component MTBF is varied. The same is true for the sensitivities of Downtime, Servicing Margin, and Cost metrics when the Reliability Threshold is varied (not as sensitive as Utility to Science is to varying Reliability Threshold).

7.4.2.2 Crossover

The distribution of values for per architecture percent changes reveals the percentage of the time that a specific trade metric delta was negative, i.e., $T_s(x_i) < T_0(x_i)$; this percentage will be referred to as the crossover percentage. For the metrics of Cost and Downtime, negative delta values and larger crossover percentages indicate better performance for a specific design parameter change. Note that this data is calculated with respect to the baseline case, so it is not necessary for the baseline case to be represented. For Utility to Science and Servicing Margin, positive delta values and lower crossover percentages indicate better performance with a specific design parameter change. A chart of the crossover percentages for each trade metric across

varying sensitivity levels is shown in Figure 88 for Component MTBF and Figure 90 for Reliability Threshold.
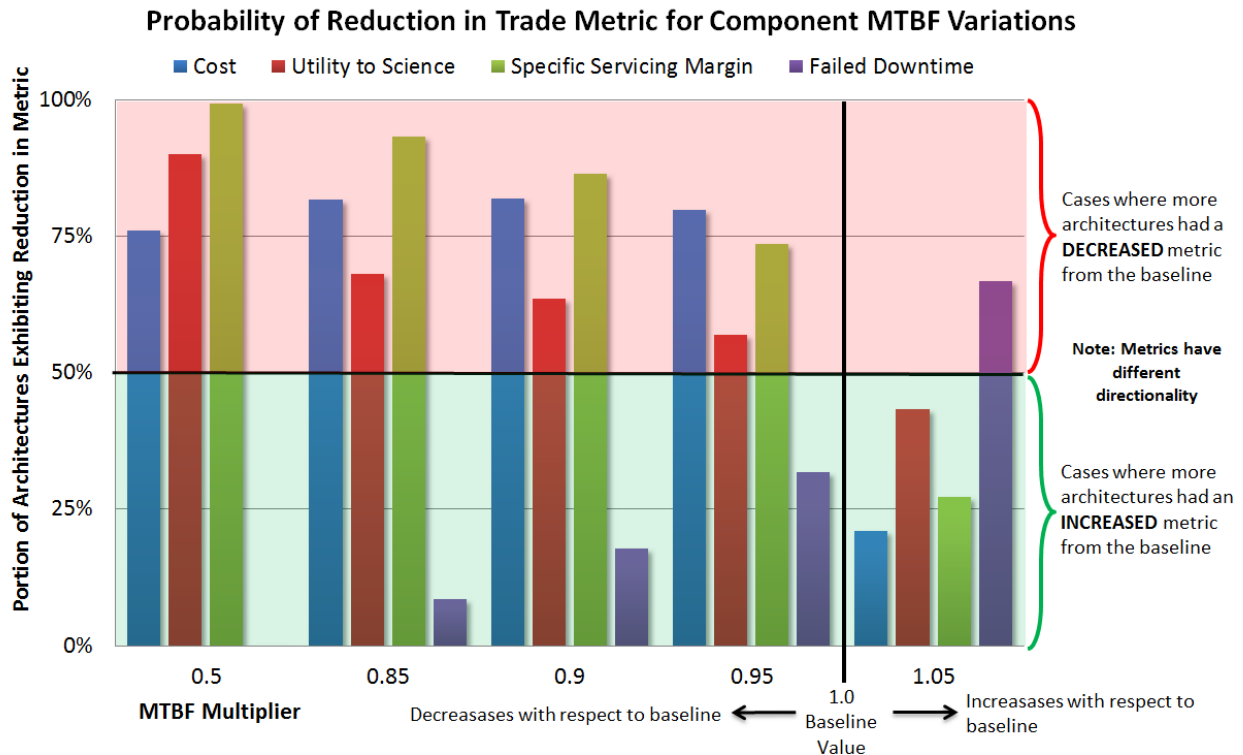
Figure 88: Crossover percentages for component MTBF variations

As expected, lowering the MTBF lowers the percentage of architectures for which $C_0(x_i) > C_s(x_i)$. Due to increased failures and increased downtime, the crossover values that exceed 50% for MTBF factors less than 100% and the greater the MTBF, the higher the crossover value (Figure 88). For the 50% MTBF case, 76% of the time the model produced a lower cost for the same architectural decision. Decreasing the MTBF values per component in the majority of architectures lowers the initial system cost. This result is because lower MTBFs correspond to less expensive components in the model; the driving assumption being components that tend to fail more often are either less expensive to make or purchase. The cost metric is determined by multiplying the initial telescope cost by the ratio of serviced mass to telescope mass. The serviced mass in the model does not fluctuate greatly with decreases in MTBF for modularity levels 1-3 and 5-6 because entire modules are replaced if at least one component has failed or is expected to fail soon, so an increase in failures does not correspond to a large increase in serviced mass. The exceptions, then, are modularity 4 and 7, where individual component families are serviced and significant increases are observed in serviced mass for increased failures (Modularity Levels with Higher Costs). For the 50% MTBF data set, the 24% of architectures for which a decreased MTBF yielded an increased cost were almost entirely composed of architectures with Modularity level 4 or 7 (Figure 89).

Figure 89: Modularity composition of architectures with higher costs at MTBF 50%

Servicing Margin is decreased when Component MTBF is decreased, as expected, due to the fact that serviced mass is not changed (for modularity levels 1-3 and 5-6) but servicing missions are increased. Decreasing the Component MTBF increases telescope downtime due to increased failures. A 50% decrease in Component MTBF is almost always worse than the baseline for the metric of downtime (Figure 88).

Trends in Figure 88 also show relationships between the trade metrics and the MTBF values of the components. It is important to note for this analysis that in this analysis the intervals between the MTBF multipliers are not constant, so it is not appropriate to comment directly on the rate of change of a metric with respect to the parameter without careful consideration of the variation in step size; that is the subject of future analysis. However, trends are shown and can be analyzed.

Cost shows an interesting trend. In general, lowering the MTBF values decreases the cost for 75-80% of the architectures; this makes sense, as the NICM cost model used to determine the cost of the instrument package is based in part on the MTBF values of the instruments, with lower MTBF values resulting in lower instrument costs. This also explains the cost increase for 20% of the architectures when the MTBF values are increased. However, it is interesting to point out that, while the proportion of architectures with decreased cost for decreased MTBF is steady at approximately 80% for MTBF multipliers of .85, .9, and .95, for an MTBF multiplier of .5 (the case where the MTBF values are reduced by half) the proportion of architectures with decreased cost drops to 75%. This implies that there is another effect that takes hold to increase the cost for lower MTBF values, but only when the change in MTBF values is low. This is most likely an increase in the serviced mass, which results in increased costs both in launch and development of replacement parts. While this increase in serviced mass is likely present for the other sensitivity analyses with reduced MTBF values, it is only when the magnitude of the reduction of MTBF

175

values is higher (reducing to 50% of the original value) that the effect of increased serviced mass overrides the effect of decreased cost.

The other trade metrics display more monotonic behavior. In general, lowering MTBF values lowers the Utility to Science with an effect proportional to the MTBF multiplier; the proportion of architectures with lower Utility to Science ranges between approximately 57% and 90% across the range of MTBF multipliers tested that were less than 1. For an increase in MTBF values, approximately 43% of the architectures exhibited increased Utility to Science. While more data from analyses with increased MTBF values would be required to verify this, these results seem to indicate that the effect of MTBF is similar for both increases and decreases, resulting in a proportional change in the percentage of architectures with increased Utility to Science.

The proportional relationship between MTBF values and Utility to Science makes sense, because the primary impact of component MTBF values on Utility to Science is in the amount of Failed Downtime; the lower the MTBF values of the components, the more often those components are expected to fail, resulting in lower downtime. To investigate this hypothesis, the Failed Downtime metric is investigated. Failed Downtime exhibits the inverse trend – the higher the MTBF values, the greater the percentage of architectures for which Failed Downtime was reduced. This supports the hypothesis. In fact, for the MTBF multiplier of 0.5, the percentage of architectures with decreased Failed Downtime is 0; for this MTBF multiplier, every architecture experienced increased downtime. This is again reflected in the fact that this MTBF multiplier experiences the highest percentage of architectures with decreased Utility to Science.

The trend in the Specific Servicing Margin shows that as the MTBF multiplier increases, the percentage of architectures with decreased Specific Servicing Margin decreases; in general, lowering the MTBF of the components in an architecture tends to decrease the Specific Servicing Margin. In fact, for an MTBF multiplier of 0.5, nearly all of the architectures experienced a decreased Specific Servicing Margin. This makes sense, as lower MTBFs result in more component failures and thus higher serviced mass. The definition of Specific Servicing Margin from Eq. 1 shows that a higher serviced mass results in a lower Specific Servicing Margin.
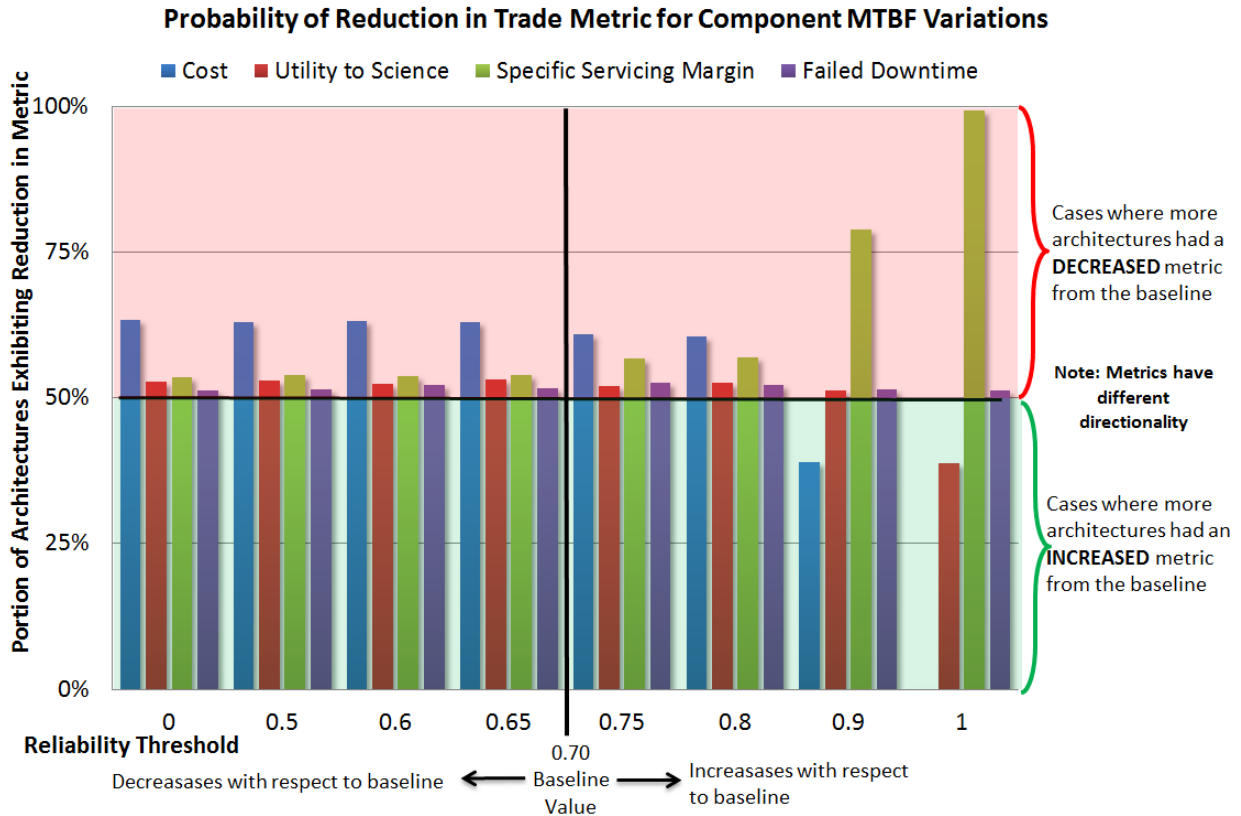
Figure 90: Crossover percentages for reliability threshold variations

The higher the Reliability Threshold, the greater the cost due to increased module servicing that increases serviced mass while not changing the initial system mass. The higher the Reliability Threshold, the greater the Utility to Science because modules are being maintained at higher reliabilities, thus decreasing downtime due to failures. On the other hand, decreasing the Reliability Threshold to values below 0.65 does not have a large impact on Utility to Science: Utility to Science is lowered but does not continue to degrade with decreasing Reliability Threshold. This trend indicates that Utility to Science is sensitive to increased changes in Reliability but not sensitive to decreases below 0.65. Similarly, Servicing Margin experiences the same sensitivities to increasing the Reliability Threshold above 0.65, but not to decreasing it.

In summary, Cost, Utility to Science, and Specific Servicing Margin are all much more sensitive to increases in the Reliability Threshold than deceases. This makes sense, as the primary interaction between these metrics and the Reliability Threshold is through the replacement of components that would not otherwise be replaced, i.e. components that are not failed but have fallen below the reliability threshold. It is expected that as the Reliability Threshold decreases the number of components serviced decreases as well, but only up to a certain point. Because random failure is also incorporated into the model, a certain number of components will be replaced regardless of the Reliability Threshold; as the Reliability Threshold decreases, the number of operational components with reliabilities below the threshold decreases due to their higher probability of having failed already. Thus, at a certain point the Reliability Threshold becomes low enough that the number of components that survive long enough for their reliability

to drop to that level is negligible, and reducing the Reliability Threshold further has no effect. Increasing the Reliability Threshold above this value, however, has a significant effect, as it significantly increases the number of components that require replacement that are not failed. Based upon this analysis, the level of Reliability Threshold at which the simulation begins replacing a significant number of components that are not failed is somewhere between 0.8 and 0.9, as this is the point where the effects in Cost and Specific Servicing Margin begin to manifest themselves.

The center of the distributions for Downtime across the varying Reliability Threshold changes is relatively constant, indicating that Downtime is not sensitive to changes in Reliability Threshold.

7.4.2.3   *Cumulative Distribution Functions*

For each sensitivity impact on a trade metric, Cumulative Distribution Functions (CDFs) were plotted to show the distribution of the Trade Metrics and percent change metric (Figure 91 and Figure 92). The steeper slopes in the CDFs indicate ranges for a metric for which there are many architectures. These CDFs also depict changes in center, spread, and shape of the data and regions where certain architectural sets are stochastically dominant. Though Figure 86 and Figure 87 allow conclusions to be more readily determined, the same conclusions can also be drawn from the CDF plots. Therefore, the CDF plots can provide the same conclusions, though they represent the data in a less concise manner as with the Tornado and Crossover figures. An example of each type of CDF is shown below.
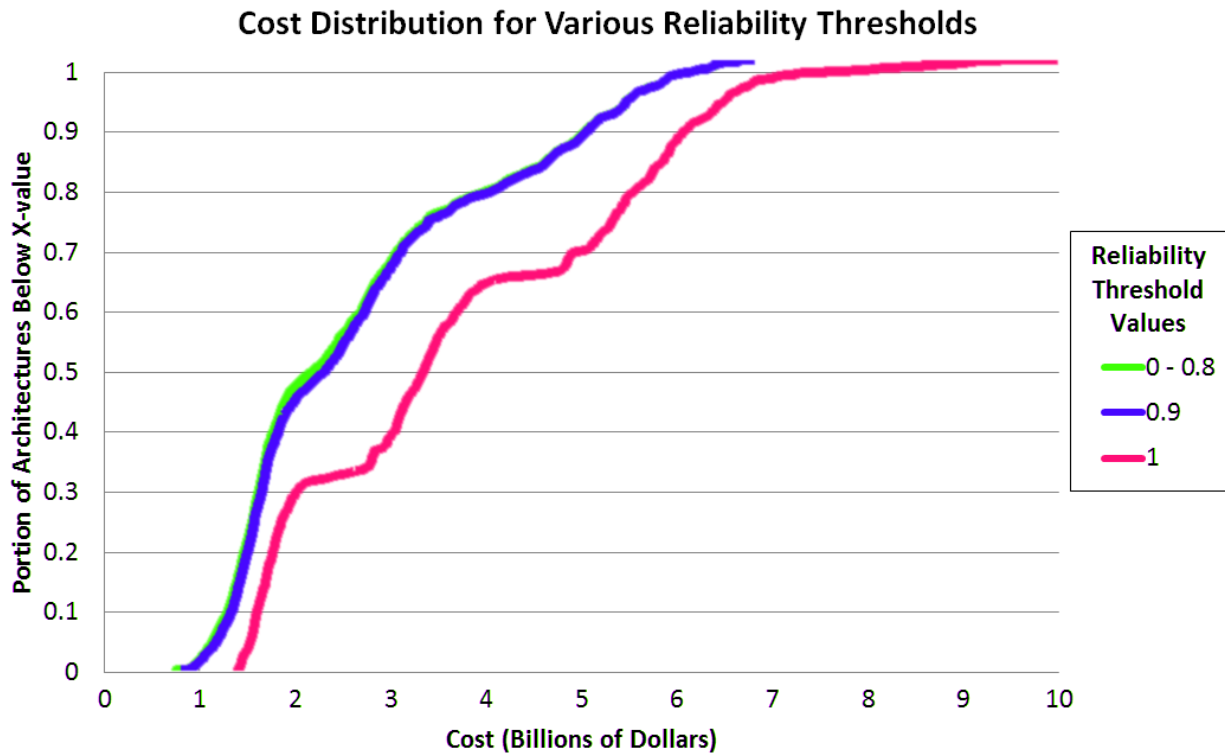
Figure 91: CDF of cost varying reliability threshold (comparing distributions)
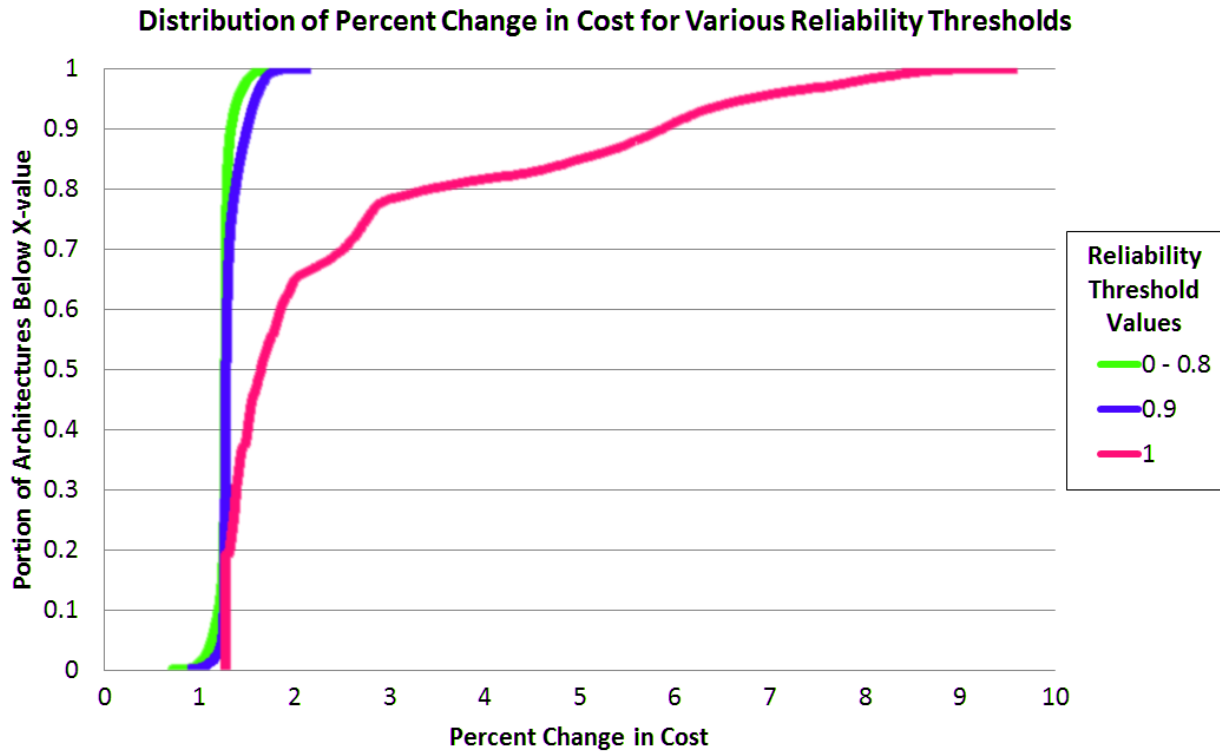
Figure 92: CDF of percent change in cost varying reliability threshold (comparing architectures)

7.4.2.4 Sensitivity of Pareto Frontier to Assumptions

In order to investigate the sensitivity of the Pareto frontier to the assumptions, a trade space exfoliation method was developed to identify layers of Pareto frontiers and the movement of architectures along the layers as a result of altering an assumption. In order to understand the results, a detailed explanation of tradespace exfoliation and Pareto layers is necessary. The following steps detail the tradespace exfoliation method:

1. For the baseline data set, identify the metrics that are traded and the number of dimensions
2. Normalize the data
3. Determine the Pareto frontier and label those architectures as Pareto layer $i=1$
4. Remove the ith Pareto frontier from the data set
5. Determine the Pareto frontier of the reduced data set (the data set without the $1{:}i^{th}$ frontier) and label as Pareto layer $i+1$
6. Continue for $i = 1{:}N$, with N being the number at which the frontier is empty, i.e., until there are no points in the data set
7. Repeat steps 2-6 for the set of architectures for which an assumption was changed
8. Compare the Pareto layer numbers for each architecture in the first Pareto layer in the baseline data set to the Pareto layer in which that architecture now resides as a result of the change in the assumption/design parameter

Figure 93 depicts the cumulative distribution of the percentage of the baseline Pareto frontier that

was moved to a given Pareto layer or lower, i.e., the tradespace with the altered assumption contains y percent of the Pareto layer 1 architectures in layers 1 to x, where y is the vertical axis and x is the horizontal axis. The solid lines in Figure 93 correspond to the distributions for changes in Component MTBF of ±5% and the dotted lines correspond to the distributions for changes in Reliability Threshold of ±0.05.

With respect to change in Component MTBF values, only 10% of the Pareto-Optimal architectures of the baseline data remain in the first Pareto layer when the MTBF values are changed. Thus, the Pareto front itself is sensitive to change in Component MTBF values. However, this analysis technique allows an investigation of "Pareto zones" rather than simply fronts; the data reveal what proportion of Pareto-Optimal architectures from the baseline data moved to each Pareto layer. Approximately 60% of the Pareto-Optimal architectures remained within the first 5 Pareto layers when the parameter was changed, indicating that over half the architectures remained fairly close to the Pareto front. Given the margin for error in the calculation of model outputs, the first 5 Pareto layers represent architectures that may be considered "pseudo-Pareto-Optimal" within the accuracy of the model. The farthest that any Pareto-Optimal architecture fell is 24 Pareto layers (out of a total of approximately 40).

For change in Reliability Threshold values, approximately 20% of the Pareto-Optimal architectures remained in the first layer, and approximately 80% fell no further than 5 Pareto layers. The farthest that any Pareto-Optimal architecture fell is 14 Pareto layers. Therefore, the Pareto frontier is more sensitive to changes in Component MTBF values than changes in Threshold Reliability. The Pareto frontier itself is quite sensitive to changes in model parameters, but inclusion of the first 5 Pareto layers as "pseudo-Pareto-Optimal" shows that the Pareto zone is more robust to changes in the model parameters.
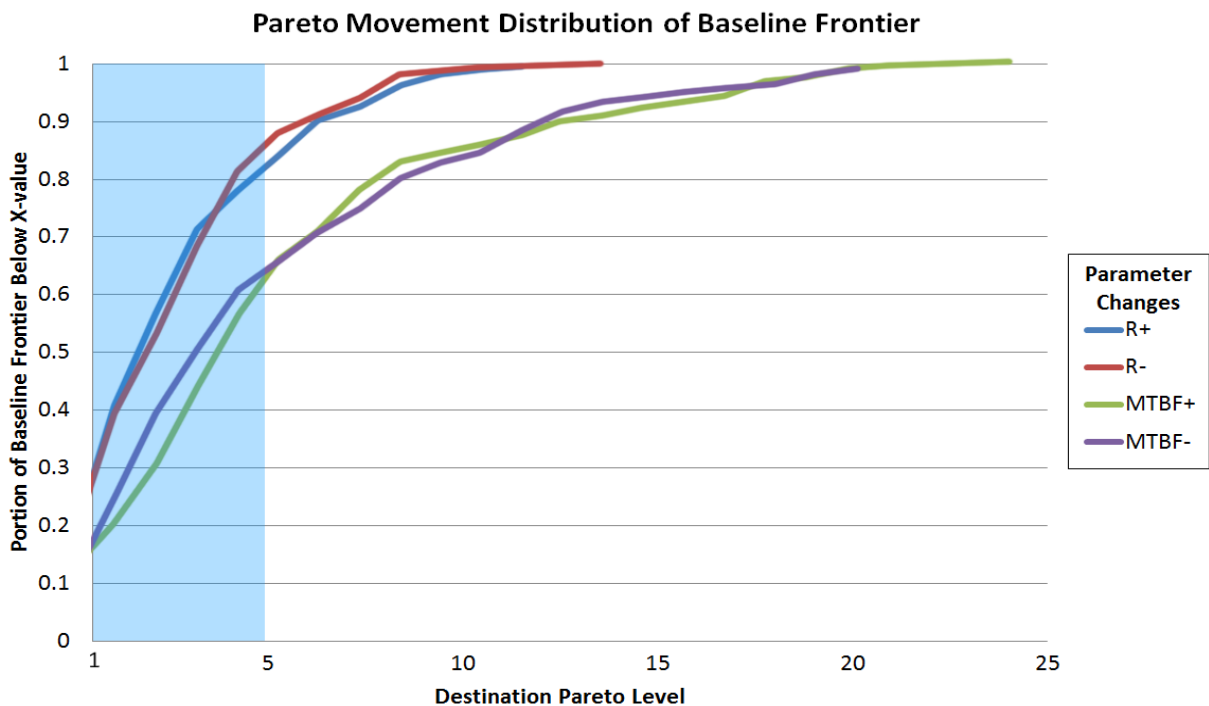
Figure 93: Pareto movement of baseline frontier

8   FUTURE WORK

There is a considerable amount of future work that can be done on this project both to increase the validity of the model and to extend the reach of conclusions achieved thus far. The main contribution of this work has been to set up a tool to evaluate possible large telescope architectures that meet the ATLAST science requirements, but many alterations should be made before the model's evaluation of architectures is to be cited confidently. As with any model and tradespace analysis, there are a great deal of points for further work and exploration; however, these are some of the immediate points that the TITANS AE team would have liked to incorporate and investigate.

8.1   Next steps to increase the validity of the model

The model serves as a tool with which the tradespace of large telescope architectures can be explored. There are many sources of uncertainty in the existing model due to, for example, low level of maturity for several considered technologies, unavailability of a full set of cost models with the appropriate ranges of validity, etc.

- *Decrease the discretization of the subsystem modules*: Because the focus of this study has been on the architecture evaluation tool, the subsystem models achieve a low level of fidelity by defining a small number of component families each subsystem can choose from. This resulted in some of the subsystem models producing only discretized architectures, which caused the trade metrics values across architectures to be less continuous than they likely are in reality.

- *Incorporate feedback loops into model*: The model does not incorporate feedback for several reasons (see Section 5.1 which talks about the N^2 and the lack of feedback). The addition of feedback into the models would decrease the number of assumptions and increase the fidelity of the subsystem architecture models.

- *Reconsider the rate of improvement in instrument discovery efficiency over the 40-year mission lifetime*: As discussed in Section 5.2.1 (utility-to-science section), the instrument improvement rate has been shown to increase exponentially, but it may not be realistic at this time to project the rate of improvement as exponential over the next 55 years.

- *Incorporate upgrades in satellite bus components*: The model incorporates advances in science instrumentation but not in engineering instrumentation. Over time, these components will only improve (i.e., become less massive, more reliable, more capable, etc.). If a model exists to obtain projected performance of engineering components, it should be implemented in order to more accurately reflect increasing engineering component capability over the telescope lifetime, which would, by extension, reflect increasing telescope capability.

- *Increase the range of validity of our architectural model so it may be further validated*: One of the biggest limitations to the model is its inability to be properly validated against even the most similar large telescope missions (i.e., JWST and HST). The assumptions made (e.g., 16.8-m-diameter primary mirror) and the way the scientific requirements

were incorporated (e.g., science data rate is a requirement for the communications system) does not make the model applicable to JWST and HST. As is natural with an ambitious study of this sort, validation is difficult and largely unattainable, but it would be useful to be able to relax the assumptions and account for requirements in a more general way so that the model can be minimally validated.

- *Track the consumption of consumables over time*: The study has assumed that the telescope will have enough consumables (e.g., propulsive fuel, coolant) to last the time between servicing missions, and that consumables are replaced during servicing missions. In the future, consumables should be considered something to be "serviced," in the sense that they can fail by being depleted between servicing missions.

- *Account for different signal latency in servicing operations*: The differences in signal latency for various assembly/servicing locations has not been taken into account in this analysis, though it surely affects operational downtime as well as the feasibility of different types of assembly/servicing technique.

8.2 Next steps for tradespace exploration

This initial tradespace exploration should be expanded upon to increase its ability to accurately differentiate between architectures based on the four trade metrics considered. Generally, the addition of and improved implementation of architectural decisions will extend the conclusions of the trade study by allowing for a more detailed analysis of architectures' cost and utility.

- *Estimate cost of servicing*: An estimate of servicing cost is critical to the evaluation of possible architectures for this mission. Such an estimate would be based on a currently nonexistent servicing cost model that could be developed based on further research and development effort on assembly and servicing methods for large space telescopes.

- *Improve the implementation of some architectural decisions considered in the study*: There are some architectural decisions that were implemented in a way that they did not result in interesting trades. For example, from our main effects plots, it is evident that the decisions of segmentation of the primary mirror and the communications architecture did not interface with other architectural decisions and did not significantly affect the trade metrics. Launch costs were the only thing affected by the segmentation of the primary mirror, and these are small compared to lifecycle cost. The different data transmission capabilities (i.e., data rates) of different communications architectures were not taken into account, so this choice did not change utility to science the way it likely would in reality.

- *Consider the baffle design*: The type of baffle could be made into an architectural decision or considered in a separate analysis. As a starting point, the baffle design could either be similar to the JWST baffle or Hubble baffle.

- *Consider assembly and servicing techniques separately*: Making these separate architectural decisions would allow for the consideration of different approaches to these distinct operational phases. Breaking these decisions out separately may produce

interesting results especially in distinguishing between designs with very different levels of modularity and segmentation.

- *Consider on-demand servicing*: It is assumed that servicing would be regularly scheduled to simplify the analysis. This is one of the most important architectural decisions that impact lifetime servicing cost. The implications of employing on-demand vs. scheduled servicing, or a hybrid of the two, are discussed in detail in Section 4.3.4.

- *Consider an external coronagraph*: It was assumed that the telescope system would not have a separate formation-flying coronagraph. However, such a coronagraph was proposed for ATLAST, and it this study would be remiss to explicitly not consider an external coronagraph in the future.

9 CONCLUSION

The steps outlined in this document describe the process for the tradespace analysis which was conducted in course 16.89, Space Systems Engineering, at MIT. The team investigated past designs of space telescopes and conducted a stakeholder analysis in order to determine the seven most important architectural decisions and enumerate an appropriate tradespace of alternatives associated with those decisions. The team determined the necessary system metrics (cost, utility to science, failed downtime, and servicing margin) which were used to evaluate each architecture.

The development of these metrics into a fully-functional and streamlined program enabled the team to efficiently evaluate the full set of enumerated architectures. Analysis of the outputs of the model has revealed a number of important dependencies. Utility to science depends most strongly on servicing frequency and servicing location, with the focus on upgrading the instruments often and minimizing downtime. Cost most strongly depends on modularity level and servicing frequency with architectures requiring a large serviced mass being most expensive. Failed downtime most strongly depends on servicing frequency, with the other architectural decisions contributing in minor ways. Architectures with infrequent servicing are more likely to experience failures leading to lengthy downtimes. Serviceability most strongly depends on modularity, servicing frequency, and assembly/servicing technique. Architectures with strong modularity serviced often with cheap servicing techniques exhibit the lowest cost per unit serviced mass. In the sensitivity analysis, utility to science was the sole trade metric to significantly feel the effects of the changes in MTBF and reliability threshold.

These dependencies reveal themselves in the analysis of the Pareto front. Clusters towards the higher end of the Pareto front use frequent servicing at Sun-Earth L2 and low modularity to achieve high utility to science but with high cost. Clusters near the middle of the Pareto front use high modularity to achieve lower cost by changing to high levels of modularity while losing some utility to science. Architectures near the bottom of the Pareto front use high levels of modularity and less frequent servicing at LEO to achieve very low cost with relatively little utility to science. The Pareto Optimal architectures changed with the variation of MTBF and reliability threshold. However, most of the original Pareto Optimal architectures remained close to the new Pareto fronts, indicating moderate sensitivity. While the other architectural decisions affect the trade metrics in small ways, our analysis has shown that servicing frequency, servicing location, and modularity are the most important decisions when architecting a space telescope—essential information for stakeholders in the selection of an optimal architecture for the next generation space telescope.

APPENDIX A: VARIABLE LIST

Code Module	Variable	Description	Units
Main	LTA	Structure to contain each architecture's design variables	[varies]
	res_vec	Results vector	[varies]
Sensitivity Analysis	modlevsensitivity	Sensitivity analysis variable - Multiplier of number of bus-segments needed per module	[unitless]
	MTBFsensitivity	Sensitivity analysis variable - Multiplier of MTBF column	[unitless]
	R_threshold	Sensitivity analysis variable - Required reliability of a given component family for a given servicing mission (would be pre-emptively replaced if below threshold)	[unitless]
Design Constants	reliability_req	Required reliability of a given subsystem for initial design (0.90)	[unitless]
	mirror_diam	Primary mirror diameter (16.8)	m
	mirror_temp_range	Mirror operating temperature range (20-22)	deg C
	shield_efficiency	Thermal shield efficiency (0.80)	[unitless]
	total_mass_estimate	Estimate of total spacecraft mass (15000)	kg
	R_earth2telescope	Distance from earth to the telescope (1.5 billion)	m
	acs_pointing_error	Pointing requirement taken from ATLAST reqs (1)	milli-arcsec
	unique_prescr	Number of unique prescriptions (6)	prescriptions
	num_rings	Number of mirror segment rings (3)	rings
	segment_diam	Diameter of mirror segments (16.8/7 = 2.3)	m
	rep_segments	Number of repeated segments (6)	segments
	lifetime_req	Requirement of mission lifetime (40)	years
Components DB and DSMs	costCol	Column of cost/unit per component family, imported from Components DB spreadsheet	$1K US FY13
	massCol	Column of cost/unit per component family, imported from Components DB spreadsheet	kg
	dimCol	Column of mass/unit per component family, imported from Components DB spreadsheet	m
	volCol	Column of stowed-volume/unit per component family, imported from Components DB spreadsheet	m^3
	compPowerAvgCol	Column of avg-power-draw/unit per component family, imported from Components DB spreadsheet	W
	compPowerPeakCol	Column of peak-power-draw/unit per component family, imported from Components DB spreadsheet	W
	powerCol	Column of avg-power-generated/unit per component family, imported from Components DB spreadsheet	W
	TRLCol	Column of total-readiness-level/unit per component family, imported from Components DB spreadsheet	level number
	MTBFCol	Column of mean-time-between-failure/unit per component family, imported from Components DB spreadsheet	years

	lifetimeCol	Column of lifetime/unit per component family, imported from Components DB spreadsheet	years
	StructuralDSM	Design structure matrix for structural interactions between component families,imported from DSM spreadsheets	binary matrix
	ThermalDSM	Design structure matrix for thermal interactions between component families,imported from DSM spreadsheets	binary matrix
	DataDSM	Design structure matrix for data interactions between component families,imported from DSM spreadsheets	binary matrix
	PowerDSM	Design structure matrix for power interactions between component families,imported from DSM spreadsheets	binary matrix
	LTA	Structure to contain each architecture's design variables	[varies]
	OpticalDSM	Design structure matrix for optical interactions between component families,imported from DSM spreadsheets	binary matrix
Design Vector	servicing_loc	Servicing Location	selection number
	servicing_freq	Servicing Frequency	years
	comm_arch	Communications Architecture	selection number
	mirror_support	Mirror Support Method	selection number
	a_s_technique	Assembly/Servicing Technique	selection number
	mirror_segmentation	Segmentation Technique of the Primary Mirror	selection number
	modularity_level	Modularity Level	level number
Optics	optics_m	Total mass of Optics subsystem (inst. only)	kg
	optics_v	Total volume of Optics subsystem (inst. only)	m^3
	optics_avg_power_req	Average power required by Optics subsystem (inst. only)	W
	optics_temp_range	Operating temperature range of Optics subsystem (cryo inst. only)	deg C
	optics_power_diss	Average power dissipated by Optics subsystem (inst. only)	W
	inst_perf_decay_rate	Rate paramter for performance decay of an instrument over time	[unitless]
	optics_data_rate	Rate at which data is transmitted from the telescope to avionics	Mbps
	optics_components	Component family choices for Optics subsystem (inst. only)	units of comp. family
	num_segments	Total number of primary mirror segments	segments
	discovery_efficiency_inst_a	Discovery efficiency (FOV*throughput) of instrument A	arcmin^2*photons/sec
	discovery_efficiency_inst_b	Discovery efficiency (FOV*throughput) of instrument B	arcmin^2*photons/sec
	discovery_efficiency_inst_c	Discovery efficiency (FOV*throughput) of instrument C	arcmin^2*photons/sec
	discovery_efficiency_inst_d	Discovery efficiency (FOV*throughput) of instrument D	arcmin^2*photons/sec
	vol_data_to_ground	Quanity of data that needs to be transmitted to ground, largest contributor is optics/science data	Mb
Comm	comm_power_diss	Average power dissipated by Comm subsystem	W

	comm_temp_range	Operating temperature range of Comm subsystem	deg C
	comm_avg_power_req	Average power required by Comm subsystem	W
	comm_peak_power	Peak power required by Comm subsystem	W
	comm_peak_length	Time for which the peak power is needed	s
	comm_peak_frequency	How often the peak power is needed	Hz
	comm_timedelay	Transmission delay of the data	s
	comm_m	Total mass of Comm subsystem	kg
	comm_v	Total volume of Comm subsystem	m^3
	comm_MTBF	Mean time between failure (MTBF) for Comm subsystem	years
	comm_QOS_BER	Quality-of-signal / Bit-error-rate of selected Comm architecture	[unitless]
	comm_SNR	Signal-to-noise ratio of selected Comm architecture	[unitless]
	comm_components	Component family choices for Comm subsystem	units of comp. family
	comm_components_MTBF	Mean time between failure (MTBF) of individual "component families" selected for Comm subsystem	years
ADCS	acs_temp_range	Operating temperature range of ADCS subsystem	deg C
	acs_avg_power_req	Average power required by ADCS subsystem	W
	acs_m	Total mass of ADCS subsystem	kg
	acs_v	Total volume of ADCS subsystem	m^3
	acs_components	Component family choices for ADCS subsystem	units of comp. family
	acs_components_MTBF	Mean time between failure (MTBF) of individual "component families" selected for ADCS subsystem	years
	acs_MTBF	Mean time between failure (MTBF) for ADCS subsystem	years
Avionics	avionics_m	Total mass of Avionics subsystem	kg
	avionics_v	Total volume of Avionics subsystem	m^3
	avionics_avg_power_req	Average power required by Avionics subsystem	W
	avionics_power_diss	Average power dissipated by Avionics subsystem	W
	avionics_temp_range	Operating temperature range of Avionics subsystem	deg C
	avionics_components	Component family choices for Avionics subsystem	units of comp. family
	avionics_components_MTBF	Mean time between failure (MTBF) of individual "component families" selected for Avionics subsystem	years
	avionics_MTBF	Mean time between failure (MTBF) for Avionics subsystem	years
	avionics_data_rate	Avionics data rate	bps
Propulsion	prop_m_nd	Propellant mass fraction (per unit spacecraft mass)	kg/kg
	prop_v_nd	Propellant volume fraction (per unit spacecraft mass)	m^3/kg
	prop_svc_time	One-way travel time between L2 and servicing location	days
	prop_avg_power_req	Average power required by Propulsion subsystem	W
	prop_temp_range	Operating temperature range of Propulsion subsystem	deg C
	prop_power_diss	Average power dissipated by Propulsion subsystem	W
	prop_components	Component family choices for Propulsion subsystem	units of comp. family

	prop_transit_time	One-way travel time between earth and L2	days
Power	power_m	Total mass of Power subsystem	kg
	power_v	Total volume of Power subsystem	m^3
	power_m_nd	Non-dimensionalized mass (per Watt required)	kg/W
	power_v_nd	Non-dimiensionalized volume (per Watt required)	m^3/W
	power_avg_power_diss	Average power dissipated due to power distribution inefficiencies	W
	power_array_area	Area of solar arrays	m^2
	power_temp_range	Operating temperature range of Power subsystem	deg C
	power_components	Component family choices for Power subsystem	units of comp. family
Thermal	thermal_m	Total mass of Thermal subsystem	kg
	thermal_v	Total volume of Thermal subsystem	m^3
	thermal_avg_power_req	Average power required by Thermal subsystem	W
	thermal_components	Component family choices for Thermal subsystem	units of comp. family
	thermal_components_MTBF	Mean time between failure (MTBF) of individual "component families" selected for Thermal subsystem	years
	thermal_MTBF	Mean time between failure (MTBF) for Thermal subsystem	years
Structures	structures_components	Component family choices for Structures subsystem	units of comp. family
	structures_pow_avg	Average power required by Structures subsystem	W
	structures_pow_peak	Peak power required by Structures subsystem	W
	structures_v	Total volume of Structures subsystem	m^3
	structures_m	Total mass of Structures subsystem	W
	structures_components_MTBF	Mean time between failure (MTBF) of individual "component families" selected for Structures subsystem	years
	overall_components	Compiled "component family" choices for entire spacecraft	units of comp. family
	sys_pow_avg	Total average power of entire spacecraft	W
	sys_pow_peak	Total peak power of entire spacecraft	W
	sys_mass	Total mass of entire spacecraft	kg
	prop_m	Final mass of Propulsion subsystem	kg
	sys_vol	Total volume of entire spacecraft	m^3
	prop_v	Final volume of Propulsion subsystem	m^3
	jitter	Jitter of the System (RMS)	mm
	module_definitions	Vector that captures which module each component is in	module number
Systems	sys_reliability	Total system reliability	[unitless]
	sys_complexity	Total system complexity (based on DSMs)	N/A
Operations	inst_del_rate	Rate parameter for the increase in instrument utility over time	[unitless]
	num_mod	Number of modules in spacecraft	modules
	t_end	Monte Carlo simulation variable - Time at which simulation ends	weeks passed
	dt	Monte Carlo simulation variable - Time-step of simulation	weeks

	time	Monte Carlo simulation variable - Vector of evaluation times for simulation	weeks passed
	architecture	Monte Carlo simulation variable - captures full spacecraft architecture's state at each servicing mission evaluation point	[varies]
	inst_replaced	Monte Carlo simulation variable - captures each instrument's state of replacement at each servicing mission evaluation point	binary vector
	downtime	Monte Carlo simulation variable - Downtime due to mass-servicing and transit to servicing location	days
	failures	Monte Carlo simulation variable - Number of failures per servicing mission	failures
	module_replacements	Monte Carlo simulation variable - Modules that were replaced per servicing mission	modules
	scope_state	Monte Carlo simulation variable - State of spacecraft per servicing mission	binary vector
	row_inst_a	Monte Carlo simulation variable - Row number of instrument A	row number
	row_inst_b	Monte Carlo simulation variable - Row number of instrument B	row number
	row_inst_c	Monte Carlo simulation variable - Row number of instrument C	row number
	row_inst_d	Monte Carlo simulation variable - Row number of instrument D	row number
	utility_inst_a	Monte Carlo simulation variable - Utility-to-science of instrument A at given evaluation time	$arcmin^2$*photons
	utility_inst_b	Monte Carlo simulation variable - Utility-to-science of instrument B at given evaluation time	$arcmin^2$*photons
	utility_inst_c	Monte Carlo simulation variable - Utility-to-science of instrument C at given evaluation time	$arcmin^2$*photons
	utility_inst_d	Monte Carlo simulation variable - Utility-to-science of instrument D at given evaluation time	$arcmin^2$*photons
	p_util_science_a	Monte Carlo simulation variable - Distribution of utility-to-science of instrument A over mission lifetime	$arcmin^2$*photons
	p_util_science_b	Monte Carlo simulation variable - Distribution of utility-to-science of instrument B over mission lifetime	$arcmin^2$*photons
	p_util_science_c	Monte Carlo simulation variable - Distribution of utility-to-science of instrument C over mission lifetime	$arcmin^2$*photons
	p_util_science_d	Monte Carlo simulation variable - Distribution of utility-to-science of instrument D over mission lifetime	$arcmin^2$*photons
	p_util_science	Monte Carlo simulation variable - Distribution of utility-to-science of spacecraft over mission lifetime	$arcmin^2$*photons
	MC_results.m_serv_mat	Monte Carlo results variable - Mass serviced per servicing mission	kg
	MC_results.downtime	Monte Carlo results variable - Total downtime due to failure, servicing, or transit at each servicing mission evaluation point	weeks

	MC_results.service_downtime_vec	Monte Carlo results variable - Downtime due to mass-servicing or transit per servicing mission	weeks
	MC_results.mean_m_serv_vec	Monte Carlo results variable - Avg serviced mass per servicing mission	kg
	mean_service_downtime	Total average downtime due to mass-servicing or transit time	weeks
	mean_downtime	Total average downtime due to failure, mass-servicing, or transit to servicing location	weeks
	failed_downtime	Total average downtime due to spacecraft failure	weeks
	service_downtime_frac	Fraction of intended mission lifetime used for servicing	[unitless]
	failed_downtime_frac	Fraction of intended mission lifetime when spacecraft is in failed state	[unitless]
Trade Metrics	stahl_cost1	Cost of developing the optics	USD FY13
	cost_flightsystem.program_level1	Cost of developing the spacecraft bus (NR)	USD FY13
	cost_flightsystem.program_level2	Cost of developing the spacecraft bus and infrastructure (NR)	USD FY13
	USCM8_cost1	Cost of developing the spacecraft bus and infrastructure (NR+R)	USD FY13
	NICM_cost_a	Cost of developing instrument A	USD FY13
	NICM_cost_b	Cost of developing instrument B	USD FY13
	NICM_cost_c	Cost of developing instrument C	USD FY13
	NICM_cost_d	Cost of developing instrument D	USD FY13
	NICM_cost	Cost of developing the instruments	USD FY13
	flightsyscost	Total cost of developing the flight system	USD FY13
	cost_servicing	Total cost of developing components for servicing missions	USD FY13
	cost_for_flightsystem	Total cost of flight system over mission lifetime	USD FY13
	cost_to_launch	Total cost of launching the flight system	USD FY13
	cost_servicing_launch	Total cost of launching servicing missions	USD FY13
	cost	Total cost of spacecraft over mission lifetime	USD FY13
	baseline_cost	Total cost of spacecraft assuming entire spacecraft is serviced every servicing mission (modularity level = 1)	USD FY13
	serviceability	Cost margin relative to the baseline cost per mass serviced in servicing missions	USD FY13
	utility_to_science	Total utility-to-science over mission lifetime	arcmin^2*photons
	state_probability	State probability matrix	[unitless]
	expected_productivity	Expected productivity	arcmin^2*photons

APPENDIX B: STAKEHOLDER QUESTIONS AND ANSWERS

- What ground stations will we use? DSN? How often should we assume passes occur and how long will they be?
- Is there a set of launch vehicles which we can use for making initial estimates?
- What are the mission goals? How does this telescope relate to current and future telescopes (ATLAST)?
- What is the expectation of the optical capability of the new telescope (optical bandwidth, aperture size, angular resolution, FOV, pointing stability, spectral resolution, contrast, inner working angle, wavefront error, wavefront stability, uninterrupted observation time, lifetime, operational efficiency)
- What operational orbits should we consider?
- What is the budget for this mission?
- Is there an available cost model for this mission (spacecraft, ground systems, launch vehicle)? Is there a cost model for a federated satellite system?
- When will this telescope operate? What is its expected lifetime? What other space assets will be available for utilization at that time?
- What mirror technologies should we consider?
- What detector technologies should we consider?
- What adaptive optics technologies should we consider?
- Are there specific technology insertion goals for this telescope?
- Does the data need to be secure?
- Who is going to receive the data?
- What data management system should we use?
- Is NASA interested in soliciting additional stakeholders for the project (ESA, Commercial, Hosted Payloads)?

Stakeholder Responses

Dan Lester

- What are the mission goals? How does this telescope relate to current and future telescopes (ATLAST)?

It's really up to the science community to define priority goals for a new space telescope. If the assumption is that this telescope is going to be a LARGE DIAMETER, OPTICAL telescope, then the best science case for that kind of telescope was probably made by the ATLAST team. But that's not really a consensus science case. It does seem perfectly reasonably to adopt the ATLAST goals as notional goals, which may or may not actually represent a consensus priority by the astronomical community. But there have been many other large telescopes (infrared, X-ray, ultraviolet, radio) proposed, so you pretty much have to decide which one you're interested in designing. These are YOUR goals. Not the goals of the community. So your "assumption/rationale" that the science goals/requirements for this telescope are the same as for ATLAST seems one sensible approach. There are many other sensible approaches. This exercise can then be taken as an existence proof as to whether there is an affordable strategy to build a telescope defined by the ATLAST requirements.

- What is the expectation of the optical capability of the new telescope (optical bandwidth, aperture size, angular resolution, FOV, pointing stability, spectral resolution, contrast, inner working angle, wavefront error, wavefront stability, uninterrupted observation time, lifetime, operational efficiency)

These are all expectations that depend on budget. You basically want a telescope you can afford that will do as much as possible. That being the case, you want a telescope that is at least a factor of three larger in diameter than what we virtually have now, which would be JWST. It's commonly understood that a flagship project, in order to be sellable, has to be an order of magnitude better than what you had before. In light gathering power, a factor of three in diameter would do it. So I think you need an 18+ m diameter telescope. Well, if this is really to be an optical (as in "visual wavelength" telescope, then maybe we're talking a factor of three over HST. That would be a 7-m telescope. But I think the reason that NASA chose to develop a 6m near-IR large telescope instead of a 6-m optical telescope is because that's where the best science was thought to be.

As to optical bandwidth, it's simple to have a telescope that can perform well across the reflectivity spectrum of aluminum. The would go longward from the near-UV. If the telescope is not going to be cold, there isn't much sense in having it work any farther into the infrared than 2-3 microns, as for HST. But be careful about UV requirements, as those will completely dominate the wavefront error, pointing, and cleanliness requirements for the telescope. An optimal UV-capable telescope could be enormously expensive.

Pointing stability should serve diffraction-limited performance of an 18+ m aperture telescope, on a time scale of at least hours. Same with wavefront error and stability.

Spectral resolution isn't about the telescope. It's about the focal plane instruments. If this is a serviceable telescope, where new instruments can be installed, this isn't an obviously important question. In any case, high spectral resolution isn't advantageous in wavelengths at which the Earth's atmosphere is transparent, because at such wavelengths, much larger ground-based telescopes will win every time for photon-hungry and background-tolerant applications like high spectral resolution.

As to lifetime, that's a dangerous game to play. If you go to NASA and ask them to buy into a telescope with a 40 year lifetime, for example, you're asking them to commit to 40 years of operating budgets. They simply won't do that, unless you give them a clear picture of the science those forty years will buy. We have no way of telling what that science might be. In fact, our science priorities evolve pretty dramatically on time scales of a decade or so. Ordinarily, I'd say a ten-year lifetime is defensible. Perhaps with a serviceable telescope, you could try for twenty. But you're going to pay a stiff price for long lifetime. I think the best idea is to design a telescope with fixed science capabilities that will last for ten years, and then make serviceability and servicing as extra-cost options. ROI isn't necessarily proportional to observing time, once you get past the highest priority questions.

Operational efficiency is pretty much dependent on what you're trying to accomplish. If you get outside of LEO, the operational efficiency could be quite high, in terms of the fraction of the time that data is being taken. I would assume that the planned scheduling efficiency of JWST,

which is something like 95%, should apply to this. That mainly dictates slew times and engineering time requirements.

I think the bottom line to all this is trying to come up with a concept for a huge telescope with optimum imaging performance, and see if you can do it in such a way that is affordable. Once you have that, there are many useful directions one can take.

- Is there an available cost model for this mission (spacecraft, ground systems, launch vehicle)? Is there a cost model for a federated satellite system?

There are plenty of cost models for federally funded space telescopes. In fact, a big piece of NASA develops and supports such cost modeling for space missions. Probably the most important part of a credible cost model is one that develops a clear picture of technological readiness. That is, you don't start cutting metal until you have cogently identified all technology needs, and made appropriate investments to relieve them. Identifying technology lapses late in the project is HUGELY expensive. Should assess the subsystems with regard to current TRL.

The cost curve for large space telescope development has a pretty well understood profile, and NASA SMD funding is simply incapable of supporting a peak funding rate of more than about $500M/yr for an astronomical telescope.

That said, to the extent this mission makes any requirements on human space flight, it would be very hard to come up with a believable cost model. We don't have good cost models for human space flight outside of LEO. That being the case, maybe you should assume that the 10-year budget is <$5B, and just make the thing optionally serviceable. Or else assume that the servicing is done robotically.

- Is there a set of launch vehicles which we can use for making initial estimates?

If you want to keep costs down, and $/lb low, you need to be looking at Falcon Heavy. I suppose you should look at SLS, but I don't have a lot of confidence that support for that launcher will continue. It might be a dead end, as we've made no serious plans about what we'd put on it, and it's already understood to be a very expensive lift option.

- What operational orbits should we consider?

For the highest performance, in terms of thermal stability, accessibility, and field of regard, you won't do better than Sun-Earth L2. DO NOT put this telescope in LEO. A very large optical telescope will be seriously compromised by putting it in LEO, for many reasons.

- What is the budget for this mission?

I frankly don't think it's sellable if the LCC (not including servicing) is over $5B. JWST is a bad example to follow, in terms of LCC affordability. NASA, Congress, and the science community will avoid such expensive instruments like the plague in the future. Some serious thought should be given to making such a telescope useful to other nations, with the hope that those other nations can invest in it. That's feasible only if those other nations see obvious roles for themselves in telescope development. Another country won't buy in to such a telescope scientifically unless they can exercise their technological expertise in building it. Nations largely

don't pay for space astronomy. They pay for technology development that leads to good space astronomy.

So therein lies the challenge. Can you design a very capable telescope three times the size of JWST for 50% less money?

- What ground stations will we use? DSN? How often should we assume passes occur and how long will they be?

That's not a big issue. Ground station operations are a function of data rate, comm architecture, and on-board data storage. That's not going to drive mission design. But for a mission at ES L2, you'd pretty much assume you're going to use a DSN-like comm station. If you had to build a completely new DSN station, just for this mission, it would be a small fraction of the mission budget.

- What mirror technologies should we consider?
- What detector technologies should we consider?
- What adaptive optics technologies should we consider?

These are things that come out of focused trade studies. It doesn't make a lot of sense to think about these before establishing the telescope requirements.

- Are there specific technology insertion goals for this telescope?

There are many aspects to this question. Technology insertion strategies can apply to system or technology obsolescence, and technology applicability to different stakeholder groups. I think an important one for this telescope is that technologies developed should allow for extensibility in telescope design. That is, whether I want to expand this particular telescope, or build a new much larger one after this one, I want the technologies developed for this one to be applicable to the next gen one. For example, one concept for ATLAST was putting the largest primary mirror possible in the largest launch shroud. That's not an extensible strategy, at least until someone decides to build a much bigger launcher. That is, the strategies that one develops here (construction, deployment, alignment, etc.) to make, say, an 18m telescope, should lead to envisioning a much larger one, or even expanding this one.

Another technology insertion goal is servicing. One would like a design that is not only ideally serviceable, but one that is amenable to new instruments. While one might not be sure about the prospects for servicing and instrument replacement, the telescope should not be designed in such a way to prevent that from happening.

- Why are hexagons used as the standard for mirror segments?

Because they fill space efficiently. Round segments don't. Since hexagons are roughly round, they are more symmetrically fabricatable.

- Does the data need to be secure?

Not "secure" in terms of national security. But it will be understood that preselected mission teams get first dibs on the data they've proposed to get.

- Who is going to receive the data?

Once the comm packages come down to Earth, the standard model is to have some institution (STScI for HST, or IPAC for IR data), manage, distribute, and archive the data. This is just a service you buy, and there are many with that experience,

- What data management system should we use?

That's up to the data management institution, and is not a decision for the observatory designers, nor an engineering decision. The observatory designers might like to set some specifications about what the data management system should be capable of doing. It clearly has to be one that serves a multitude of worldwide users who can't be assumed to have any engineering expertise.

- Is NASA interested in soliciting additional stakeholders for the project (ESA, Commercial, Hosted Payloads)?

I don't think "hosted payloads" has much to do with this. Commercial? That would require that industry see observatory operations as a money-making concept. I don't think that would happen. Certainly other national space agencies -- ESA, Roscosmos, JAXA, CSA, etc. could be polled about this, as per my suggestion above. But this isn't an engineering question except, as I said above, to the extent of assessing how their engineering expertise overlaps.

Lee Feinberg

I agree with almost all of your observatory requirements but I personally would advocate you go larger than 16.8-meters. I know that size was chosen for the deployed ATLAST and so there is some existing work done at that scale but once you buy into the idea of assembly and economies of scale based on identical mirrors and modules then 20+meters makes a lot more sense (I'm OK bigger than 20-meters but 16.8-meters is still at the size that you would consider deployment and not enough bang for the buck). This argument is supported by the next generation of hexagonal mirror ground telescopes which are 30 meters (TMT) and 39 meters (EELT). The argument of course is that the major costs are in the NRE of making the first modules, facilitizing, and solving how to assemble - the incremental cost of additional area is not significant. For size and high contrast dynamics and pointing may actually be the limiting issue (we want to take advantage of the resolution) but the hope is active solutions can mitigate this (an area I urge you to focus on!). Conveniently, the 20-meter telescope size we chose using JWST segment size has exactly the number of hexagonal elements as the next generation deformable mirror from Boston micro-machines that the VNC group is using and which is critical to achieving high contrast. In addition, Marc Postman has done some thinking about the science for a 20-meter (and hopefully will spend more time on this issue in the future) and can comment on that aspect of things.

I'm very interested to hear what you are thinking on where and how assembly will be accomplished - that seems to be a key nut to crack. With respect to servicing, do you want to consider two key roles for human involvement: troubleshooting (if there is a major issue that robots cannot solve) and reduced latency telerobotics.

With regards to cost, TMT's model relies quite a bit on international contributions (China, India and Japan are all contributing significantly) and on economies of scale. We've studied mirror segment economies of scale from JWST and a ground telescope but a lot more needs to be done

here. I suspect there are other economies of scale arguments that would be very helpful to explaining why bigger doesn't cost that much more and I would urge you to talk to your economist colleagues at MIT to help with that. Also, I'm not sure how you cost the assembly piece so you may want to study the HST cost arguments.

Swati Mohan

- What are the mission goals? How does this telescope relate to current and future telescopes (ATLAST)?

1.   Find earth-like planets around other stars and determine if they carry the signature of life.

2.   Look at the universe as far back in time as possible and understand our origins.

3.   Look at galactic centers to understand their structure, formation, etc.

4.   STScI has a lot of information on this.

5.   We would think it relates closely to ATLAST.

- What is the expectation of the optical capability of the new telescope (optical bandwidth, aperture size, angular resolution, FOV, pointing stability, spectral resolution, contrast, inner working angle, wavefront error, wavefront stability, uninterrupted observation time, lifetime, operational efficiency).

1.   80% Strehl ratio at 633 nm.

2.   Rules of thumb you can use for an F1 primary are:

Radius of curvature of PM = 2 * PM_diameter

Radius of curvature of SM = 0.25 * PM_diameter

PM-SM_distance = 0.9 * PM_Diameter

SM_Diameter = 0.15 * PM_Diameter

3.   You should decide the telescope operational temperature requirements based on the mission objectives. Is this UV, optical, IR or some combination?

4.   The rest of the requirements depend on the application and will be determined based on the mission objectives.

- Is there an available cost model for this mission (spacecraft, ground systems, launch vehicle)? Is there a cost model for a federated satellite system?

1.   We don't know of any available cost model. Or a model for a federated satellite system.

- Is there a set of launch vehicles which we can use for making initial estimates?

1.   Atlas V, Delta IV heavy, the SLS with either the Atlas V or Delta IV heavy fairing, the SLS with 8 and 10 meter fairings that are on the drawing board. Could also look at Dragon.

- What operational orbits should we consider?

1. Fixed at ESL2.

2. Other Lagrange points.

3. GEO (to assemble?).

- What is the budget for this mission?

1. $5-10B in 2013 $.

- What ground stations will we use? DSN? How often should we assume passes occur and how long will they be?

1. If at SE-L2 (or L1) would use the 34 m antennas at DSN.

2. If Earth orbiting would use TDRSS.

3. Full coverage for critical events. One 8 hour pass a day otherwise.

- What mirror technologies should we consider?

1. Actuated hybrid mirrors with either a nanolaminate or polished silicon carbide surface.

- What detector technologies should we consider?

1. Suggest you pick a representative set of instruments and base the detectors on current state of the art.

- What adaptive optics technologies should we consider?

1. Actuated hybrid mirrors with rigid body actuators for the primary.

2. Actuated hybrid mirrors with rigid body actuators for the secondary and a primary with rigid body actuators.

- Are there specific technology insertion goals for this telescope?

1. A great deal of technology needs to be developed to enable the telescope. Marc Postman has a chart that summarizes these. OpTIIX does a number of them: on-orbit assembly and servicing, actuated hybrid mirrors, laser metrology, wavefront sensing and control.

- Why are hexagons used as the standard for mirror segments?

1. They are stackable and reasonably close to circles which makes them easier to polish. Manufacturing inertia (machines, tooling, etc. already developed) will likely keep it that way.

- Does the data need to be secure?

1. Data security should be the same as a for a NASA science mission.

- Who is going to receive the data?

1. Assuming mission is at L2, Level 0 data will come through the DSN to the GDS at the institution operating the mission; JPL, GSFC, etc. The data will then be processed into Level 1 data and shipped to the institution(s) in charge of science; STScI, universities, etc.

- What data management system should we use?

1. We would expect the institution managing the project/mission to choose. JPL has more experience with planetary missions. GSFC with Earth orbiting. We would probably pick something at JPL since mission is at L2.

2. This shouldn't be a driver for this study.

- Is NASA interested in soliciting additional stakeholders for the project (ESA, Commercial, Hosted Payloads)?

1. Not something that we can answer other than the cost is so high that NASA will likely want partners to help defray it.

Tupper Hyde

- What ground stations will we use? DSN? How often should we assume passes occur and how long will they be?

DSN, mainly Australia site for 4 hours per day. Same as JWST.

- Is there a set of launch vehicles which we can use for making initial estimates?

Any EELV, Falcon 9, F9 Heavy, Ariane, SLS

- What are the mission goals? How does this telescope relate to current and future telescopes (ATLAST)?

UVOIR Astronomy and Earth-size exoplanets. Same science goals as ATLAST 16.8-m. Should consider servicing to enable 40+ year life.

- What is the expectation of the optical capability of the new telescope (optical bandwidth, aperture size, angular resolution, FOV, pointing stability, spectral resolution, contrast, inner working angle, wavefront error, wavefront stability, uninterrupted observation time, lifetime, operational efficiency).

Same as assumed for ATLAST 16.8-m design.

- What operational orbits should we consider?

SE-L2 for science. Any for assembly/servicing.

- What is the budget for this mission?

Cost should be an output of the trade. $10B (of today's dollars) is not unreasonable. I bet the range will be like $5-15B.

- Is there an available cost model for this mission (spacecraft, ground systems, launch vehicle)? Is there a cost model for a federated satellite system?

Several large telescope cost models are in the literature. I would recommend the one by Phil Stahl. NASA will provide DSN costs.

- When will this telescope operate? What is its expected lifetime? What other space assets will be available for utilization at that time?

Assume mission start in 2020 and launch by 2030. It should operate at least 10 years or up to 40 with servicing. You could assume a geo servicer such as the NASA Restore mission would be operating regularly by 2028 (ssco.gsfc.nasa.gov)

- What mirror technologies should we consider?

Glass and AHM segments. Size and number of segments is a trade.

- What detector technologies should we consider?

Same at ATLAST.

- What adaptive optics technologies should we consider?

Image and/or laser truss wavefront sensing with mirror actuation. Bandwidth (update rate) of wavefront control depends on thermal time constants. Coronagraphs will have additional deformable mirrors.

- Are there specific technology insertion goals for this telescope?

In the servicing options, upgrades for new technology in instruments should be considered.

- Does the data need to be secure?

No

- Who is going to receive the data?

A space telescope science institute (such as STScI) would archive the data and provide it to investigators

- What data management system should we use?
- Is NASA interested in soliciting additional stakeholders for the project (ESA, Commercial, Hosted Payloads)?

We expanded the stakeholder names at the meeting. I don't think adding ESA or commercial for this scope of study will be useful.

APPENDIX C: COMPONENTS DATABASE

This page is a large rotated landscape spreadsheet/table of spacecraft subsystem components and parameters. The text is extremely dense and rotated; the readable content is transcribed below.

Reference / Source	Component Description
edu/~nso/telecom/media/aw_r-29-09/Henshaw%20FREND%20Overview%207_29_09.pdf	Robotic Arm
RINGS coil	Electromagnetic Coil
UDP	Universal Docking Port
JWST	Mirror Segment
	Surface Normal Actuator
	Surface Parallel Actuator
http://www.jwst.nasa.gov/faq.html	Backframe per mirror segment
	Structural Support
	Magnetic Isolation Device
	Viscoelastic Isolation Device
	Active Damping Device
Hubble Gimbal	Deployment Device
	Gimballing Device
	Universal Docking Port Comm
	Universal Docking Port Power
MIT Lincoln Labs, http://spaceflightnow.com/news/n1108/22technology/	Laser communications type of comm box
Hubble References	Radio frequency type of comm box
ATLAST	Antenna for direct downloads
Indium NEXT (Rantec Microwave Antenna)	Crosslink antenna
	Memory required to store data prior to downlink
97sd3232	Power Converter
PXI220	Command and Data Link Interface between other subsystems
Hubble	Wide Field of View, Low Spectral Resolution, NUV-VIS-VISNIR, Partially coronographic
Hubble References	Non-imaging, Medium/High Spectral Resolution, FUV-NUV-VIS, Non coronographic
Hubble References	Orientation navigation
Hubble References	Imaging, Low/Medium Spectral Resolution, VISNIR-NIR-ExtNIR, Coronographic -
	High Resolution Imaging, Low/Medium Spectral Resolution, FUV-NUV-VIS-VISNIR, Coronographic -
	Thermal Insulation, Thermal Isolation
	Thermal rejection
	Cooling mechanism
	Cooling mechanism
	Heating mechanism
	Heat transfer mechanism
	Thermal sensing
Honeywell HR16 MW (Nms)	Attitude Control System
Custom	Attitude Control System
Ball CT-633 Stellar AS	Attitude Determination System
Triple Junction In/Gas cells	100 watt solar array unit (assuming 5 meter size folded
Lithium Ion battery	1 watt-hour battery unit (assuming cube volume)
VPT converters	100 watt distribution/converters) unit (assuming cube volume)
General connector and wiring	Connectors wires needed from voltage bus to modules
Hubble from Margaret	Protect the telescope optics from stray light
ATLAST 8m scaled by ratio of length to radius	Deployment Device
Hubble	Mirror Segment
Hubble	Protect against light impingement
Hubble	Avionics Central Processing Unit
	Process, format, code/decode messages
	Heating mechanism
	Heating mechanism
	Thermal sensing
	Thermal sensing
	Thermal Insulation, Thermal Isolation
	Structural Support
	Thruster
	Thruster
	Thruster
	Propellant Tank + Propellant

Notes in margin columns: "80-600Mbps", "To be removed (Redundant)", "AntDevCo: Spacecraft Antennas and Ant...", "M/P/V allocated based on previous progr..."

APPENDIX D: STRUCTURAL DSM

#	DSM	1	2	3	4	5	6	7	8	9	10	11	12	13	14	15	16	17	18	19	20	21	22	23	24	25	26	27	28	29	30	31	32	33	34	35	36	37	38	39	40	41	42	43	44	45	46	47	48	49	50	51	52	53	54	55	56	57
1	Robotic Arm	0	0	0	0	0	0	0	0	0	0	0	0	0	0	0	0	0	0	0	0	0	0	0	0	0	0	0	0	0	0	0	0	0	0	0	0	0	0	0	0	0	0	0	0	0	0	0	0	0	0	0	0	0	0	0	0	0
2	EM Coil	0	0	0	0	0	0	0	0	0	0	0	0	0	0	0	0	0	0	0	0	0	0	0	0	0	0	0	0	0	0	0	0	0	0	0	0	0	0	0	0	0	0	0	0	0	0	0	0	0	0	0	0	0	0	0	0	0
3	UDP	1	0	0	0	0	0	0	0	0	0	0	0	0	0	0	0	0	0	0	0	0	0	0	0	0	0	0	0	0	0	0	0	0	0	0	0	0	0	0	0	0	0	0	0	0	0	0	0	0	0	0	0	0	0	0	0	0
4	Primary Mirror Segment	0	0	0	0	0	0	0	0	0	0	0	0	0	0	0	0	0	0	0	0	0	0	0	0	0	0	0	0	0	0	0	0	0	0	0	0	0	0	0	0	0	0	0	0	0	0	0	0	0	0	0	0	0	0	0	0	0
5	Surface Normal Actuator	0	0	0	1	0	0	0	0	0	0	0	0	0	0	0	0	0	0	0	0	0	0	0	0	0	0	0	0	0	0	0	0	0	0	0	0	0	0	0	0	0	0	0	0	0	0	0	0	0	0	0	0	0	0	0	0	0
6	Surface Parallel Actuator	0	0	0	1	1	0	0	0	0	0	0	0	0	0	0	0	0	0	0	0	0	0	0	0	0	0	0	0	0	0	0	0	0	0	0	0	0	0	0	0	0	0	0	0	0	0	0	0	0	0	0	0	0	0	0	0	0
7	Backframe per segment	0	1	1	1	1	1	0	0	0	0	0	0	0	0	0	0	0	0	0	0	0	0	0	0	0	0	0	0	0	0	0	0	0	0	0	0	0	0	0	0	0	0	0	0	0	0	0	0	0	0	0	0	0	0	0	0	0
8	Bus structure	1	1	1	0	0	0	1	0	0	0	0	0	0	0	0	0	0	0	0	0	0	0	0	0	0	0	0	0	0	0	0	0	0	0	0	0	0	0	0	0	0	0	0	0	0	0	0	0	0	0	0	0	0	0	0	0	0
9	Magnetic Isolation Device	0	0	0	0	0	0	0	1	0	0	0	0	0	0	0	0	0	0	0	0	0	0	0	0	0	0	0	0	0	0	0	0	0	0	0	0	0	0	0	0	0	0	0	0	0	0	0	0	0	0	0	0	0	0	0	0	0
10	Viscoelastic Isolation Device	0	0	0	0	0	0	0	1	0	0	0	0	0	0	0	0	0	0	0	0	0	0	0	0	0	0	0	0	0	0	0	0	0	0	0	0	0	0	0	0	0	0	0	0	0	0	0	0	0	0	0	0	0	0	0	0	0
11	Active Damper	0	0	0	0	0	0	1	0	0	0	0	0	0	0	0	0	0	0	0	0	0	0	0	0	0	0	0	0	0	0	0	0	0	0	0	0	0	0	0	0	0	0	0	0	0	0	0	0	0	0	0	0	0	0	0	0	0
12	Deployment Device for Solar Array	0	0	1	0	0	0	1	1	1	1	1	0	0	0	0	0	0	0	0	0	0	0	0	0	0	0	0	0	0	0	0	0	0	0	0	0	0	0	0	0	0	0	0	0	0	0	0	0	0	0	0	0	0	0	0	0	0
13	Gimbal Device	0	1	1	0	0	0	0	1	0	0	0	0	0	0	0	0	0	0	0	0	0	0	0	0	0	0	0	0	0	0	0	0	0	0	0	0	0	0	0	0	0	0	0	0	0	0	0	0	0	0	0	0	0	0	0	0	0
14	UDP Comm interface	1	0	1	0	0	0	0	0	0	0	0	0	0	0	0	0	0	0	0	0	0	0	0	0	0	0	0	0	0	0	0	0	0	0	0	0	0	0	0	0	0	0	0	0	0	0	0	0	0	0	0	0	0	0	0	0	0
15	UDP Power interface	1	0	1	0	0	0	0	0	0	0	0	0	0	0	0	0	0	0	0	0	0	0	0	0	0	0	0	0	0	0	0	0	0	0	0	0	0	0	0	0	0	0	0	0	0	0	0	0	0	0	0	0	0	0	0	0	0
16	Laser Communications Box	0	0	0	0	0	0	0	0	0	0	0	0	0	0	0	0	0	0	0	0	0	0	0	0	0	0	0	0	0	0	0	0	0	0	0	0	0	0	0	0	0	0	0	0	0	0	0	0	0	0	0	0	0	0	0	0	0
17	RF Communications Box	0	0	0	0	0	0	0	0	0	0	0	0	0	0	0	0	0	0	0	0	0	0	0	0	0	0	0	0	0	0	0	0	0	0	0	0	0	0	0	0	0	0	0	0	0	0	0	0	0	0	0	0	0	0	0	0	0
18	Direct Downlink Antennas	0	0	0	0	0	0	0	0	0	0	0	0	0	0	0	0	0	0	0	0	0	0	0	0	0	0	0	0	0	0	0	0	0	0	0	0	0	0	0	0	0	0	0	0	0	0	0	0	0	0	0	0	0	0	0	0	0
19	Crosslink Antennas	0	0	0	0	0	0	0	0	0	0	0	0	0	0	0	0	0	0	0	0	0	0	0	0	0	0	0	0	0	0	0	0	0	0	0	0	0	0	0	0	0	0	0	0	0	0	0	0	0	0	0	0	0	0	0	0	0
20	RAM	0	0	0	0	0	0	0	0	0	0	0	0	0	0	0	0	0	0	0	0	0	0	0	0	0	0	0	0	0	0	0	0	0	0	0	0	0	0	0	0	0	0	0	0	0	0	0	0	0	0	0	0	0	0	0	0	0
21	Power Convertor Unit (PCU)	0	0	0	0	0	0	0	0	0	0	0	0	0	0	0	0	0	0	0	0	0	0	0	0	0	0	0	0	0	0	0	0	0	0	0	0	0	0	0	0	0	0	0	0	0	0	0	0	0	0	0	0	0	0	0	0	0
22	Data Interface Unit (DIU)	0	0	0	0	0	0	0	0	0	0	0	0	0	0	0	0	0	0	0	0	0	0	0	0	0	0	0	0	0	0	0	0	0	0	0	0	0	0	0	0	0	0	0	0	0	0	0	0	0	0	0	0	0	0	0	0	0
23	Instrument A	0	0	0	0	0	0	1	0	0	0	0	0	0	0	0	0	0	0	0	0	0	0	0	0	0	0	0	0	0	0	0	0	0	0	0	0	0	0	0	0	0	0	0	0	0	0	0	0	0	0	0	0	0	0	0	0	0
24	Instrument B	0	0	0	0	0	0	1	0	0	0	0	0	0	0	0	0	0	0	0	0	0	0	0	0	0	0	0	0	0	0	0	0	0	0	0	0	0	0	0	0	0	0	0	0	0	0	0	0	0	0	0	0	0	0	0	0	0
25	Fine Guidance Sensors	0	0	0	0	0	0	0	0	0	0	0	0	0	0	0	0	0	0	0	0	0	0	0	0	0	0	0	0	0	0	0	0	0	0	0	0	0	0	0	0	0	0	0	0	0	0	0	0	0	0	0	0	0	0	0	0	0
26	Instrument C	0	0	0	0	0	0	0	0	0	0	0	0	0	0	0	0	0	0	0	0	0	0	0	0	0	0	0	0	0	0	0	0	0	0	0	0	0	0	0	0	0	0	0	0	0	0	0	0	0	0	0	0	0	0	0	0	0
27	Instrument D	0	0	0	0	0	0	0	0	0	0	0	0	0	0	0	0	0	0	0	0	0	0	0	0	0	0	0	0	0	0	0	0	0	0	0	0	0	0	0	0	0	0	0	0	0	0	0	0	0	0	0	0	0	0	0	0	0
28	Thermal blanket {bus}	0	0	0	0	0	0	1	0	0	0	0	0	0	0	0	0	0	0	0	0	0	0	0	0	0	0	0	0	0	0	0	0	0	0	0	0	0	0	0	0	0	0	0	0	0	0	0	0	0	0	0	0	0	0	0	0	0
29	External radiator {bus}	0	0	0	0	0	0	1	0	0	0	0	0	0	0	0	0	0	0	0	0	0	0	0	0	0	0	0	0	0	0	0	0	0	0	0	0	0	0	0	0	0	0	0	0	0	0	0	0	0	0	0	0	0	0	0	0	0
30	Thermoelectric cooler (TEC) {optics}	0	0	1	0	0	0	0	0	0	0	0	0	0	0	0	0	0	0	0	0	0	0	0	0	0	0	0	0	0	0	0	0	0	0	0	0	0	0	0	0	0	0	0	0	0	0	0	0	0	0	0	0	0	0	0	0	0
31	Cryocooler {inst}	0	0	0	0	0	0	0	0	0	0	0	0	0	0	0	0	0	0	0	0	0	0	1	1	1	1	1	0	0	0	0	0	0	0	0	0	0	0	0	0	0	0	0	0	0	0	0	0	0	0	0	0	0	0	0	0	0
32	Thermostatic heater {optics}	0	0	1	0	0	0	0	0	0	0	0	0	0	0	0	0	0	0	0	0	0	0	0	0	0	0	0	0	0	0	0	0	0	0	0	0	0	0	0	0	0	0	0	0	0	0	0	0	0	0	0	0	0	0	0	0	0
33	Heat pipe network {bus}	0	0	0	0	0	0	1	0	0	0	0	0	0	0	0	1	1	1	1	1	1	1	0	0	0	0	0	0	0	0	0	1	0	1	0	0	0	0	0	0	0	0	0	0	0	0	0	0	0	0	0	0	0	0	0	0	0
34	Thermal sensor {optics}	1	1	1	1	1	1	1	0	1	1	1	1	1	1	1	0	0	0	0	0	0	0	0	0	0	0	0	0	0	0	1	0	1	0	0	0	0	0	0	0	0	0	0	0	0	0	0	0	0	0	0	0	0	0	0	0	0
35	Momentum Wheel	0	0	0	0	0	0	0	0	0	0	0	0	0	0	0	0	0	0	0	0	0	0	0	0	0	0	0	0	0	0	0	0	0	1	0	0	0	0	0	0	0	0	0	0	0	0	0	0	0	0	0	0	0	0	0	0	0
36	Solar Sail	0	0	0	0	0	0	0	0	0	0	0	0	0	0	0	0	0	0	0	0	0	0	0	0	0	0	0	0	0	0	0	0	0	0	0	0	0	0	0	0	0	0	0	0	0	0	0	0	0	0	0	0	0	0	0	0	0
37	Star Tracker	0	0	0	0	0	0	0	0	0	0	0	0	0	0	0	0	0	0	0	0	0	0	0	0	0	0	0	0	0	0	0	0	0	1	0	0	0	0	0	0	0	0	0	0	0	0	0	0	0	0	0	0	0	0	0	0	0
38	Solar Array per 100 watts	0	0	0	0	0	0	1	0	0	0	0	0	0	0	0	0	0	0	0	0	0	0	0	0	0	0	0	0	0	0	0	0	0	0	0	0	0	0	0	0	0	0	0	0	0	0	0	0	0	0	0	0	0	0	0	0	0
39	Battery per watt-hour	0	0	0	0	0	0	0	0	0	0	0	0	0	0	0	0	0	0	0	0	0	0	0	0	0	0	0	0	0	0	0	0	0	0	0	0	0	1	0	0	0	0	0	0	0	0	0	0	0	0	0	0	0	0	0	0	0
40	Distribution per 100 watts	0	0	0	0	0	0	1	0	0	0	0	0	0	0	0	0	0	0	0	0	0	0	0	0	0	0	0	0	0	0	0	0	0	0	0	0	0	0	0	0	0	0	0	0	0	0	0	0	0	0	0	0	0	0	0	0	0
41	Connectors and Wiring	0	0	0	0	0	0	1	0	0	0	0	0	0	0	0	0	0	0	0	0	0	0	0	0	0	0	0	0	0	0	0	0	0	0	0	0	0	0	0	0	0	0	0	0	0	0	0	0	0	0	0	0	0	0	0	0	0
42	Light Shield	0	0	0	0	0	0	1	0	0	0	0	0	0	0	0	0	0	0	0	0	0	0	0	0	0	0	0	0	0	0	0	0	0	0	0	0	0	0	0	0	0	0	0	0	0	0	0	0	0	0	0	0	0	0	0	0	0
43	Deployment Device for Antenna	0	0	0	0	0	0	0	1	1	1	1	1	0	0	0	1	1	0	0	0	0	0	0	0	0	0	0	0	0	0	0	0	0	0	0	0	0	0	0	0	0	0	0	0	0	0	0	0	0	0	0	0	0	0	0	0	0
44	Secondary Mirror Segment	0	0	0	0	1	1	1	0	0	0	0	0	0	0	0	0	0	0	0	0	0	0	0	0	0	0	0	0	0	0	0	0	0	0	0	0	0	0	0	0	0	0	0	0	0	0	0	0	0	0	0	0	0	0	0	0	0
45	Primary Mirror Baffle	0	0	0	0	0	0	1	0	0	0	0	0	0	0	0	0	0	0	0	0	0	0	0	0	0	0	0	0	0	0	0	0	0	0	0	0	0	0	0	0	0	0	0	0	0	0	0	0	0	0	0	0	0	0	0	0	0
46	CPU	0	0	0	0	0	0	0	0	0	0	0	0	0	0	0	0	0	0	0	0	0	0	0	0	0	0	0	0	0	0	0	0	0	0	0	0	0	0	0	0	0	0	0	0	0	0	0	0	0	0	0	0	0	0	0	0	0
47	Data Management Unit (DMU)	0	0	0	0	0	0	0	0	0	0	0	0	0	0	0	0	0	0	0	0	0	0	0	0	0	0	0	0	0	0	0	0	0	0	0	0	0	0	0	0	0	0	0	0	0	0	0	0	0	0	0	0	0	0	0	0	0
48	Thermostatic heater {inst}	0	0	0	0	0	0	0	0	0	0	0	0	0	0	0	0	0	0	0	0	0	0	1	1	1	1	1	0	0	0	0	0	0	0	0	0	0	0	0	0	0	0	0	0	0	0	0	0	0	0	0	0	0	0	0	0	0
49	Thermostatic heater {bus}	0	0	0	0	0	0	1	0	0	0	0	0	0	0	0	1	1	0	1	0	0	0	0	0	0	0	0	0	0	0	0	0	1	0	0	0	0	0	0	0	0	0	0	0	0	0	0	0	0	0	0	0	0	0	0	0	0
50	Thermal sensor {inst}	0	0	0	0	0	0	0	0	0	0	0	0	0	0	0	0	0	0	0	0	0	0	1	1	1	1	1	0	0	0	0	0	0	0	0	0	0	0	0	0	0	0	0	0	0	0	0	0	0	0	0	0	0	0	0	0	0
51	Thermal sensor {bus}	0	0	0	0	0	0	1	0	0	0	0	0	0	0	0	1	1	1	1	1	1	1	0	0	0	0	0	0	0	0	0	0	1	0	0	0	0	0	0	0	0	0	0	0	0	0	0	0	0	0	0	0	0	0	0	0	0
52	Thermal blanket {inst}	0	0	0	0	0	0	0	0	0	0	0	0	0	0	0	0	0	0	0	0	0	0	1	1	1	1	1	0	0	0	0	0	0	0	0	0	0	0	0	0	0	0	0	0	0	0	0	0	0	0	0	0	0	0	0	0	0
53	Science Payload support structure	0	0	0	0	0	0	1	0	0	0	0	0	0	0	0	0	0	0	0	0	0	0	0	0	0	0	0	0	0	0	0	0	0	0	0	0	0	0	0	0	0	0	0	0	0	0	0	0	0	0	0	0	0	0	0	0	0
54	Monopropellant hydrazine thruster	0	0	0	0	0	0	1	0	0	0	0	0	0	0	0	0	0	0	0	0	0	0	0	0	0	0	0	0	0	0	0	0	0	0	0	0	0	0	0	0	0	0	0	0	0	0	0	0	0	0	0	0	0	0	0	0	0
55	Arcjet thruster	0	0	0	0	0	0	1	0	0	0	0	0	0	0	0	0	0	0	0	0	0	0	0	0	0	0	0	0	0	0	0	0	0	0	0	0	0	0	0	0	0	0	0	0	0	0	0	0	0	0	0	0	0	0	0	0	0
56	Hall thruster	0	0	0	0	0	0	1	0	0	0	0	0	0	0	0	0	0	0	0	0	0	0	0	0	0	0	0	0	0	0	0	0	0	0	0	0	0	0	0	0	0	0	0	0	0	0	0	0	0	0	0	0	0	0	0	0	0
57	Propellant (and tank)	0	0	0	0	0	0	1	0	0	0	0	0	0	0	0	0	0	0	0	0	0	0	0	0	0	0	0	0	0	0	0	0	0	0	0	0	0	0	0	0	0	0	0	0	0	0	0	0	0	0	0	0	0	0	0	0	0

APPENDIX E: THERMAL DSM

DSM	1	2	3	4	5	6	7	8	9	10	11	12	13	14	15	16	17	18	19	20	21	22	23	24	25	26	27	28	29	30	31	32	33	34	35	36	37	38	39	40	41	42	43	44	45	46	47	48	49	50	51	52	53	54	55	56	57
1 Robotic Arm	0	0	0	0	0	0	0	0	0	0	0	0	0	0	0	0	0	0	0	0	0	0	0	0	0	0	0	0	0	0	0	0	0	0	0	0	0	0	0	0	0	0	0	0	0	0	0	0	0	0	0	0	0	0	0	0	0
2 EM Coil	0	0	0	0	0	0	0	0	0	0	0	0	0	0	0	0	0	0	0	0	0	0	0	0	0	0	0	0	0	0	0	0	0	0	0	0	0	0	0	0	0	0	0	0	0	0	0	0	0	0	0	0	0	0	0	0	0
3 UDP	0	0	0	0	0	0	0	0	0	0	0	0	0	0	0	0	0	0	0	0	0	0	0	0	0	0	0	0	0	0	0	0	0	0	0	0	0	0	0	0	0	0	0	0	0	0	0	0	0	0	0	0	0	0	0	0	0
4 Primary Mirror Segment	0	0	0	0	0	0	0	0	0	0	0	0	0	0	0	0	0	0	0	0	0	0	0	0	0	0	0	0	0	0	0	0	0	0	0	0	0	0	0	0	0	0	0	0	0	0	0	0	0	0	0	0	0	0	0	0	0
5 Surface Normal Actuator	0	0	1	0	0	0	0	0	0	0	0	0	0	0	0	0	0	0	0	0	0	0	0	0	0	0	0	0	0	0	0	0	0	0	0	0	0	0	0	0	0	0	0	0	0	0	0	0	0	0	0	0	0	0	0	0	0
6 Surface Parallel Actuator	0	0	0	1	1	0	0	0	0	0	0	0	0	0	0	0	0	0	0	0	0	0	0	0	0	0	0	0	0	0	0	0	0	0	0	0	0	0	0	0	0	0	0	0	0	0	0	0	0	0	0	0	0	0	0	0	0
7 Backframe per segment	0	0	0	0	0	0	0	0	0	0	0	0	0	0	0	0	0	0	0	0	0	0	0	0	0	0	0	0	0	0	0	0	0	0	0	0	0	0	0	0	0	0	0	0	0	0	0	0	0	0	0	0	0	0	0	0	0
8 Bus structure	0	1	0	0	0	0	0	0	0	0	0	0	0	0	0	0	0	0	0	0	0	0	0	0	0	0	0	0	0	0	0	0	0	0	0	0	0	0	0	0	0	0	0	0	0	0	0	0	0	0	0	0	0	0	0	0	0
9 Magnetic Isolation Device	0	0	0	0	0	0	0	1	0	0	0	0	0	0	0	0	0	0	0	0	0	0	0	0	0	0	0	0	0	0	0	0	0	0	0	0	0	0	0	0	0	0	0	0	0	0	0	0	0	0	0	0	0	0	0	0	0
10 Viscoelastic Isolation Device	0	0	0	0	0	0	0	0	0	0	0	0	0	0	0	0	0	0	0	0	0	0	0	0	0	0	0	0	0	0	0	0	0	0	0	0	0	0	0	0	0	0	0	0	0	0	0	0	0	0	0	0	0	0	0	0	0
11 Active Damper	0	0	0	0	0	0	0	0	0	0	0	0	0	0	0	0	0	0	0	0	0	0	0	0	0	0	0	0	0	0	0	0	0	0	0	0	0	0	0	0	0	0	0	0	0	0	0	0	0	0	0	0	0	0	0	0	0
12 Deployment Device for Solar Array	0	0	0	0	0	0	1	0	0	0	0	0	0	0	0	0	0	0	0	0	0	0	0	0	0	0	0	0	0	0	0	0	0	0	0	0	0	0	0	0	0	0	0	0	0	0	0	0	0	0	0	0	0	0	0	0	0
13 Gimbal Device	0	0	0	0	0	0	0	0	0	0	0	0	0	0	0	0	0	0	0	0	0	0	0	0	0	0	0	0	0	0	0	0	0	0	0	0	0	0	0	0	0	0	0	0	0	0	0	0	0	0	0	0	0	0	0	0	0
14 UDP Comm interface	0	0	0	0	0	0	0	0	0	0	0	0	0	0	0	0	0	0	0	0	0	0	0	0	0	0	0	0	0	0	0	0	0	0	0	0	0	0	0	0	0	0	0	0	0	0	0	0	0	0	0	0	0	0	0	0	0
15 UDP Power interface	0	0	0	0	0	0	0	0	0	0	0	0	0	0	0	0	0	0	0	0	0	0	0	0	0	0	0	0	0	0	0	0	0	0	0	0	0	0	0	0	0	0	0	0	0	0	0	0	0	0	0	0	0	0	0	0	0
16 Laser Communications Box	0	0	0	0	0	0	0	0	0	0	0	0	0	0	0	0	0	0	0	0	0	0	0	0	0	0	0	0	0	0	0	0	0	0	0	0	0	0	0	0	0	0	0	0	0	0	0	0	0	0	0	0	0	0	0	0	0
17 RF Communications Box	0	0	0	0	0	0	0	0	0	0	0	0	0	0	0	0	0	0	0	0	0	0	0	0	0	0	0	0	0	0	0	0	0	0	0	0	0	0	0	0	0	0	0	0	0	0	0	0	0	0	0	0	0	0	0	0	0
18 Direct Downlink Antennas	0	0	0	0	0	0	0	0	0	0	0	0	0	0	0	0	0	0	0	0	0	0	0	0	0	0	0	0	0	0	0	0	0	0	0	0	0	0	0	0	0	0	0	0	0	0	0	0	0	0	0	0	0	0	0	0	0
19 Crosslink Antennas	0	0	0	0	0	0	0	0	0	0	0	0	0	0	0	0	0	0	0	0	0	0	0	0	0	0	0	0	0	0	0	0	0	0	0	0	0	0	0	0	0	0	0	0	0	0	0	0	0	0	0	0	0	0	0	0	0
20 RAM	0	0	0	0	0	0	0	0	0	0	0	0	0	0	0	0	0	0	0	0	0	0	0	0	0	0	0	0	0	0	0	0	0	0	0	0	0	0	0	0	0	0	0	0	0	0	0	0	0	0	0	0	0	0	0	0	0
21 Power Convertor Unit (PCU)	0	0	0	0	0	0	0	0	0	0	0	0	0	0	0	0	0	0	0	0	0	0	0	0	0	0	0	0	0	0	0	0	0	0	0	0	0	0	0	0	0	0	0	0	0	0	0	0	0	0	0	0	0	0	0	0	0
22 Data Interface Unit (DIU)	0	0	0	0	0	0	0	0	0	0	0	0	0	0	0	0	0	0	0	0	0	0	0	0	0	0	0	0	0	0	0	0	0	0	0	0	0	0	0	0	0	0	0	0	0	0	0	0	0	0	0	0	0	0	0	0	0
23 Instrument A	0	0	0	0	0	0	0	0	0	0	0	0	0	0	0	0	0	0	0	0	0	0	0	0	0	0	0	0	0	0	0	0	0	0	0	0	0	0	0	0	0	0	0	0	0	0	0	0	0	0	0	0	0	0	0	0	0
24 Instrument B	0	0	0	0	0	0	0	0	0	0	0	0	0	0	0	0	0	0	0	0	0	0	0	0	0	0	0	0	0	0	0	0	0	0	0	0	0	0	0	0	0	0	0	0	0	0	0	0	0	0	0	0	0	0	0	0	0
25 Fine Guidance Sensors	0	0	0	0	0	0	0	0	0	0	0	0	0	0	0	0	0	0	0	0	0	0	0	0	0	0	0	0	0	0	0	0	0	0	0	0	0	0	0	0	0	0	0	0	0	0	0	0	0	0	0	0	0	0	0	0	0
26 Instrument C	0	0	0	0	0	0	0	0	0	0	0	0	0	0	0	0	0	0	0	0	0	0	0	0	0	0	0	0	0	0	0	0	0	0	0	0	0	0	0	0	0	0	0	0	0	0	0	0	0	0	0	0	0	0	0	0	0
27 Instrument D	0	0	0	0	0	0	0	0	0	0	0	0	0	0	0	0	0	0	0	0	0	0	0	0	0	0	0	0	0	0	0	0	0	0	0	0	0	0	0	0	0	0	0	0	0	0	0	0	0	0	0	0	0	0	0	0	0
28 Thermal blanket {bus}	0	0	0	0	0	0	0	0	0	0	0	0	0	0	0	0	0	0	0	0	0	0	0	0	0	0	0	0	0	0	0	0	0	0	0	0	0	0	0	0	0	0	0	0	0	0	0	0	0	0	0	0	0	0	0	0	0
29 External radiator {bus}	0	0	0	0	0	0	0	0	0	0	0	0	0	0	0	0	0	0	0	0	0	0	0	0	0	0	0	0	0	0	0	0	0	0	0	0	0	0	0	0	0	0	0	0	0	0	0	0	0	0	0	0	0	0	0	0	0
30 Thermoelectric cooler (TEC) {optics}	0	0	1	0	0	0	0	0	0	0	0	0	0	0	0	0	0	0	0	0	0	0	0	0	0	0	0	0	0	0	0	0	0	0	0	0	0	0	0	0	0	0	1	0	0	0	0	0	0	0	0	0	0	0	0	0	0
31 Cryocooler {inst}	0	0	0	0	0	0	0	0	0	0	0	0	0	0	0	0	0	0	0	0	0	0	1	1	1	1	1	0	0	0	0	0	0	0	0	0	0	0	0	0	0	0	0	0	0	0	0	0	0	0	0	0	0	0	0	0	0
32 Thermostatic heater {optics}	0	0	1	0	0	0	0	0	0	0	0	0	0	0	0	0	0	0	0	0	0	0	0	0	0	0	0	0	0	0	0	0	0	0	0	0	0	0	0	0	0	0	1	0	0	0	0	0	0	0	0	0	0	0	0	0	0
33 Heat pipe network {bus}	0	0	0	0	0	0	0	0	1	0	0	0	0	0	0	1	1	1	1	1	1	0	0	0	0	0	0	0	0	1	0	0	0	0	0	0	0	0	0	0	0	0	0	0	0	0	0	0	0	0	0	0	0	0	0	0	0
34 Thermal sensor {optics}	1	1	1	1	1	1	1	1	0	1	1	1	1	1	1	1	0	0	0	0	0	0	0	0	0	0	0	0	0	0	0	0	0	0	0	0	0	0	0	0	0	0	0	0	0	0	0	0	0	0	0	0	0	0	0	0	0
35 Momentum Wheel	0	0	0	0	0	0	0	0	0	0	0	0	0	0	0	0	0	0	0	0	0	0	0	0	0	0	0	0	0	0	0	0	0	0	0	0	0	0	0	0	0	0	0	0	0	0	0	0	0	0	0	0	0	0	0	0	0
36 Solar Sail	0	0	0	0	0	0	0	0	0	0	0	0	0	0	0	0	0	0	0	0	0	0	0	0	0	0	0	0	0	0	0	0	0	0	0	0	0	0	0	0	0	0	0	0	0	0	0	0	0	0	0	0	0	0	0	0	0
37 Star Tracker	0	0	0	0	0	0	0	0	0	0	0	0	0	0	0	0	0	0	0	0	0	0	0	0	0	0	0	0	0	0	0	0	0	1	0	0	0	0	0	0	0	0	0	0	0	0	0	0	0	0	0	0	0	0	0	0	0
38 Solar Array per 100 watts	0	0	0	0	0	0	1	0	0	0	0	0	0	0	0	0	0	0	0	0	0	0	0	0	0	0	0	0	0	0	0	0	0	1	0	0	0	0	0	0	0	0	0	0	0	0	0	0	0	0	0	0	0	0	0	0	0
39 Battery per watt-hour	0	0	0	0	0	0	0	0	0	0	0	0	0	0	0	0	0	0	0	0	0	0	0	0	0	0	0	0	0	0	0	0	0	1	0	0	0	0	0	0	0	0	0	0	0	0	0	0	0	0	0	0	0	0	0	0	0
40 Distribution per 100 watts	0	0	0	0	0	0	1	0	0	0	0	0	0	0	0	0	0	0	0	0	0	0	0	0	0	0	0	0	0	0	0	0	0	1	0	0	0	0	0	0	0	0	0	0	0	0	0	0	0	0	0	0	0	0	0	0	0
41 Connectors and Wiring	0	0	0	0	0	0	0	0	0	0	0	0	0	0	0	0	0	0	0	0	0	0	0	0	0	0	0	0	0	0	0	0	0	1	0	0	0	0	0	0	0	0	0	0	0	0	0	0	0	0	0	0	0	0	0	0	0
42 Light Shield	0	0	0	0	0	0	0	0	0	0	0	0	0	0	0	0	0	0	0	0	0	0	0	0	0	0	0	0	0	0	0	0	0	1	0	0	0	0	0	0	0	0	0	0	0	0	0	0	0	0	0	0	0	0	0	0	0
43 Deployment Device for Antenna	0	0	0	0	0	0	0	0	0	0	0	0	0	0	0	0	0	0	0	0	0	0	0	0	0	0	0	0	0	0	0	0	0	1	0	0	0	0	0	0	0	0	0	0	0	0	0	0	0	0	0	0	0	0	0	0	0
44 Secondary Mirror Segment	0	0	0	0	0	0	0	0	0	0	0	0	0	0	0	0	0	0	0	0	0	0	0	0	0	0	0	0	0	0	0	0	0	1	0	0	0	0	0	0	0	0	0	0	0	0	0	0	0	0	0	0	0	0	0	0	0
45 Primary Mirror Baffle	0	0	0	0	0	0	0	0	0	0	0	0	0	0	0	0	0	0	0	0	0	0	0	0	0	0	0	0	0	0	0	0	0	1	0	0	0	0	0	0	0	0	0	0	0	0	0	0	0	0	0	0	0	0	0	0	0
46 CPU	0	0	0	0	0	0	0	0	0	0	0	0	0	0	0	0	0	0	0	0	0	0	0	0	0	0	0	0	0	0	0	0	0	1	0	0	0	0	0	0	0	0	0	0	0	0	0	0	0	0	0	0	0	0	0	0	0
47 Data Management Unit (DMU)	0	0	0	0	0	0	0	0	0	0	0	0	0	0	0	0	0	0	0	0	0	0	0	0	0	0	0	0	0	0	0	0	0	1	0	0	0	0	0	0	0	0	0	0	0	0	0	0	0	0	0	0	0	0	0	0	0
48 Thermostatic heater {inst}	0	0	0	0	0	0	0	0	0	0	0	0	0	0	0	0	0	0	0	0	0	0	1	1	1	1	1	0	0	0	1	0	0	0	0	0	0	0	0	0	0	0	0	0	0	0	0	0	0	0	0	0	0	0	0	0	0
49 Thermostatic heater {bus}	0	0	0	0	0	0	1	0	0	0	0	0	0	0	0	1	1	0	1	0	1	0	0	0	0	0	0	0	0	1	0	0	1	0	0	0	0	1	0	1	0	0	1	0	0	0	0	0	0	0	0	0	0	0	0	0	0
50 Thermal sensor {inst}	0	0	0	0	0	0	0	0	0	0	0	0	0	0	0	0	0	0	0	0	0	0	1	1	1	1	1	0	0	0	1	0	0	0	0	0	0	0	0	0	0	0	0	0	0	0	0	1	0	0	0	0	0	0	0	0	0
51 Thermal sensor {bus}	0	0	0	0	0	0	1	0	0	0	0	0	0	0	0	1	1	1	1	1	1	0	0	0	0	0	0	0	0	1	0	0	1	0	0	0	0	1	0	1	0	0	1	0	0	0	0	0	1	1	0	0	0	0	0	0	0
52 Thermal blanket {inst}	0	0	0	0	0	0	0	0	0	0	0	0	0	0	0	0	0	0	0	0	0	0	0	0	0	0	0	0	0	0	0	0	0	0	0	0	0	0	0	0	0	0	0	0	0	0	0	0	0	0	0	0	0	0	0	0	0
53 Science Payload support structure	0	0	0	0	0	0	0	0	0	0	0	0	0	0	0	0	0	0	0	0	0	0	0	0	0	0	0	0	0	0	0	0	0	0	0	0	0	0	0	0	0	0	0	0	0	0	0	0	0	0	0	0	0	0	0	0	0
54 Monopropellant hydrazine thruster	0	0	0	0	0	0	0	0	0	0	0	0	0	0	0	0	0	0	0	0	0	0	0	0	0	0	0	0	0	0	0	0	0	0	0	0	0	0	0	0	0	0	0	0	0	0	0	0	0	0	0	0	0	0	0	0	0
55 Arcjet thruster	0	0	0	0	0	0	0	0	0	0	0	0	0	0	0	0	0	0	0	0	0	0	0	0	0	0	0	0	0	0	0	0	0	0	0	0	0	0	0	0	0	0	0	0	0	0	0	0	0	0	0	0	0	0	0	0	0
56 Hall thruster	0	0	0	0	0	0	0	0	0	0	0	0	0	0	0	0	0	0	0	0	0	0	0	0	0	0	0	0	0	0	0	0	0	0	0	0	0	0	0	0	0	0	0	0	0	0	0	0	0	0	0	0	0	0	0	0	0
57 Propellant (and tank)	0	0	0	0	0	0	0	0	0	0	0	0	0	0	0	0	0	0	0	0	0	0	0	0	0	0	0	0	0	0	0	0	0	0	0	0	0	0	0	0	0	0	0	0	0	0	0	0	0	0	0	0	0	0	0	0	0

APPENDIX F: DATA DSM

DSM	1	2	3	4	5	6	7	8	9	10	11	12	13	14	15	16	17	18	19	20	21	22	23	24	25	26	27	28	29	30	31	32	33	34	35	36	37	38	39	40	41	42	43	44	45	46	47	48	49	50	51	52	53	54	55	56	57
1 Robotic Arm	0	0	0	0	0	0	0	0	0	0	0	0	0	0	0	0	0	0	0	0	0	0	0	0	0	0	0	0	0	0	0	0	0	0	0	0	0	0	0	0	0	0	0	0	0	0	0	0	0	0	0	0	0	0	0	0	0
2 EM Coil	0	0	0	0	0	0	0	0	0	0	0	0	0	0	0	0	0	0	0	0	0	0	0	0	0	0	0	0	0	0	0	0	0	0	0	0	0	0	0	0	0	0	0	0	0	0	0	0	0	0	0	0	0	0	0	0	0
3 UDP	1	0	0	0	0	0	0	0	0	0	0	0	0	0	0	0	0	0	0	0	0	0	0	0	0	0	0	0	0	0	0	0	0	0	0	0	0	0	0	0	0	0	0	0	0	0	0	0	0	0	0	0	0	0	0	0	0
4 Primary Mirror Segment	0	0	0	0	0	0	0	0	0	0	0	0	0	0	0	0	0	0	0	0	0	0	0	0	0	0	0	0	0	0	0	0	0	0	0	0	0	0	0	0	0	0	0	0	0	0	0	0	0	0	0	0	0	0	0	0	0
5 Surface Normal Actuator	0	0	0	0	0	0	0	0	0	0	0	0	0	0	0	0	0	0	0	0	0	0	0	0	0	0	0	0	0	0	0	0	0	0	0	0	0	0	0	0	0	0	0	0	0	0	0	0	0	0	0	0	0	0	0	0	0
6 Surface Parallel Actuator	0	0	0	0	0	0	0	0	0	0	0	0	0	0	0	0	0	0	0	0	0	0	0	0	0	0	0	0	0	0	0	0	0	0	0	0	0	0	0	0	0	0	0	0	0	0	0	0	0	0	0	0	0	0	0	0	0
7 Backframe per segment	0	0	0	0	0	0	0	0	0	0	0	0	0	0	0	0	0	0	0	0	0	0	0	0	0	0	0	0	0	0	0	0	0	0	0	0	0	0	0	0	0	0	0	0	0	0	0	0	0	0	0	0	0	0	0	0	0
8 Bus structure	0	0	0	0	0	0	0	0	0	0	0	0	0	0	0	0	0	0	0	0	0	0	0	0	0	0	0	0	0	0	0	0	0	0	0	0	0	0	0	0	0	0	0	0	0	0	0	0	0	0	0	0	0	0	0	0	0
9 Magnetic Isolation Device	0	0	0	0	0	0	0	0	0	0	0	0	0	0	0	0	0	0	0	0	0	0	0	0	0	0	0	0	0	0	0	0	0	0	0	0	0	0	0	0	0	0	0	0	0	0	0	0	0	0	0	0	0	0	0	0	0
10 Viscoelastic Isolation Device	0	0	0	0	0	0	0	0	0	0	0	0	0	0	0	0	0	0	0	0	0	0	0	0	0	0	0	0	0	0	0	0	0	0	0	0	0	0	0	0	0	0	0	0	0	0	0	0	0	0	0	0	0	0	0	0	0
11 Active Damper	0	0	0	0	0	0	0	0	0	0	0	0	0	0	0	0	0	0	0	0	0	0	0	0	0	0	0	0	0	0	0	0	0	0	0	0	0	0	0	0	0	0	0	0	0	0	0	0	0	0	0	0	0	0	0	0	0
12 Deployment Device for Solar Array	0	0	0	0	0	0	0	0	0	0	0	0	0	0	0	0	0	0	0	0	0	0	0	0	0	0	0	0	0	0	0	0	0	0	0	0	0	0	0	0	0	0	0	0	0	0	0	0	0	0	0	0	0	0	0	0	0
13 Gimbal Device	0	0	0	0	0	0	0	0	0	0	0	0	0	0	0	0	0	0	0	0	0	0	0	0	0	0	0	0	0	0	0	0	0	0	0	0	0	0	0	0	0	0	0	0	0	0	0	0	0	0	0	0	0	0	0	0	0
14 UDP Comm interface	1	0	0	0	0	0	0	0	0	0	0	0	0	0	0	0	0	0	0	0	0	0	0	0	0	0	0	0	0	0	0	0	0	0	0	0	0	0	0	0	0	0	0	0	0	0	0	0	0	0	0	0	0	0	0	0	0
15 UDP Power interface	1	0	0	0	0	0	0	0	0	0	0	0	0	0	0	0	0	0	0	0	0	0	0	0	0	0	0	0	0	0	0	0	0	0	0	0	0	0	0	0	0	0	0	0	0	0	0	0	0	0	0	0	0	0	0	0	0
16 Laser Communications Box	0	0	0	0	0	0	0	0	0	0	0	0	0	0	0	0	0	0	0	0	0	0	0	0	0	0	0	0	0	0	0	0	0	0	0	0	0	0	0	0	0	0	0	0	0	0	0	0	0	0	0	0	0	0	0	0	0
17 RF Communications Box	0	0	0	0	0	0	0	0	0	0	0	0	0	0	0	0	0	0	0	0	0	0	0	0	0	0	0	0	0	0	0	0	0	0	0	0	0	0	0	0	0	0	0	0	0	0	0	0	0	0	0	0	0	0	0	0	0
18 Direct Downlink Antennas	0	0	0	0	0	0	0	0	0	0	0	0	0	0	0	0	0	0	0	0	0	0	0	0	0	0	0	0	0	0	0	0	0	0	0	0	0	0	0	0	0	0	0	0	0	0	0	0	0	0	0	0	0	0	0	0	0
19 Crosslink Antennas	0	0	0	0	0	0	0	0	0	0	0	0	0	0	0	0	0	0	0	0	0	0	0	0	0	0	0	0	0	0	0	0	0	0	0	0	0	0	0	0	0	0	0	0	0	0	0	0	0	0	0	0	0	0	0	0	0
20 RAM	0	0	0	0	0	0	0	0	0	0	0	0	0	0	0	0	0	0	0	0	0	0	0	0	0	0	0	0	0	0	0	0	0	0	0	0	0	0	0	0	0	0	0	0	0	0	0	0	0	0	0	0	0	0	0	0	0
21 Power Convertor Unit (PCU)	0	0	0	0	0	0	0	0	0	0	0	0	0	0	0	0	0	0	0	0	0	0	0	0	0	0	0	0	0	0	0	0	0	0	0	0	0	0	0	0	0	0	0	0	0	0	0	0	0	0	0	0	0	0	0	0	0
22 Data Interface Unit (DIU)	0	0	0	0	0	0	0	0	0	0	0	0	0	0	0	0	0	0	0	0	0	0	0	0	0	0	0	0	0	0	0	0	0	0	0	0	0	0	0	0	0	0	0	0	0	0	0	0	0	0	0	0	0	0	0	0	0
23 Instrument A	0	0	0	0	0	0	0	0	0	0	0	0	0	0	0	0	0	0	0	0	0	0	0	0	0	0	0	0	0	0	0	0	0	0	0	0	0	0	0	0	0	0	0	0	0	0	0	0	0	0	0	0	0	0	0	0	0
24 Instrument B	0	0	0	0	0	0	0	0	0	0	0	0	0	0	0	0	0	0	0	0	0	0	0	0	0	0	0	0	0	0	0	0	0	0	0	0	0	0	0	0	0	0	0	0	0	0	0	0	0	0	0	0	0	0	0	0	0
25 Fine Guidance Sensors	0	0	0	0	0	0	0	0	0	0	0	0	0	0	0	0	0	0	0	0	0	0	0	0	0	0	0	0	0	0	0	0	0	0	0	0	0	0	0	0	0	0	0	0	0	0	0	0	0	0	0	0	0	0	0	0	0
26 Instrument C	0	0	0	0	0	0	0	0	0	0	0	0	0	0	0	0	0	0	0	0	0	0	0	0	0	0	0	0	0	0	0	0	0	0	0	0	0	0	0	0	0	0	0	0	0	0	0	0	0	0	0	0	0	0	0	0	0
27 Instrument D	0	0	0	0	0	0	0	0	0	0	0	0	0	0	0	0	0	0	0	0	0	0	0	0	0	0	0	0	0	0	0	0	0	0	0	0	0	0	0	0	0	0	0	0	0	0	0	0	0	0	0	0	0	0	0	0	0
28 Thermal blanket {bus}	0	0	0	0	0	0	0	0	0	0	0	0	0	0	0	0	0	0	0	0	0	0	0	0	0	0	0	0	0	0	0	0	0	0	0	0	0	0	0	0	0	0	0	0	0	0	0	0	0	0	0	0	0	0	0	0	0
29 External radiator {bus}	0	0	0	0	0	0	0	0	0	0	0	0	0	0	0	0	0	0	0	0	0	0	0	0	0	0	0	0	0	0	0	0	0	0	0	0	0	0	0	0	0	0	0	0	0	0	0	0	0	0	0	0	0	0	0	0	0
30 Thermoelectric cooler (TEC) {optics}	0	0	0	0	0	0	0	0	0	0	0	0	0	0	0	0	0	0	0	0	0	0	0	0	0	0	0	0	0	0	0	0	0	0	0	0	0	0	0	0	0	0	0	0	0	0	0	0	0	0	0	0	0	0	0	0	0
31 Cryocooler {inst}	0	0	0	0	0	0	0	0	0	0	0	0	0	0	0	0	0	0	0	0	0	0	1	1	1	1	1	0	0	0	0	0	0	0	0	0	0	0	0	0	0	0	0	0	0	0	0	0	0	0	0	0	0	0	0	0	0
32 Thermostatic heater {optics}	0	0	0	0	0	0	0	0	0	0	0	0	0	0	0	0	0	0	0	0	0	0	0	0	0	0	0	0	0	0	0	0	0	0	0	0	0	0	0	0	0	0	0	0	0	0	0	0	0	0	0	0	0	0	0	0	0
33 Heat pipe network {bus}	0	0	0	0	0	0	0	0	0	0	0	0	0	0	0	0	0	0	0	0	0	0	0	0	0	0	0	0	0	0	0	0	0	0	0	0	0	0	0	0	0	0	0	0	0	0	0	0	0	0	0	0	0	0	0	0	0
34 Thermal sensor {optics}	0	0	0	0	0	0	0	0	0	0	0	0	0	0	0	0	0	0	0	0	0	0	0	0	0	0	0	0	0	0	0	0	0	0	0	0	0	0	0	0	0	0	0	0	0	0	0	0	0	0	0	0	0	0	0	0	0
35 Momentum Wheel	0	0	0	0	0	0	0	0	0	0	0	0	0	0	0	0	0	0	0	0	0	0	0	0	0	0	0	0	0	0	0	0	0	0	0	0	0	0	0	0	0	0	0	0	0	0	0	0	0	0	0	0	0	0	0	0	0
36 Solar Sail	0	0	0	0	0	0	0	0	0	0	0	0	0	0	0	0	0	0	0	0	0	0	0	0	0	0	0	0	0	0	0	0	0	0	0	0	0	0	0	0	0	0	0	0	0	0	0	0	0	0	0	0	0	0	0	0	0
37 Star Tracker	0	0	0	0	0	0	0	0	0	0	0	0	0	0	0	0	0	0	0	0	0	0	0	0	0	0	0	0	0	0	0	0	0	0	0	0	0	0	0	0	0	0	0	0	0	0	0	0	0	0	0	0	0	0	0	0	0
38 Solar Array per 100 watts	0	0	0	0	0	0	0	0	0	0	0	0	0	0	0	0	0	0	0	0	0	0	0	0	0	0	0	0	0	0	0	0	0	0	0	0	0	0	0	0	0	0	0	0	0	0	0	0	0	0	0	0	0	0	0	0	0
39 Battery per watt-hour	0	0	0	0	0	0	0	0	0	0	0	0	0	0	0	0	0	0	0	0	0	0	0	0	0	0	0	0	0	0	0	0	0	0	0	0	0	0	0	0	0	0	0	0	0	0	0	0	0	0	0	0	0	0	0	0	0
40 Distribution per 100 watts	0	0	0	0	0	0	0	0	0	0	0	0	0	0	0	0	0	0	0	0	0	0	0	0	0	0	0	0	0	0	0	0	0	0	0	0	0	0	0	0	0	0	0	0	0	0	0	0	0	0	0	0	0	0	0	0	0
41 Connectors and Wiring	1	1	0	0	1	0	1	0	0	1	0	1	1	1	0	0	1	0	1	1	0	1	0	0	0	0	1	0	0	0	0	0	0	0	0	0	0	0	0	0	0	0	1	0	0	0	0	0	0	0	0	0	0	0	0	0	0
42 Light Shield	0	0	0	0	0	0	0	0	0	0	0	0	0	0	0	0	0	0	0	0	0	0	0	0	0	0	0	0	0	0	0	0	0	0	0	0	0	0	0	0	0	0	0	0	0	0	0	0	0	0	0	0	0	0	0	0	0
43 Deployment Device for Antenna	0	0	0	0	0	0	0	0	0	0	0	0	0	0	0	0	0	0	0	0	0	0	0	0	0	0	0	0	0	0	0	0	0	0	0	0	0	0	0	0	0	0	0	0	0	0	0	0	0	0	0	0	0	0	0	0	0
44 Secondary Mirror Segment	0	0	0	0	0	0	0	0	0	0	0	0	0	0	0	0	0	0	0	0	0	0	0	0	0	0	0	0	0	0	0	0	0	0	0	0	0	0	0	0	0	0	0	0	0	0	0	0	0	0	0	0	0	0	0	0	0
45 Primary Mirror Baffle	0	0	0	0	0	0	0	0	0	0	0	0	0	0	0	0	0	0	0	0	0	0	0	0	0	0	0	0	0	0	0	0	0	0	0	0	0	0	0	0	0	0	0	0	0	0	0	0	0	0	0	0	0	0	0	0	0
46 CPU	1	1	0	0	1	1	1	0	0	0	1	1	1	1	0	1	1	0	1	1	0	1	1	1	1	1	1	0	0	0	1	0	0	0	0	0	1	0	0	0	0	0	0	0	0	0	0	0	0	0	0	0	0	0	0	0	0
47 Data Management Unit (DMU)	1	1	0	0	1	1	1	0	0	0	1	1	1	1	0	1	1	0	1	1	0	1	1	1	1	1	1	0	0	0	1	0	0	0	0	0	1	0	0	0	0	0	0	0	0	0	0	0	0	0	0	0	0	0	0	0	0
48 Thermostatic heater {inst}	0	0	0	0	0	0	0	0	0	0	0	0	0	0	0	0	0	0	0	0	0	0	0	0	0	0	0	0	0	0	0	0	0	0	0	0	0	0	0	0	0	0	0	0	0	1	1	0	0	0	0	0	0	0	0	0	0
49 Thermostatic heater {bus}	0	0	0	0	0	0	0	0	0	0	0	0	0	0	0	0	0	0	0	0	0	0	0	0	0	0	0	0	0	0	0	0	0	0	0	0	0	0	0	0	0	0	0	0	0	1	1	0	0	0	0	0	0	0	0	0	0
50 Thermal sensor {inst}	0	0	0	0	0	0	0	0	0	0	0	0	0	0	0	0	0	0	0	0	0	0	0	0	0	0	0	0	0	0	0	0	0	0	0	0	0	0	0	0	0	0	0	0	0	1	1	0	0	0	0	0	0	0	0	0	0
51 Thermal sensor {bus}	0	0	0	0	0	0	0	0	0	0	0	0	0	0	0	0	0	0	0	0	0	0	0	0	0	0	0	0	0	0	0	0	0	0	0	0	0	0	0	0	0	0	0	0	0	1	1	0	0	0	0	0	0	0	0	0	0
52 Thermal blanket {inst}	0	0	0	0	0	0	0	0	0	0	0	0	0	0	0	0	0	0	0	0	0	0	0	0	0	0	0	0	0	0	0	0	0	0	0	0	0	0	0	0	0	0	0	0	0	0	0	0	0	0	0	0	0	0	0	0	0
53 Science Payload support structure	0	0	0	0	0	0	0	0	0	0	0	0	0	0	0	0	0	0	0	0	0	0	0	0	0	0	0	0	0	0	0	0	0	0	0	0	0	0	0	0	0	0	0	0	0	0	0	0	0	0	0	0	0	0	0	0	0
54 Monopropellant hydrazine thruster	0	0	0	0	0	0	0	0	0	0	0	0	0	0	0	0	0	0	0	0	0	0	0	0	0	0	0	0	0	0	0	0	0	0	0	0	0	0	0	0	0	0	0	0	0	0	1	1	0	0	0	0	0	0	0	0	0
55 Arcjet thruster	0	0	0	0	0	0	0	0	0	0	0	0	0	0	0	0	0	0	0	0	0	0	0	0	0	0	0	0	0	0	0	0	0	0	0	0	0	0	0	0	0	0	0	0	0	0	1	1	0	0	0	0	0	0	0	0	0
56 Hall thruster	0	0	0	0	0	0	0	0	0	0	0	0	0	0	0	0	0	0	0	0	0	0	0	0	0	0	0	0	0	0	0	0	0	0	0	0	0	0	0	0	0	0	0	0	0	0	1	1	0	0	0	0	0	0	0	0	0
57 Propellant (and tank)	0	0	0	0	0	0	0	0	0	0	0	0	0	0	0	0	0	0	0	0	0	0	0	0	0	0	0	0	0	0	0	0	0	0	0	0	0	0	0	0	0	0	0	0	0	0	0	0	0	0	0	0	0	0	0	0	0

APPENDIX G: POWER DSM

DSM	1	2	3	4	5	6	7	8	9	10	11	12	13	14	15	16	17	18	19	20	21	22	23	24	25	26	27	28	29	30	31	32	33	34	35	36	37	38	39	40	41	42	43	44	45	46	47	48	49	50	51	52	53	54	55	56	57
1 Robotic Arm	■	0	0	0	0	0	0	0	0	0	0	0	0	0	0	0	0	0	0	0	0	0	0	0	0	0	0	0	0	0	0	0	0	0	0	0	0	0	0	0	0	0	0	0	0	0	0	0	0	0	0	0	0	0	0	0	0
2 EM Coil	0	■	0	0	0	0	0	0	0	0	0	0	0	0	0	0	0	0	0	0	0	0	0	0	0	0	0	0	0	0	0	0	0	0	0	0	0	0	0	0	0	0	0	0	0	0	0	0	0	0	0	0	0	0	0	0	0
3 UDP	0	0	■	0	0	0	0	0	0	0	0	0	0	0	0	0	0	0	0	0	0	0	0	0	0	0	0	0	0	0	0	0	0	0	0	0	0	0	0	0	0	0	0	0	0	0	0	0	0	0	0	0	0	0	0	0	0
4 Primary Mirror Segment	0	0	0	■	0	0	0	0	0	0	0	0	0	0	0	0	0	0	0	0	0	0	0	0	0	0	0	0	0	0	0	0	0	0	0	0	0	0	0	0	0	0	0	0	0	0	0	0	0	0	0	0	0	0	0	0	0
5 Surface Normal Actuator	0	0	0	0	■	0	0	0	0	0	0	0	0	0	0	0	0	0	0	0	0	0	0	0	0	0	0	0	0	0	0	0	0	0	0	0	0	0	0	0	0	0	0	0	0	0	0	0	0	0	0	0	0	0	0	0	0
6 Surface Parallel Actuator	0	0	0	0	0	■	0	0	0	0	0	0	0	0	0	0	0	0	0	0	0	0	0	0	0	0	0	0	0	0	0	0	0	0	0	0	0	0	0	0	0	0	0	0	0	0	0	0	0	0	0	0	0	0	0	0	0
7 Backframe per segment	0	0	0	0	0	0	■	0	0	0	0	0	0	0	0	0	0	0	0	0	0	0	0	0	0	0	0	0	0	0	0	0	0	0	0	0	0	0	0	0	0	0	0	0	0	0	0	0	0	0	0	0	0	0	0	0	0
8 Bus structure	0	0	0	0	0	0	0	■	0	0	0	0	0	0	0	0	0	0	0	0	0	0	0	0	0	0	0	0	0	0	0	0	0	0	0	0	0	0	0	0	0	0	0	0	0	0	0	0	0	0	0	0	0	0	0	0	0
9 Magnetic Isolation Device	0	0	0	0	0	0	0	0	■	0	0	0	0	0	0	0	0	0	0	0	0	0	0	0	0	0	0	0	0	0	0	0	0	0	0	0	0	0	0	0	0	0	0	0	0	0	0	0	0	0	0	0	0	0	0	0	0
10 Viscoelastic Isolation Device	0	0	0	0	0	0	0	0	0	■	0	0	0	0	0	0	0	0	0	0	0	0	0	0	0	0	0	0	0	0	0	0	0	0	0	0	0	0	0	0	0	0	0	0	0	0	0	0	0	0	0	0	0	0	0	0	0
11 Active Damper	0	0	0	0	0	0	0	0	0	0	■	0	0	0	0	0	0	0	0	0	0	0	0	0	0	0	0	0	0	0	0	0	0	0	0	0	0	0	0	0	0	0	0	0	0	0	0	0	0	0	0	0	0	0	0	0	0
12 Deployment Device for Solar Array	0	0	0	0	0	0	0	0	0	0	0	■	0	0	0	0	0	0	0	0	0	0	0	0	0	0	0	0	0	0	0	0	0	0	0	0	0	0	0	0	0	0	0	0	0	0	0	0	0	0	0	0	0	0	0	0	0
13 Gimbal Device	0	0	0	0	0	0	0	0	0	0	0	0	■	0	0	0	0	0	0	0	0	0	0	0	0	0	0	0	0	0	0	0	0	0	0	0	0	0	0	0	0	0	0	0	0	0	0	0	0	0	0	0	0	0	0	0	0
14 UDP Comm interface	0	0	0	0	0	0	0	0	0	0	0	0	0	■	0	0	0	0	0	0	0	0	0	0	0	0	0	0	0	0	0	0	0	0	0	0	0	0	0	0	0	0	0	0	0	0	0	0	0	0	0	0	0	0	0	0	0
15 UDP Power interface	0	0	0	0	0	0	0	0	0	0	0	0	0	0	■	0	0	0	0	0	0	0	0	0	0	0	0	0	0	0	0	0	0	0	0	0	0	0	0	0	0	0	0	0	0	0	0	0	0	0	0	0	0	0	0	0	0
16 Laser Communications Box	0	0	0	0	0	0	0	0	0	0	0	0	0	0	0	■	0	0	0	0	0	0	0	0	0	0	0	0	0	0	0	0	0	0	0	0	0	0	0	0	0	0	0	0	0	0	0	0	0	0	0	0	0	0	0	0	0
17 RF Communications Box	0	0	0	0	0	0	0	0	0	0	0	0	0	0	0	0	■	0	0	0	0	0	0	0	0	0	0	0	0	0	0	0	0	0	0	0	0	0	0	0	0	0	0	0	0	0	0	0	0	0	0	0	0	0	0	0	0
18 Direct Downlink Antennas	0	0	0	0	0	0	0	0	0	0	0	0	0	0	0	0	0	■	0	0	0	0	0	0	0	0	0	0	0	0	0	0	0	0	0	0	0	0	0	0	0	0	0	0	0	0	0	0	0	0	0	0	0	0	0	0	0
19 Crosslink Antennas	0	0	0	0	0	0	0	0	0	0	0	0	0	0	0	0	0	0	■	0	0	0	0	0	0	0	0	0	0	0	0	0	0	0	0	0	0	0	0	0	0	0	0	0	0	0	0	0	0	0	0	0	0	0	0	0	0
20 RAM	0	0	0	0	0	0	0	0	0	0	0	0	0	0	0	0	0	0	0	■	0	0	0	0	0	0	0	0	0	0	0	0	0	0	0	0	0	0	0	0	0	0	0	0	0	0	0	0	0	0	0	0	0	0	0	0	0
21 Power Convertor Unit (PCU)	0	0	0	0	0	0	0	0	0	0	0	0	0	0	0	0	0	0	0	0	■	0	0	0	0	0	0	0	0	0	0	0	0	0	0	0	0	0	0	0	0	0	0	0	0	0	0	0	0	0	0	0	0	0	0	0	0
22 Data Interface Unit (DIU)	0	0	0	0	0	0	0	0	0	0	0	0	0	0	0	0	0	0	0	0	0	■	0	0	0	0	0	0	0	0	0	0	0	0	0	0	0	0	0	0	0	0	0	0	0	0	0	0	0	0	0	0	0	0	0	0	0
23 Instrument A	0	0	0	0	0	0	0	0	0	0	0	0	0	0	0	0	0	0	0	0	0	0	■	0	0	0	0	0	0	0	0	0	0	0	0	0	0	0	0	0	0	0	0	0	0	0	0	0	0	0	0	0	0	0	0	0	0
24 Instrument B	0	0	0	0	0	0	0	0	0	0	0	0	0	0	0	0	0	0	0	0	0	0	0	■	0	0	0	0	0	0	0	0	0	0	0	0	0	0	0	0	0	0	0	0	0	0	0	0	0	0	0	0	0	0	0	0	0
25 Fine Guidance Sensors	0	0	0	0	0	0	0	0	0	0	0	0	0	0	0	0	0	0	0	0	0	0	0	0	■	0	0	0	0	0	0	0	0	0	0	0	0	0	0	0	0	0	0	0	0	0	0	0	0	0	0	0	0	0	0	0	0
26 Instrument C	0	0	0	0	0	0	0	0	0	0	0	0	0	0	0	0	0	0	0	0	0	0	0	0	0	■	0	0	0	0	0	0	0	0	0	0	0	0	0	0	0	0	0	0	0	0	0	0	0	0	0	0	0	0	0	0	0
27 Instrument D	0	0	0	0	0	0	0	0	0	0	0	0	0	0	0	0	0	0	0	0	0	0	0	0	0	0	■	0	0	0	0	0	0	0	0	0	0	0	0	0	0	0	0	0	0	0	0	0	0	0	0	0	0	0	0	0	0
28 Thermal blanket {bus}	0	0	0	0	0	0	0	0	0	0	0	0	0	0	0	0	0	0	0	0	0	0	0	0	0	0	0	■	0	0	0	0	0	0	0	0	0	0	0	0	0	0	0	0	0	0	0	0	0	0	0	0	0	0	0	0	0
29 External radiator {bus}	0	0	0	0	0	0	0	0	0	0	0	0	0	0	0	0	0	0	0	0	0	0	0	0	0	0	0	0	■	0	0	0	0	0	0	0	0	0	0	0	0	0	0	0	0	0	0	0	0	0	0	0	0	0	0	0	0
30 Thermoelectric cooler (TEC) {optics}	0	0	0	0	0	0	0	0	0	0	0	0	0	0	0	0	0	0	0	0	0	0	0	0	0	0	0	0	0	■	0	0	0	0	0	0	0	0	0	0	0	0	0	0	0	0	0	0	0	0	0	0	0	0	0	0	0
31 Cryocooler {inst}	0	0	0	0	0	0	0	0	0	0	0	0	0	0	0	0	0	0	0	0	0	0	0	0	0	0	0	0	0	0	■	0	0	0	0	0	0	0	0	0	0	0	0	0	0	0	0	0	0	0	0	0	0	0	0	0	0
32 Thermostatic heater {optics}	0	0	0	0	0	0	0	0	0	0	0	0	0	0	0	0	0	0	0	0	0	0	0	0	0	0	0	0	0	0	0	■	0	0	0	0	0	0	0	0	0	0	0	0	0	0	0	0	0	0	0	0	0	0	0	0	0
33 Heat pipe network {bus}	0	0	0	0	0	0	0	0	0	0	0	0	0	0	0	0	0	0	0	0	0	0	0	0	0	0	0	0	0	0	0	0	■	0	0	0	0	0	0	0	0	0	0	0	0	0	0	0	0	0	0	0	0	0	0	0	0
34 Thermal sensor {optics}	0	0	0	0	0	0	0	0	0	0	0	0	0	0	0	0	0	0	0	0	0	0	0	0	0	0	0	0	0	0	0	0	0	■	0	0	0	0	0	0	0	0	0	0	0	0	0	0	0	0	0	0	0	0	0	0	0
35 Momentum Wheel	0	0	0	0	0	0	0	0	0	0	0	0	0	0	0	0	0	0	0	0	0	0	0	0	0	0	0	0	0	0	0	0	0	0	■	0	0	0	0	0	0	0	0	0	0	0	0	0	0	0	0	0	0	0	0	0	0
36 Solar Sail	0	0	0	0	0	0	0	0	0	0	0	0	0	0	0	0	0	0	0	0	0	0	0	0	0	0	0	0	0	0	0	0	0	0	0	■	0	0	0	0	0	0	0	0	0	0	0	0	0	0	0	0	0	0	0	0	0
37 Star Tracker	0	0	0	0	0	0	0	0	0	0	0	0	0	0	0	0	0	0	0	0	0	0	0	0	0	0	0	0	0	0	0	0	0	0	0	0	■	0	0	0	0	0	0	0	0	0	0	0	0	0	0	0	0	0	0	0	0
38 Solar Array per 100 watts	0	0	0	0	0	0	0	0	0	0	0	0	0	0	0	0	0	0	0	0	0	0	0	0	0	0	0	0	0	0	0	0	0	0	0	0	0	■	0	0	0	0	0	0	0	0	0	0	0	0	0	0	0	0	0	0	0
39 Battery per watt-hour	0	0	0	0	0	0	0	0	0	0	0	0	0	0	0	0	0	0	0	0	0	0	0	0	0	0	0	0	0	0	0	0	0	0	0	0	0	0	■	0	0	0	0	0	0	0	0	0	0	0	0	0	0	0	0	0	0
40 Distribution per 100 watts	0	0	0	0	0	0	0	0	0	0	0	0	0	0	0	0	0	0	0	0	0	0	0	1	1	1	0	1	0	0	0	0	0	0	0	0	0	0	1	■	0	0	0	0	0	0	0	0	0	0	0	0	0	0	0	0	0
41 Connectors and Wiring	1	1	0	0	1	1	0	0	1	0	1	1	1	0	0	1	1	0	0	0	1	0	1	1	0	1	0	1	0	0	0	0	0	0	0	0	0	0	0	1	■	0	0	0	0	0	0	0	0	0	0	0	0	0	0	0	0
42 Light Shield	0	0	0	0	0	0	0	0	0	0	0	0	0	0	0	0	0	0	0	0	0	0	0	0	0	0	0	0	0	0	0	0	0	0	0	0	0	0	0	0	0	■	0	0	0	0	0	0	0	0	0	0	0	0	0	0	0
43 Deployment Device for Antenna	0	0	0	0	0	0	0	0	0	0	0	0	0	0	0	0	0	0	0	0	0	0	0	0	0	0	0	0	0	0	0	0	0	0	0	0	0	0	0	0	0	0	■	0	0	0	0	0	0	0	0	0	0	0	0	0	0
44 Secondary Mirror Segment	0	0	0	0	0	0	0	0	0	0	0	0	0	0	0	0	0	0	0	0	0	0	0	0	0	0	0	0	0	0	0	0	0	0	0	0	0	0	0	0	0	0	0	■	0	0	0	0	0	0	0	0	0	0	0	0	0
45 Primary Mirror Baffle	0	0	0	0	0	0	0	0	0	0	0	0	0	0	0	0	0	0	0	0	0	0	0	0	0	0	0	0	0	0	0	0	0	0	0	0	0	0	0	0	0	0	0	0	■	0	0	0	0	0	0	0	0	0	0	0	0
46 CPU	0	0	0	0	0	0	0	0	0	0	0	0	0	0	0	0	0	0	0	0	0	0	0	0	0	0	0	0	0	0	0	0	0	0	0	0	0	0	0	0	0	0	0	0	0	■	0	0	0	0	0	0	0	0	0	0	0
47 Data Management Unit (DMU)	0	0	0	0	0	0	0	0	0	0	0	0	0	0	0	0	0	0	0	0	0	0	0	0	0	0	0	0	0	0	0	0	0	0	0	0	0	0	0	0	0	0	0	0	0	0	■	0	0	0	0	0	0	0	0	0	0
48 Thermostatic heater {inst}	0	0	0	0	0	0	0	0	0	0	0	0	0	0	0	0	0	0	0	0	0	0	0	0	0	0	0	0	0	0	0	0	0	0	0	0	0	0	0	1	0	0	0	0	0	0	0	■	0	0	0	0	0	0	0	0	0
49 Thermostatic heater {bus}	0	0	0	0	0	0	0	0	0	0	0	0	0	0	0	0	0	0	0	0	0	0	0	0	0	0	0	0	0	0	0	0	0	0	0	0	0	0	0	1	0	0	0	0	0	0	0	0	■	0	0	0	0	0	0	0	0
50 Thermal sensor {inst}	0	0	0	0	0	0	0	0	0	0	0	0	0	0	0	0	0	0	0	0	0	0	0	0	0	0	0	0	0	0	0	0	0	0	0	0	0	0	0	1	0	0	0	0	0	0	0	0	0	■	0	0	0	0	0	0	0
51 Thermal sensor {bus}	0	0	0	0	0	0	0	0	0	0	0	0	0	0	0	0	0	0	0	0	0	0	0	0	0	0	0	0	0	0	0	0	0	0	0	0	0	0	0	1	0	0	0	0	0	0	0	0	0	0	■	0	0	0	0	0	0
52 Thermal blanket {inst}	0	0	0	0	0	0	0	0	0	0	0	0	0	0	0	0	0	0	0	0	0	0	0	0	0	0	0	0	0	0	0	0	0	0	0	0	0	0	0	0	0	0	0	0	0	0	0	0	0	0	0	■	0	0	0	0	0
53 Science Payload support structure	0	0	0	0	0	0	0	0	0	0	0	0	0	0	0	0	0	0	0	0	0	0	0	0	0	0	0	0	0	0	0	0	0	0	0	0	0	0	0	0	0	0	0	0	0	0	0	0	0	0	0	0	■	0	0	0	0
54 Monopropellant hydrazine thruster	0	0	0	0	0	0	0	0	0	0	0	0	0	0	0	0	0	0	0	0	0	0	0	0	0	0	0	0	0	0	0	0	0	0	0	0	0	0	0	0	0	0	0	0	0	0	0	0	0	0	0	0	0	■	0	0	0
55 Arcjet thruster	0	0	0	0	0	0	0	0	0	0	0	0	0	0	0	0	0	0	0	0	0	0	0	0	0	0	0	0	0	0	0	0	0	0	0	0	0	0	0	0	0	0	0	0	0	0	0	0	0	0	0	0	0	0	■	0	0
56 Hall thruster	0	0	0	0	0	0	0	0	0	0	0	0	0	0	0	0	0	0	0	0	0	0	0	0	0	0	0	0	0	0	0	0	0	0	0	0	0	0	0	0	0	0	0	0	0	0	0	0	0	0	0	0	0	0	0	■	0
57 Propellant (and tank)	0	0	0	0	0	0	0	0	0	0	0	0	0	0	0	0	0	0	0	0	0	0	0	0	0	0	0	0	0	0	0	0	0	0	0	0	0	0	0	0	0	0	0	0	0	0	0	0	0	0	0	0	0	0	0	0	■

APPENDIX H: OPTICAL DSM

DSM	1	2	3	4	5	6	7	8	9	10	11	12	13	14	15	16	17	18	19	20	21	22	23	24	25	26	27	28	29	30	31	32	33	34	35	36	37	38	39	40	41	42	43	44	45	46	47	48	49	50	51	52	53	54	55	56	57
1 Robotic Arm	0	0	0	0	0	0	0	0	0	0	0	0	0	0	0	0	0	0	0	0	0	0	0	0	0	0	0	0	0	0	0	0	0	0	0	0	0	0	0	0	0	0	0	0	0	0	0	0	0	0	0	0	0	0	0	0	0
2 EM Coil	0	0	0	0	0	0	0	0	0	0	0	0	0	0	0	0	0	0	0	0	0	0	0	0	0	0	0	0	0	0	0	0	0	0	0	0	0	0	0	0	0	0	0	0	0	0	0	0	0	0	0	0	0	0	0	0	0
3 UDP	0	0	0	0	0	0	0	0	0	0	0	0	0	0	0	0	0	0	0	0	0	0	0	0	0	0	0	0	0	0	0	0	0	0	0	0	0	0	0	0	0	0	0	0	0	0	0	0	0	0	0	0	0	0	0	0	0
4 Primary Mirror Segment	0	0	0	0	0	0	0	0	0	0	0	0	0	0	0	0	0	0	0	0	0	0	0	0	0	0	0	0	0	0	0	0	0	0	0	0	0	0	0	0	0	0	0	0	0	0	0	0	0	0	0	0	0	0	0	0	0
5 Surface Normal Actuator	0	0	0	0	0	0	0	0	0	0	0	0	0	0	0	0	0	0	0	0	0	0	0	0	0	0	0	0	0	0	0	0	0	0	0	0	0	0	0	0	0	0	0	0	0	0	0	0	0	0	0	0	0	0	0	0	0
6 Surface Parallel Actuator	0	0	0	0	0	0	0	0	0	0	0	0	0	0	0	0	0	0	0	0	0	0	0	0	0	0	0	0	0	0	0	0	0	0	0	0	0	0	0	0	0	0	0	0	0	0	0	0	0	0	0	0	0	0	0	0	0
7 Backframe per segment	0	0	0	0	0	0	0	0	0	0	0	0	0	0	0	0	0	0	0	0	0	0	0	0	0	0	0	0	0	0	0	0	0	0	0	0	0	0	0	0	0	0	0	0	0	0	0	0	0	0	0	0	0	0	0	0	0
8 Bus structure	0	0	0	0	0	0	0	0	0	0	0	0	0	0	0	0	0	0	0	0	0	0	0	0	0	0	0	0	0	0	0	0	0	0	0	0	0	0	0	0	0	0	0	0	0	0	0	0	0	0	0	0	0	0	0	0	0
9 Magnetic Isolation Device	0	0	0	0	0	0	0	0	0	0	0	0	0	0	0	0	0	0	0	0	0	0	0	0	0	0	0	0	0	0	0	0	0	0	0	0	0	0	0	0	0	0	0	0	0	0	0	0	0	0	0	0	0	0	0	0	0
10 Viscoelastic Isolation Device	0	0	0	0	0	0	0	0	0	0	0	0	0	0	0	0	0	0	0	0	0	0	0	0	0	0	0	0	0	0	0	0	0	0	0	0	0	0	0	0	0	0	0	0	0	0	0	0	0	0	0	0	0	0	0	0	0
11 Active Damper	0	0	0	0	0	0	0	0	0	0	0	0	0	0	0	0	0	0	0	0	0	0	0	0	0	0	0	0	0	0	0	0	0	0	0	0	0	0	0	0	0	0	0	0	0	0	0	0	0	0	0	0	0	0	0	0	0
12 Deployment Device for Solar Array	0	0	0	0	0	0	0	0	0	0	0	0	0	0	0	0	0	0	0	0	0	0	0	0	0	0	0	0	0	0	0	0	0	0	0	0	0	0	0	0	0	0	0	0	0	0	0	0	0	0	0	0	0	0	0	0	0
13 Gimbal Device	0	0	0	0	0	0	0	0	0	0	0	0	0	0	0	0	0	0	0	0	0	0	0	0	0	0	0	0	0	0	0	0	0	0	0	0	0	0	0	0	0	0	0	0	0	0	0	0	0	0	0	0	0	0	0	0	0
14 UDP Comm interface	0	0	0	0	0	0	0	0	0	0	0	0	0	0	0	0	0	0	0	0	0	0	0	0	0	0	0	0	0	0	0	0	0	0	0	0	0	0	0	0	0	0	0	0	0	0	0	0	0	0	0	0	0	0	0	0	0
15 UDP Power interface	0	0	0	0	0	0	0	0	0	0	0	0	0	0	0	0	0	0	0	0	0	0	0	0	0	0	0	0	0	0	0	0	0	0	0	0	0	0	0	0	0	0	0	0	0	0	0	0	0	0	0	0	0	0	0	0	0
16 Laser Communications Box	0	0	0	0	0	0	0	0	0	0	0	0	0	0	0	0	0	0	0	0	0	0	0	0	0	0	0	0	0	0	0	0	0	0	0	0	0	0	0	0	0	0	0	0	0	0	0	0	0	0	0	0	0	0	0	0	0
17 RF Communications Box	0	0	0	0	0	0	0	0	0	0	0	0	0	0	0	0	0	0	0	0	0	0	0	0	0	0	0	0	0	0	0	0	0	0	0	0	0	0	0	0	0	0	0	0	0	0	0	0	0	0	0	0	0	0	0	0	0
18 Direct Downlink Antennas	0	0	0	0	0	0	0	0	0	0	0	0	0	0	0	0	0	0	0	0	0	0	0	0	0	0	0	0	0	0	0	0	0	0	0	0	0	0	0	0	0	0	0	0	0	0	0	0	0	0	0	0	0	0	0	0	0
19 Crosslink Antennas	0	0	0	0	0	0	0	0	0	0	0	0	0	0	0	0	0	0	0	0	0	0	0	0	0	0	0	0	0	0	0	0	0	0	0	0	0	0	0	0	0	0	0	0	0	0	0	0	0	0	0	0	0	0	0	0	0
20 RAM	0	0	0	0	0	0	0	0	0	0	0	0	0	0	0	0	0	0	0	0	0	0	0	0	0	0	0	0	0	0	0	0	0	0	0	0	0	0	0	0	0	0	0	0	0	0	0	0	0	0	0	0	0	0	0	0	0
21 Power Convertor Unit (PCU)	0	0	0	0	0	0	0	0	0	0	0	0	0	0	0	0	0	0	0	0	0	0	0	0	0	0	0	0	0	0	0	0	0	0	0	0	0	0	0	0	0	0	0	0	0	0	0	0	0	0	0	0	0	0	0	0	0
22 Data Interface Unit (DIU)	0	0	0	0	0	0	0	0	0	0	0	0	0	0	0	0	0	0	0	0	0	0	1	1	1	1	1	0	0	0	0	0	0	0	0	0	0	0	0	0	0	0	0	0	0	0	0	0	0	0	0	0	0	0	0	0	0
23 Instrument A	0	0	0	0	0	0	0	0	0	0	0	0	0	0	0	0	0	0	0	0	0	1	0	0	0	0	0	0	0	0	1	1	1	0	1	0	0	0	0	0	0	0	0	0	0	0	0	0	0	0	0	0	0	0	0	0	0
24 Instrument B	0	0	0	0	0	0	0	0	0	0	0	0	0	0	0	0	0	0	0	0	0	1	0	0	0	0	0	0	0	0	1	1	1	0	1	0	0	0	0	0	0	0	0	0	0	0	0	0	0	0	0	0	0	0	0	0	0
25 Fine Guidance Sensors	0	0	0	0	0	0	0	0	0	0	0	0	0	0	0	0	0	0	0	0	0	1	0	0	0	0	0	0	0	0	1	1	1	0	1	0	0	0	0	0	0	0	0	0	0	0	0	0	0	0	0	0	0	0	0	0	0
26 Instrument C	0	0	0	0	0	0	0	0	0	0	0	0	0	0	0	0	0	0	0	0	0	1	0	0	0	0	0	0	0	0	1	1	1	0	1	0	0	0	0	0	0	0	0	0	0	0	0	0	0	0	0	0	0	0	0	0	0
27 Instrument D	0	0	0	0	0	0	0	0	0	0	0	0	0	0	0	0	0	0	0	0	0	1	0	0	0	0	0	0	0	0	1	1	1	0	1	0	0	0	0	0	0	0	0	0	0	0	0	0	0	0	0	0	0	0	0	0	0
28 Thermal blanket {bus}	0	0	0	0	0	0	0	0	0	0	0	0	0	0	0	0	0	0	0	0	0	0	0	0	0	0	0	0	0	0	0	0	0	0	0	0	0	0	0	0	0	0	0	0	0	0	0	0	0	0	0	0	0	0	0	0	0
29 External radiator {bus}	0	0	0	0	0	0	0	0	0	0	0	0	0	0	0	0	0	0	0	0	0	0	0	0	0	0	0	0	0	0	0	0	0	0	0	0	0	0	0	0	0	0	0	0	0	0	0	0	0	0	0	0	0	0	0	0	0
30 Thermoelectric cooler (TEC) {optics}	0	0	0	0	0	0	0	0	0	0	0	0	0	0	0	0	0	0	0	0	0	0	0	0	0	0	0	0	0	0	0	0	0	0	0	0	0	0	0	0	0	0	0	0	0	0	0	0	0	0	0	0	0	0	0	0	0
31 Cryocooler {inst}	0	0	0	0	0	0	0	0	0	0	0	0	0	0	0	0	0	0	0	0	0	0	0	0	0	0	0	0	0	0	0	0	0	0	0	0	0	0	0	0	0	0	0	0	0	0	0	0	0	0	0	0	0	0	0	0	0
32 Thermostatic heater {optics}	0	0	0	0	0	0	0	0	0	0	0	0	0	0	0	0	0	0	0	0	0	0	0	0	0	0	0	0	0	0	0	0	0	0	0	0	0	0	0	0	0	0	0	0	0	0	0	0	0	0	0	0	0	0	0	0	0
33 Heat pipe network {bus}	0	0	0	0	0	0	0	0	0	0	0	0	0	0	0	0	0	0	0	0	0	0	0	0	0	0	0	0	0	0	0	0	0	0	0	0	0	0	0	0	0	0	0	0	0	0	0	0	0	0	0	0	0	0	0	0	0
34 Thermal sensor {optics}	0	0	0	0	0	0	0	0	0	0	0	0	0	0	0	0	0	0	0	0	0	0	0	0	0	0	0	0	0	0	0	0	0	0	0	0	0	0	0	0	0	0	0	0	0	0	0	0	0	0	0	0	0	0	0	0	0
35 Momentum Wheel	0	0	0	0	0	0	0	0	0	0	0	0	0	0	0	0	0	0	0	0	0	0	0	0	0	0	0	0	0	0	0	0	0	0	0	0	0	0	0	0	0	0	0	0	0	0	0	0	0	0	0	0	0	0	0	0	0
36 Solar Sail	0	0	0	0	0	0	0	0	0	0	0	0	0	0	0	0	0	0	0	0	0	0	0	0	0	0	0	0	0	0	0	0	0	0	0	0	0	0	0	0	0	0	0	0	0	0	0	0	0	0	0	0	0	0	0	0	0
37 Star Tracker	0	0	0	0	0	0	0	0	0	0	0	0	0	0	0	0	0	0	0	0	0	0	0	0	0	0	0	0	0	0	0	0	0	0	0	0	0	0	0	0	0	0	0	0	0	0	0	0	0	0	0	0	0	0	0	0	0
38 Solar Array per 100 watts	0	0	0	0	0	0	0	0	0	0	0	0	0	0	0	0	0	0	0	0	0	0	0	0	0	0	0	0	0	0	0	0	0	0	0	0	0	0	0	0	0	0	0	0	0	0	0	0	0	0	0	0	0	0	0	0	0
39 Battery per watt-hour	0	0	0	0	0	0	0	0	0	0	0	0	0	0	0	0	0	0	0	0	0	0	0	0	0	0	0	0	0	0	0	0	0	0	0	0	0	0	0	0	0	0	0	0	0	0	0	0	0	0	0	0	0	0	0	0	0
40 Distribution per 100 watts	0	0	0	0	0	0	0	0	0	0	0	0	0	0	0	0	0	0	0	0	0	0	0	0	0	0	0	0	0	0	0	0	0	0	0	0	0	0	0	0	0	0	0	0	0	0	0	0	0	0	0	0	0	0	0	0	0
41 Connectors and Wiring	0	0	0	0	0	0	0	0	0	0	0	0	0	0	0	0	0	0	0	0	0	0	0	0	0	0	0	0	0	0	0	0	0	0	0	0	0	0	0	0	0	0	0	0	0	0	0	0	0	0	0	0	0	0	0	0	0
42 Light Shield	0	0	0	0	0	0	0	0	0	0	0	0	0	0	0	0	0	0	0	0	0	0	0	0	0	0	0	0	0	0	0	0	0	0	0	0	0	0	0	0	0	0	0	0	0	0	0	0	0	0	0	0	0	0	0	0	0
43 Deployment Device for Antenna	0	0	0	0	0	0	0	0	0	0	0	0	0	0	0	0	0	0	0	0	0	0	0	0	0	0	0	0	0	0	0	0	0	0	0	0	0	0	0	0	0	0	0	0	0	0	0	0	0	0	0	0	0	0	0	0	0
44 Secondary Mirror Segment	0	0	1	0	0	0	0	0	0	0	0	0	0	0	0	0	0	0	0	0	0	0	0	0	0	0	0	0	0	0	0	0	0	0	0	0	0	0	0	0	0	0	0	0	0	0	0	0	0	0	0	0	0	0	0	0	0
45 Primary Mirror Baffle	0	0	0	0	0	0	0	0	0	0	0	0	0	0	0	0	0	0	0	0	0	0	0	0	0	0	0	0	0	0	0	0	0	0	0	0	0	0	0	0	0	0	0	0	0	0	0	0	0	0	0	0	0	0	0	0	0
46 CPU	0	0	0	0	0	0	0	0	0	0	0	0	0	0	0	0	0	0	0	0	0	0	0	0	0	0	0	0	0	0	0	0	0	0	0	0	0	0	0	0	0	0	0	0	0	0	0	0	0	0	0	0	0	0	0	0	0
47 Data Management Unit (DMU)	0	0	0	0	0	0	0	0	0	0	0	0	0	0	0	0	0	0	0	0	0	0	0	0	0	0	0	0	0	0	0	0	0	0	0	0	0	0	0	0	0	0	0	0	0	0	0	0	0	0	0	0	0	0	0	0	0
48 Thermostatic heater {inst}	0	0	0	0	0	0	0	0	0	0	0	0	0	0	0	0	0	0	0	0	0	0	0	0	0	0	0	0	0	0	0	0	0	0	0	0	0	0	0	0	0	0	0	0	0	0	0	0	0	0	0	0	0	0	0	0	0
49 Thermostatic heater {bus}	0	0	0	0	0	0	0	0	0	0	0	0	0	0	0	0	0	0	0	0	0	0	0	0	0	0	0	0	0	0	0	0	0	0	0	0	0	0	0	0	0	0	0	0	0	0	0	0	0	0	0	0	0	0	0	0	0
50 Thermal sensor {inst}	0	0	0	0	0	0	0	0	0	0	0	0	0	0	0	0	0	0	0	0	0	0	0	0	0	0	0	0	0	0	0	0	0	0	0	0	0	0	0	0	0	0	0	0	0	0	0	0	0	0	0	0	0	0	0	0	0
51 Thermal sensor {bus}	0	0	0	0	0	0	0	0	0	0	0	0	0	0	0	0	0	0	0	0	0	0	0	0	0	0	0	0	0	0	0	0	0	0	0	0	0	0	0	0	0	0	0	0	0	0	0	0	0	0	0	0	0	0	0	0	0
52 Thermal blanket {inst}	0	0	0	0	0	0	0	0	0	0	0	0	0	0	0	0	0	0	0	0	0	0	0	0	0	0	0	0	0	0	0	0	0	0	0	0	0	0	0	0	0	0	0	0	0	0	0	0	0	0	0	0	0	0	0	0	0
53 Science Payload support structure	0	0	0	0	0	0	0	0	0	0	0	0	0	0	0	0	0	0	0	0	0	0	0	0	0	0	0	0	0	0	0	0	0	0	0	0	0	0	0	0	0	0	0	0	0	0	0	0	0	0	0	0	0	0	0	0	0
54 Monopropellant hydrazine thruster	0	0	0	0	0	0	0	0	0	0	0	0	0	0	0	0	0	0	0	0	0	0	0	0	0	0	0	0	0	0	0	0	0	0	0	0	0	0	0	0	0	0	0	0	0	0	0	0	0	0	0	0	0	0	0	0	0
55 Arcjet thruster	0	0	0	0	0	0	0	0	0	0	0	0	0	0	0	0	0	0	0	0	0	0	0	0	0	0	0	0	0	0	0	0	0	0	0	0	0	0	0	0	0	0	0	0	0	0	0	0	0	0	0	0	0	0	0	0	0
56 Hall thruster	0	0	0	0	0	0	0	0	0	0	0	0	0	0	0	0	0	0	0	0	0	0	0	0	0	0	0	0	0	0	0	0	0	0	0	0	0	0	0	0	0	0	0	0	0	0	0	0	0	0	0	0	0	0	0	0	0
57 Propellant (and tank)	0	0	0	0	0	0	0	0	0	0	0	0	0	0	0	0	0	0	0	0	0	0	0	0	0	0	0	0	0	0	0	0	0	0	0	0	0	0	0	0	0	0	0	0	0	0	0	0	0	0	0	0	0	0	0	0	0

APPENDIX I: DESCRIPTION OF ATLAST REQUIREMENTS AND THEIR IMPLICATIONS

As previously referenced, the optical and instrument baselines used in the TITANS AE architectural model originate in the ATLAST requirements as developed by NASA for the proposed 16.8-m class space observatory. This baseline does not vary substantially within the tradespace explored in this project; accordingly, the relevant subsystem models have been simplified to streamline the evaluation process. However, the imposed ATLAST requirements (**Table XXXIV**) do offer substantial guidance for the design of these subsystems which may be of interest to the reader. The proposed design implementation of the ATLAST requirements for the TITANS AE set of architectures is documented here.

Table XXXIV: ATLAST Key Optical Performance Requirements and Goals[5]

Requirement Name	Requirement	Goal	Science Drivers
Optical Bandwidth	0.2 – 2.5 μm	0.11 – 2.5 μm	Solar system exploration
Aperture Size	16.8 m		
Angular Resolution	6 – 12 mas	3.5 mas	
Field of View	5 arcmin		Extragalactic star formation
Pointing Stability	1 mas		Exoplanet characterization, life detection
Spectroscopic Resolution	300	120000	Extragalactic star formation
Contrast	1e+07	1e+10	Exoplanet characterization, life detection
Inner Working Angle	50 -100 mas	40 -50 mas	Exoplanet characterization, life detection
Wavefront Error	37 nm	0.07 nm	Exoplanet characterization, life detection
Wavefront Stability	10 nm	0.07 nm	Exoplanet characterization, life detection
Uninterrupted Observation Time	2 hours		
Operational Efficiency	90%		

For the optical train, three ATLAST requirements drive design considerations relevant to TITANS AE: (1) optical bandwidth; (2) aperture size; and (3) wavefront error. The optical bandwidth indicated here stretches across the ultraviolet (UV), optical (O/VIS), and near infrared (IR/NIR) wavelength ranges and drives the selection of mirror coatings. A variety of aluminum and silver-based coatings exist which are appropriate for this range of wavelengths; however, many coatings experience a substantial reflectance fall-off in the extreme ('far') UV ranges.[80] Accordingly, the use of separate channels for more and less reflection-sensitive instruments may be appropriate (see below).

As in the ATLAST case, mirror diameter has been fixed at the 16.8-meter size class. (This in turn drives the angular resolution requirements specified in Table 1). The TITANS AE design also uses the three-ring hexagonal mirror format common to the ATLAST proposal. This approach minimizes wavefront complications due to mirror segmentation while still permitting launch of the primary mirror. (The appropriate balance between segmentation and mirror size is further addressed in Appendix K.)

Finally, the wavefront error requirement of 37 nm specifies the tolerance for manufacturing errors and polishing imperfections within the optical train. Because this number specifies the total error budget for the observatory, the wavefront error contribution of each element must represent only a fraction of this value. This value represents an incremental improvement on the expected performance of the JWST optical train.[81] More challenging, however, is the "goal" error of .07 nm. Such accuracy can only be achieved with adaptive optics. The TITANS AE design presupposes such an adaptive optics system is integrated into secondary mirror assembly, permitting fine control of wavefront across the entire FOV of the telescope.

At the instrument level, the ATLAST requirements most important for instrument design include the majority of the remaining requirements. The FOV requirement of 5 arcmin necessitates the inclusion of a wide field of view instrument. The stability requirements drive the design of the fine guidance sensors. Meeting the spectral resolution requirement (R=300) suggests an imaging spectrometer design; the higher resolution "goal" (R=12000) on the other hand necessitates a dedicated, likely slit-based spectrograph/detector approach. The contrast and inner working requirements specify the performance for coronographic elements. Finally, the optical bandwidth requirement imposes an additional constraint (in addition to those it imposes on the optical train): each instrument will require additional detector channels for each of the UV, VIS and NIR wavelength ranges it attempts to analyze, due to the nature of detector technologies.

ATLAST meets and exceeds the requirements specified above with the following combination of instruments (Figure I.1).

Telescope	TMA Focal Plane Instruments				Cass Focal Plane Instruments		
	Vis/NIR Wide-field Imager	Vis/NIR Multi-Object Spectrograph	Vis/NIR IFU	FGS (FOV per FGS unit)	UV IFU & Spectrograph	Starlight Suppression	Exoplanet Imager & Spectrograph
8-m, 9.2-m	8x8 arcmin	4x4 arcmin	2x2 arcmin	3x3 arcmin	30 arcsec	Internal Coronagraph or Starshade Sensor	~10 arcsec
16.8-m	4x4 arcmin	3x3 arcmin	1x1 arcmin	~1x3 arcmin	15 arcsec		~10 arcsec

Figure 94: Tentative ATLAST Science Instruments and their FOV[17]

The decision to include both a Three-Mirror Anastigmat (TMA) and Cassegrain focal plane helps balance the tradeoff between FOV control and throughput losses associated with the inclusion of additional mirrors and interfaces in the optical pathway. For the particularly photon-starved (reflectivity-loss-sensitive) instruments, the Cassegrain focal plane minimizes bounces, compensating for the lower reflectivity of the optics in the UV, and the general lack of photons available to be collected for exoplanet purposes. The TMA focal plane allows many instruments to "pick off" light from the observatory field of view for various scientific purposes. As suggested above, these include fine guidance sensing, WFOV imaging and lower-resolution and/or imaging (relatively wide area) spectroscopy.

Because the TITANS AE architectural model does not require the degree of specificity included in the ATLAST model, these instruments have been incorporated into four "packages" for launch, assembly and servicing purposes. This decision reflects the wide range of functionalities any instrument package may possess (including multiple modes and detector planes) while meeting the outlined scientific objectives.

APPENDIX J: FORMS AND FUNCTIONS FOR HISTORICAL MISSIONS

Structures Subsystem	Hubble	JWST	Kepler	IRIDIUM
Protecting				
Radiation Protecting	Light Shield			
Dust Protecting	Aperture door, light shield		Photometer Dust Cover	
Micrometeoroid Protecting	Aperture door, light shield	2-layer aluminum meteoroid shields	Graphite Cyanite Structure	
Stray Light Protecting	Aperture door, light shield	Sun shield, central baffle	Sun Shield	N/A
Temperature Protecting	Multi-layer insulation; heaters; thermal blankets	Sun shield, radiator shades, MLI	Focal Plane Radiator	
Supporting	Aluminum shell; graphite-epoxy frame; storage bay ring; solar arrays, high gain antennas - latches on light shield	primary mirror - backplane; secondary mirror - "tripod" booms; bus electronics - bus electronics box; instruments - ISIM truss structure	Solar panels - fixed to side of telescope structure; support system electronics - honeycomb aluminum box at base of photometer	electronics - spacecraft bus; antennas - communication panel
Pointing				
Bus Pointing		solar pressure trim flap, reaction wheels, thrusters	Reaction Wheels; thrusters	thrusters
Articulated Pointing		primary mirror segments - hexapod with actuators; HG antenna - two-axis gimbal		N/A
Preventing Jitter		Tower structure	(operational) Reaction wheels as only moving part	N/A
Deploying	N/A	Extendable booms; spreader bars; stem deployers; gimbals; tension cables	N/A	N/A
Stowing	N/A	Unitized pallet structure; hold-downs	N/A	N/A
Interfacing				
Launch Vehicle Interfacing		Clamp-band	Vehicle Adapter Ring with umbilicals	
Ground System Interfacing		Omni antenna, high gain antenna	High gain antenna; 2x omnidirectional low gain antennas	K-band antenna panel, L-band phased array antenna x3
AIT Interfacing	Gas purge system	test port		test port
Access Providing				
Physical Access Providing	Outer doors; latches; handrails; footholds	N/A	N/A	N/A
Digital Access Providing		N/A	N/A	test port
On-orbit Assembling				
Manipulating	N/A	N/A	N/A	N/A
Integrating	N/A	N/A	N/A	K-band inter-satellite antenna panel

Power Subsystem				
Power Generating	Solar Array		Solar Array	Solar Array
Size (Surface area or mass)	19 m²		10.2 m²	
Amount	2800 W		1100 W	2000 W

Power Storing	Batteries		Battery (Lithium ion)	

Thermal Subsystem

Insulating spacecraft	Multi-layer insulation (MLI) ; new layers (NOBL) added	5-layer sunshield	MLI	MLI and/or thermal shields
Controlling temperature of optics (ie: mirrors)	Thermostatically controlled heaters	Central baffle / radiator (cooling)	Controlled heaters; Thermal blankets (cooling)	
Controlling temperature of spacecraft bus and subsystems				Standard active and/or passive thermal designs
Cooling instrument and/or detectors	Thermoelectric coolers, Heat pipes, Capillary Pumped Loop subsystems; Cryogenic dewar	Passive radiator enclosure; Cryogenic dewar; Joule-Thomson cooler	Propane and ammonia heat pipes; External radiator	Standard active and/or passive thermal designs
Isolating instrument(s) from warm sources on spacecraft	Thermal insulation; Thermal isolation	Thermal insulation; Thermal isolation	Thermal insulation; Thermal isolation	Thermal insulation; Thermal isolation

Avionics/Comm Subsystem

Avionics functions

Data collecting from target	Collected by Science Instrument Control & Data Handling (SICDH)	From interface with optics subsystem	Photometer, CCD Radiator	L-band antenna
Data processing from target	Data Management System(DF-224 computers)	Moongoose 5 processor	RAD750 Processor	on-board processor
Storing of data from target	Engineering/Science Tape Recorder, Solid State Recorder	Solid state recorder (471Gbits)	16 GB Solid State Recorder	N/A
Scheduling of tasks and resources between telescope subsystems	Data Management System(DF-224 computers)	Moongoose 5 processor	RAD750 Processor	teleport network (= teleports connecting the satellites through Earth stations to a MPLS Multiprotocol Label Switching)
Scheduling of tasks and resources between FSS satellites	Data Management System(DF-224 computers)	Moongoose 5 processor	RAD750 Processor	teleport network (= teleports connecting the satellites through Earth stations to a MPLS Multiprotocol Label Switching)
Interfacing with FSS	Data Management System (Data Interface Units)	Moongoose 5 processor	RAD750 Processor	teleport network (= teleports connecting the satellites through Earth stations to a MPLS Multiprotocol Label Switching)
Processing received data from the ground station	Data Management System(DF-224 computers)	Moongoose 5 processor	RAD750 Processor	on-board processor
Storing of the received data	Engineering/Science Tape Recorder, Solid State Recorder	Moongoose 5 processor, Solid state recorder	RAD750 Processor, 16 GB SSR	on-board processor
Formatting the data for sending / receiving	Data Management System(DF-224 computers)	Moongoose 5 processor	RAD750 Processor	on-board processor

Comm functions

Transmitting target data (image) to ground		Far omni antenna, high-gain antenna, near omni antenna		single, 48 beam TX/RX phased array antenna, one omni antenna, also two fixed and two steerable antennas
Receiving data from the ground station	Low gain and high gain antenna Communications loop between HST and Tracking and Data Relay System Satellite (TDRSS)		parabolic-dish high gain antenna, 2 TX low gain, 2 RX low gain	
Electrical power distributing between all subsystems	1 x Power Control Unit, 4 x Power Distribution Units	Electrical power unit	20 amp-hr rechargeable lithium-ion battery	Electrical power unit
Electrical power collecting / generating	Solar arrays, batteries, charge current controllers	Solar arrays, 37Ah NiH2 battery	4 non-coplanar solar panels	solar arrays, 2000W

Systems

Launching

Launch Vehicle	Shuttle Discovery	Ariane 5 ECA	United Launch Alliance Delta II 7925	Dnepr, Falcon 9
Launch Location	KSC	Kourou, French Guiana	Cape Canaveral Air Force Station	TBD
Launch Date	April, 1990	2018?	March, 2009	2015-2017?
Orbit	600 km	L2	Earth-trailing heliocentric	780 km
Operations				
Deploy	Single Shuttle launch	Fold-up in Ariane 5 rocket to L2	Boeing Delta II to Earth-trailing heliocentric	10 satellites, 7 launches on Spacex Falcon 9
Control	Goddard (partial pre-program, partial real-time)	Space Telescope Science Institute	LASP (mostly auto-rolls every 6 months)	Analysis and monitoring of performance
Collect Data	Cassegrain reflector - 2.4 m mirror	6.5 m mirror	1.4 m mirror, .95 m photometer	Cross-linked architecture captures device signals (like cell towers)
Distribute Data	TDRSS	Deep Space Network	Deep Space Network	Gateway facility to telephone and internet infrastructures
Decommission	Piece-by-piece until robotically-assisted de-orbit	10 year lifespan based on fuel, unclear decommission plan	??	Atmospheric burn-up after orbital decay
Manufacturing				
Measuring light (http://www.jwst.nasa.gov/mirrors.html)	2.4-m-diameter primary mirror	6.5-m-diameter primary mirror	1.4-m-diameter primary mirror	N/A
Being lightweight	Inch-thick top and bottom plates sandwiching a honeycomb lattice	Use of beryllium (strong but light material) (1/10 of the mass of Hubble's mirror per unit area)		N/A
Mirror fitting into a rocket	N/A	18 segments on a structure that folds up	N/A	N/A
Fitting without gaps (high filling factor)	1-segment mirror	Hexagonal shape for each segment	1-segment mirror	N/A
Providing a 6-fold symmetry to reduce the number optical prescriptions	N/A	Hexagonal shape for each segment	N/A	N/A
Focusing the light into the most compact region on the detectors	Circular shape for primary mirror	Approximately circular shape for primary mirror	Circular shape for primary mirror	N/A
Focusing correctly on faraway galaxies	N/A	6 actuators attached to the back of each primary and secondary mirror segment + 1 actuator in the center to correct curvature	N/A	N/A
Keeping cold at -220°C	N/A	Cryogenic system	N/A	N/A
Shaping, smoothing, polishing	Computer-controlled polishing machines	Industrial machines		N/A
Testing the change in mirror segment shape due to the exposure to cryogenic temperatures	Support the mirror on both sides with 138 rods exerting varying amounts of force	PhaseCam Laser interferometer		N/A
Improving the mirror's reflectivity	65-nm-thick aluminum coating (+ protective 25-nm-thick magnesium fluoride coating)	Gold coating	Enhanced silver coating	N/A
Seeing newly forming stars, and faintly visible comets as well as objects in the Kuiper Belt.		MIRI (http://ircamera.as.arizona.edu/MIRI/instrument.htm)		N/A
Studying thousands of galaxies in 5 years		NIRSpec and microshutters (http://www.jwst.nasa.gov/nirspec.html)	105-square-degree field of view	N/A
Imaging in the NIR		NIRCam (http://www.jwst.nasa.gov/nircam.html)		N/A
Pointing		FGS/NIRISS (http://www.jwst.nasa.gov/fgs.html)	4 CCDs located on science focal plane	N/A
Measuring large aspheres		SSI-A (http://www.nasa.gov/topics/technology/features/web b-spinoffs.html)		N/A
Compensating spherical aberration			Schmidt corrector	N/A
Mass-producing satellites on a gimbal	N/A	N/A	N/A	Patented technology by the engineer who set up the automated factory for Apple's Macintosh
Providing utmost reliability				Microwave inter-satellite communications links

APPENDIX K: PROPOSED METHODOLOGY FOR CALCULATING INSTRUMENT-LEVEL SCIENCE VALUE

Although detailed calculation of science utility was unnecessary for evaluation of the TITANS AE tradespace, the ability to accurately assess the relative values of various discoveries and the observatories and instruments which produce them remains a desirable capability for future comparisons between system architectures. This appendix offers a partial proposal for accomplishing this objective, with emphasis on instrument-level characterization.

For general a general set of astronomical observations, the total science utility can be expressed as a function of the value of each discovery weighted relative to the value of the given class of discoveries:

$$Total\ Science\ Utility = \sum_{i=1}^{n}(Discovery\ Value_i * Number\ of\ Discoveries)$$

<div align="right">Eq. K.1</div>

Where *i* represents the class of discovery for *n* classes of discovery. A discovery "class" for these purposes represents a kind of observation, e.g., "faint object characterization," where an observation is defined as the set of photons collected for the purpose. Developing relative weightings and valuations of discovery classes is difficult and inherently subjective, but may be accomplished with reference to the decadal survey or direct communication/polling of stakeholders (scientists). The decadal survey already suggests priorities for various kinds of missions and scientific efforts, which implies that a weighting schema is feasible.

Within a single class of discoveries/observations, a second set of weightings is desirable to distinguish how *useful* a given observation/set of photons is from a scientific perspective. The usefulness of a photon can be described as our ability to distinguish it (via optics and instruments) from other photons. This discrimination can come in a variety of dimensions: photometric, spatial, spectral or polarimetric, among others. For different classes of observations, certain kinds of discrimination have greater value than others; spatial discrimination is more valuable for surveys and imaging operations, while spectral characterization is arguably more valuable for exoplanet characterization. For a given weighting associated with each discrimination class *z*, optics and instruments can be evaluated against observation class *i* by referencing their discovery efficiency:

$$Discovery\ Value_i = \left[\sum_{z=1}^{q}(Discrimination\ Weighting_z)\right] * Discovery\ Efficiency$$

<div align="right">Eq. K.2</div>

As suggested, discovery efficiency here refers to the capabilities of a given combination of instrument and optical train to discriminate between classes of photons. This equation suggests

that doubling an instrument's capacity to discriminate photons (e.g., doubling spectral resolution) only doubles discovery value if, for the current class of discoveries, such a doubling is useful (and is so reflected in the discrimination capacity weightings).

These first two equations capture the bulk of the subjective elements of utility estimation, permitting objective evaluation of optics and instrument performance in the forgoing discussion. Objective evaluation of performance is a non-trivial problem on its own, with much of the challenge lying in a determination of the appropriate units. Past efforts have suggested units such as "productivity rate" (images per unit time) or another form of "discovery efficiency" (throughput * FOV, or photons per arcmin^2, occasionally photons per arcmin^2 per unit wavelength).[24,13] While each of these options captures some aspects of instrument performance, they collectively focus imaging operations for comparison (arguably, they are equations 'optimized' for imaging systems comparison). As the bulk of astronomical observations includes a non-imaging component, or are entirely non-imaging, a more general equation is required to fully assess such systems' performance. Such observations have only one parameter which is fundamentally comparable across all operations: the amount of time required to complete them.

At a theoretical level, for a given observation target, the amount of time required to confirm detection of the target is related to the photon flux density collected from the target and the sensitivity of the instrument/optics train. For these purposes, both sensitivity and flux density may be appropriately defined in Janskies or AB magnitude (Janksy/flux units used here for simplicity). The Jansky, defined as 10^{-26} Watts per m^2 per Hz, is the integral of the spectral radiance over the source solid angle, and may be applied to point or extended sources. Sensitivity, meanwhile, provides the minimum effective flux which can be extracted as signal from background noise in a given integration time and over a given wavelength range. Such values have been calculated for existing systems (Figure K.1).

photometric performance, point source, 10σ in 10^4s
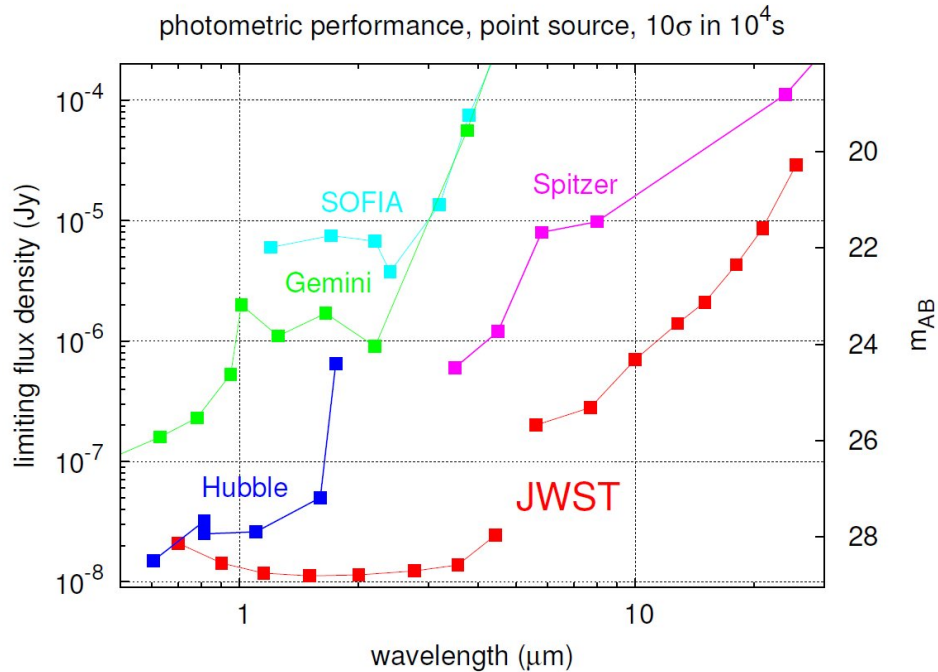
Figure K.1: The faintest flux that can be detected at 10σ in a 10^4s integration for a variety of telescope systems.[82]

Below the specified sensitivity threshold, any photons detected will not generate meaningful science; to make use of them, it would be necessary to increase the integration time or improve instrument performance. By contrast, sources above this threshold flux density will be observable in a smaller amount of time, or for the same time allocation, can be observed at a higher degree of discrimination/granularity. In this way, any photons collected above the sensitivity threshold can be "spent" on decreasing the integration time (allowing for more science operations), or increasing the fidelity of the current science operation (by discriminating in more detail between the kinds of photons), effectively increasing the number of unidimensional science operations.

In designing and evaluating instruments, available technologies allow for the optimization of certain science operations. At a basic level, any instrument is capable of discriminating the photons associated with a target in any dimension (spectral/spatial//photometric/polarimetric), provided that instrument is equipped with detectors, a limited set of tools and enough time. Using a one-pixel detector, a coronagraph and an adjustable slit/grating, a spatial and spectral image cube at very high contrast and high resolution over a wide field of view can be created…in a very long time. What distinguishes instruments from a scientific standpoint is how they are optimized for one or more of these discrimination tasks, and how efficiently they use the available flux density. The first of these parameters – optimization – addresses the overhead time cost associated with each science operation. An imaging instrument can be used to take spectral measurements if a filter wheel is applied. For a multispectral image, three (or more) images are taken, one at each filter wavelength range. The time required to collect enough flux to reach an SNR of 10 is directly linked to the amount of flux available (and hence, the number of ways the available flux is being subdivided). So, collecting 5 wavelength subranges takes five

times as long as collecting one panchromatic image of that target (assuming an even spectral distribution of flux in this degenerate case). Additionally, because time is required to adjust the filter wheels, an additional 5x penalty is occurred relative to the baseline panchromatic option. By comparison, the imaging aspect of the operation incurs much less penalty. Dividing a single detector into 1000 pixels over the same FOV means the image takes 1000 times as long to collect. However, no overhead cost is incurred, because all detectors collect simultaneously/in parallel. This reflects the efficient use of the available flux density per unit time associated with the two dimensional detector. In effect, less input flux is wasted as a result of parallelization. To use another example, a single spectrograph replaced by a cluster of spectrographs (as in JWST's NIRSpec) increases the parallelization and thus efficiency of collections. NIRSpec could be used for imaging operations by simply iterating the spectral collections over a large spatial area – but at a substantial time penalty[2].

Once photons are detected and discriminated/separated, a final step involves accounting for the actual collection capability of the optics system. The size of the primary mirror and associated resolving power determine the amount of light collected from each detection and also the degree to which that light can be resubdivided. Taken together, these factors suggest the following qualitative formula:

$$Discovery\ Efficiency$$
$$= Photons\ Collected\ *\ Photons\ Discriminated\ *\ Photons\ Detected$$

Eq. 91

Where "photons collected" loosely corresponds to optical performance, "photons discriminated" accounts for the design of the instrument-level optics pathway, and "photons detected" captures the sensitivity and capability of the detectors themselves.

This conceptual framework can be made quantitative by returning to the flux density notation introduced previously. For a given class of target at a specified distance, an expected flux density profile, angular size and working area can be specified (where working area refers to the presence or absence of alternative signal sources in the vicinity). This total flux (10^{-26} $W/(m^2*Hz*s)$), when collected by an optical train with a specified mirror collection area, after experiencing differential throughput losses associated with the optical train yields the total flux collected and available for sensing at the optical bench ("photons collected"). At this point, the target is "picked off" by an instrument (in whole or in part) for analysis. (Larger targets may have an effective angular size greater than the FOV of the instrument, necessitating additional observations). The relevant photons are divided spectrally, spatially and polarimetrically by the instrument workbench, with losses associated with each discrimination accounted for ("photons discriminated"). Finally, with any extraneous signals suppressed (via coronagraphy or other methods), detectors of a given size, well depth and pixel density can record the target to a degree

---

[2] Arguably, opening all of the microshutters at once converts NIRspec into a sort of imaging system. But assuming that only a few could be open at a time, an image could still be produced with enough time penalty.

of photometric accuracy within the limitations of the detector sensitivity ("photons detected"). These factors, when combined, yield the following equation:

$$(TFD * MCA * OTL) * \left(\frac{IFOV * SWR}{ETS * SB * NPOL} * ITL \right) * \left[\frac{(CSF * \frac{EPF}{ESF} * EDD)}{EDS} \right]$$
$$= Discovery\ Efficiency\ (units: discoveries\ per\ 10^4 s\ @\ SNR = 10$$

<div align="right">Eq. 92</div>

where:

TFD   = *Total (source) Flux Density (10^{-26} W/(m^2*Hz))*
MCA = *Mirror Collection Area (m^2)*
OTL   = *Optical Train Losses (expressed as % of original remaining)*
SWR   = *Spectral Wavelength Range (required wavelength coverage, Hz or λ)*
SB   = *Spectral Bandwidth (number of subdivisions in wavelength range – unitless)*
IFOV = *Instrument Field of View (arcmin^2)*
ETS   = *Effective Target Size (arcmin^2)*
NPOL = *Number of desired polarization characterizations*
ITL   = *Instrument Throughput Losses (expressed as % of original remaining)*
CSF   = *Contrast/Suppression Factor (ratio of intensity of target & suppressed source)*
EPF   = *Effective Parallelization Factor (# of sub-observations conducted in parallel)*
ESF   = *Effective Serialization Factor (# of sub-observations conducted in series)*
EDD   = *Effective Detector Density (degree of sampling of diffraction limit)*
EDS   = *Effective Detector Sensitivity (10^{-26} W/Hz)*

This equation, while not fully characterized, captures the core logic of discovery efficiency – the amount of time it takes to make a notional discovery/observe a notional target. It appropriately penalizes complex science operations through the time mechanic. It also captures that some complexity/increased discrimination of photons is easier than other complexity for a given instrument. Finally, it captures that a given instrument may be more efficient for some discoveries than for others; a wide field instrument with a limited coronographic capability and set of spectral filter wheels will have a lower discovery efficiency against the exoplanet mission set (still non-zero), but a higher discovery efficiency for surveys.

Future work to on this proposed framework can leverage the rich history of existing instruments and observatories to revise and validate the model. Such efforts can leverage past efforts to evaluate new telescope proposals: the ATLAST final report includes several assessments of observatory performance phrased in similar units and terms (Figure K.2). James Webb's resources include Exposure Time Calculators, which provide results relevant to a discovery efficiency analysis.[82]
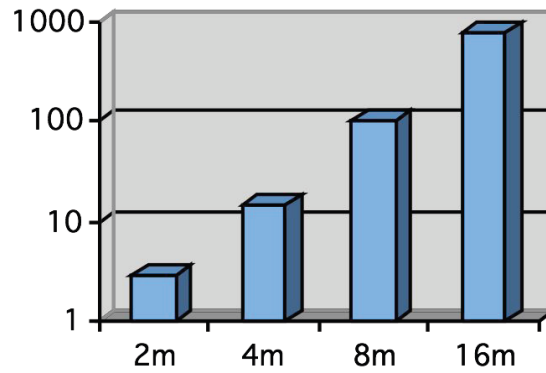
Figure 2. The average number of F, G, K stars where SNR=10 R=70 spectrum of an Earth twin could be obtained in < 500 ksec as a function of telescope aperture, D. The growth in the sample size scales as D3.[17]

Additionally, the Hubble legacy of upgrades (and historical attempts to determine discovery efficiency) offers a rich dataset for model assessment, with extensibility to other systems and wavelength regimes following thereafter.

APPENDIX L: LAUNCH MASS CAPABILITY CALCULATIONS

In order to determine the launch cost of servicing missions for the EM-L2 and LOTUS servicing locations, the launch mass capability of the various launch systems to these orbits must be determined. Due to a lack of reported data, the launch mass capability was estimated based upon known data for mass-to-LEO and mass-to-SE-L2 capabilities for each system. The rocket equation was used for this analysis:

$$\Delta V = v_e \ln\left(\frac{m_0}{m_1}\right)$$

Eq. 93

where the variables are described in **Table XXXV**.

Table XXXV: Variables of the rocket equation, with units

Variable	Description	Units
ΔV	Change in Speed	m/s
v_e	Effective Exhaust Velocity	m/s
m_0	Initial Total Mass	kg
m_1	Final Total Mass	kg

For this calculation, three assumptions are made. First, the ΔV requirement for both EM-L2 and LOTUS orbits is assumed to be approximately the ΔV requirement for Lunar orbit. Second, the final total mass m_1 is assumed to be approximately the mass of the payload, m, in kilograms. Finally, the initial total mass m_0 is assumed to be approximately the sum of the payload mass m and the mass of the rocket and propellant, p, in kilograms. Thus, the effects of staging are not encompassed in this calculation. However, this is meant to be a first-approximation value of the mass-to-orbit capability of these rockets, and thus these assumptions are considered to be valid. For final implementation of this model, actual mass-to-orbit data for each launch system for each destination orbit should be obtained from the manufacturer.

The ΔV requirement for each orbit is known, and the payload mass capability of each launch system is known for LEO and SE-L2. Therefore, the rocket equation can be rearranged and used to develop a system of two equations with two unknowns:

$$\Delta V_{LEO} = v_e \ln\left(\frac{m_{LEO}+p}{m_{LEO}}\right)$$

Eq. 94

$$\Delta V_{SEL2} = v_e \ln\left(\frac{m_{SEL2}+p}{m_{LEO}}\right)$$

Eq. 95

where ΔV and m are the change in velocity and payload mass for the orbit indicated in the subscript (known values), and v_e and p are the effective exhaust velocity and rocket/propellant mass for the launch system under consideration (unknown values). Using this set of equations, approximations for the effective exhaust velocity and the rocket/payload mass for each launch system can be calculated, and are documented in Table XXXVI.

Table XXXVI: Calculated effective exhaust velocity and rocket/payload mass for the launch systems under consideration

Launch System	Effective Exhaust Velocity v_e [m/s]	Rocket/Payload Mass p [kg]
SLS	3056	851261
Falcon 9	7659	18489
Falcon Heavy	2194	1801390
Atlas V	4904	114857
Delta IV Heavy	8425	34977

Once these parameters for each launch system have been calculated, the mass-to-lunar-orbit capability for each launch system can be calculated, again via rearrangement of the rocket equation:

$$m_{lunar} = \frac{p}{e^{\frac{\Delta V_{lunar}}{v_e}} - 1}$$

Eq. 96

The results of this calculation are documented in Table XXXVII.

Table XXXVII: Payload mass to lunar orbit capability of the launch systems under consideration

Launch System	Payload Mass to Lunar Orbit [kg]
SLS	35815
Falcon 9	7113
Falcon Heavy	20836
Atlas V	17967
Delta IV Heavy	15870

REFERENCES

[1] Golkar, A. (2013 April). Federated Satellite Systems (FSS): A vision Towards an Innovation in Space Systems Design. In Smith L. J. (Chair), Session 7: Special Aspects. Symposium conducted at the 9th IAA Symposium on Small Satellites for Earth Observation, Berlin, Germany.

[2] Committee for a Decadal Survey of Astronomy and Astrophysics and the National Research Council, *New Worlds, New Horizons in Astronomy and Astrophysics*, The National Academies Press, Washington, DC, 2010.

[3] "NRO Gifts NASA Two Leftover Space Telescopes, Euclid to Cost NASA $40-50 Million, GEMS Not Confirmed." *SpacePolicyOnline.com*. Space and Technology Policy Group, 04 June 2012. Web.

[4] Postman, M., Traub, W., Krist, J., Stapelfeldt, K., Brown, R., Oegerle, W., Lo, A., Clampin, M., Soummer, R., Wiseman, J., Mountain, M., "Advanced Technology Large-Aperture Space Telescope (ATLAST): Characterizing Habitable Worlds" *ASP Conference Series, 2010*, Barcelona. 2009.

[5] Redding, D.C., Hickey, G., Agnes, G., Eisenhardt, P., Green, J.J., Krist, J., Peterson L., Stapelfeldt, K., Traub, W., Unwin, S., Werner, M., "Active Optics for a 16-Meter Advanced Technology Large Aperture Space Telescope." SPIE Astronomical Instrumentation Symposium, Marseilles. 2008.

[6] "The James Webb Space Telescope: About Webb's Orbit"
[http://www.jwst.nasa.gov/orbit.html. Accessed 3/10/2012.]

[7] Contract marks new generation for Deep Space Network. [Online] Retrieved from http://www.oriondeepspace.com/index.php?option=com_content&view=article&id=295:contract-marks-new-generation-for-deep-space-network&catid=41:space-science&Itemid=62

[8] Iridium Satellite Constellation. [Online] Retrieved from http://spacecollaborative.com.au/2030%20Sydney/Research/Network/Iridium_Sat.html

[9] Golkar, A. (2013 April). Federated Satellite Systems (FSS): A vision Towards an Innovation in Space Systems Design. In Smith L. J. (Chair), Session 7: Special Aspects. Symposium conducted at the 9th IAA Symposium on Small Satellites for Earth Observation, Berlin, Germany.

[10] T. Tolker-Nielsen, J-C. Guillen. SILEX: The First European Optical Communication Terminal in Orbit. ESA Bulletin 96 – November 1988. Retrieved from http://www.esa.int/esapub/bulletin/bullet96/NIELSEN.pdf

[11] How It Works: NASA's Experimental Laser Communication System. Retrieved from http://www.popularmechanics.com/science/space/nasa/how-it-works-nasas-experimental-laser-communication-system

[12] Vincent W.S. Chan and JohnE.Kaufman. Coherent Optical Inter-satellite Crosslinks. MIT Lincoln Laboratory. Military Communications Conference, 1988. MILCOM 88, Conference Record. 21st Century Military Communications – What's Possible? 1988 IEEE.

[13] Baldessera, M. "A Decision-Making Framework to Determine the Value of On-Orbit Servicing Compared to Replacement of Space Telescopes." S.M. Thesis, Department Of Aeronautics and Astronautics, Massachusetts Institute of Technology, Cambridge, MA, 2007.

[14] Hastings, Daniel E., and Carole Joppin. "On-Orbit Upgrade and Repair: The Hubble Space Telescope Example." Journal of Spacecraft and Rockets 43.3 (2006): 614-25.

[15] National Aeronautics and Space Administration. On-Orbit Satellite Servicing Study: Project Report. NP-2010-08-162-GSFC Vol., 2010. Print.

[16] Gardner, J.P. et al. "The James Webb Space Telescope." *Space Science Reviews* 123.4 (2006): 485-606. Print.

[17] Postman, M. et al. "Advanced Technology Large-Aperture Space Telescope (ATLAST): A Technology Roadmap For The Next Decade." Space Telescope Science Institute, May 2009.

[18] Gralla, E., and De Weck, O., "Strategies for On-Orbit Assembly of Modular Spacecraft". *JBIS,* Vol 60, 2007. pp. 219-227.

[19] "Phoenix." *DARPA RSS*. Web. 20 Feb. 2013.
<http://www.darpa.mil/our_work/tto/programs/phoenix.aspx>.

[20] Gettliffe, Gwendolyn. "High-Temperature Superconductors as Electromagnetic Deployment and Support Structures in Spacecraft." Masters Thesis. Massachusetts Institute of Technology. 2012.

[21] Mohan, Swati. "Quantitative Selection and Design of Model Generation Architectures for On-Orbit Autonomous Assembly." PhD Thesis. Massachusetts Institute of Technology. 2010.

[22] Stewart, A. M., "Design and Optimization of Lightweight Space Telescope Structures," S.M. Thesis, Department of Aeronautics and Astronautics, Massachusetts Institute of Technology, Cambridge, MA, 2007.

[23] "Primary Mirror," ESA Science & Technology, February 2004. [http://sci.esa.int/science-e/www/object/index.cfm?fobjectid=34702. Accessed 3/10/13.]

[24] "Hubble Space Telescope Primer for Cycle 21: 4.7 Instrument Comparisons," Space Telescope Science Institute, Maryland, December 2012. [http://www.stsci.edu/hst/proposing/documents/primer/Ch_48.html. Accessed 5/7/2013.]

[25] Stahl, P., Henrichs, T., and Dollinger, C., "Parametric Cost Models for Space Telescopes," *International Conference on Space Optics*, 2010.

[26] Wertz, J. R., Everett, D. F., Pischell, J. J., *"Space Mission Engineering: The New SMAD"*, Microcosm Press, 2011, Ch. 24.

[27] Postman, Marc, et al. "Advanced Technology Large-Aperture Space Telescope (ATLAST): A Technology Roadmap for the Next Decade." NASA Astrophysics Strategic Mission Concept Study, *Space Telescope Science Institute,* (May 2009)

[28] Sirianni, Marco and Mutchler, Max. "Radiation Damage in HST Detectors." STScI Report. SDW 2005.

[29] Sirianni, Marco et al., "Radiation Damage in Hubble Space Telescope Detectors." IEEE Explore 2007.

[30] Wertz, J. R., Everett, D. F., Pischell, J. J., *"Space Mission Engineering: The New SMAD"*, Microcosm Press, 2011, Ch. – Chapter 16 "Communication Payloads" page 455

[31] Muriel Noca - Space system engineering, October 2010, EPFL

[32] John Farserotu – Satellite communications class, October 2010, EPFL

[33] NASA DSN antennas characteristics, http://deepspace.jpl.nasa.gov/dsn/antennas/index.html

[34] Link budget introduction, http://complextoreal.com/wp-content/uploads/2013/01/linkbud.pdf

[35] NASA Optical Link Study Group (OLSG) Final Report, Interagency Operations Advisory Group - Optical Link Study Group, 5 June 2012

[36] Goddard Space Flight Center. *Hubble Facts: Hubble Space Telescope Servicing Mission 3A: New Advanced Computer.* Retrieved from http://asd.gsfc.nasa.gov/archive/hubble/a_pdf/news/facts/FS09.pdf

[37] Maxwell Technologies. *97SD3232 1Gb SDRAM.* Retrieved from http://www.maxwell.com/products/microelectronics/docs/97sd3232_rev3.pdf

[38] *Maxwell Introduces First Fully Qualified and Radiation Characteried Die-Based Memory Component for the Space Industry.* (May 1, 2003) Retrieved from http://www.spaceref.com/news/viewpr.html?pid=11415

[39] Lockheed Martin: Missiles and Space. *Hubble Space Telescope: Servicing Mission 3A Media Reference Guide.* Retrieved from http://asd.gsfc.nasa.gov/archive/hubble/a_pdf/news/SM3A-MediaGuide.pdf

[40] TDK Lambda: PXD Series. Retrieved from http://us.tdk-lambda.com/lp/ftp/Specs/pxd.pdf

[41] Sonn, C. (2011). APM5003: *Exploring methodology for psychological research* [Class lecture slides]. School of Social Sciences and Psychology, Victoria University, Melbourne, Australia.

[42] Cattrysse, Jill M. "Space Telescope Mission Design For L 2 Point Stationing."*54 the International Astronautical Congress of the International Astronautical Federation(IAF)*. 2003.

[43] Howell, K. C., and Kakoi, M., "Transfers Between The Earth-Moon and Sun-Earth Systems Using Manifolds and Transfer Orbits," *Acta Astronautica,* 59, 2006, pp. 367-380.

[44] Truesdale, Nick. "Using Invariant Manifolds of the Sun-Earth L2 Point for Asteroid Mining Operations." ASEN 5050 Space Flight Dynamics final report. University of Colorado. 2012.

[45] Sutton, George Paul., and Oscar Biblarz. *Rocket Propulsion Elements*. New York: John Wiley & Sons, 2001. Print.

[46] Lozano, Paulo. "Lecture 1: Missions and Thrusters". 16.522 Space Propulsion. Massachusetts Institute of Technology. 2013.

[47] Wertz, J. R., Everett, D. F., Pischell, J. J., *"Space Mission Engineering: The New SMAD"*, Microcosm Press, 2011.

[48] Gilmore, D. G. "Space Thermal Control Handbook – Volume I: Fundamental Technologies." 2002, 2nd edition. AIAA. Reston, Virginia.

[49] Donabedian, M. "Space Thermal Control Handbook – Volume II: Cryogenics." 2003. AIAA. Reston, Virginia.

[50] Ross, Jr. R. G. "A Study of the Use of 6K ACTDP Cryocoolers for the MIRI Instrument on JWST." *Cryocoolers 13*. 2005. International Cryocooler Conference.

[51] Kittle, P. "Cryocooler Performance Estimator." *Cryocoolers 14*. 2007. International Cryocooler Conference.

[52] "eTEC HV37 Thin-Film Thermoelectric Cooler Data Sheet." Document APS0023, rev 2.0. Nextreme Thermal Solutions, Inc.

[53] Durning, J., "The James Webb Space Telescope Fast Facts," NASA/ESA/CSA. Web. 20 April 2013. <http://www.jwst.nasa.gov/facts.html>

[54] Nelson, Buddy, editor. Lockheed Martin. "Hubble Space Telescope Servicing Mission 4-Media Reference Guide. Revision 1." *United States National Aeronautics and Space Administration*. May 2009. Web. 5 May 2013. <http://www.nasa.gov/pdf/327688main_09_SM4_Media_Guide_rev1.pdf>

[55] Uebelhart, Scott. "Non-Deterministic Design and Analysis of Parameterized Optical Structures during Conceptual Design." PhD Thesis. Massachusetts Institute of Technology. 2006.

[56] ""Modular Optical Space Telescope (MOST) Poster." Current Programs. Space Systems Laboratory, n.d. Web. 12 May 2013. <http://ssl.mit.edu/research/Posters/MOST_Poster_2006.pdf>.

[57] "How to Provide High-Resolution Vision," Review of Optometry, December 2006. [http://cms.revoptom.com/index.asp?ArticleType=SiteSpec&Page=osc/105418/lesson.htm. Accessed 5/8/13.]

[58] Masterson, R. A. "Development and Validation of Empirical and Analytical Reaction Wheel Disturbance Models." S.M. Thesis, Department Of Aeronautics and Astronautics, Massachusetts Institute of Technology, Cambridge, MA, 1999.

[59] Gutierrez, H. L. "Performance Assessment and Enhancement of Precision Controlled Structures During Conceptual Design." PhD Thesis, Department Of Aeronautics and Astronautics, Massachusetts Institute of Technology, Cambridge, MA, 1999.

[60] Sinha, K. and de Weck, O. "Structural Complexity Metric for Engineered Complex Systems and its Application," *14th International Design Structure Matrix (DSM) Conference*, 2012.

[61] Sternberg, D., et al., "A Bottom-up Modeling Approach for the Profit Analysis of Cellularized Spacecraft Architectures", *IAC-13 Congress,* Beijing, China, 2013. Abstract Accepted.

[62] Wertz, J., and Miller, D., "Expected productivity-based risk analysis in conceptual design," Acta Astronautica 59 (2006), 420-429.

[63] Keys, A. et al. (2008). Radition Hardened Electronics for Space Environments (RHSE) Project Overview. [PowerPoint slides]. Retrieved from Georgia Tech website: https://smartech.gatech.edu/bitstream/handle/1853/26381/97-168-1-PB.pdf?sequence=1

[64] Jun, I. (2009). Radiation Shielding Design: Protecting Electronics from the Environment. [PowerPoint slides]. Retrieved from NASA website: http://opfm.jpl.nasa.gov/files/N-Jun-Radiation%20Shielding1.pdf

[65] Hemmati, H., Free-Space Optical Communications at JPL/HASA. Retrieved from http://opticalcomm.jpl.nasa.gov/PAPERS/REVIEW/overview.pdf

[66] Cattrysse, Jill M. "Space Telescope Mission Design For L 2 Point Stationing."54 the International Astronautical Congress of the International Astronautical Federation(IAF). 2003.

[67]"Hubble Essentials: Quick Facts." *HubbleSite.org*. Web. 8 May 2013. <http://hubblesite.org/the_telescope/hubble_essentials/quick_facts.php>.

[68] Wall, Mike. "NASA's Huge New Rocket May Cost $500 Million Per Launch." *Space.com*., 12 Sept. 2012. Web. 08 Apr. 2013.

[69] "SpaceX Falcon." *SpaceX*., 2013. Web. 08 Apr. 2013.

[70] "Atlas V Product Card." *United Launch Alliance, LLC*. ULA, 2013. Web. 08 Apr. 2013.

[71] "Delta IV Overview." *Boeing: Defense, Space & Security*. Web. 10 Apr. 2013.

[72] "Delta IV - Specifications." *Delta IV - Specifications*. Andrews Space & Technology, Web. 10 Apr. 2013.

[73] de Weck O.L., Nadir W.D., Wong J.G., Bounova G. and Coffee T.M., "Modular Structures for Manned Space Exploration: The Truncated Octahedron as a Building Block", AIAA-2005-2764,

1st Space Exploration Conference: Continuing the Voyage of Discovery, 30 Jan - 1 Feb 2005, Orlando, Florida

[74] Overbye, D. "Refurbishments Complete, Astronauts Let Go of Hubble." New York Times

[75] Leone, D. "NASA Acknowledged James Webb Telescope Costs Will Delay Other Science Missions." Space News

[76] Morgan, D. "CRS Report for Congress – Hubble Space Telescope: NASA's Plans for Servicing Mission." Online. http://www.fas.org/sgp/crs/space/RS21767.pdf

[77] Hubble_SM4_Media_Guide_rev1. Online.

http://www.nasa.gov/pdf/327688main_09_SM4_Media_Guide_rev1.pdf

[78] Stockman, P. "James Webb Space Telescope (JWST)." Online. http://www.stsci.edu/jwst/doc-archive/presentations/JWST-STScI-000432.pdf

[79] Zagarola, M., "Demonstration of a Two-Stage Turbo- Brayton Cryocooler for Space Applications", International Cryocooler Conference, Boulder, CO, 2009. Online. https://www.google.com/url?sa=t&rct=j&q=&esrc=s&source=web&cd=9&cad=rja&ved=0CJQ BEBYwCA&url=http%3A%2F%2Fconferences.library.wisc.edu%2Findex.php%2Ficc15%2Fart icle%2Fdownload%2F234%2F234&ei=2YaFUevHINO54AOdkYH4Bw&usg=AFQjCNFSwKQ 6AgaApwO5JttDs5sb3Ttpyg&sig2=E3SuQJtTaCNnywMKzMm1wQ&bvm=bv.45960087,d.dm g

[80] CVI Melles Griot Technical Guide: Chapter 5: Optical Coatings. Online. http://www.cvimellesgriot.com/Products/Documents/TechnicalGuide/Optical-Coatings.pdf

[81] James Webb Space Telescope – Image Quality. *Space Telescope Science Institute.* Online. http://www.stsci.edu/jwst/ote/image-quality

[82] "James Webb Space Telescope – JWST Sensitivity" Space Telescope Science Institute. Available at http://www.stsci.edu/jwst/science/sensitivity. Prototype ETC available at http://jwstetc.stsci.edu/etc/.

GIUSEPPE CATALDO

Massachusetts Institute of Technology
Department of Aeronautics and Astronautics
Cambridge, MA 02139, USA

Phone: +1 617 253 9869
Fax: +1 617 258 8111
E-mail: gcataldo@mit.edu

EDUCATION

2012–present **Massachusetts Institute of Technology (MIT), Cambridge, USA**
PhD candidate in Space Systems Engineering, Minor: Space Policy

2010, Nov. **Institut Supérieur de l'Aéronautique et de l'Espace (ISAE) SUPAERO, Toulouse, France**
MSc in Aerospace Engineering (Highest Honor), Major: Aerodynamics, Minor: Automatic Controls

2010, Nov. **Polytechnic Institute of Turin, Italy**
MSc in Aerospace Engineering (High Honor), Major: Systems Engineering

2010, Oct. **Polytechnic Institute of Milan, Italy**
MSc in Aeronautical Engineering (High Honor), Major: Aerodynamics

2007, Jul. **Polytechnic Institute of Milan, Italy**
BSc in Aerospace Engineering (Highest Honors)

RESEARCH AND WORK EXPERIENCE

2012–present **Massachusetts Institute of Technology (MIT), Fellow Research Assistant**
Thesis proposal: The International Space Station as an observing platform for space astrophysics and Earth science
Other projects: Mission concept study of a lunar far-side radio observatory

2012–present **NASA Goddard Space Flight Center (GSFC), Research Scientist I**
1. **Micro-X**: Supervision of the installation, integration, and testing of the GSFC-supplied hardware at MIT, design of hardware components for the payload, launch operations
2. **Micro-Spec** for the SPace Infrared telescope for Cosmology and Astrophysics, **SPICA**
   Lead: Modeling of asymmetric resonator transmission data with complex baselines from non-ideal microwave resonant circuits applied to superconducting devices used for Micro-Spec
   Lead: Software development and testing for kinetic inductance parameter evaluation

2010–2012 **NASA GSFC, Research Associate Scientist**
1. **James Webb Space Telescope (JWST)**
   Analysis and reduction of noise data by modeling previously unmodelable noise sources, aimed at maximizing sensitivity of Near-Infrared Spectrograph (**NIRSpec**)
2. **Micro-Spec** for **SPICA**
   Lead: Design and optimization of an ultra-compact high-performance far-infrared spectrometer implemented on superconducting microstrip transmission lines
3. **Optical Properties of Astronomical Silicates with Infrared Techniques** (**OPASI-T**)
   Lead: Development and testing of advanced numerical tools for the computation, analysis, and interpretation of the dielectric functions of astrophysical dust analogs in the infrared

2010 **NASA GSFC, Visiting Scholar**
Performed research within the OPASI-T project

2009 **NASA GSFC and European Space Agency (ESA), Visiting Research Associate**
2009 NASA Academy, performed research within the OPASI-T and Odysseus projects

2007–2009 **Thales Alenia Space Italy, Polytechnic Institutes of Milan and Turin, Systems Engineer**
"Space Hotel Design" Multidisciplinary Project (pre-phase A)

PRIZES AND AWARDS

Sigma Xi, European Space Agency (ESA) Research Grants, John Mather Nobel Scholar Award, NASA Academy Award, Arthur Gelb Fellowship, Mayoux Dauriac Prize, Pegasus Award, High Polytechnic School Award, Top Industrial Managers for Europe (TIME) Excellence Scholarship, High Polytechnic School Excellence Scholarship, "You deserve more" Scholarship, Antonio Aquilino Prize, Eagle Scout

LEADERSHIP EXPERIENCE

NASA Leadership Development Training, NASA Academy Application Scoring & Interview Committees, NASA Academy Alumni Association Vice President of Operations, Public Outreach Lead for the Embassy of Italy to the USA

PROFESSIONAL ACTIVITIES AND SKILLS

Referee for peer-reviewed journal articles. Member of several professional associations. Fluent in: Italian, English, French, Spanish, German. Proficient in Windows, Linux, C, Fortran 77/90, Python, Visual Basic, MATLAB, Simulink, Solid Edge, XFoil, Microsoft Office, LaTeX. Violin and piano player, choir director, scuba diver, skier, swimmer.

PUBLICATIONS

Journal articles: 3 published, 1 submitted, 3 in preparation; 3 NASA technical reports; 25+ conference proceedings, papers, abstracts, and posters; 18 invitations for seminars, talks, interviews, TV shows; 15+ press releases in social media.

Mark Chodas

84 Gardner St, Apt. 7, Allston, MA 02134   Email: mchodas@gmail.com

Phone: (818) 395-4796   Citizenship: US

Career Objective

I'm interested in advancing the state of the art of systems engineering to enable more complex and cheaper missions.

Education

Massachusetts Institute of Technology – Cambridge, MA   **2008-2014 (anticipated)**

- S.B. in Aerospace Engineering - 2012
  - GPA: 4.7
  - Won the James Means Award for Excellence in Space Systems Engineering
- M.S. in Aerospace Engineering - 2014 (anticipated)
  - GPA: 4.5
  - NSTRF 2013 Fellow

School Project Experience

Instrument Systems Engineer – REXIS   **Fall 2011 – Spring 2013**

- Imaging X-ray spectrometer being built for the OSIRIS-REx mission
- Developed and managed the requirements tree and verification plans
- Developed and managed the instrument-level schedule
- Developed a detailed test plan for thermal-vacuum testing
- Developed a model for the science performance of a solar observing Silicon Drift Diode
- Developed the MEL/PEL/Risk Matrix and implemented processes for updates

6.270 Robotics Competition   **January 2012**

- MIT-wide robotics competition of autonomous robots made of LEGO with sensors, actuators, and a microcontroller that compete head to head
- Developed the movement and strategy code in C
- Won 1st place out of 24 teams

Work Experience

Intern – Jet Propulsion Laboratory, Pasadena, CA   **Summer 2012**

- Assisted the Europa Habitability Mission team develop and maintain SysML models
- Developed a Jython script to export SysML parametric diagrams as systems of equations to Mathematica to support automated PEL generation

Intern – Jet Propulsion Laboratory, Pasadena, CA   **Summer 2011**

- Studied global dust transport using data from the MISR instrument
- Developed a QVT script for extracting data from a SysML model and creating an input file for an FEA modeling suite

Papers

- Gunderson, A., and M. Chodas, "An Investigation of Cloud Cover Probability for the HyspIRI Mission using MODIS Cloud Mask Data", IEEE Aerospace Conference, March 5-12, 2011.
- Mercury, M., R. Green, S. Hook, B. Oaida, W. Wu, A. Gunderson, M. Chodas, "Global cloud cover for assessment of optical satellite observation opportunities: A HyspIRI case study," Remote Sensing of Environment, Volume 126, November 2012, Pages 62–71.

Technical Skills

Proficient In:

- Microsoft Office
- MATLAB
- SysML
- MagicDraw

Familiar With:

- Java
- C
- QVT

PRATIK K. DAVÉ

pdave87@yahoo.com

11 Douglass Street   Cambridge, MA 02139   (609) 876-6187

EDUCATION:

Massachusetts Institute of Technology   Cambridge, MA
S.M., Aeronautics and Astronautics   September 2012 - Present
Space Systems Laboratory   GPA: 5.0 / 5.0

University of Maryland   College Park, MD
B.S., Aerospace Engineering   Degree Awarded: May 21, 2009
Aerospace Honors, University Honors, Gemstone   GPA: 3.83 / 4.00

HONORS AND AWARDS:

Honor Societies	Sigma Gamma Tau - National Honor Society in Aerospace Engineering	Fall 2006
	Omicron Delta Kappa - National Leadership Honor Society	Fall 2008
	Tau Beta Pi - The Engineering Honor Society	Fall 2008
Awards	AIAA Undergraduate Scholarship Award	July 2007
	John Mather Nobel Scholars Award	July 2008

RESEARCH AND PROFESSIONAL EXPERIENCE:

MIT Space Systems Laboratory   Cambridge, MA
THERMAL ENGINEER, SYSTEMS ENGINEER   September 2012 - Present
- CubeSat Development Project - MicroMAS: Micro-sized Microwave Atmospheric Satellite
- Thesis Research - Analyses on the Operations and Design of a Microwave Radiometer CubeSat with In-situ Planetary Limb Calibration using GPS Radio Occultation
- Advisor - Dr. Kerri Cahoy, Assistant Professor in Department of Aeronautics and Astronautics, MIT

MIT Lincoln Laboratory   Lexington, MA
ASSISTANT STAFF, LINCOLN SCHOLAR   August 2009 - Present
- Research methods to improve the performance of precision orbit determination algorithms, create software to incorporate algorithmic improvements, and test algorithms against measurements
- Construct real-time data acquisition software for electro-optic sensors used for precision space tracking
- Model the performance of space tracking sensors and networks, validate models with field measurements
- Investigate impacts of adverse space weather on communications, sensing, and satellite navigation

UMD Department of Aerospace Engineering   College Park, MD
HUMAN FACTORS ENGINEER   October 2008 - May 2009
- Team Senior Design Project - Project Alshain: A Lunar Flying Vehicle for Rapid Universal Surface Access
- Advisor - Dr. David Akin, Associate Professor, Director of Space Systems Laboratory, UMD

Honeywell Aerospace   Lanham, MD
NASA GSFC SAWDRIP INTERN   June 2008 - December 2008
- Investigated correlations between historical space weather data, spacecraft orbital data, and known spacecraft anomalies using NASA ViSBARD visualization software (AIAA Region I-MA Student Conf, 2009)

Integral Systems, Inc.   Lanham, MD
PROCEDURE DEVELOPMENT INTERN   January 2008 - May 2008
- Developed commands and telemetry-integrated GUIs for satellite monitoring and ground operations

TECHNICAL SKILLS:
Windows + Linux OS, STK, CAD, MATLAB, C/C++, Scripting, Monte Carlo simulations, Thermal testing/modeling

Atray C. Dixit

70 Pacific Street, Apt 112C
Cambridge, MA 02139
Phone: 516-474-5612
acdixit@mit.edu

Current Position

Massachusetts Institute of Technology, Predoctoral Student
Harvard-MIT Health Sciences and Technology, PhD program in Medical Engineering Medical Physics
Speciality training in Bioastronautics. Funding: National Space Biomedical Research Institute Fellowship
Affiliations: Massachusetts General Hospital; Brigham and Women's Hospital, Broad Institute of MIT and Harvard

Education

2008–2012 Princeton, NJ	**Princeton University**, BSE in Mechanical and Aerospace Engineering magna cum laude, GPA: 3.67 Major GPA: 3.83 Certificates/Minors: Robotics, Materials, Engineering Biology

Recent Awards

2012	Lore von Jaskowsky Memorial Prize
2012	John Marshall II Memorial Prize
2012 & 2011	M. Tyler Campbell Trophy
2011	Morgan W. McKinsie '93 Senior Thesis Fund Award
2011	Academic All-Ivy

Recent Research Experience

1st Year PhD Lab Rotations, MIT/Harvard/MGH/BWH   Cambridge, MA; Sep 2012-
Research Lab for Electronics: Micron scale 3D protein printing. *Broad Institute of MIT and Harvard*: Developed computational pipeline to analyze RNA and ChIP-seq data in uncharacterized stem cell population.

Autonomous UAV Systems   Princeton, NJ and Cambridge, MA; 2011–
Spearheaded a team of four on a project to automatically control the flight path of an UAV using an onboard iPhone/Arduino microprocessor and a ground based laptop. Integrated autonomous UAV agents into a simulated airspace architecture.

Howard Stone, Complex Fluids Laboratory   Princeton, NJ; May 2010-2012
Investigated biomimetic viscoelastic wrinkling and folding similar to structures found on the leaves of plants. Thesis quantified relationship between fibroblast cell traction forces and initial cell culture density.

Wellman-HST Summer Institute for Biomedical Optics   Boston, MA; Jun-Aug 2011
Designed, automated (in LabVIEW), and calibrated a device to noninvasively measure the stiffness of tissue. Tested on human cancer samples as well as *in vitro* metastatic models. Worked with Professor Seemantini Nadkarni

Society Memberships

Sigma Xi, Materials Research Society, Biomedical Engineering Society, American Institute of Aeronautics and Astronautics

Journal Articles

Scott MA, Liu MC, Wu Y, **Dixit AC**, Yanik MF. Rapid Three-dimensional Laser Microprinting of Scaffolds Containing Internal Patterns of Proteins. Nature Communications (submitted May 2013)

Kim P, Abkarian M, **Dixit AC**, Stone HA, Dynamics of interacting folds under biaxial compressive stresses. Soft Materials (in prep, abstract APS 2013)

Conference Articles

Dixit AC, Falusi J, Kim S, Savit G, and Stengel RF. [Three articles] **1**. Development of an iPhone-controlled UAV, **2**. Flight Test of a UAV Operating in a Simulated Airspace, and **3**. Integration of UAV in Flight and Ground Operations. AIAA Infotech@Aerospace 2013.

Roy A, Steele L, Blanchard E, **Dixit AC**, and Wisnivesky J. The Association between Asthma Education and Use of Environmental Control Practices. 2010 Pediatric Academic Societies.

Other Experience

Technical Skills

Fabrication: Micro/nano fabrication techniques, CNC, machine shop skills (mill, lathe); **Computer**: MATLAB, LabVIEW, CAD Creo Elements, HTML, R, ImageJ, UNIX, Illustrator, Java, LaTeX; **Imaging Tools**: SEM, XRD, AFM, TEM, Confocal; **Aerospace**: Certified private pilot, experimental aircraft design, control systems, networked architectures **Languages**: Basic conversational knowledge of Italian and Gujrati

Leadership

Volunteer Instructor: MIT Museum; **Captain:** Princeton Varsity Sprint Football;
Co-Founder: Princeton Biomedical Engineering Society; **Co-President:** Princeton Materials Engineering Society

Sherrie Hall

shall6@mit.edu   70 Pacific St., Apt. 642B
706-713-6713   Cambridge, MA 02139

Education:
- Massachusetts Institute of Technology – Cambridge, Massachusetts
  - PhD, Aeronautics and Astronautics: 2016
  - GPA – 5.00
- Georgia Institute of Technology – Atlanta, Georgia
  - Master of Science in Aerospace Engineering: August 3, 2012
  - GPA – 3.88
  - Bachelor of Science in Aerospace Engineering, Highest Honors: May 8, 2011
  - GPA – 3.95
    - Honors Program, Music Certificate
- Cedar Shoals High School – College Preparatory Diploma
  - Overall GPA – 4.40, Valedictorian

Experience:
- MIT Man Vehicle Lab and Space Systems Lab – Graduate research as Systems Engineer for joint human and robotic geologic Lunar surface exploration. Coordinating with Skolkovo Tech.
- Caltech Space Challenge 2013 – Expedition ASAPH (Team Voyager). In five days, designed a detailed, feasible human mission to Phobos with robotic reconnaissance missions to Phobos and Demos
- University NanoSat Program 7 – Prox-1 Propulsion Team Lead, lead low-thrust propulsion design, test, and integration on Prox-1 satellite (Georgia Tech) through PQR. PROX-1 granted launch through AFRL. TERSat Science Payload Engineer, worked with design, test, and integration of the scientific payload (VLF transmitter and receiver) on the TERSat spacecraft (MIT) leading up to FCR.
- Boeing Satellite Development Center, El Segundo – Test Engineer. Summer intern working on the IntelSat program during the second Integration Verification Test and Environmental Build test phases of the first 702MP spacecraft, IS-22 (in orbit), and the next in line, IS-21
- Georgia Tech High Power Electric Propulsion Lab – Graduate research studying anomalous charged particle mobility in crossed electric and magnetic fields using magnetized ions to model trapped electrons Undergraduate research working with Helicon Hall Thrusters for spacecraft propulsion systems

Publications:
- *Expedition ASAPH,* Caltech Space Challenge, Team Voyager Final Report, Published online (2013)
- *Journal of the Stockholm Junior Water Prize*, *Radionuclides in the* Water Environment Federation, *Miocene Aquifers of Coastal Georgia* (2006)
- *Groundwater*, *Radionuclides in the Miocene Aquifers of Coastal Georgia* National Groundwater Association, (abstract) (2006)

Memberships and Volunteerism:
- Member of Phi Sigma Pi National Honor Fraternity, AIAA, Sigma Gamma Tau, Tau Beta Pi, SAME, National Society of Collegiate Scholars, Golden Key National Honor Society
- Co-leader of Girl Scout troop 12042 and member of Northeast GA Gold Award Committee
- Georgia Tech Oxford Summer Study Abroad Program, 2009
- Society of Women Engineers and Girl Scout engineering outreach volunteer
- GT Symphony Orchestra – first Violin fall 2007- fall 2010 (second violin fall and spring 2009)

Competencies: Matlab, Solid Edge, Autocad, Mathematica, STK 8/9, Microsoft Office, Space Propulsion, Satellite Systems, Human Factors, Systems Engineering, Integration and Testing, collaborative team design projects

Awards:
- National Science Foundation Graduate Research Fellowship
- President's Fellowship (Georgia Tech)
- David C. Garret President's Scholar (Georgia Tech)
- Points of Light National Community Service Award – Bronze, 2006; Silver, 2007; Bronze, 2008
- Girl Scouts of the USA Social Responsibility Award, 2009
- Boeing Scholar
- Georgia Engineering Foundation Scholarship – 2007, 2008, 2009, 2010
- Girl Scout Gold and Silver Award Recipient

ROBERT (ROBBIE) J. HARRIS, JR.
3278 Patterson Drive
Pearl, MS 39208
769-226-4102
robbie.harris@sloan.mit.edu

EDUCATION

MASSACHUSETTS INSTITUTE OF TECHNOLOGY   Cambridge, MA
Leaders for Global Operations (LGO) Fellow   2012 - Present
Candidate for MBA, MIT Sloan School of Management, June 2014
Candidate for SM, Aeronautics and Astronautics (Space Systems Focus), MIT School of Engineering, June 2014
- New Student Recruiting Committee; Web Forums Sub-committee Co-chair; InterviewFest Sub-committee Co-chair
- LGO Seminar Committee

GEORGIA INSTITUTE OF TECHNOLOGY   Atlanta, GA
BS in Mechanical Engineering   2006 – 2007
- Recipient of Shell scholarship for students selected by dean

UNIVERSITY OF MISSISSIPPI   Oxford, MS
BBA in Management (Behavioral Focus), magna cum laude   2001 - 2005
- President of Alpha Kappa Psi Professional Business Fraternity, Rho Tau Chapter
- Re-founding Father of Delta Kappa Epsilon Fraternity, Chi Chapter

EXPERIENCE

EATON – AEROSPACE DIVISION   Jackson, MS
Senior Project Engineer (promoted from Project Engineer)   2008 - 2012
Leadership and Teamwork
- Led $500K design and development for business jet reservoir while maintaining 99% on-time milestone completion
- Coordinated design and test activities with major corporate customers to maintain "green" customer ratings
- Managed qualification testing efforts for multiple aerospace hydraulic components to fulfill FAA requirements
- Directed 10 technical professionals to accomplish project objectives to support delivery schedules
- Volunteered to lead 6S implementation initiative in office area of 100 employees

Innovation and Strategy
- Created reservoir design tool to streamline and standardize work, making future effort weeks shorter and error-proof
- Taught workshop on optimal reservoir design to build strategic organizational capability that would allow Eaton to progress from proposing components to proposing systems
- Developed design concepts and budgets for proposed hydraulic components to aid in capture of $100M contract
- Investigated and advocated new sub-component supplier to facilitate improved reservoir design for savings of $4M
- Performed research to develop appropriate product requirements, eliminating unnecessary design and testing
- Completed Design For Six Sigma (DFSS) Green Belt training to learn robust, efficient design process

HONEYWELL – AEROSPACE & DEFENSE DIVISION   Torrance, CA
Project Engineer   2007 - 2008
- Oversaw $400K testing effort for proposed cooling systems to prove feasibility in new airliner
- Generated and tracked detailed budgets and schedules for $4.9M project to maintain accountability
- Designed test plans to efficiently demonstrate specifications and simulate service conditions
- Supervised project work for lab engineers and technicians to meet all testing milestones
- Authored test reports based on experimental results to support innovative system proposal
- Defined key design parameters for supplemental cooling and turbomachinery systems by analyzing requirements

CATERPILLAR   Oxford, MS
Intern   Fall 2005
- Constructed new quality-tracking system based on stakeholder input and product research to allow for automated statistical process control
- Recruited peers to aid with quality-tracking system installation to facilitate setup for entire plant within 3 months

ACTIVITIES AND INTERESTS
- Speaker and small group leader for Kairos Prison Ministry
- Co-chair of Missions committee for St. Mark's United Methodist Church, Brandon, MS (2010 – 2011)
- Lead for company relay team in the Mississippi Blues Marathon
- Hobbies: family time, reading, triathlon, weight training, travel

Fernando Mier Hicks

550 Memorial Dr. APT 17B2
Cambridge, MA 02139

E-mail: fernandomierhicks@gmail.com
Research webpage: fernandomierhicks.blogspot.com

EDUCATION

2012-present   Massachusetts Institute of Technology.

S.M Aeronautics and Astronautics. Space Propulsion Laboratory. Graduating December 2013

2007-11   Monterrey Institute of Technology and Higher Education.

Mechatronics engineer, graduated with honors.

EXTRACURRICULAR ACTIVITIES AND AWARDS

2012   Recipient of CONACYT scholarship.

2012   Appearance in MIT news, Popular Science website and others.

2012   Best mechatronics Engineer graduate award by ANFEI.

2011   1st place on national robotics competition "Robochallenge Advanced 2011".

2011   Recipient of Roberto Rocca Fellowship.

2010   1st place on regional line-follower robot competition "Robochallenge 2010".

2010   Prominent Mechatronic student 2010 award.

2010   1st place on national robotics competition, "Robochallenge Advanced 2010".

2009   1st place on regional robotics competition "I bet you can't 2009".

2009   Suspension analysis of the ITESM FormulaSAE car in CAD software.

2009   Member of student associations AEAGS, Mechatronics Congress and Compromiso.

2008   Team leader of electric Go-Kart design competition "Electrathon" representing ITESM.

RESEARCH EXPERIENCE

2011   Four month internship at **Willow Garage**, a revolutionizing robotics company based in Sillicon Valley. The project focused on a new successful underactuaded adaptive gripper design

2011   Summer research internship at **Massachusetts Institute of Technology** in the Space Propulsion Laboratory, under the guidance of Dr. Paulo Lozano.

2010   Summer research internship on planetary robotics with **Carnegie Mellon University** team pursuing the Google Lunar X prize, under the leadership of Dr. Red Whittaker.

PUBLICATIONS

Matei C, Hicks F, Stanford S.," Kinetic and Dimensional Optimization for a Tendon-driven Gripper " 2013 IEEE International Conference on Robotics and Automatitation. ICRA

Perna, L. E., Hicks, F. M. (2012) Progress Toward Demonstration of Remote, Autonomous Attitude Control of a CubeSat Using Ion Electrospray Propulsion Systems. 48th AIAA/ASME/SAE/ASEE Joint Propulsion Conference

CHRISTOPHER MICHAEL JEWISON

Current Address:	*Permanent Address:*	*Contact Information:*
70 Pacific Street, #839B	103 Horizon Drive	jewisonc@mit.edu
Cambridge, MA 02139	Venetia, PA 15367	Cell: (724)-986-9048

Education

Massachusetts Institute of Technology, Cambridge, MA   *September 2012 – May 2014*
Candidate for Master of Science in the Department of Aeronautics and Astronautics

Cornell University, Ithaca, NY   *August 2008 – January 2012*
B.S. in Mechanical Engineering, summa cum laude
3.95/4.0 cumulative GPA

Peters Township High School, McMurray, PA   *August 2004 – June 2008*
4.46/5.0 cumulative GPA – Graduated Valedictorian

Previous Work, Research and Leadership Experience

Space Systems Lab, Research Assistantship, MIT   *September 2012 – present*

- Researching resource aggregated reconfigurable control under the support of Professor David Miller
- Developing the hardware and software to expand the SPHERES experimental satellite testbed on the International Space Station to allow for the research of robotic servicing, assembly and repurposing

Space Systems/Loral, Sr. College Co-op Technical Intern, Palo Alto, CA   *August 2010 – August 2012*

- Worked in the Systems Mechanical department of the Spacecraft System Engineering organization
- Streamlined the process of analyzing deployment shock data to qualify satellites' parts for flight
- Served as systems floor support for the duration of a spacecraft's dynamics testing phase

Flux Pinning Research Team, Structural Lead, Space Systems Design Studio   *May 2010 – May 2012*

- Researched the feasibility of docking and reconfiguring nano-sat modules through the use of flux pinning interfaces under the guidance of Associate Professor Mason Peck and a graduate student team
- Designed and built mock-up nano-sat modules and test equipment as lead of the structures sub-team

CUAir – Project/Design Team, Airframe Lead, Cornell University   *February 2010 – June 2012*

- Dedicated to the development and systems integration of an autonomous intelligence seeking airplane
- Designed and constructed the airplane as the lead of the mechanical engineering sub-team
- Placed 2nd overall and 1st in the mission portion of the AUVSI Student UAS competition in June 2012

Fluid Dynamics Research Lab, Energy Group, Cornell University   *August 2011 – May 2012*

- Investigated the effects of design parameters on the efficiency of lift based, vertical-axis wind turbines for energy harvesting in a small scale, urban environment under the guidance of Professor C.H.K. Williamson
- Developed a theoretical model and computer simulation to predict turbine performance
- Fabricated and experimented on prototypes to determine the optimal configuration for power generation

Skills

<u>Computer:</u>	SolidWorks – Pro E – ANSYS – FLUENT – C – MATLAB – VBA
<u>Hands-on:</u>	Design lab, machine shop, soldering, experimental design and testing
<u>Language:</u>	German (intermediate writing and speaking)

Memberships and Awards

Member of American Society of Mechanical Engineers (ASME)
Member of American Institute of Aeronautics and Astronautics (AIAA)

Engineering Learning Initiative Grant (2011), College of Engineering, Cornell University
Frank O. Ellenwood Prize (2012), Sibley School of Mechanical and Aerospace Engineering, Cornell University

Ioana JOSAN-DRINCEANU

Address	70 Pacific Street, Apartment 204, 02139 Cambridge, MA, USA
Mobile	(+1) 617 – 583 2385
Email	ijosand@mit.edu
Nationality	Romanian
Date of birth	July 9, 1986

Objective

My goal is to actively contribute to the advancement of Environmental Control and Life Support Systems (ECLSS) technology so that humans can be sustained in space for longer periods of time. This would allow astronauts to explore even farther destinations from Earth and enrich our understanding of the Universe.

Education

2012 – present PhD candidate in Aeronautics and Astronautics, MIT (Massachusetts Institute of Technology), USA
- Main research direction in the field of Environmental Control and Life Support Systems (ECLSS) for human space habitats

2009 – 2011 Master studies in Electrical Engineering, EPFL (Swiss Federal Institute of Technology, Lausanne), Switzerland
- Major specialization in electronics and microelectronics
- Admitted with an excellence scholarship for 2 years
- Minor specialization in space technologies at the Swiss Space Center

Selected projects

September 2012 – January 2013 Model-based amphibious racing challenge (MBARC)
- Aeronautics and Astronautics department, MIT, "Fundamentals of Systems Engineering" class
- Participated in the DARPA MBARC competition: I was part of the MIT team challenged to build an amphibious vehicle, I was in charge of the electrical systems for our vehicle, we won the first place in the final competition at Camp Pendelton, San Diego, CA in January 2013.

November 2010 – December 2011 Gravity Gradient Earth Sensor (GGES) REXUS experiment
- Swiss Space Center, EPFL and Microsystems for Space Technologies Laboratory, EPFL
- As part of the team that was selected by ESA to participate in the REXUS program (Rocket Experiments for University Students), I was in charge of the hardware and software design of the payload boards of this experiment. The goal of GGES was to test a MEMS attitude determination sensor. The payload boards are responsible for MEMS sensor and inertial data collection. This was the topic of my Master thesis (which took place from February 2011 to July 2011).

Additional training

- Radioamateur HB9 licence
- C, C++, LabVIEW, LaTeX, basic VHDL, VHDL-AMS

Languages

English, German, French, Romanian

References available on request

ANDREW OWENS

235 Albany Street #1026B, Cambridge, MA 02139
(t) 678-358-0458, (e) acowens@mit.edu

EDUCATION

Massachusetts Institute of Technology, Cambridge, MA
Master of Science in Space Systems (Advisor: Prof. Olivier de Weck), September 2012-Present
GPA: 5.00/5.00
Rice University, Houston, TX
Bachelor of Science in Mechanical Engineering, Graduation May 2012
GPA: 3.80/4.00 (*cum laude*)
University of Technology – Sydney, Sydney, NSW, Australia
Semester abroad Fall 2009

MASTER'S THESIS TOPIC

Investigation into component failure impact analysis, reconfigurability, and failure recovery in Environmental Control and Life Support Systems; specifically, modeling of the effect of component failure on system functionality and determination of potential reconfigurations for full or partial function recovery.

RELEVANT SKILLS

- *Design Experience*: Team Leadership, Project Planning, Budgeting, Fundraising, Requirements Definition, Concept Generation/Evaluation, Modeling, Prototyping, Fabrication, Testing and Analysis, Technical Writing and Presentation, Troubleshooting, On-Site Repair and Reconfiguration
- *Software*: SolidWorks, Autodesk Inventor, Pro/ENGINEER, Creo Elements/Pro, Windchill, MATLAB, LabVIEW, LaTeX, Microsoft Office, ImageJ, OriginPro. Familiar with Windows and Macintosh operating systems.

RECENT EXPERIENCE

Strategic Engineering Research Group, MIT, Cambridge, MA, 2012-Present
HabNet Research Team Member, 2012-Present
- Collaborated with 3 other team members under Prof. Olivier de Weck to develop generalized modeling environment for space habitat environmental control and life support system (ECLSS) architectures
- Utilized Object-Process Methodology to perform a functional decomposition of ECLSS
- Developed method for decomposition into modular, interchangeable systems to enable the rapid investigation and characterization of various technology choices
- Interfaced with Mars Surface Strategy Team at Johnson Space Center for project guidance and NASA input
- Developed framework for modeling of spacecraft and habitat thermal control systems
- Researched historical, current, and proposed life support technologies
- Implemented framework using the Extravehicular Mobility Unit (EMU) ECLSS as a case study
- Developed flexible MATLAB/Simulink modeling techniques for simulation of ECLSS architectures

Rice University Solar Car Team, Rice University, Houston, TX, 2010-2012
Co-Founder and President, 2010-2011; Presidential Advisor 2012
- Created largest student-led engineering design project at Rice to build Rice's first solar car
- Placed 2nd in the solar power division at the Shell Eco-Marathon 2012
- Coordinated fundraising efforts, contacting 15-20 companies and applying to grants to raise over $85,000
- Planned and led 1 semester, 4 credit design class offering course credit to 28 students for solar car design work
- Recruited over 100 team members from all academic years and more than 10 disciplines
- Recruited advisory board of 5 faculty members and 1 industry expert
- Proposed 2 solar-car based senior design projects for capstone design class, recruited faculty sponsors, and presented to over 150 mechanical, electrical, and bioengineering students
- Drafted club constitution and formed official Rice club
- Corresponded with faculty, administration, and students to generate support

PUBLICATIONS AND AWARDS

- "Increasing the Efficiency of Single Walled Carbon Nanotube Amplification by Fe-Co Catalysts Through the Optimization of CH4/H2 Partial Pressures" by Alvin W. Orbaek, Andrew C. Owens, and Andrew R. Barron (*Nano Letters,* 2011)
- MIT Odge Diversity Award, Spring 2013
- MIT Lemelson Minority Engineering Presidential Fellowship, Fall 2012
- Rice University Outstanding Senior Mechanical Engineering Student Recognition Award, 2012
- Leadership Rice Director's 11 (Student Advisory Board) Member, 2011-2012
- National Merit Rice University Scholarship, 2008-2012

Eric D. Peters

92 Webster Ave, Cambridge, MA 02141 • e_peters@mit.edu • 617.401.7437

Education

Massachusetts Institute of Technology, Cambridge, MA — June 2014 (Expected)
Candidate for Master of Science in Aerospace Engineering
Research Assistant in Space Systems Laboratory under Prof. David Miller

Massachusetts Institute of Technology, Cambridge, MA — June 2011
Bachelor of Science in Aerospace Engineering
GPA: 4.2/5.0

Relevant Courses

Space Systems Engineering, Satellite Engineering, Space Propulsion, Structural Mechanics, Dynamics, Computational Methods, Aerodynamics, Principles of Automatic Control, Thermodynamics, Fluid Mechanics

Experience

Graduate Researcher – MIT Space Systems Laboratory — May 2012 – Present
Massachusetts Institute of Technology — Cambridge, MA
- Supporting hardware fabrication, integration, and testing for MicroMAS picosatellite in preparation for flight hardware delivery
- Matured structural truss and electronics box designs of REXIS X-ray Spectrometer to PDR level
- Research interests include structural modeling and early-stage design optimization

Research Specialist – MIT Space Systems Laboratory — July 2011 – May 2012
Massachusetts Institute of Technology — Cambridge, MA
- Lead structural engineer for REXIS X-ray Spectrometer
- Structural design/test lead for MicroMAS, including leading vibration and thermal-vacuum tests.
- Designed motor to facilitate rotation of MicroMAS payload in vacuum environment
- Served as mechanical/structures mentor to undergraduate students in Space Systems Engineering class.

Undergraduate Researcher – MIT Space Systems Laboratory — February 2010 – May 2011
Massachusetts Institute of Technology — Cambridge, MA
- Responsible for design and structural analysis of components for CASTOR nanosatellite.
- Redesigned structural trusses to comply with CDR feedback and matured hardware design for University Nanosatellite Program flight competition review (FCR)
- Instrumental in fabrication and assembly of Engineering Test Unit.

Student Investigator – MIT Man Vehicle Laboratory — September 2009 – May 2010
Massachusetts Institute of Technology — Cambridge, MA
- Developed an experiment to test the metabolic implications of varying the stiffness of a space suit ankle joint.
- Designed and fabricated ankle joint exoskeleton for use in experiment.
- Conducted experiment on human subjects.

Undergraduate Researcher – Mars Gravity Biosatellite Program — September 2008 – June 2009
Massachusetts Institute of Technology — Cambridge, MA
- Developed experiment to assess effectiveness of exiting Waste Collection System hardware in microgravity.
- Fabricated test equipment and conducted experiment onboard a parabolic research flight.

Robotics Phase II Teacher — July 2008
Peddie Summer Science Institute — Hightstown, NJ
- Taught a hands-on, intermediate-level robotics class to 15 high school juniors that focused on completing several team-based, competitive challenges intended to teach the basics of gear ratios, motorized steering, variable-speed transmissions, and autonomous control.

Activities

Rocket Team: Developing numerical simulation to aid in the development of liquid-fueled rocket engines.

Skills

Computer-Aided Design: SolidWorks, Kubotek KeyCreator
Structural Analysis: Ansys Workbench, Femap, NEi Nastran
Programming: Java, MATLAB, Unix, HTML
Mechanical: Skilled in the operation and programming of CNC mills, lathes, and OMAX Water Jet Machining Centers

Publications

- Peters, E. D., Corbin, B. A., and Kendrick, D. P., "Validating Waste Collection System Hardware Developed for the Mars Gravity Biosatellite Program Aboard a Parabolic Research Flight," *AIAA Region I-NE Student Conference*, AIAA, Boston, MA, 2010.
- Blackwell, WJ, et al. 2012. "Nanosatellites for Earth Environmental Monitoring: The MicroMAS Project," *Proceedings of the AIAA/USU Conference on Small Satellites*, The Horizon, SSC12-I-2.

MARGARET M. SHAW

Apt. 810, 70 Pacific Street, Cambridge, MA 02139 (U.S. Citizen) | mmshaw@mit.edu | (908) 500-0252

EDUCATION

Massachusetts Institute of Technology, Cambridge, MA   **August 2012-Present**

S.M. Candidate, Aeronautics and Astronautics
GPA: 5.0/5.0

Princeton University, Princeton, NJ   **September 2008-June 2012**

B.A. Astrophysics; Certificate in Planets and Life
High Honors

PUBLICATIONS

- *"A Modeling Approach for the Profit Analysis of Cellularized Spacecraft Architectures"*, IAC 2013 Conference

- *"Measuring NIR Atmospheric Extinction Using a Global Positioning System Receiver,"* Blake, C.H. and **Shaw, M.M.** 2011, *PASP*, 123, 1302

- *"The Nyquist-Shannon sampling theorem and the atomic pair distribution function,"* Farrow, C.L., **Shaw, M.M.**, Kim, H., Juhas, P., and Billinge, S.J.L. 2011, *Phys. Rev. B*, 84, 13

HONORS AND MEMBERSHIPS

- NSF Graduate Research Fellowship (2012-2015)

- Donald W. Douglas Fellowship (2012-2013)

- Sigma Xi, American Institute of Aeronautics and Astronautics

- AT&T Foundation Scholarship and William H. Cane Scholarship (2008-2012)

RECENT RESEARCH EXPERIENCE

Strategic Engineering Research Group, Aeronautics & Astronautics Dept., MIT   **August 2012-Present**

- Research Area: Environmental Control and Life Support Systems (ECLSS) for Deep Space Habitation.
  Thesis advisor: Prof. Olivier de Weck

- Developing HabNet, an integrated framework for architecting and modeling crewed habitation systems. Physicochemical and bioregenerative technologies as well as in-situ resource utilization methods are considered.

- S.M. topic (tentative): investigating the optimal use of physicochemical and bioregenerative technologies for long-duration, nearly closed ECLSS. A trade is expected to exist between complexity and robustness of partial ecosystems.

Electric Propulsion and Plasma Dynamics Lab, Mech./Aero. Engineering Dept., Princeton Univ. **Fall 2011-Spring 2012**

- Senior thesis project entitled *A Novel Thrust Measurement Method For Plasma Rockets With Magnetic Nozzles Using B-field Measurements.* Advisors: Profs. Edgar Choueiri (Mech./Aero. Engineering Dept.) & Jeremy Goodman (Astrophysics Dept.).

- Developed a way to measure the thrust produced by high-power plasma propulsion devices that employ magnetic nozzles (e.g., VASIMR). The B-field thrust measurement method indirectly determines the thrust by measuring the perturbations to the magnetic field due to the accelerated plasma in the vicinity of the magnetic nozzle.

COMPUTER SKILLS

Experience with UNIX operating systems. Programming experience in Matlab, Simulink, LabView, IDL, Java, Python, SM, Fortran, C, and Mathematica. Extensive experience using Object Process Methodology (a functional/formal decomposition tool). Experience with emacs and Latex text editors. Familiar with the Satellite Toolkit for orbital maneuver design.

LEADERSHIP AND ACTIVITIES

Massachusetts Institute of Technology
Co-President, Graduate Association of Aeronautics and Astronautics; Presenter, MIT Women's Initiative; Co-Coordinator, Sidney Pacific Inter-Cultural Exchange; Graduate Women at MIT; Women's Club Soccer

School Address   **David Sternberg**   *Home Address*
70 Pacific Street   davister@mit.edu   835 Springbank Lane
Cambridge, MA 02139   (610) 420-6425   Wayne, PA 19087
US Citizen

Objective: To obtain a challenging position in the aerospace field to enhance my knowledge of space systems.

Education: **Massachusetts Institute of Technology**   Cambridge, MA
Candidate for Master of Science in Space Systems Engineering in the Space Systems Lab   June 2014
Structural and Systems researcher for ARMADAS, MEDUSA, and PHOENIX Projects; Research Assistantship
Thesis Area: Use of fully autonomous satlets for on-orbit servicing and assembly.
Bachelor of Science in Aerospace Engineering, *Minor* in Science, Technology, and Society   June 2012
Graduate GPA: 5.0/5.0
Undergraduate GPA: 4.8/5.0   Merit Scholarship

The Haverford School   Haverford, PA
Cum Laude Society, GPA: 4.2/4.3-unweighted   June 2008

Experience: **Boeing Company**   Ridley Park, PA
Engineering Designer for Chinook Programs   Summer 2012
Redesigned in CATIA V5 M60 machine gun pintle mounts for the MH-47G to accommodate the conversion to machined frames. Created a revision history for the UK Mk6 Interior stencils and marking stickers to determine which were placed incorrectly on the aircraft or on the engineering drawings themselves.

NASA Jet Propulsion Laboratory   Pasadena, CA
Comet Sample Return Prototyper, Tester, and Analyst   Summer 2011
Developed, tested, and analyzed new Comet Sample Return tools for a 2014 JPL mission. Created comet simulant and comparatively tested the performance of prototyped tool design with existing technologies. Machined several tools after creating SolidWorks models for each. Led to data collection and analysis for paper and proposal writing.

SPHERES Team, MIT   Cambridge, MA
Engineering and Machining UROP; Zero Robotics Researcher; Fluid Slosh Researcher   January 2009-Spring 2012
Provided the mechanical support by CAD modeling and machining improved battery holders, expansion port covers, and docking mechanisms to further their mission capabilities on the International Space Station. Led two teams to develop several new game designs for Zero Robotics STEM competitions. Co-wrote a white paper for LEGO designing, programming, and testing. Developed a Fluid Slosh system in collaboration with FIT and ERAU. *Total of Nine UROP opportunities*.

Piasecki Aircraft Corporation   Essington, PA
UAV Flight Research Intern   Summer 2010
Led the development work on FCS Class II and III UAVs. Removed slop, improved engine performance, and lightened body components. Designed, manufactured, and tested new components.
Summer Research Intern   Summer 2007
Video recorded test flights, assisted in resource procurement, and enhanced documentation and cataloguing of project plans and components on the X-49A Speedhawk. Led to ahead of schedule card completion.

Washington Naval Station   Washington D.C.
NAVSEA Intern, Interim SECRET Clearance   January 2010
Calculated and analyzed the loads applied to helicopter tiedowns to reduce radar signature of DDG-1000 destroyers. Assisted in testing of a LIDAR anemometer. Supported the systems engineering of the boat handling system.

Leadership/Activities:
- MIT Associate Advisor with Prof. Miller – advise seven freshmen with their coursework and MIT life 2011-Present
- MIT Unified Grader and Lab TA- Grade 54 students' assignments weekly and lab Teaching Assistant   2010-12
- MIT Rocket Team Payload Section Lead / MIT UAV Team   2010
- First Place Team in GE Challenge, GE Intern for a Day, Third Place Team in Unified Flying Competition   2010
- Volunteer at the American Helicopter Museum, West Chester, PA running their flight simulator for   2007-08
  visitors. Taught the basics of helicopter flight to 25+ people per day, six year olds and up.

Memberships:
Tau Beta Pi- MIT Chapter, Aircraft Owners and Pilot Association, Aero Club of PA, Experimental Aircraft Association-Chapter 106, MIT Aero Club, American Institute of Aeronautics and Astronautics, National Society of Collegiate Scholars

Skills and Awards:
- Microsoft Office; C, JAVA; MATLAB; LabView; SolidWorks; CATIA V5; Altium V5; DWG TrueView; Machine Shop manufacturing; Design, build, and launch model rockets and aircraft; Engineering Release, Defective Material Report, and Mylar drawing creation; NAUI scuba diver, 200 hour Complex Private Pilot since July 25, 2008
- Aero Club of PA Bob Shannon Scholarship, Drexel University Book Award; William Wallace Prize; Rensselaer Polytechnic Institute Medal; D.A.R. History Prize; Latin Honor Society; John C. Lober Prize in Mathematics; Barton Sensenig Science Prize; The Federal Reserve Bank of Philadelphia Prize in Economics

Publications and Invited Talks:
- "A Modeling Approach for the Profit Analysis of Cellularized Spacecraft Architectures", IAC 2013 Conference
- SPHERES: An ISS Facility for Control Algorithm Development; Lecture to NSCU Commercial Space Club, Jan. 2012

KATHLEEN VOELBEL

134 3rd Street #1, Cambridge, MA 02141 • Cell: 386-479-3402 • email: kathleen@sdm.mit.edu

EDUCATION

Massachusetts Institute of Technology, Cambridge, MA
School of Engineering and Sloan School of Management; System Design and Management Fellow
Master of Science in Engineering and Management   February 2014

Bachelor of Science in Aerospace Engineering with Information Technology   2007

EXPERIENCE

MIT Humans and Automation Laboratory (HAL), Cambridge, MA   February 2012-Present
Research Assistant

- Design interactive moving map for locomotive engineers to aid Situational Awareness and decision-making en route using human factors methods
- Supervise software development of working prototype for usability studies and experimental testing in train simulators
- Present and report progress and findings to Federal Railroad Administration (FRA) sponsors

United States Air Force Reserve (USAFR), Huntsville, AL   2011-Present
USAFR Modeling and Simulation Project Lead (Part Time)

- Develop performance analysis models incorporating Computational Fluid Dynamics (CFD) coefficients with potential savings of $450K per system
- Identify and implement solutions from other domains resulting in 6x process and schedule improvement
- Lead kick-off of tri-service, multi-agency project by developing innovative prioritization approach

Raytheon Integrated Defense Systems (IDS), Andover, MA   2007-2012
Lead - System Test Interoperability (2010-2012)

- Aligned technical and logistical requirements for military tactical communications for multi-million dollar flight tests
- Interfaced with multiple government agencies including customers (government program offices)

Representative - System Test customer interface to Integrated Product Team (IPT) (2009-2012)

- Managed IPT test strategies and execution by comparing system-level and sub-system level requirements as stakeholder, approval authority and direct customer for requirements sell-off

Manager - Government Furnished Equipment (GFE) (2008-2009)

- Negotiated agreement to receive a high-demand, program-critical item on loan from the Air National Guard to off-set 3 months of schedule risk
- Maintained accountability for GFE and Communications Secure (COMSEC) equipment valued at over $2.6 million

Engineer - System Integration, Test and Whole Life (2007-2008)

- Lead the time-critical retrofit effort of a deployed system in order to prevent down time and safety hazards of a persistent surveillance system

United States Army National Guard, Cambridge, MA   2007-2011
Company Executive Officer (Part Time) (2010-2011)

- Led 74 enlisted soldiers and 13 officers as second in command to fulfill short-term and long-term mission requirements
- Oversaw maintenance program consisting of over $500K of sensitive items
- Addressed mental health, medical and financial solider issues and mentored junior officers

Platoon Leader, Assistant Platoon Leader & Tactical Intelligence Officer (Part Time) (2007-2010)

- Awarded Army Commendation Medal for reinventing unit's security clearance processing, increasing unit medical readiness from 8% to 60% and organizing esprit de corps training

ADDITIONAL INFORMATION

- **Programming Languages**- MATLAB, Objective C, Simulink
- **Publications-** A Foot Placement Planning Algorithm for a Walking Quadruped, AIAA
  Infotech@Aerospace Conference (co-author/co-presenter)
- **Security Clearance-** Active DoD clearance

MARCUS WU SHIHONG

Massachusetts Institute of Technology, Master of Science in Technology and Policy, Master of Science in Aeronautics and Astronautics
235 Albany Street #2027B, Ashdown House, Cambridge, MA 02139
marcuswu@mit.edu | 917 982 4951

EDUCATION

2014   **MASSACHUSETTS INSTITUTE OF TECHNOLOGY**   Cambridge, MA
Master of Science in Technology and Policy, Master of Science in Aeronautics and Astronautics
- Research at MIT Systems Engineering Advancement Research Initiative (SEAri):
  - Application of tradespace exploration methods in designing for affordability in aerospace systems
  - Professional Publication: "Enabling Design for Affordability: An Epoch-Era Analysis Approach" (2013)
- Classes: Satellite Engineering, Space Systems Engineering, Engineering Apollo, Science Technology and Public Policy, Modeling and Assessment for Policy, Law Technology and Public Policy, Microeconomics
- Leadership activities: President of Singapore Student Society, Social Officer in graduate dormitories,

2012   **IMPERIAL COLLEGE LONDON**   London, United Kingdom
Bachelors of Engineering in Electrical & Electronic Engineering (1st Class Honors)
- Academic Achievements: Nujira Prize for Outstanding Final Year Project (2012)
  Engineering Dean's List (2010, 2011, 2012)
- Classes: Communications, Control Systems, Energy Systems, Signal Processing, Electronic Devices, Analogue and Digital Electronics, Computer Architecture, Algorithms, Finance Management
- Group Projects: Design of an 'EEBug': an electronic toy car that is activated by sound (2010), Assessing the feasibility of implementing piezoelectric flooring in London Underground stations (2011)
- Individual Final Year Project: 'Memristor Modeling Optimization' (2012)
  - Developed a software model that predicts behavior of memristors developed within Imperial College London and proposed applications of memristor technology in neuromorphic applications
  - Professional Publications: "Modeling of Current Percolation Channels in Emerging Resistive Switching Elements" (2012), "Computing Shortest Paths in 2D and 3D Memristive Networks" (2013)
- Leadership Activities:
  - Talent Manager, AIESEC Imperial (*Association Internationale des Étudiants en Sciences Économiques et Commerciales*): Organized activities and leadership tournaments for UK colleges
  - Investment Club, Electrical Engineering Society, Singapore Society, Fellwanderers

EXPERIENCE

2011, 2009   **DEFENCE SCIENCE & TECHNOLOGY AGENCY (DSTA)**   Singapore
Scholar Intern (Guided Weapons and Armaments Program Centre, Naval and Land Systems Division)
DSTA provides leading-edge technological solutions to the Singapore Armed Forces (SAF)
- Did two internships spanning 6 months and 3 months in 2009 and 2011 respectively
- Awarded Certificate of Excellence for outstanding performance on both internships
- 2009 Project: 'Unmanned Aerial Vehicles (UAV) for naval platforms'
  - Managed the acquisition and development of naval UAVs for the Republic of Singapore Navy (RSN)
  - Assessed performance of naval UAVs during sea trials for RSN landing ship tanks and stealth frigates
  - Evaluated electromagnetic interference and compatibility of UAV with shipboard electronics
- 2011 Project: 'Evaluation of search and recovery methods in asset tracking and monitoring'
  - Conducted in-depth research into asset search and recovery techniques in military settings
  - Analyzed feasibility of solutions leveraging on Radio Frequency Identification (RFID) technology
  - Proposed system operation concept and future scope of development to senior management

2007-2008   **SINGAPORE ARMED FORCES**   Singapore
Combat Medic Specialist, Headquarters Medical Corps (SAF HQ MC)
- Completed courses and trained personnel in frontline medical care, resuscitation and evacuation
- Assisted in the management of medical scholarships and deployment of medical officers

SKILLS AND ACTIVITIES

- Computer Skills: MATLAB, C++, C#, SPICE, Pascal, Microsoft Windows applications (Word, Excel, PowerPoint, Visio)
- Languages: Proficient in written and spoken Mandarin and Japanese
- Interests: Enjoys travelling, professional photography, football, music, reading and leadership activities